Evaluation of neuropathology and neurodegeneration in experimental models of Parkinson's disease based on alpha synuclein preformed fibrils or 6-hydroxydopamine

Pang, Cindy

Awarding institution:
King's College London

Evaluation of neuropathology and neurodegeneration in experimental models of Parkinson's disease based on alpha synuclein preformed fibrils or 6-hydroxydopamine

Cindy Chi Ching Pang

Ph.D Thesis

The University of Hong Kong and King's College London

2021

Abstract of thesis titled

Evaluation of neuropathology and neurodegeneration in experimental models of Parkinson's disease based on alpha synuclein preformed fibrils or 6-hydroxydopamine

Submitted by

Cindy Chi Ching Pang

For the joint degree of Doctor of Philosophy at The University of Hong Kong and King's College London

In May 2021

Parkinson's disease (PD) is a complex multisystem neurodegenerative disorder with no cure. Many PD patients will develop dementia, referred to as Parkinson's disease dementia (PDD). The characteristic neuropathological hallmarks of PD are Lewy bodies (LBs) and Lewy neurites (LNs) that are composed primarily of misfolded α–synuclein. α–Synuclein pathology spreads to different regions of the brain as disease progresses and the presence of LBs and LNs correlate closely with the clinical features of PD. However, it is not yet understood which events are necessary to cause dementia in PD. With this in mind, it is important to understand events that facilitate the spread of phosphorylated α-synuclein to neuroanatomically connected regions, and the consequences of this spread on cellular events that lead to altered

cognition. In rodents, injection into the brain of α–synuclein preformed fibrils (PFFs) has previously been shown to induce human-like Lewy body pathology, leading to neurodegeneration after prolonged periods of time, whereas injection of the free radical 6-hydroxydopamine (6-OHDA) induces rapid neurotoxicity of dopaminergic neurons and motor deficits in the apparent absence of α–synuclein modifications.

To further investigate the brain changes underlying cognitive dysfunction in PD, the PD-related effects of PFFs and 6-OHDA were examined following their unilateral stereotactic injection into the medial forebrain bundle (MFB) of Sprague-Dawley (SD) rats. Behaviour tests to measure motor, executive and visuospatial related cognitive impairments were used. Tissues were collected at 60, 90 and 120 days post injection (d.p.i.) of PFFs or vehicle. Phosphorylated α–synuclein was examined in regions connected to the MFB, with a focus on the frontal cortex and hippocampal areas that control cognition. These areas were also examined for changes in tau, synaptic proteins, oxidative stress and astrocyte reactivity. Synaptic disruptions underlie cognitive decline. Synaptic fractions were therefore isolated from rat tissues and immunoblotting techniques were used to study changes in synaptic proteins. To investigate the impact of rapid neuronal loss in the substantia nigra (SN) on α–synuclein spreading and neurodegenerative events important for cognition, a similar experimental approach was taken following unilateral MFB lesions with 6-hydroxydopamine (6-OHDA). Validation tests were conducted at 3 weeks post injection (w.p.i.) to confirm dopaminergic loss within the SN.

Results from this thesis established that injection of α–synuclein PFFs into rat MFB can lead to phosphorylation of endogenous α-synuclein and apparent “spreading” of phosphorylated α–synuclein to regions connected to the MFB. However, α–synuclein PFF injection did not

cause alterations in tau, synapses or cause disruptions to rat behaviour or cognition up to 120 d.p.i., in partial agreement with previous findings. In contrast, 6-OHDA injection into rat MFB resulted in rapid mass neuronal loss in the SN, phosphorylation and "spreading" of phosphorylated α–synuclein to MFB connected regions that was associated with altered synaptic marker levels, and cognitive impairments. These results extend previously published reports and suggest that rapid neuronal loss in the SN may initiate a cascade of events that facilitates the phosphorylation and/or spread of α–synuclein, ultimately leading to cognitive deficits.

The study elucidates events that facilitate α–synuclein modifications and neurodegenerative changes linked to cognitive dysfunction in PD. Oxidative stress-induced rapid neuronal loss may stimulate neuronal alterations that lead to the induction of oxidative stress and the appearance of phosphorylated α-synuclein in neuroanatomically connected regions, synaptic changes and cognitive abnormalities, whereas α–synuclein alone does not cause these neurodegenerative changes, at least not at the time points examined here. A future therapeutic intervention to reduce dementia related to α–synuclein in PD may therefore be an antioxidant or neuroprotective agent, rather than α–synuclein targeted therapy. Such a therapy could prevent the progression of a full-blown neurodegeneration cascade that results in PDD.

*(An abstract of exactly **584** words)*

Evaluation of neuropathology and neurodegeneration in experimental models of Parkinson's disease based on alpha synuclein preformed fibrils or 6-hydroxydopamine

Cindy Chi Ching Pang

(BSc, MSc)

A thesis submitted in partial fulfilment of the requirements for the Joint degree of Doctor of Philosophy at The University of Hong Kong and King's College London

2021

"All models are wrong, but some are useful"

George E.P. Box

Declaration

I hereby declare that all the work presented in this thesis represents my own, except where due acknowledgement is made.

Chapter 2, section 2.2.2. Rat primary neuron culture studies were performed by Mr Cyrus Liu (The University of Hong Kong).

Chapter 3, section 4.72. Optimisation of antibodies against total and phosphorylated tau, Htau and wild-type mouse lysates were provided by Dr Matthew Wade (King's College London)

Figure 2.5 was adapted from Mr Cyrus Liu's final year project thesis, submitted in 2017

Figure 2.9 Schematic diagram of the synaptoneurosome isolation methods was created by Dr Martina Hughes

Signed..... 

Acknowledgements

Reflecting back, I think I have always been fascinated by the brain. We all have one, yet each one is so unique. As an undergraduate student studying Biomedical sciences, it became apparent very early on that I was most interested in neurodegeneration related lectures. I remember a lecture about Parkinson's disease and although the lecture consisted of us watching a video for the entire duration, I was so fascinated and curious to understand more. My literature review topic was neuro related, and so it was inevitable that my MSc was also in Neuroscience. In hindsight, even my favourite characters from TV series were also neuro related. So, it was no surprise that when given a list of projects and research laboratory to choose from on the HKU website, I instantly picked one with a project on Parkinson's disease.

This PhD has been an emotional ride but I am really glad I persevered. I am even more grateful that I did not have to deal with all the hurdles throughout the 4 years alone. I have been extremely lucky to have experienced some of the best mentorships and support throughout. With that, I would like to truly thank those who have offered their kind words, a helping hand, technical help, a smile, and anything else that made those hurdles easier.

Firstly, I would like to thank my two supervisors, Dr Raymond Chang and Dr Wendy Noble, for this opportunity. I would like to thank The University of Hong Kong and King's College London for this joint adventure. The experience really has been invaluable.

Wendy, under your mentorship I have always felt very well looked after and loved. Thank you for being an incredible mentor giving me endless encouragement, reassurance and support in and outside of my project. Thank you for our discussions about science and career development. I have enjoyed learning a great deal from you about research, also how to do it well. Regardless of the situation there is always a light at the end of the tunnel.

Drs Virginia Lee and John Trojanowski, the three months in CNDR has genuinely been a highlight in my PhD journey. I have loved listening to your life adventures. It was truly inspirational and exciting to learn from you both. Thank you for your guidance and continuous mentorship. I would also like to extend my thanks to the CNDR team; Bin, Kelvin, Fares, Sylvia, Chao, Esteban, Sam, Hao, Quihui Wu, Lakshmi, Sneha, Sue, JR, Mo and Medha. A truly wonderful family, so enthusiastic, willing to teach and explain.

Dr Clemens Kiecker, I am so lucky to have had you as my MSc supervisor and mentor. Thank you for inspiring me and giving me the confidence to pursue a PhD.

Dr Peter Giese, thank you for the opportunity to present on ARUK Science Day.

I would also like to thank Professor Steve Gentleman for your words of wisdom and offering me your microtome in times of desperation.

At HKU, I would like to thank LND members; Becky, Rachel, Krit, Carmen, Samantha, Chunxia and Anuri for your assistance throughout. Clara, Sally and Summer, thank you for your training in character building. Maja, thank you for your hard work and support from the moment you arrived. Jeff, John and Haydn, thank you for being such a great laugh and looking out for me in and outside the lab.

Smara, thank you for being my PhD buddy and helping me with all matters HKU related. I am so grateful (and miss) our long weekend brunches. Shawn, thank you for being so cheery. Brian thank you for your advice with my western blots. LAU staff, Joseph Ip and 冬姐, thank you very much for looking after the animals and me. 小燕姐**,** thank you for offering me your home-grown sweet potatoes in the morning for breakfast and being so lenient with the behaviour room. Phyllis, thank you for being so organised with the surgery room. I have really enjoyed our conversations and thank you for your kind words and encouragement. Alla, thank you for sharing all your knowledge of histological staining with me and trusting me with your histology room. I have thoroughly enjoyed learning from you. Dr Tipoe and Dr Jian Yang thank you for sharing your passion about dissection and anatomy with me during those TA sessions. I have enjoyed learning from the anatomy team. Mr Edmond Kam thank you for providing the key essentials for navigating around HKU.

At KCL, I would like to thank Diane, Bea and Maria. Team Tau members, Katie, Diana, Chen, Saskia, Kate, Aurelio, Despoina, Matt and Emily, it has been wonderful being in such a friendly and supportive group with you all. Rebecca, Louisa and Paula, thank you for being great office buddies. Huzefa, thank you for our little science chats and for making me laugh all the time. The Miller lab, thank you for lending me absolutely everything. Ricky, thank you for the unlimited supply of herbal teas. Marie, thank you for your calming words before all of my talks. Aunty Sarah, thank you for being such a good friend and listener. Also for sharing your protein ladder with me. Lizzie, thank you for your advice on all my presentations and the coffee catch ups. Dawn, thank you for being such a supportive friend for matters in and outside of the lab. I have enjoyed eating away my PhD stipend with you. I would like to also extend my thank you to David and Kate, for making my crazy requests happen with access and sorting all the technical matters. Martin, thank you for being so cheery in the morning.

I would also like to thank all HKU and KCL summer, BSc, MSc and MSci students; Cyrus Liu, Catherine, Jessica, Maggie, Angel, Alvin, Glen, Suzanna, Tiffany, Matt, Vesela and Sarika. It has been a pleasure mentoring you all and thank you all for teaching me a great deal too.

Dr Alan Liu, thank you for being my go-to person and my PhD buddy despite never being in the same city. You have helped me enormously with matters in and outside of the lab. Thank you for taking the time to discuss my project with me and making me think.

Rocky, thank you for explaining the anatomy aspect of perfusion, “apex, ventricle, atrium and aorta” and willingly wait until 10pm for dinner. Thank you for always seeing the best in me and for your endless encouragement and support.

Uncle Chris and auntie Carrie, thank you for helping me settle in Hong Kong. I am forever thankful for your generosity and care. Your advice on survival in Hong Kong has been incredibly helpful.

Lastly, I would like to thank my HK and UK family members for the support and love. 我想多謝我的公公，婆婆和嫲嫲。多謝你們由我出世到現在都對我照顧有加，相信我的能力，永遠都是我的頭號支持者。 To my brother, Jeremy. Your hilarious stories have cheered me up on multiple occasions and brightened up my day (Mr Normen-Clature). I am glad to have you at home for our nerdy discussions about pharma and science. Mum and Dad, you are both the hardest working people I know. Thank you for your selfless love, care and support, the opportunities you have given me, for being so proud of me and for always being interested in listening to my PhD antics.

Table of Contents

Abbreviations and Symbols

α–synuclein	Alpha-Synuclein
β-actin	Beta actin
4HNE	4-hydroxy-2-nonenal
5-CSRTT	5-choice serial reaction time task
6-OHDA	6-hydroxydopamine
8OHG	8-hydroxyguanosine
AD	Alzheimer's disease
AldhL1	Aldehyde dehydrogenase 1 family member L1
APP	Amyloid precursor protein
ARSA	Arylsulfatase A
AT8	Tau phosphorylated at Serine 205 and Threonine 202
Aβ	Amyloid beta
BBB	Blood brain barrier
BG	Basal ganglia
BNE	BrainNetwork Europe
BSA	Bovine serum albumin
CA1	Hippocampus CA1
CA3	Hippocampus CA3
CD68	Cluster of differentiation 68
CNS	Central nervous system
Crtx	Cortex
DA	Dopamine
DBS	Deep brain stimulation
DFur	5'-deoxy-5'-fluorouridine
DJ-1	PARK7
DLB	Dementia with Lewy bodies
DNA	Deoxyribonucleic acid
dPBS	Dulbeccos phosphate buffer
D.p.i.	Days post injection
ELISA	Enzyme-linked immunosorbent assay

FPLC	Fast protein liquid chromatography
GBA	Glucocerebrosidase
GFAP	Glial fibrillary acid protein
GPe	External global pallidus
GPi	Globus pallius internus
GSK3-β	Glycogen synthase kinase beta 3
h.p.i.	Hour post injection
H_2O_2	Hydrogen peroxide
HPLC	High performance liquid chromatography
HS	High salt buffer
I.P.	Intraperitoneal
Iba1	Ionised calcium binding adaptor molecule 1
IHC	Immunohistochemical
iPSC	Induced pluripotent stem cells
ITI	Intertrial interval
L-DOPA	L-3,4-dihydroxyphenylamin
LBs	Lewy bodies
LNs	Lewy neurites
LCN2	Lipocalin-2
LRP10	Low-density lipoprotein receptor-related protein 10
LRRK2	Leucine-rich repeat kinase 2
MAPT	Microtubule associated tau protein
MFB	Medial forebrain bundle
m.p.i.	Months post injection
MPTP	1-methyl-4-phenyl1-1,2,3,6-tetrahydropyridine
MWM	Morris water maze
NAC	Non-amyloid binding component
NADPH	Nicotinamide adenine dinucleotide phosphate
NFT	Neurofibrillary tangles
NUS1	NUS1 dehydrodolichyl diphosphate synthase subunit
OF	Open field test
Paraquat	N,N'-dimethyl-4-4'-bipiridinium

PBS	Phosphate buffered saline
PBS-T	Phosphate buffered saline- Tween-20
PD	Parkinson's disease
PDD	Parkinson's disease dementia
PDGF	Platelet derived growth factor
PFA	Paraformaldehyde
PFFs	Pre-formed fibrils
PHF1	Paired helical filaments
PINK1	PTEN induced kinase 1
PRKN	Parkin RBR E3 ubiquitin protein ligase
PrP^{Sc}	Scrapie prion proteins
pS396	Tau phosphorylate on serine 396
pS404	Tau phosphorylated on serine 404
PSEN1	Presenilin
pSer129	α–Synuclein phosphorylated on serine 129
PSD-95	Post synaptic density protein-95
REM	Rapid eye movement
ROS	Reactive oxygen species
RT	Room temperature
SAP97	Synapse associated protein 97
S.C.	Subcutaneous
SD	Sprague-Dawley
SDS	Sodium dodecyl sulfate
SerpinA3	Serpin Family A Member 3
SN	Substantia nigra
SNpc	Substantia nigra pars compacta
SNr	Substantia nigra reticulata
SNCA	Alpha synuclein
STn	Subthalamic nuclei
TBS	Tris-buffered saline
TDP-43	TAR DNA binding protein-43
Tg	Transgenic

ThT	Thioflavin T
TMEM230	Transmembrane protein 230
TX	High salt buffer Triton-X
VPS35	Vacuolar protein sorting-associated protein 35
VTA	Ventral tegmental area
W.p.i.	weeks post injection
WT	Wild-type
XO	Xanthine oxidase

List of Figures

List of Tables

Papers/conference presentations arising from this thesis

Paper

PANG, C. C., KIECKER, C., O'BRIEN, J. T., NOBLE, W. & CHANG, R. C. 2019. Ammon's Horn 2 (CA2) of the Hippocampus: A Long-Known Region with a New Potential Role in Neurodegeneration. *Neuroscientist,* 25**,** 167-180.

In Preparation

***Cindy C.C. Pang**, Maja H. Sørensen, Krit Lee, Kelvin C. Luk, John Q. Trojanowski, Virginia M.Y. Lee, Wendy Noble, and Raymond C.C. Chang. 2021. Investigating key factors underlying neurodegeneration linked to α-synuclein spread*

Conference presentations

2016

1. **Pang C.C.C**., Noble W., Chang R.C.C. (2016) Investigating the impacts of Parkinson's Disease Dementia (PDD) by using an animal in PD. *The 4th International Anatomical Sciences and Cell Biology Conference (IASCBC 2016), The University of Hong Kong, Hong Kong.*

2017

1. **Pang, C.C.C**., Man, S.C., Lee, K., Noble. W., Chang, R.C.C. (2017) Establishing pre-clinical therapeutics. *International Alzheimer's Conference 2017. Hong Kong.*
2. **Pang, C.C.C**., Chang, R.C.C. (2017) Investigating tau and alpha-synuclein in Parkinson's disease dementia model. *13th International Conference on Alzheimer's & Parkinson's Diseases, Vienna, Austria.*
3. **Pang, C.C.C.,** Man, S.C., Noble, W., Chang, R.C.C (2017) Investigating the impacts of Parkinson's disease dementia (PDD) by using an animal model in PD. *The 12th International Symposium on Healthy Aging, Hong Kong.*

2019

1. **Pang, C.C.C**, Sorensen, M.H, Lee, K., Luk, K.C., Lee, V.M., Trojanowski, J.Q.T., Noble. W., Chang, R.C.C. (2019). Investigating the links between cognitive dysfunction and

neuropathology in experimental rat models of Parkinson's disease. *The 14th International Conference on Alzheimer's & Parkinson's Diseases, Lisbon, Portugal.*

2. **Pang, C.C.C**, Sorensen, M.H, Lee, K., Luk, K.C., Lee, V.M., Trojanowski, J.Q.T., Noble. W., Chang, R.C.C. (2019). Investigating the links between cognitive dysfunction and neuropathology in experimental rat models of Parkinson's disease. *Alzheimer's Research UK conference 2019. Harrogate, UK.*

2020

1. **Pang, C.C.C,** Sorensen, M.H, Lee, K., Luk, K.C., Lee, V.M., Trojanowski, J.Q.T., Noble. W., Chang, R.C.C. (2020). Using 6-OHDA and aSyn PFFs to explore the role of tau mediated loss of synaptic dysfunction leading to cognitive dysfunction in Parkinson's disease. *The 121st Meeting of the British Neuropathological Society, London.UK.*

Talks

1. **Pang C.C.C**., Noble W., Chang R.C.C. (2018) Investigating the impacts of Parkinson's Disease Dementia (PDD) by using an animal in PD. *External seminar at The University of Pennsylvania, 2018, USA.*
2. **Pang, C.C.C**, Sorensen, M.H, Lee, K., Luk, K.C., Lee, V.M., Trojanowski, J.Q.T., Noble. W., Chang, R.C.C. (2019). Investigating the links between cognitive dysfunction and neuropathology in experimental rat models of Parkinson's disease. *Neuroscience PhD symposium 2019, King's College London, UK.*
3. **Pang, C.C.C**, Sorensen, M.H, Lee, K., Luk, K.C., Lee, V.M., Trojanowski, J.Q.T., Noble. W., Chang, R.C.C. (2019). Investigating the links between cognitive dysfunction and neuropathology in experimental rat models of Parkinson's disease. *Alzheimer's Research UK Science Day at King's College London, UK.*

Grants

1. **Pang., C.C.C and Rupawala, H**. Investigation of the relationship between cysteine string protein alpha (CSP-α) and alpha synuclein (αSyn) in Parkinson's disease dementia. *Alzheimer's Research UK King's College London Network Centre, Pump Priming grant*, 2019

Chapter 1 Introduction

1.1 Parkinson's disease

1.11 A brief history of Parkinson's disease

Parkinson's disease (PD) was first described over two hundred years ago by the English neurosurgeon James Parkinson in "An Essay on the Shaking Palsy". In his essay, James Parkinson described his encounters with a handful of patients, all of whom displayed tremor at rest, bradykinesia, akinesia accompanied with stooped posture and festinating gait (Goetz, 2011). A clear distinction in tremor was also distinguishable between those with passive and resting tremor in Paralysis agitans compared to tremor from those due to excess alcohol consumption, advanced aging or brain lesions (Goetz, 2011). It is now known as the most prevalent movement disorder (Alexander, 2004) and the second most common form of neurodegenerative disorder, after Alzheimer's disease (Cabreira and Massano, 2019).

PD was initially mentioned from as early on as the 12th century B.C, where the symptoms were described in the Bible, in Egyptian papyrus and Leonardo da Vinci's notebooks (Raudino, 2010). A Hungarian physician, Ferenc Papai Pariz (1649-1716) also noted some of the clinical symptoms of PD in a textbook (Bereczki, 2010). Later in the Ming Dynasty, Yikvi Sun, further recorded that tremors involved the head, hands and feet (Raudino, 2001).

Although ancient literature provided descriptive features of PD-like symptoms in abundance, James Parkinson first observed that patients suffering from Paralysis agitans originally had their intellect and senses spared, although he noted that further disease progression usually led to a common end stage phenomenon of "constant sleepiness, slight delirium and extreme

exhaustion". This was suggestive that the disease was far more complex and beyond the visible motor impairment.

Fifty years later, a French neurologist Jean-Martin Charcot further elaborated on the comprehensive description and anatomopathological basis of the disease. Charcot denoted the name Parkinson's disease as a distinctive clinical entity to credit James Parkinson's work. Charcot identified differences in the variations of tremors. Tremors were either of slow 4-6 Hz or of high frequency 8-9 Hz, with the former being characteristic of PD. Charcot also observed the non-motor symptoms Parkinson previously mentioned, such as autonomic dysfunctions, fatigue and pain (Garcia-Ruiz et al., 2014). Brissaud further suggested that the substantia nigra (SN) was the possible lesion site in PD (Okun and Koehler, 2007). However, it was not until much later that Tretiakoff (1919) provided neuropathological evidence of changes in the SN in PD (Holdorff, 2002; Lees et al., 2009). Depigmentation of the SN was observed to occur as a result of the loss of SN neurons. The microscopic loss of neuromelanin-positive neurons was also associated with gliosis and Lewy bodies (LBs), so named after their description by Fredrich Lewy in 1912. These lesions are now a central focal point of neuropathological studies of PD. Surprisingly initial observations described LB inclusions as being absent in the SN, but localised within the dorsal nucleus of the vagus nerve and substantia innominate (Holdorff, 2002).

Dopamine dysregulation was first recognised as contributing to PD in the 1900s. Fluorescent and histochemical methods showed that dopamine is present in vertebrate brain (Carlsson et al., 1958), and that the striatum has the highest brain concentration of dopamine (Carlsson, 1959; Sano et al., 1959). However, it was Carlsson et al. (1957) who reported the functional

role of dopamine and showed that the dopamine precursor, L-3,4-dihydroxyphenylamine (L-DOPA) was sufficient to reverse reductions in dopamine levels (Lees et al., 2015). This further encouraged George Cotzias to treat PD patients with L-dopa, and this treatment remains as the gold standard today (Lees et al., 2015).

Great advances have since been made in understanding the origin and pathogenesis of PD, and several alternative treatments for PD have been discovered, including deep brain stimulation (DBS), and stem cell therapy (in animal models) (Bjorklund et al., 2002), with many other disease-modifying therapies under investigation (Bjørklund et al., 2020). Several animal models of PD have been developed, and these will be discussed in more detail below. Rodent models in which the neurotoxins 6-hydroxydopamine (6-OHDA) and 1-methyl-4-phenyl1-1,2,3,6-tetrahydropyridine (MPTP) are injected are commonly used to study preclinical PD (Kin et al., 2019). The identification of familial causative PD gene mutations (Aharon-Peretz et al., 2004; Polymeropoulos et al., 1997) led to the generation of many genetically modified rodent models (Lee et al., 2012). Braak and colleagues proposed a staging system for PD based on the specific pattern of α–synuclein spread in postmortem PD brain (Braak et al., 2003). More recently, the identification of "cell to cell transmission" and propagation of α–synuclein (Luk et al., 2012a) (Luk et al., 2012b) has led to a colossal number of studies investigating the progressive spread of pathology in models of PD, including investigates of the strain of α–synuclein that allows spread and/or leads to neurodegeneration (including this investigation). Figure 1.1 summarises some of the key figures and their contributions during the 200-year history of PD.

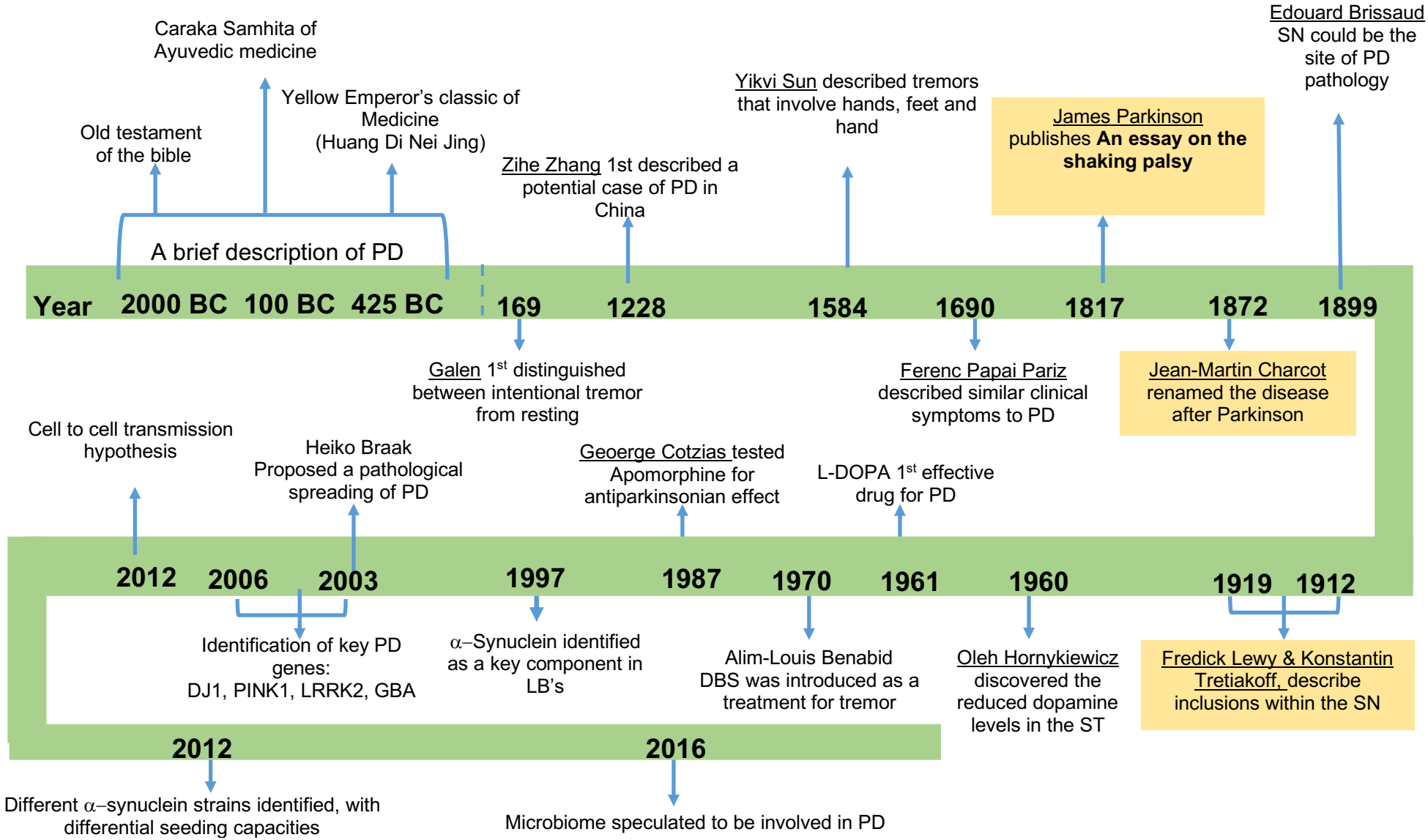

Figure 1.1 A brief history of Parkinson's disease from 2000 BC, through to 20th Century. Key discoveries in shaping the understanding of Parkinson's disease are highlighted, experimental discoveries and clinical trial results are excluded. PD, Parkinson's disease, SN, substantia nigra, ST, striatum, DBS, deep brain stimulation, LB, Lewy bodies.

1.2 PD as a multifaceted disorder

PD is a chronic, progressive neurodegenerative movement disorder, with no cure for the disease and treatments address only symptoms (Bandres-Ciga et al., 2020). From 2016 there were an estimated 6 million PD cases globally and the number of cases is predicted to increase to over 12 million by 2040 (Feigin et al., 2020). Incidentally, PD is also the fastest growing neurological disorder (Feigin et al., 2020). Age is an irrefutable risk factor for PD with average age of onset being approximately 60 years of age. Typically, a diagnosis under the age of 40 is considered as early onset PD and these patients tend to have a longer disease duration compared to patients diagnosed at the age of 70 and over, where there is a more rapid disease progression (McCann et al., 2014). Men are disproportionately affected by PD compared to women (Wright Willis et al., 2010). The progression of PD symptoms varies upon the individual but can take fifteen to twenty years or more to develop (Davie, 2008). The symptoms of PD are both complex and diverse, involving both motor and non-motor components. Key characteristic clinical symptoms of PD include the presence of two or more of the cardinal motor symptoms bradykinesia, rigidity, gait instability and resting tremor (Poewe et al., 2017). A wide range multifactorial causes including genetic and environmental factors have been proposed to contribute to PD etiology (Blauwendraat et al., 2020), though the molecular basis remains not entirely clear. Potential triggering causes include mitochondrial dysfunction, oxidative stress and the misfolding of α–synuclein. It is unlikely that these factors act independently, but their complex interplay is likely to contribute to PD pathogenesis (Obeso et al., 2010).

1.2.1 Genetics of PD

The majority of PD cases (90-95%) are sporadic without an identified genetic component (Duffy et al., 2018a). A small percentage of cases are known to harbour mutations in known PD genes that have large effects and cause familial forms of PD, which include genes that encode synuclein (*SNCA),* Leucine-rich repeat kinase 2 *(LRRK2),* vacuolar protein sorting-associated protein 35 (*VPS35),* parkin RBR E3 ubiquitin protein ligase *(PRKN),* PTEN induced kinase 1 (*PINK1),* glucocerebrosidase (*GBA)* and *DJ-1* (*PARK7*) (Polymeropoulos et al., 1997; Zimprich et al., 2011; Bonifati et al., 2003; Valente et al., 2004; Tayebi et al., 2001; Vilarino-Guell et al., 2011; Liu et al., 2014; Oczkowska et al., 2013). Pathogenic variants of *PARK7, PRKN, PINK1* and *DJ-1* have been implicated in mitochondrial and mitophagy functions, while *GBA, LRRK2* and *VPS35* are thought to be associated with lysosomal and trafficking pathways (Blauwendraat et al., 2020). Mutations in the *SNCA* gene were first identified in 1997 in a large Italian kindred and three unrelated Greek families (Polymeropoulos et al., 1997). A causative missense mutation was identified at *A53T*, and additional mutations at *A30P, E46K* and *H50Q* and *A53E* have since been identified (Kruger et al., 1998; Lesage et al., 2013). In addition to point mutations in *SNCA*, duplications or triplications of wild-type *SNCA* also cause familial PD (Duffy et al., 2018a) and show gene-dosage effects with *SNCA* triplication carriers exhibiting earlier and more rapid progression compared to those with duplications (Singleton et al., 2003); (Farrer et al., 2004);(Olgiati et al., 2015). In contrast, evidence supporting elevated mRNA and protein levels of α–synuclein in idiopathic patients is lacking (Tan et al., 2005); (Su et al., 2017). Postmortem analysis reveals only modest changes in α–synuclein protein levels compared to age-matched controls (Zhou et al., 2011). Therefore, examining total expression levels of α–synuclein is a useful means of distinguishing familial from

sporadic forms of the disease. However, both familial and sporadic PD brain exhibits changes in membrane association, solubility and the abundance of post-translationally modified forms of α–synuclein (Tong et al., 2010; Burre et al., 2018). A notable shift in the ratio of soluble to insoluble α–synuclein is observed, but without changes in total α–synuclein. A decrease in soluble monomeric α–synuclein occurs with concurrent increases in soluble phosphorylated α–synuclein in susceptible regions such as the SN and cortex in sporadic and *SNCA* triplication carriers (Gibb and Lees, 1988b); Irizarry et al., 1998; Tong et al., 2010). Together, these findings emphasise the critical role of α–synuclein phosphorylation in PD pathophysiology in both sporadic and familial forms of PD.

Additional gene variants are associated with PD, including in the genes encoding transmembrane protein 230 (*TMEM230),* low-density lipoprotein receptor-related protein 10 *(LRP10),* NUS1 dehydrodolichyl diphosphate synthase subunit *(NUS1)* and arylsulfatase *A (ARSA) (*Blauwendraat et al., 2020). However, the consequences of these variants for PD risk are still debated and additional studies are required to elucidate their involvement in PD etiology.

PD related genes	Biological consequence	References
Alpha-synuclein (SNCA)	Misfolding of aSyn protein	Polymeropoulos et al., 1997
Vacuolar protein sorting-associated protein 35 (VPS35)	Associated with lysosomal and trafficking pathways	Vilarino-Guell et al., 2011
Glucocerebrosidase (GBA)		Tayebi et al., 2001
Leucine-rich repeat kinase 2 (LRRK2)		Li et al., 2014
DJ-1 (PARK7)	Mitochondrial and mitophagy functions	Bonifati et al., 2003
Parkin RBR E3 ubiquitin protein ligase (PRKN)		Oczkowska et al., 2013
PTEN induced kinase 1 (PINK1)		Valente et al., 2004
Transmembrane protein 230 (TMEM230	Implications unknown, additional studies required	Blauwendraat et al., 2020
Low-density lipoprotein receptor-related protein 10 (LRP10),		
NUS1 dehydrodolichyl diphosphate synthase subunit (NUS1		
Arylsulfatase A (ARSA)		

Table 1.1 Summary of genes implicated in PD, indicating the primary biological pathways in which their encoded proteins function.

1.2.2 Motor impairment and the basal ganglia

The basal ganglia (BG) circuitry consists of several important neuroanatomical regions in the brain that are affected in PD. This circuitry has a critical role in controlling goal-directed behaviour and habits. The loss of dopamine in PD leads to the disruption of the two main striatal projection systems resulting in the inability to respond appropriately to cortical and thalamic signals, causing bradykinesia (Zhai et al., 2018). The main components of the BG include the striatum, which itself consists of the dorsal striatum (caudate nucleus and putamen) (Lipton et al., 2019). The dorsal striatum receives dopaminergic input from the SN and has long been demonstrated to play a central role in compulsion, goal-directed and habitual reinforcement as indicated by animal studies (Ahmari, 2016), while the ventral striatum which is made up of nucleus accumbens and olfactory tubercle is associated with the "reward pathway" and addiction (Luscher, 2016). Other anatomical components of the BG include the globus pallidus, the ventral pallidum, the substantia nigra and the subthalamic nucleus.

By understanding the BG network, it is possible to appreciate the importance of dopamine for motor output and to understand the detrimental consequences of dopaminergic neuron loss in the midbrain and how this leads to circuit-level changes that underlie the motor symptoms of PD.

The striatal medium spiny neurons (MSNs) can be considered as two populations - the direct and indirect pathway MSNs, depending on their projection targets. In the direct pathway, MSNs project directly to the BG and decrease BG output, disinhibiting the thalamus and hence promoting movement. Conversely, indirect pathway MSNs project to the BG indirectly via the

GPe and STN. They also express Gi-coupled D2-like dopamine receptors (Gerfen et al., 1990; Mahul-Mellier et al., 2020; McGregor and Nelson, 2019). Activating the indirect pathway to increases BG output and inhibits the thalamus thereby reducing movement. Dopamine is thought to have opposing effects on these two populations, increasing or decreasing MSN activity. The overall effect of dopaminergic signalling is to promote movement by suppressing BG output from the GPi. However, in PD, dopamine loss leads to imbalanced activity between the two pathways, especially at the striatal level. Excessive indirect pathway activity is thought to supress GPe firing, increase STN activity and result in an increased GPi-mediated thalamic inhibition. In contrast, diminished direct pathway firing disinhibits GPi neurons and further suppresses the thalamus and cortex (Figure 1.2).

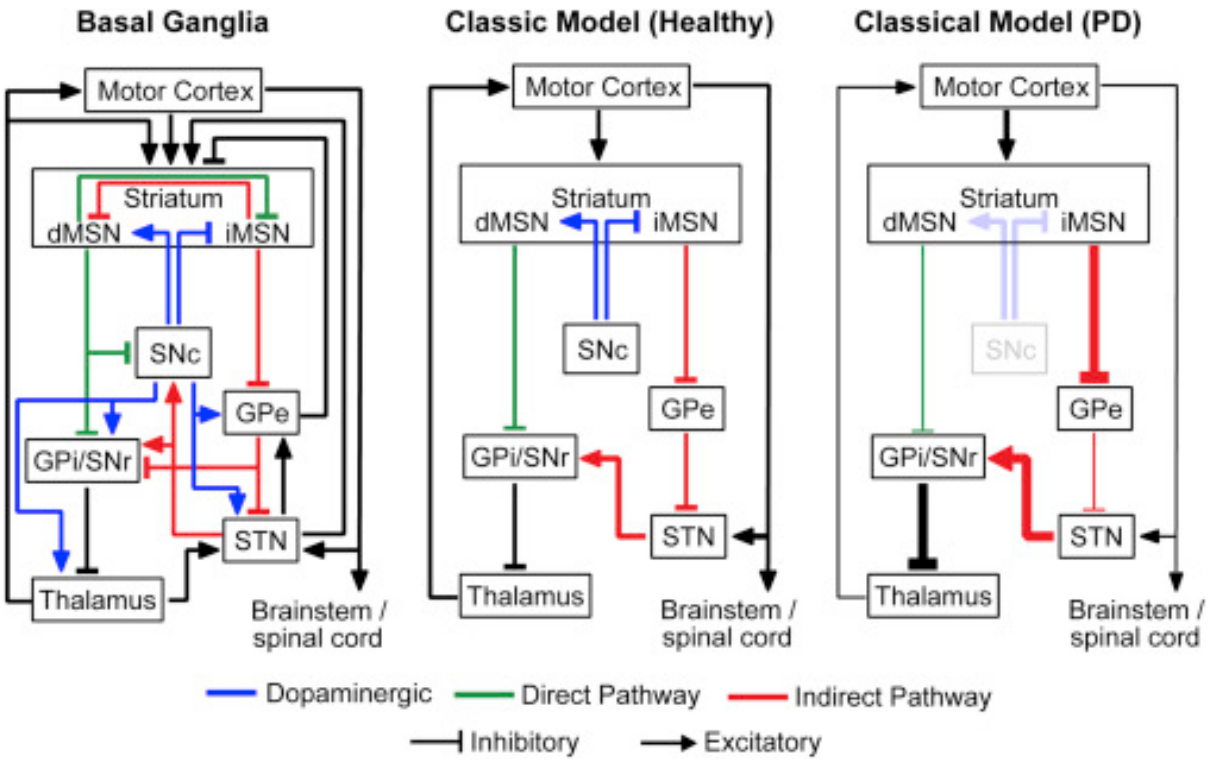

Figure 1.2 Left panel: basal ganglia diagram highlights the role of dopamine on both direct and indirect pathway activity and motor output. The centre diagram represents "healthy condition" where dopamine from the SNc to the striatum activities the direct pathway and inhibits the indirect pathway MSNs. This subsequently decreases GPi output, releasing inhibition on the thalamus and cortex and promoting movement. The right panel diagram represents Parkinsonian conditions. The loss of SNc dopamine leads to hypoactivity of the direct pathway and hyperactivity of the indirect pathway leading to excessive GPi output. This ultimately causes over-inhibition of the thalamus and cortex and suppression of movement. Figure taken from McGregor and Nelson (2019), with permission.

1.2.3 Cognitive impairment in Parkinson's disease

Robust evidence has shown that in comparison with age matched controls without PD, those with PD are at a much higher risk of developing dementia and show a tendency for cognitive decline involving several cognitive domains (Aarsland et al., 2017). The prevalence of cognitive impairment in PD is approximately 30 % (Aarsland et al., 2003), while approximately 80 % of longitudinally followed patients with PD developed dementia over the course of their disease progression, if they survived for more than 10 years after diagnosis (Hely et al., 2008); (Aarsland et al., 2003); (Irwin and Hurtig, 2018). The onset of dementia in PD leads to a diagnosis of Parkinson's disease dementia (PDD). The major cognitive domains affected in PDD are executive function, visual perceptual ability, attention and memory (Gratwicke et al., 2015; Aarsland et al., 2017).

Executive function encompasses various cognitive abilities such as inhibition, problem solving, planning/sequencing, rule-shifting/maintenance, task switching and manipulation of working memory (Marshall et al., 2019). The fronto-striatal network, strong functional connections between the prefrontal cortex and the striatum via parallel dopamine dependent cortico-striatal loops, is partially responsible for executive function (Lewis et al., 2003). However, the mesocortical dopamine network, which originates in the midbrain ventral tegmental area (VTA) (A10) and projects diffusely to neocortical areas such as the cingulate cortices, insular and prefrontal regions may also contribute to executive dysfunction (Gratwicke et al., 2015). Visuospatial deficits include subtle difficulties in perception of personal space (Levin et al., 1991); (Montse et al., 2001) and evidence from voxel-based morphometry MRI analysis found that in PD patients with mild cognitive impairment (PD-MCI), alterations in occipito-temporal and dorsal parietal connections underlie cognitive deficits (Pereira et al., 2012). Attention is

considered to comprise of three different subsystems; executive control, alerting and orienting, and involve the fronto-parietal, cortico-occipital cholinergic and noradrenergic networks (Petersen and Posner, 2012).

The mechanisms leading to cognitive decline in PD are still poorly understood. Cognition itself is rarely dominated by a single neural network, but is instead influenced by several interacting neural networks including cholinergic, serotonergic, noradrenergic and glutamatergic systems (Del Tredici et al., 2002); (Braak et al., 2003). Evidence from the Tg2576 mouse model of AD that expresses mutant human APP demonstrated that progressive dopaminergic neuron loss within the mesolimbic pathway is correlated with impairment in CA1 plasticity and memory performance (Nobili et al., 2017).

In addition to cognitive impairment in PD, some of the non-cognitive disturbances in PD may involve the following (as listed in Table 1.2): autonomic system (sexual dysfunction, hypotension), gastrointestinal (constipation, difficulty in voiding bowels), sensory (dystonia, visceral pain), sleep (REM sleep disorders) and neuropsychiatric (depression) features leading to a significant reduction in quality of life (Chaudhuri et al., 2006; Mahul-Mellier et al., 2020); (Docherty and Burn, 2010).

Parkinson's disease symptoms	
Early symptoms	-Mild tremors, -Lack of movement of limbs, -Abnormal facial expression,
Primary Motor	- Tremor - Rigidity - Bradykinesia - Postural instability
Secondary motor	- Muscle cramps, dystonia - Difficulty in swallowing, chewing - Sexual dysfunction
Primary non-motor	- Dementia (executive dysfunction, hallucinations) - Fatigue, REM sleep disorders - Pain
Secondary non-motor	- Constipation - Hypotension - Emotional changes

Table 1.2 The main symptoms of PD. Table summarises the clinical features presented during PD progression. An individual may not necessarily experience all of these symptoms and may show secondary prior to primary symptoms.

1.3 Pathological proteins in PD

1.3.1 Neuropathological hallmarks of PD

The characteristic neuropathological hallmarks of PD include the loss of nigrostriatal dopaminergic neurons and the presence of intraneuronal proteinaceous cytoplasmic inclusions, referred to as Lewy bodies (LBs). The cell bodies of nigrostriatal neurons in the SN contain conspicuous quantities of neuromelanin (Marsden, 1983) and therefore depigmentation is evident upon neuronal loss (Figure 1.3). The extent of SN cell loss parallels the decline of dopamine (DA) transporter expression (Uhl et al., 1994). Typically, at the onset of motor symptoms 60% of the dopaminergic neurons within the SN are lost, and putamenal DA has been depleted by 80% (Uhl et al., 1985).

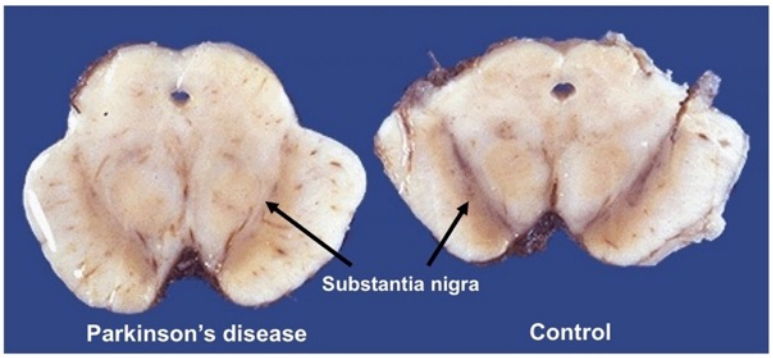

Figure 1.3 Loss of substantia nigra (SN) neurons in PD compared to control brain. In Parkinson's disease, there is evident loss of dopaminergic neurons in contrast to dense pigmentation caused by neuromelanin-positive dopaminergic neurons in the SN observed in controls. Figure adapted from Mercer University of Medicine (www.Medicine.tamu.edu). Copyright permission from Dr Klatt.

Spillatini et al (1998) were the first to discover that α–synuclein is the main constituent of LBs, along with neurofilaments, p63 and ubiquitin. The formation of LBs consists of several phases, starting with the pre-Lewy body where phosphorylated α–synuclein is minimal. Typically, LBs observed during postmortem investigations appear as immature LBs, also referred to as pale bodies, at early stages of disease. As disease progresses, pale bodies develop into intracellular diffuse and granular eosinophilic material with ill-defined borders. At advanced stages of PD, mature cytoplasmic LBs dominate over pale bodies (Gibb and Lees, 1988a); (Irizarry et al., 1998); (Stefanis, 2012). Mature LBs and accompanying Lewy neurites (LNs) show dense cores with radiating filaments that stain positive for thioflavin S, and are resistant to digestion by proteinase K (Neumann et al., 2002). As LBs mature, they contain an increased abundance of phosphorylated α–synuclein, and the cytosolic to membrane ratio of α–synuclein also changes. Pre-Lewy bodies consist of 2:1 cytosolic/membrane-bound α–synuclein, while in mature LBs, approximately equal forms of α-synuclein are found in the cytosolic and membrane-bound (Zhou et al., 2011);(Murphy and Halliday, 2014). An image depicting the various α-synuclein pathology is shown in Figure 1.4.

Lewy-related pathology, particularly in the cortex, is considered to be most important for the development of cognitive impairment in PD since it correlates closely with dementia in PD (Aarsland et al., 2003{Halliday, 2014 #1613; Compta et al., 2011; Irwin et al., 2012).

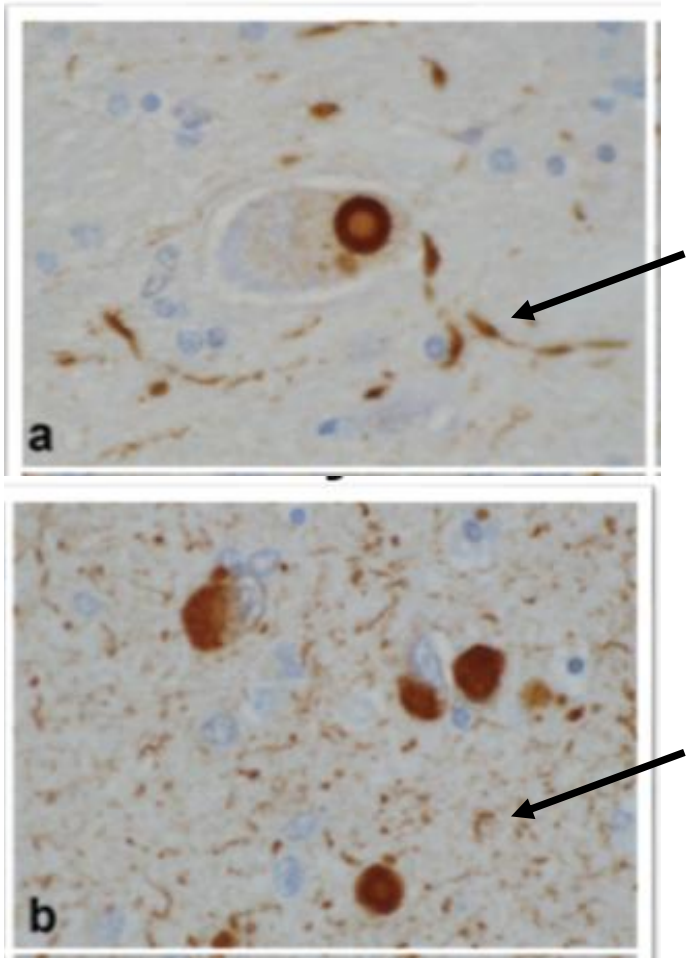

Figure 1.4 Images of α–synculein pathology at postmortem. a) shows large Lewy Body next to a nucleus, with lewy surrounding lewy neurites b) cytoplasmic lewy bodies that are smaller in size with other aggregates in neurites. Arrows point to Lewy neurites. Images are taken from Alforum.org, courtesy of Dennis Dickson, Mayo Clinic.

1.3.2 Alpha Synuclein

1.3.2.1 Alpha synuclein structure

α–Synuclein is a relatively small protein of 140 amino acids, first reported by Maroteaux and Scheller (1991). Biochemically α–synuclein consists of three main domains; the N-terminus, residues 1-60, which is rich in leucine and has seven highly conserved hexameric motifs that form the amphipathic alpha-helix structure (Uversky, 2007). A point mutation at amino acid 53, A53T, leads to familial PD. The "NAC" region in the middle of the molecule contains the non-amyloid binding component (residues 61-95). The hydrophobicity of this region contributes to the ability of α–synuclein to self-aggregate. The C-terminus of α–synuclein, amino acids 96-140, is enriched with charged residues and contains multiple phosphorylation sites, one of which is Serine 129 (Ser129) (Figure 1.5).

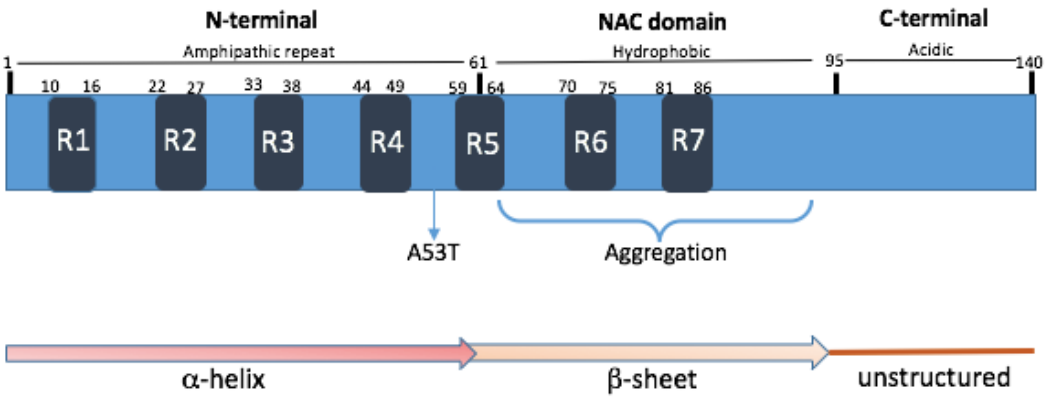

Figure 1.5 A representation of the biochemical structure of a-synuclein. The N-terminus, consisting of four amphipathic repeats typically gives rise to β-helix structures. The non-amyloid-binding component (NAC) is hydrophobic and is prone to aggregate into β-sheet structures. The C-terminal domain includes many phosphorylation sites including Ser129. R denotes repeat regions. Figure created by Cindy Pang.

1.3.2.2 Alpha synuclein functions in health and disease

Within the central nervous system (CNS), α–synuclein is predominantly expressed by neurons and is found in presynaptic vesicles. When α–synuclein exists in the physiological, soluble and monomeric form, it participates in regulating exocytosis, vesicle membrane fusion, vesicle clustering, and within dopaminergic neurons mediates presynaptic neurotransmitter release (Duffy et al., 2018a);(Chandra et al., 2005). Mice lacking the *SNCA* gene show impaired release of dopamine (Abeliovich et al., 2000). Knockout of α–synuclein alone gives rise to only modest phenotypes (Burre et al., 2010), whereas ablation of all three synuclein members leads to premature death of small presynaptic boutons (Greten-Harrison et al., 2010).

Under environmental conditions where the rate of nucleation, growth and fragmentation are favorable, α–synuclein protein is capable of spontaneously generating amyloid structures due to protein misfolding (Jucker and Walker, 2013). This property is not unique to α–synuclein as all proteins are capable of doing so (Dobson, 1999). In the process of amyloidogenesis, intermediate assemblies occur, referred to as oligomers and protofibrils (Jucker and Walker, 2013). The aggregation of proteins can result in loss of functions, whereby molecules are sequestered within aggregates, disrupting their physiological functions. The aggregates may in turn cause toxic gains of function. Figure 1.6 provides a schematic representation of the conversion from monomeric synuclein to toxic, aggregated and fibrillar forms of α–synuclein.

Misfolded, oligomeric and aggregated forms of α–synuclein can induce a variety of toxic effects including mitochondrial dysfunction and oxidative stress (Lin and Beal, 2006), impaired

axonal transport (Volpicelli-Daley, 2017) and altered protein clearance and degradation (Xilouri et al., 2009).

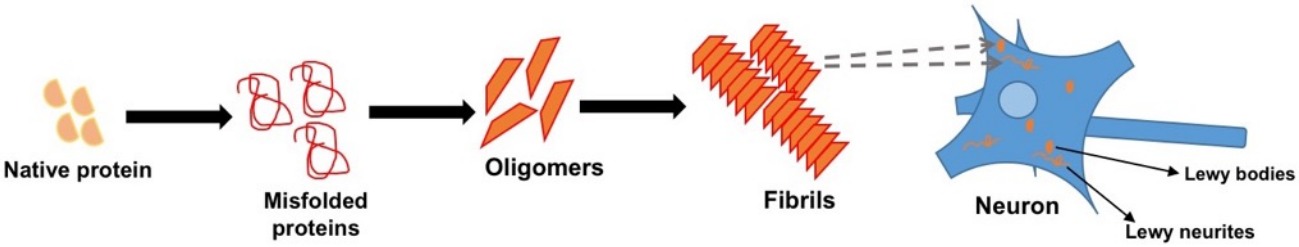

Figure 1.6 Schematic diagram representing the steps in producing α–synuclein fibrils from native monomeric α–synuclein. In response to changes in the local environment, native monomeric forms of α–synuclein misfold and form oligomers. Some of the oligomeric α–synuclein may form fibrils, which can accumulate inside neurons to form Lewy bodies. Figure created by Cindy Pang.

1.3.2.3 Spreading of alpha synuclein

The pathologic changes observed in PD occur gradually and progressively over many years (Halliday et al., 2014). In 2003, Braak and colleagues conducted a detailed neuropathological examination of a large number of PD and control cases. This led to the proposition that the α–synuclein neuropathology spreads through the brain in a region specific and predictable manner (Braak et al., 2003).

At stage 1, α–synuclein pathology is present in the olfactory nucleus and dorsal motor nucleus of the vagus nerve (Ordonez et al., 2018), which may provide an explanation for the enteric system involvement and hyposmia reported at early stages of disease (Marras and Chaudhuri, 2016);(Holmqvist et al., 2014). By stage 2, α–synuclein pathology can be observed in the medulla oblongata and pontine tegmentum with both the raphe nuclei and locus coeruleus affected, leading to depressive symptoms (Boeve et al., 2007). Only at stage 3 of the disease is pathology found within the midbrain, affecting predominantly the SN and amygdala. This stage is considered as the pre-symptomatic stage and rapid eye movement (REM) sleep disorder and motor impairments are common (Boeve et al., 2007). Pathology spreads into the anteromedial temporal mesocortex at stage 4, when overt parkinsonism is evident. The neocortex remains minimally involved at this stage. In the final two stages (stage 5 and 6), pathology reaches prefrontal neocortex, premotor areas and primary sensory areas, including the primary motor field. The key feature of stage 6 is the involvement of almost the entire neocortex. PD patients manifest the full spectrum of clinical symptoms and cognitive impairment is most apparent at these stages (Braak et al., 2003) (Figure 1.7)

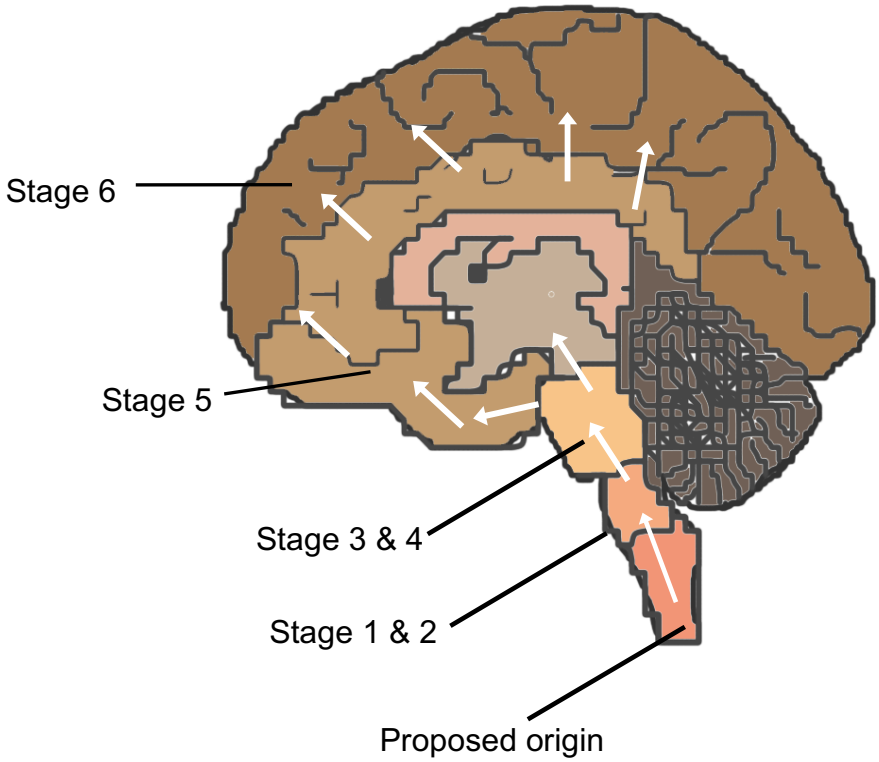

Proposed origin= Peripheral and enteric nervous system, Stages 1 & 2= Medulla oblongata and Pontine tegmentum, Stages 3 & 4= Basal mid and forebrain, hypothalamus, thalamus, Stage 5= Mesocortex, allocortex. Stage 6= Neocortex

Figure 1.7 Illustration depicting Braaks hypothesis on the origin and spread of α–synuclein pathology in Parkinson's disease. According to Braak et al (2003), PD originates in the enteric nervous system, and spreads to the CNS along the vagus nerve to the dorsal vagus motor nucleus. α–Synuclein pathology then spreads in a spatiotemporally defined manner into medulla areas, followed by the midbrain, mesocortex and lastly to all neocortical regions. Figure created by Cindy Pang.

Braak's hypothesis is not without controversy. Although many cases do indeed follow Braak's proposed staging system, there are cases where the distribution of pathology does not follow the proposed spreading pattern. Eighty-three percent of PD patients appear to follow Braak's staging, however, approximately 7-11% do not show Lewy pathology in the dorsal motor nucleus of vagus, despite other brain regions being affected (Kalaitzakis et al., 2008). Some cases also do not show the predicted clinical symptoms (Colosimo et al., 2003); (Galvin et al., 2006), with 55% of PD cases exhibiting Braak stage 5-6 pathology but lacking clinical evidence of dementia (Parkkinen et al., 2008); (Gratwicke et al., 2015). In some cases, neurodegeneration in the SN also precedes Lewy pathology (Milber et al., 2012). An alternative theory suggests that instead of a stepwise accumulation of Lewy pathology, the spread of Lewy pathology occurs in parallel and is based upon differential vulnerability profiles of the different cell types within different regions (Engelender and Isacson, 2017).

Many experimental studies corroborate the spreading hypothesis proposed by Braak et al (2003), whereby initiation of α–synuclein pathology in the enteric system spreads to the CNS. For example, when α–synuclein preformed fibrils (PFFs) were injected into the duodenal wall of rats, it spread through the vagal nerve to the dorsal motor vagus nerve and from there into the rest of the CNS (Holmqvist et al., 2014). Injection of α–synuclein PFFs into the duodenal and pyloric muscularis layers also led to the spreading of α–synuclein along the vagus nerve into relevant regions such as dorsal motor nucleus, caudal portions of the hindbrain including locus coeruleus and the basolateral amygdala, dorsal ralphe nucleus and SN. Importantly, truncal vagotomy prevented the spread of α–synuclein pathology from gut to brain and the associated behavioural deficits in mice (Kim et al., 2019).

Evidence for CNS spread of α–synuclein includes intracerebral injection of α–synuclein PFFs into various anatomical regions of rodents (Polinski et al., 2018);(Patterson et al., 2019), resulting in inclusions that closely resemble human Lewy pathology. Depending on the site of injection, pathology can be observed both contralateral and ipsilateral to the injection site (Luk et al., 2012a; Rey et al., 2013). For an extensive list of α–synuclein PFF rodent studies, see Table 1.3.

α–Synuclein is also known to interact with other neurodegenerative disease proteins. For example, studies using DLB-AD transgenic mice in which the M83-h line (expressing A53T mutant human α–synuclein) of mice were crossed with 3xTg (transgenic) AD mice (expressing mutant human *APP* (amyloid precursor protein), *PSEN1* (presenilin) and *MAPT* (microtubule associated tau protein) genes, have shown that α–synuclein, Aβ and tau act synergistically to exacerbate pathology, behavioural impairments and neurodegeneration (Clinton et al., 2010). β-Amyloid species present in amyloid plaques in the 5xFAD mouse model of AD were found to facilitate the seeding and spreading of fibrillar α–synuclein, causing further degeneration (Bassil et al., 2020), while in the 3xTg AD mouse model, reduction of α–synuclein led to a reversal of AD pathology (Spencer et al., 2016).

1.3.2.4 Mechanism of transmission

The mechanism of cell-to-cell α–synuclein transmission involves pathological seeds from a donor cell acting as a template to induce endogenous counterparts in recipient cells to misfold, resulting in the amplification of the pathological protein conformation (referred to as "templated amplification") (Peng et al., 2020). The mechanism underlying the formation of pathological seeds remains unclear, but this is considered to be a result of the local cellular

environment leading to native α-synuclein protein misfolding, becoming oligomerised and forming small aggregates with the capacity to be released from donor cells, internalised by recipient cells and sequester endogenous proteins. Thus, the transmission process can be divided into three parts; intracellular transportation, release of pathological seeds and lastly internalisation by recipient cells (Figure 1.8).

The initial transmission process occurs when pathological seeds are formed and amplified in the donor cell. These pathological seeds are transported intracellularly to the site of release, where exosome-based secretion is thought to mediate their release. Exosomes are nano sized (30-130 nm) membrane bound extracellular vesicles, that are formed as internal vesicles of a multivesicular body. They are released into the extracellular environment after fusion with the plasma membrane (Turturici et al., 2014). Cell culture and human plasma and CSF studies have shown the presence of α–synuclein within exosomes (Emmanouilidou et al., 2010);(Poehler et al., 2014);(Danzer et al., 2012). Alternatively, seeds may enter the extracellular space as "free" proteins.

The released pathological seeds must then be internalised by recipient cells. Primary hippocampal culture experiments suggest that endocytosis is the most prominent pathway that allows their internalisation (Wu et al., 2019); (Volpicelli-Daley et al., 2011). However, alternative mechanisms have been proposed including direct penetration of the plasma membrane by macropinocytosis (Holmes et al., 2013), or fluid-phase endocytosis (Guo and Lee, 2011). Lastly, nanotubes have also been proposed to transfer α–synuclein PFFs between neurons inside lysosomes (Wani et al., 2011). Stressed lysosomes that function as the vehicle of transport inside the nanotubes have been suggested to allow fibrils to escape, enabling the

seeding of cytosolic protein (Kanimalla et al., 2013). Introduction of α−synuclein PFFs to the medium of cultured cells also led to an increase in the number of tunneling nanotubes (Costanzo et al., 2013);(Abounit et al., 2016). The intercellular transmission and templated amplification of these pathological seeds can lead to the spread of pathological protein aggregates along neuronal networks, in both anterograde and retrograde directions (Rietdijk et al., 2017).

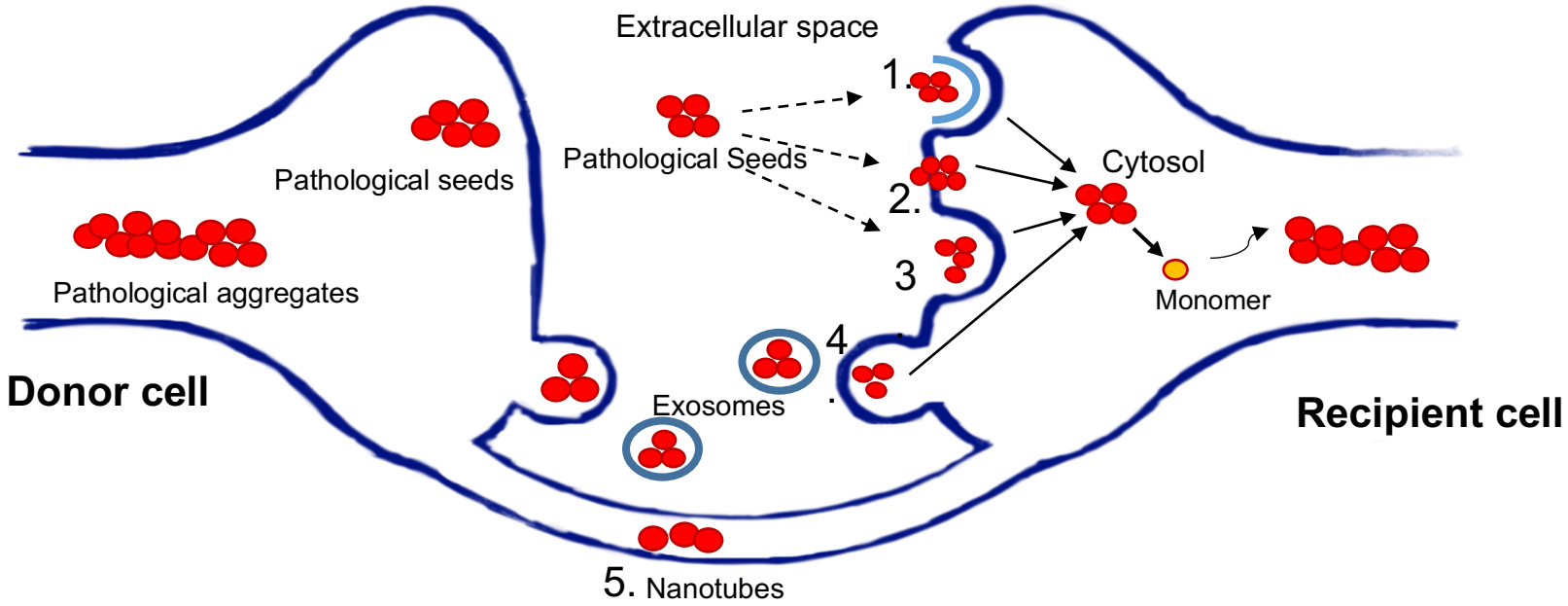

Figure 1.8 The transmission mechanism of α–synuclein PFFs. Pathological seeds are released from the donor cell into the extracellular space. Pathological seeds are a results of spontaneous protein misfolding, leading to the formation of oligomers and fibrils which eventually accumulate inside neurons as Lewy bodies. Small protein aggregates (seeds) can enter into the extracellular space either as free protein or in association with exosomes. Uptake from the extracellular space to recipient cells can be via several means; 1) receptor mediated endocytosis, 2) direct uptake across the plasma membrane, 3) fluid phase endocytosis, 4) internalization via fusion with vesicles in the plasma membrane, 5) nanotubes, protrusions that extend from plasma membrane facilitating the communications between cells. Templated amplification occurs where pathological seeds induce further native protein monomers (orange circle) to misfold. Figure adapted from (Peng et al., 2019) and created by Cindy Pang.

Inside the recipient neuron, pathological seeds can rupture vesicles (Flavin et al., 2017) and exit the endosomal vesicle to gain access to cytosolic proteins and begin the amplification process (Falcon et al., 2018). The seeds require an available substrate to template, which is generally the native form of the pathological protein in the cytoplasm. The difference in expression level of the normal protein in different cell types/sub-types has been proposed as a key factor that could explain the selective vulnerability of different neuronal populations (Luna et al., 2018).

1.3.3 Tau

Human tau is encoded by the *MAPT* gene, located on chromosome 17. It is comprised of 16 exons and alternative splicing of exons 2 and 3 leads to tau isoforms with 0, 1 or 2 N-terminal inserts. Exclusion or inclusion of exon 10 gives rise to tau isoforms with three (3R) or four (4R) microtubule binding repeats. Thus, tau can exist as six isoforms in the adult human CNS. The expression of tau isoforms is developmentally regulated. In foetal brain, only a single tau isoform (0N3R) is present. The ratio of 3R:4R isoforms in the healthy CNS is approximately equal, but can be altered in some tauopathies (Narasimhan et al., 2017).

Tau is best recognised as a microtubule-associated protein that maintains the cell cytoskeleton and regulates axonal transport. Several additional functions of tau have recently been identified including membrane-associated cell signaling and DNA protection (Guo et al., 2017). Disruption to tau homeostasis can result in several loss and gain of functions that contribute to tauopathies (Guo et al., 2017).

1.3.3.1 Structure, function and dysfunction of tau

Tau is a highly phosphorylatable protein, containing 85 phosphorylation sites - 45 Serine, 35 threonine and 5 tyrosine residues. Tau is highly phosphorylated in tauopathy brain. For example, tau phosphorylated at pS396/404 (PHF1) is characteristic of abnormally modified tau in disease, and tau phosphorylated at S404 and S396 individually can be found at basal levels in control human brain, but phosphorylation at these sites is increased in AD (Hanger et al., 2007). Abnormal and hyperphosphorylation of tau is believed to contribute to disease by effecting tau structure and propensity to aggregate, protein interactions and localisation (Noble et al., 2013; Hanger et al., 2009);(Guo et al., 2017).

In healthy brain, tau is localised predominantly in the axons of mature neurons with low levels of tau found in somatodendritic compartments, nuclei, mitochondria and the plasma membrane. Low levels of tau are also found in human astrocytes and oligodendrocytes. Retention of tau within the axonal compartment is ensured via several mechanisms. Firstly, low basal levels of phosphorylation promote tau binding to microtubules. Secondly, the axon initial segment enables tau to enter axons but prevents it from travelling back towards the dendrites and soma (Guo et al., 2017; Hanger et al., 2019). However, elevated tau phosphorylation reduces the affinity of tau for microtubules, leading to cytosolic tau accumulation and the mis-sorting of tau from axons into the somatodendritic compartment. This subsequently leads to a compromised axonal microtubule integrity and disruptions in synaptic function (Hanger et al., 2019).

A number of studies have corroborated the notion that synaptic tau disrupts synaptic function (Pooler et al., 2014); (Hanger et al., 2019); (Noble and Spires-Jones, 2019). Synapses from post mortem AD, but not control brain contain phosphorylated tau oligomers (Tai et al., 2012; Zempel and Mandelkow, 2014). Indeed, the presence of hyperphosphorylated soluble tau multimers in the synaptic compartment correlates with dementia in AD (Perez-Nievas et al., 2013. This tau mislocalisation may result from A causing increased tau phosphorylation, tau detachment from microtubules and trafficking to dendritic spines where tau mediates excitotoxic responses {Ittner, 2010 #2043; Hoover et al., 2010) or pre-synapses where phosphorylated tau disrupts synaptic vesicle release (McInnes et al., 2018). Indeed, soluble forms of tau and Aβ may act in concert at the synapse causing neural network dysfunction (Crimins et al., 2013)

1.3.3.2 Tau in Parkinson's Disease

Modified tau has been reported in PD and PDD brain (Irwin et al., 2012; Irwin et al., 2013); (Irwin and Hurtig, 2018). It is also not uncommon to see neurofibrillary tangles (NFTs) and LBs present within the brain or cell (Iseki et al., 2003). NFTs have been noted in the SN of PD patients (Schneider et al., 2006) and the presence of phosphorylated tau is seen in dopaminergic neurons of PD and PDD subjects (Wills et al., 2010). Similarly, increases in α–synuclein and phosphorylated tau at Ser396/404, detected by the PHF-1 antibody was observed in the striatum of PD patients compared to control subjects (Haggerty et al., 2011). Carriers of LRRK2 mutations that cause familial PD also demonstrate AD-like tau features, including neuritic plaques, neurofibrillary tangles and neuropil threads. This phenomenon was not observed in control or schizophrenic cases (Henderson et al., 2019b). PD cases with A53T mutations show severe tau pathology with an increased tendency to develop early onset cognitive impairments (Teravskis et al., 2018). Lastly, phosphorylated tau at epitopes Ser396, Ser202, 396/404 have also been noted in PD cortex synapses (Muntane et al., 2008).

Cell culture and rodent studies have also reflected the co-occurrence of tau and α–synuclein as seen in human patients. Using K114 fluorometry as a sensitive and quantitative measure for the presence of amyloid fibril formation, co-incubation of tau and α–synuclein led to greater K114 fluorescence (Giasson et al., 2003). Although α–synuclein alone also resulted in the generation of amyloid-like polymers, an increased polymerisation was evident at higher α–synuclein concentrations. In comparison, incubation of tau T40 (2N/4R), the longest tau isoform expressed within the CNS, did not lead to notable K114 fluorescence. This was also reflected in rodent studies. In a Tg mouse model with overexpression of human A53T, in

addition to the motor phenotype and α–synuclein inclusion, a subset of mice also exhibited abundant tau-positive grains, threads and spheroids. Inclusions were not noted in control mice and from co-labelling pathological inclusions were composed of either both tau and α–synuclein, or tau, or α–synuclein (Giasson et al., 2003).

Several studies utilising the 1-methyl-4-phenyl1-1,2,3,6-tetrahydropyridine (MPTP) mouse model, found an upregulation in levels of phosphorylated tau, α–synuclein and glycogen synthase beta 3 (GSK-3β) within the hippocampus and SN (Hu et al., 2020) and striatum (Duka et al., 2006). The presence of α–synuclein contributes to GSK-3β activation, subsequently hyperphosphorylation of tau. In α–synuclein -/- mice there was a lack of phosphorylated tau formation (Duka et al., 2009). Inhibitors of GSK-3β (lithium) reversed phosphorylated α–synuclein accumulation and tau hyperphosphorylation in SHSY-5Ycells (Duka et al., 2009). In an another Tg mouse model of PD, with overexpression of the human α–synuclein transgene under the platelet derived growth factor (PDGF) promoter, tau pathology was associated with an age-dependent increase in the expression of α–synuclein. Phosphorylated tau was only observed in 11 month-old mice where α–synuclein pathology was present, but not in 4 month old mice in the absence of synuclein pathology (Haggerty et al., 2011). Lastly, in symptomatic A30P α–synuclein mutant mice, phosphorylated tau changes were observed at sites Ser202 and Ser396/404 in the brainstem. Other regions were unfortunately not examined (Frasier et al., 2005).

1.3.3.3 α–Synuclein and Tau interaction in disease

Proteins associated with neurodegenerative disorders have long been postulated to act synergistically to exacerbate neurodegeneration (Clinton et al., 2010) and co-pathology is a common finding in postmortem brain (Spires-Jones et al., 2017); (Compta et al., 2011). In PD post mortem cases, in addition to α-synuclein pathology, Aβ (plaque) and tau (neurofibrillary) pathology are frequently observed (Irwin and Hurtig, 2018). Indeed, AD pathology is the most prominent pathology alongside aSyn pathology in PD/PDD (Hely et al., 2008). In the presence of A53T α-synuclein mutations that cause PD, tau pathology was present particularly within the parahippocampus and hippocampal regions of the brain (Nishioka et al., 2020). This co-pathology phenomenon is also noted in animals models since tau pathology was also found in a subset of mice expressing mutant human A53T α-synuclein (Waxman and Giasson, 2011). Furthermore, tau aggregation is promoted by α-synuclein seeds (Waxman and Giasson, 2011) and specific strains of aSyn can induce tau phosphorylation (Guo and Lee, 2011).

Although α-synuclein and tau show differently distributions under physiological conditions with tau being predominantly axonal and α-synuclein residing in presynaptic vesicles, both proteins share some common features. Both are abundant neuronal proteins, and adopt an unfolded confirmation in healthy environments, but polymerise into fibrils in disease. α–Synuclein can self-polymerise whereas it appears that tau requires co-factors (Meade et al., 2019). α-Synuclein is a small protein of 140 amino acids, and its middle hydrophobic region which drives filament formation is exposed. It is believed that this may facilitate intermolecular interactions leading to fibrillisation (Meade et al., 2019). In contrast, tau is a larger protein and the repeat region of tau which is required for filament formation is likely

shielded by the flanking region, which renders tau less susceptible to misfolding (Meade et al., 2019).

Protein kinases may facilitate the synergistic interactions of α-synuclein and tau. For example, α-synuclein was found to stimulate protein kinase A when bound to tau, leading to further tau phosphorylation at residues Serine 262 and 356 (Jensen et al., 1999). In PC12 cells, extracellular α-synuclein increased tau phosphorylation at Serine 396 and led to microtubule destabilisation, which was prevented by addition of a GSK-3β inhibitor. In an MPTP-based mouse model of PD, GSK-3β was found to be activated in brain regions displaying phosphorylated α-synuclein and tau. The utilisation of the GSK-3β inhibitor AZD1080 reduced the levels of phosphorylated tau and reversed motor impairments in these animals (Hu et al., 2020). These examples highlighting the involvement of protein kinases as a potential linking mechanism between tau and α-synuclein abnormalities in PD (Gassowska et al., 2014). Other co-factors are likely to exist, but are not yet identified (Hijaz and Volpicelli-Daley, 2020).

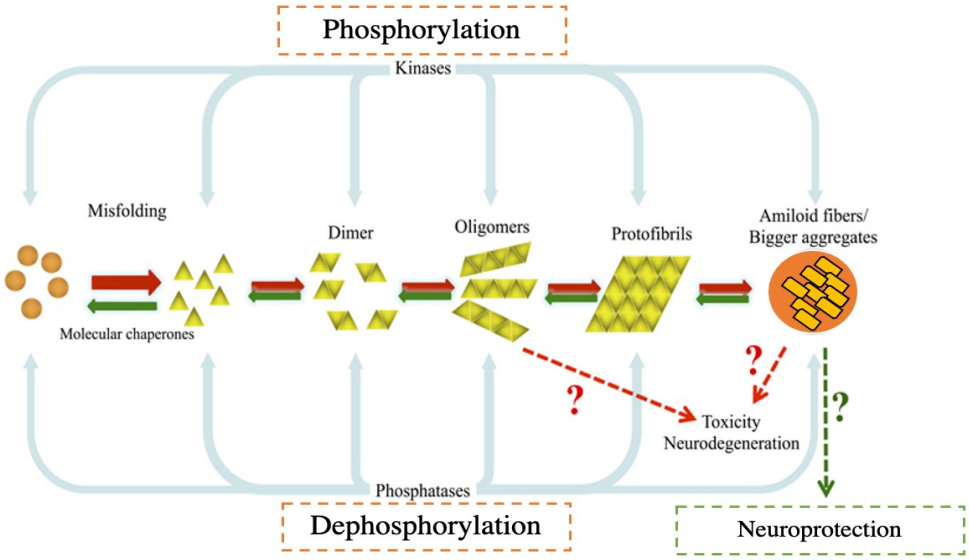

Figure 1.9 The potential interplay between α-synuclein and tau. Under pathological conditions, influenced by environmental factors and spontaneous events, normal highly soluble α-synuclein and tau may misfold and converted into pathological and larger species may fibrillise and convert into LB's and Lewy neurites or paired helical filaments (PHFs) and neurofilbrillary tangles (NFTs). Once this occurs, normal cellular mechanisms (ubiquitin system, phagosome/lysosome system) are not able to counteract such changes or reverse protein misfolding and they remain as pathological aggregates and amyloid fibrils. Figure adpated from Tenreiro et al., 2014.

1.4 Oxidative stress in PD

Oxidative stress is the imbalance of redox states, involving the excessive generation of reactive oxygen species (ROS) and a dysfunctional antioxidant pathway (Kim et al., 2015; Andersen, 2004). ROS are a group of reactive molecules derived from oxygen. Due to the two unpaired electrons present in the outer electron shell, oxygen is more susceptible to free radical formation (Bolisetty and Jaimes, 2013) and through consecutive reduction of oxygen through additional electrons, a variety of ROS are generated. The ROS family includes: free radicals (superoxide, O_2^-), hydroxyl radicals (·OH) and non-radicals (hydrogen peroxide, H_2O_2) (Figure 1.9). Prolonged elevation of oxidative stress levels can induce a diverse range of effects, including cell membrane damage from lipid peroxidation, structural damage to DNA and changes in protein structure and function due to protein oxidation (Hwang, 2013). The brain is particularly vulnerable to ROS due to its high oxygen demand. Metals such as iron or copper exist abundantly in the CNS which are both involved in catalysing ROS (Zhao and Zhao, 2013); (Blesa et al., 2015).

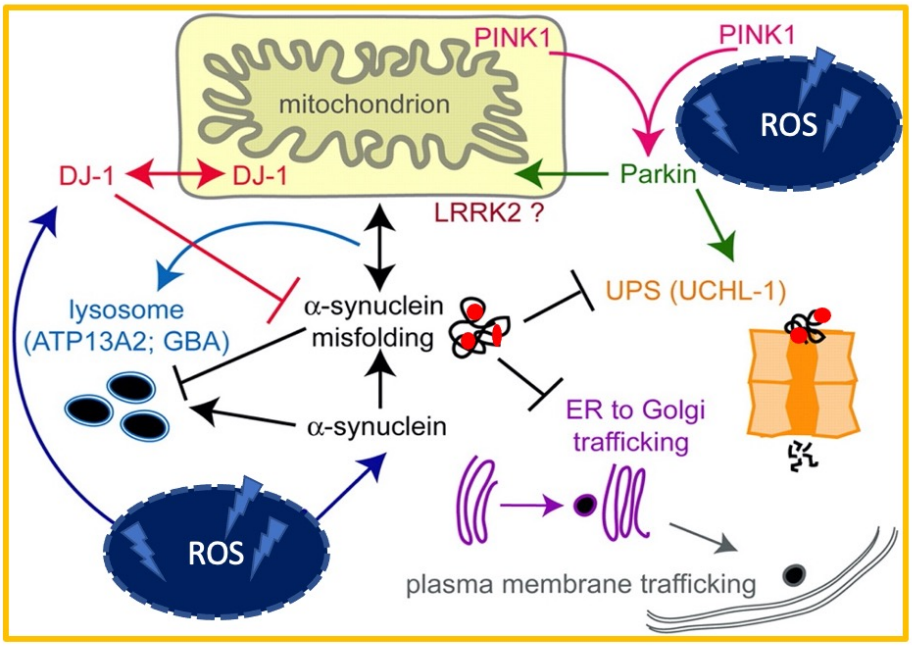

Figure 2.1 A summary of the PD associated gene products and their prospective sites of cellular function and contribution in ROS generation. The dysfunction of protein degradation components, including mechanisms associated with lysosome and autophagy and ubiquitin proteasome system are thought to contribute to PD pathogenesis. Impairment in protein clearance is assumed to promote misfolding of proteins leading to a blocked intracellular trafficking and increased cytotoxicity. Mutations in Parkin (an E3 ubiquitin ligase), ubiquitin C terminal hydrolase-1 (UCHL-1), lysosomal ATPase (ATP13A2) and glucocerebrosidase (GBA) have been further implicated in protein degradation. Genes linked to mitochondrial function, DJ-1, PTEN-induced kinase (PINK1) are thought to be contributors to ROS generation which in turn accelerate protein damage and neurodegeneration. Mutation in LRRK2 protein is the most heritable mutation in PD. Figure adapted from Caldwell and Caldwell, 2008.

Oxidative stress is a complex process that can arise due to both exogenous and endogenous influences. Exogenous sources include ultraviolet light and ionising radiation, while environmental toxins and chemicals can also produce ROS as a by-product of their metabolism (Chen et al., 2012). Endogenous production of ROS is mediated by mitochondrial and non-mitochondrial ROS generating enzymes including xanthine oxidase (XO), cytochrome P450 from the endoplasmic reticulum, flavin oxidases from peroxisomes and nicotinamide adenine dinucleotide phosphate (NADPH) oxidase (Nox). Under physiological conditions, ROS regulate key cellular pathways and enzymes necessary for cellular homeostasis, including mitogen-activated protein kinase and phosphoinositide 3-kinsase pathways (Fujino et al., 2007). However, the persistent imbalance of redox states with elevated levels of ROS is problematic and is considered to be a major contributor to disease pathogenesis across neurodegenerative disorders (Andersen, 2004).

In PD, genetic or environmental insults can lead to induction of oxidative stress responses. This in turn, can exacerbate the effects of misfolded proteins which themselves further activate oxidative stress pathways leading to a vicious cycle of elevated oxidative stress (Ganguly et al., 2017). PD patients are prone to oxidative stress insults as the neurotransmitter DA is normally stored in vesicles, but excess cytosolic DA can be easily oxidised making DA a source of oxidative stress itself (Hwang, 2013); (Andersen, 2004). Postmortem examinations revealed an increase in the intensity of oxidative stress markers such as cytoplasmic 8-hydroxyguanosine (8OHG) (Zhang et al., 1999) and 4-hydroxy-2-nonenal (4HNE) (Yoritaka et al., 1996) in the SN of PD brain, further highlighting the association between oxidative stress and PD pathogenesis.

Compelling evidence from animal and cell culture studies shows a link between α–synuclein pathology and oxidative stress levels (Scudamore and Ciossek, 2018). Oxidative stress was proposed to cause alterations in α–synuclein itself, further contributing to protein misfolding and reduced degradation of α–synuclein (Norris and Giasson, 2005). In a recent rat hippocampal cell culture study, α–synuclein PFFs induced toxicity that was dependent on α-synuclein and mediated by oxidative stress (Luna et al., 2018). The exposure to simultaneous treatments of superoxide and nitric oxide led to the formation of α–synuclein aggregates in transfected HEK cells (Paxinou et al., 2001). In addition when N,N'-dimethyl-4-4'-bipiridinium (paraquat) was used as an oxidative reagent, vagal neurons exhibited parkinsonian pathology with enhanced intracellular α–synuclein transfer (Musgrove et al., 2019). Therefore, α–synuclein and oxidative stress may act bi-directionally to form a vicious cycle of neurodegeneration in PD.

1.5 Non-neuronal contributions to PD

The term neuroinflammation defines the inflammatory process occurring in the central nervous system. Neuroinflammation can induce both beneficial and harmful effects, including at different stages of disease (Guzman-Martinez et al., 2019).

Findings from clinical studies (Gerhard et al., 2006) and rodent models of PD (Duffy et al., 2018a) have confirmed a role for oxidative stress and pro-inflammatory responses in dopaminergic degeneration early in PD. It has been proposed that α–synuclein pathology may act in parallel with inflammatory changes in the brain and periphery (Kannarkat et al., 2013). The application of inflammatory interventions for reducing dopaminergic cell death have long

been deliberated (Gagne and Power, 2010) yet the precise contribution of neuroinflammation in PD remains poorly understood.

1.5.1 Astrocytes

Astrocytes are the most abundant cells in the brain and contribute to the development and plasticity of the CNS (Gelders et al., 2018); (Joe et al., 2018). In normal physiological states, astrocytes play a critical role in regulating glucose metabolism in the brain by taking up glucose from blood and through glycolysis supplying energy to neurons in the form of lactate (Jha and Morrison, 2018). Astrocytes are also crucial for maintaining the blood brain barrier (BBB), which is known to be disrupted in PD (Gray and Woulfe, 2015). But, in response to injury or an altered local environment, astrocytes can become activated/reactive and astrogliosis occurs. Astrogliosis occurs with the intention to control and contain the damage however, prolonged states of reactivity can harbor more damaging than beneficial consequences (Sofroniew and Vinters, 2010). Depending on the stimulus detected, astrocytes can produce anti- and/or pro-inflammatory mediators (Heneka et al., 2015).

Reactive astrogliosis is a common feature in PD (Mirza et al., 2000). Emerging evidence suggests that astrocytes play a beneficial role in PD and contribute to clearing extracellular α–synuclein aggregates (Loria et al., 2017; Sacino et al., 2017);(di Domenico et al., 2019). When astrocytes derived from induced pluripotent stem cells (iPSC) from donors with familial LRRK2 mutations were co-cultured with healthy neurons, the neurons showed signs of neurodegeneration including a reduced number of neurites, abnormal α–synuclein in the soma and neurite arborisation. In contrast, co-culturing healthy astrocytes with PD derived neurons led to a partial rescue of neurodegeneration (di Domenico et al., 2019). These data

indicate that astrocytes in PD are altered such that they promote neuronal toxicity. In co-cultures of primary neurons and astrocytes (Loria et al., 2017), fibrillar α–synuclein efficiently transferred between astrocytes and neurons, via lysosomes (Loria et al., 2017); (Sacino et al., 2017)), suggesting that astrocytes might aid in clearance of α–synuclein aggregates. Interestingly, however, some astrocytes showed large intracellular deposits of α–synuclein, suggestive of an overwhelmed endo-lysosomal machinery leading to incomplete digestion of α–synuclein aggregates (Lindstrom et al., 2017); (Sacino et al., 2017)). Together, these findings suggest that upon an initial encounter with α–synuclein aggregates, astrocytes may act to protect neurons by internalizing seeds via endocytosis to clear extracellular α–synuclein aggregates. However, as the α–synuclein burden increases, a threshold is reached and as the endo-lysosomal system is compromised astrocytes can no longer digest the remaining α–synuclein aggregates (Filippini et al., 2019). Thus, the role of astrocytes in PD may depend on disease stage.

1.6 Animal models of Parkinson's disease

Several animal models have been developed that recapitulate aspects of PD. Neurotoxin models are based on local (intracerebral) or systemic administration of substances. A classic systemic model uses MPTP, whereby administration of MPTP into primates produces features highly reminiscent of human disease (DeLong, 1990; Wichmann and DeLong, 2003) including LB inclusions following chronic administration (Fornai et al., 2005). However, LB-like inclusions are less consistent when rats are injected with MPTP, possibly due to reduced sensitivity to MPTP and differential MPP+ sequestration (toxic metabolite from the prodrug MPTP) (Schmidt and Ferger, 2001). Rotenone is a potent inhibitor of the mitochondrial enzyme complex I. Rotenone administration to rats causes nigrostriatial damage and

development of LB-like inclusions, but also has a high mortality rate in rats (Fleming et al., 2004).

Genetically modified models (Dawson and Dawson, 2010) and virally induced models of PD (Kirik et al., 2003) have also been generated. As PD is primarily a sporadic disorder and genetic models rely on expression of familial PD-causing genetic mutations, genetically altered rodents may not replicate features of sporadic PD. Virally induced gene expression is ideal for targeting expression of a gene to a specific area of interest, but most leads to limited spread of pathology, and findings can be very variable (Volpicelli-Daley et al., 2016).

Recently, since the emergence of the cell to cell transmission hypothesis, models of α-synuclein spread have also been generated. In line with the aims and objectives of this thesis, only the classic PD mimetic 6-OHDA and the α–synuclein PFFs model of spread will be further elaborated below.

1.6.1 6-hydroxydopamine (6-OHDA)

Since 1968 when Ungerstedt demonstrated that injection of 6-OHDA into the SN was able to induce anterograde degeneration of the nigrostriatal dopaminergic system (Ungerstedt, 1968), 6-OHDA has remained one of the most popular neurotoxins of choice for experimental modelling of PD (Blandini et al., 2008). Depending on the site of toxin injection, varying degrees of nigrostriatal lesions can be achieved, enabling the study of the various stages of disease. Common sites of injection include the SN and medial forebrain bundle (MFB) which causes rapid and full lesions (Park et al., 2018), whereas injection into the striatum results in partial lesions (Winkler et al., 2002). Although less common, 6-OHDA has also been utilised in

other animal species including guinea pigs, dogs, cats and monkeys (Bezard and Przedborski, 2011).

6-OHDA is typically injected into one hemisphere only, leaving the unlesioned side as an internal control. To ensure success of injection, systemic injection of dopamine receptor agonists (apomorphine, L-dopa) or dopamine releasing compounds such as amphetamine can be used to induce asymmetric rotational behaviour. Ipsilateral rotational behaviour is caused by amphetamine which acts as a presynaptic stimulator, due to the release of dopamine from striatal terminals especially on the intact side (Meredith and Kang, 2006). The magnitude of lesions correlates with the severity of circling motor behaviour (Ungerstedt and Arbuthnott, 1970). However, a major disadvantage of this neurotoxin is that LB inclusions are not commonly associated with this model, as seen in human disease (Bove et al., 2005).

1.6.2 Administration of α–synuclein preformed fibrils (PFFs) to rodents

In addition to WT mouse α–synuclein PFFs, some studies also utilise human WT α–synuclein PFFs to induce α–synuclein pathology in rodents (Luk et al., 2012; Masuda-Suzukak et al., 2014; Sacino et al, 2014; Paumier et al., 2015). However, possibly due to a species barrier human PFFs were found to seed far less efficiently in rodents compared to WT mouse α–synuclein PFFs. The molecular and biology compatibility with host α-synuclein is a key influencer in fibril pathogenicity (Luk et al., 2016). The sequence of the α–synuclein PFFs is important for efficient seeding, as is the correct preparation of PFFs. Various protocols have been published describing the generation of α–synuclein PFFs (Polinski et al., 2018; Patterson et al., 2019; Volpicelli-Daley et al., 2014) that may account for variation in the reported findings. Furthermore, adequate quality control checks are essential to include when

generating α–synuclein PFFs, and these are not always reported. For this study WT mouse α–synuclein PFFs were made from recombinant mouse α–synuclein monomers and these were sonicated to generate 50 nm fibrils (Volpicelli-Daley et al., 2011). Once introduced to neuron cell cultures, PFFs are internalised by neurons, where they can recruit and template endogenous α–synuclein into inclusions of insoluble α–synuclein (Luk et al., 2009); (Volpicelli-Daley et al., 2011); (Volpicelli-Daley et al., 2014a), making α–synuclein PFFs an ideal tool for studying the cell to cell spreading of α–synuclein. The toxicity of α–synuclein PFFs is predominantly influenced by the presence of endogenous α–synuclein since in α–synuclein deficient neurons, no α–synuclein inclusions are observed upon application of PFFs (Volpicelli-Daley et al., 2014b). However, it is still unclear if α–synuclein PFFs act in a dose-dependent manner, since a wide range of concentrations has been used in publications as shown in Table 1.3 (Page 72).

Direct intracerebral injection of rodent and human α–synuclein PFFs into rats, mice and non-human primates can recapitulate features of human PD, including Lewy pathology strikingly similar to that observed in human brain (Paumier et al., 2015); (Luk et al., 2012a); (Manfredsson et al., 2018). Phosphorylated α–synuclein will typically be observed in regions that are anatomically connected to the injection site. For example, injection into the ipsilateral striatum of WT mice lead to the appearance of phosphorylated α–synuclein in the ipsilateral striatum, SN, contralateral neocortex, amygdala and frontal cortex regions (Luk et al., 2012a) whereas injection into the olfactory bulb of mice resulted in α–synuclein pathology in the anterior olfactory nucleus, entorhinal cortex, hippocampus, piriform cortex and other areas (Rey et al.,2018). Bilateral development of pathology due to ipsilateral injection is less frequently observed in mice, but is more common in rats (Paumier et al., 2015; Abdelmotilib

et al., 2017). The reasoning for this is not entirely clear, however, brain extracts of tau aggregates were demonstrated to spread through white matter tracts that interconnect anatomical regions (Ahmed et al.,2014) therefore, α-synuclein PFFs may also be transmitted via this manner, particularly in rats. Neurons that develop α–synuclein inclusions ultimately degenerate (Osterberg et al., 2015). Early inclusions in the SN resulting from α–synuclein PFF injection resemble pale bodies, and can be granular, diffuse and cytoplasmic (Duffy et al., 2018a. In due course, these inclusions condense and form compact aggregates {Mahul-Mellier, 2020 #3148; Mahul-Mellier et al., 2020)Inclusions co-localise with markers commonly observed in human LBs (Baba et al., 1998) such as p62, ubiquitin, thioflavin S, and they are proteinase K resistant (Giasson et al., 2000), mimicking the inclusions seen in late stages of PD.

The presence and spread of LB and LN pathology in rodents injected with α–synuclein PFFs are highly dependent on accurate preparation of the PFFs and the site of injection. Table 1.3 provides a compilation of rodent studies in which α–synuclein PFFs have been used. Typically, PFFs are able to spread to regions that innervate the initial injection site. This is in support of the concept of retrograde transport and templating of endogenous α–synuclein within neurons, and appears to confirm that axon terminals are able to internalise PFFs (Halliday et al., 2011). The distribution of α–synuclein inclusions appears to show selective vulnerability and degeneration of specific neuronal subpopulations (Luna et al., 2018; Maingay et al., 2006).

Injection site	Time point	Background strain/ species of animal	Concentration of PFFs	Main findings	Author(s)
Striatum	30, 90 and 180 d.p.i.	C57BL6/C3H F1, C57BL6/SJL F1, and CD1 mice	5 µg mouse α-syn per hemisphere	aSyn pffs were able to induce and transmit disease pathology and incur neurodegeneration in non-Tg mice. Progressive dopaminergic cell loss in SN with reduced dopamine innervations in dorsal striatum. Motor deficits noted at 180 d.p.i.	Luk et al., 2012
	30, 60 and 180 d.p.i.	6 week old, adult male Sprague-Dawley rats	8 µg of mouse or human aSyn PFFs	aSyn PFFs sufficient to seed, propagate and convert endogenous form to pathological. Bilateral reductions in nigral dopamine neurons at 180 d.p.i. No motor impairment overall.	Paumier et al., 2015
	3 and 6 m.p.i.	3-month-old C57BL/6J mice	5 µL of 10 µg/µL aSyn monomer, 2 µg/µL LPS(−) fibril seed, and 2 µg/µL LPS(+) fibril seed	In the presence of LPS, aSyn showed self-renewal and resulted in a structurally distinct fibril strain. Exposure to exogenous pathogens, led to amyloid fibrils with self-renewable structures which cause distinct type of proteinopathies.	Kim et al., 2016
	60 d.p.i.	2- to 4-month-old male and female wild-type C57BL6/C3H mice and α-	4.25 µg (4 µL) of WT PFFs, phosphorylated S129 PFFs and	All three types of PFFS caused seeding of endogenous aSyn. Only pSyn S129 PFFS triggered the greatest formation of aSyn inclusions within the SN, exacerbated	Karampetsou, et al. 2017

	Syn-/- mice (C57BL6/JOlaHsd mice)	phosphorylation S129 incompetent PFFs.	pathology in the cortex and dopaminergic neuronal loss, accompanied by fine motor impairment by 60 d.p.i. Early changes in innate immune response including macrophage recruitment and IL-10 release noted. pSyn S129 PFFs facilitated fibril uptake in neurons	
6 m.p.i.	8-10 week old mice (C3H/HeJ and C57BL/6J strain) and rats (Sprague Dawley)	10 µg (mice) or 20 µg (rats) of mouse or human aSyn PFFs	C3H/HeJ strain is more sensitive to fibril exposures than C57BL/6J, with more dopaminergic degeneration and inclusions. In rats, injection into the SN led to inclusion spread and dopaminergic degeneration similar to ST injections. Inclusion correlated with dopaminergic neurodegeneration.	Abdelmotilib et al.2017
1 and 6.5 w.p.i. 3 and 6 m.p.i.	2- to 3-month-old C57BL/6J mice	5 µg/2.5 µL of recombinant mouse or human aSyn PFFs	aSyn seeds rapidly disseminated through neuronal circuits after injection	Okuzumi et al. 2018
6 m.p.i.	2-month-old male Fischer mice	2µL of 2 µg/µl, mouse aSyn PFFs	Reactive microglia morphology observed in the SN 2 months following injection and 3 months prior to nigral neuronal loss. Correlation between SN pSyn inclusion and the number of MHC-II expressing microglia.	Duffy et al 2018
4 m.p.i.	C57BL/6 mice	5 µg (2.5 µL) of human aSyn PFFs	Upon aSyn PFF injection, DNA damage (YH2AX and 53BP1) and activation of DNA damage response is noted, involving oxidative stress and mitochondrial dysfunction. Effects	Milanese et al. 2018

			reversed by either endo or exogenous antioxidants.	
3 m.p.i.	10-week-old C57BL/6J mice	5 µL (150 µM) of human WT or truncated aSyn PFFs	The truncation of aSyn can influence its prion like pathogenicity. C terminally 20 residue truncated fibrils exhibited enhanced seeding activity in cultured cells. N terminally 10- or 30 residue truncated human aSyn fibrils induced more abundant aSyn pathologies than WT fibrils in mice.	Terada et al. 2018
6, 7, w.p.i.	2-3 month old, male Wistar rats	1 µL of 1 mg/ml human aSyn PFFs per site	Visuospatial learning deficits, accompanied with reduced function of GluN2A NMDA receptor subunit (suggestive of specific targeting of this subunit). Treatment with aSyn targeted antibodies reduced the loss of long term potentiation and synaptic localisation of GluN2A NMDA receptor subunit (may counteract synaptic dysfunction).	Durante et al., 2019
2, 4 or 6 m.p.i.	3 month old Fisher rats	8 or 16 µg aSyn PFFs in total	A quantity dependent increase in the magnitude of ipsilateral SN inclusion formation (2 mpi), bilateral loss of nigral dopamine neurons at 6 mpi. 16ug resulted in modest sensorimotor deficits at 6 mpi.	Patterson et al., 2019

Somatosensory cortex and dorsal neostriatum	30 and 90 d.p.i.	M83 mice on C57BL/C3H background, aSyn -/- mice maintained on C57BL/6 background	5 µg human aSyn or WT full length human aSyn	Synthetic PFFs can initiate PD like LBs/LNs and transmit disease in vivo. Cell to cell propagation and cell transmission of misfolded aSyn underlie the spread of CNS LBs/LNs	Luk et al 2012
Dorsal striatum	30, 60 and 90 d.p.i., 5 and 9 m.p.i.	2 month old (PDGF-h-aSyn) mice	5 µL (25 µg) of mouse aSyn PFFs	Detrimental effects of seeded aSyn aggregates on dendritic architecture. Spine loss and dystrophic deformation of dendritic shafts in layer V pyramidal neurons.	Blumenstock et al.2017
	1, 3, or 6 m.p.i.	G2019S mice and non Tg mice C57BL/BJ	5µg (2.5 µl) aSyn PFFs	aSyn pathology through the brain connectome is modulated by **a)** anatomical connectivity **b)** endogenous α-synuclein expression. G2019S LRRK2 expression selectivity enhances aSyn pathology in resilient populations of neurons. Rate of connectivity based spread of aSyn pathology is globally reduced in G2019S mice.	Henderson et al. 2018
Inferior colliculus and caudate putamen	3 m.p.i.	26 month old marmosets	50 µL of 4 mg/mL mouse aSyn PFFs	Dissemination of aSyn pathology does not necessarily follow neuroanatomical connections. Intra-astrocytic pathology suggests glial cells have a role in aSyn transmission.	Sorrentino et al. 2017

Substantia nigra, striatum and intravenous	4 m.p.i.	6-7 week old, female Wistar rats	2 µL of 5 µg/µL aSyn PFFs	Out of fibrils, oligomers and ribbon, fibrillar aSyn was the most toxic strain leading to progressive motor impairment and cell death. Ribbons cause histopathological phenotype similar to MSA. aSyn PFFs cross BBB and into CNS following intravenous injections. Distinct aSyn strains display differential seeding capacities.	Peelaerts et al. 2015
Substantia nigra and ventra tegmental area	10 d.p.i.	9 week old, female Sprague Dawley rats	2.5 µL of full-length recombinant human aSyn PFFs (10 µg total) per site	Combined approach of AAV mediated overexpression of human aSyn and human aSyn PFFs can reproduce cardinal features of human disease, Lewy like pathology, neuroinflammation and progressive dopaminergic cell loss. Short time span, ideal for neuroprotection studies.	Thakur et al. 2017
Substantia nigra	15 m.p.i.	4- to 6-month-old female C57BL/6J mice	10 µg of mouse or human aSyn PFFs	Injections led to abundant LBs/LNs like pathology, whereas injection of soluble aSyn did not. Endogenous mouse aSyn accumulated 3mpi, while human aSyn PFFs disappeared in 1 week.	Masuda-Suzukake et al. 2013
Hippocampus	1,2 and 4 m.p.i.	2-month-old M83 mice and M20 mice	4 µg mouse PFFs of human 21–140 aSyn PFFs or 71–82 aSyn (Only mouse PFFs and human 21-140 aSyn PFFs are amyloidogenic)	A broad disruption of proteostasis occurs after injection, glial activation, markers of neuronal injury response.	Sacino et al. 2014

Hippocampus and cortex	3 m.p.i. and 6 m.p.i.	5xFAD Tg mice (Tg6799 line, overexpress familial AD (FAD) mutations in APP, under Thy1 promoter	Mouse aSyn PFFs, 2µg/µl, 5ug per site	Feed forward mechanism, A**b** plaques enhance aSyn seeding over time	Bassil et al., 2020
	3,6, and 9 m.p.i.	2- to 3-month-old PS19 mice or C57BL6/C3H F1 mice	5 µg of aSyn PFFs	Strain A demonstrated rare cells with abnormal accumulation of phospho Tau near injection site. Strain B, exhibited substantially more tau inclusions, in more rostral and caudal area (brainstem, locus coeruleus), also contralateral to injection site.	Guo et al. 2013
Anterior Hippocampus	45 or 90 d.p.i.	Female C57Bl6/C3H	5 µg of aSyn PFFs	Selective vulnerability of hippocampal neuron subpopulations. GABAergic neurons general more susceptible to aSyn toxicity, GABAergic neurons more resilient.	Luna et al., 2018
Cortex	2,3, and 4 m.p.i.	2- to 3-month-old α-syn-GFP mice	2.5 µL of 2 mg/mL mouse WT aSyn PFFs	aSyn PFFs seed aggregation of both transgenically expressed and endogenous aSyn in neurons. Somatic inclusions undergo phases of maturation. Compaction coinciding with decreased soluble somatic and nuclear aSyn with progression. Mature inclusions bear post-translational hallmarks human LB.	Osterberg et al 2015
Intravascular injection	2, 4 m.p.i.	8 week old, female Sprague Dawley rats	aSyn PFFs was mixed at a 10:1 molar ratio with peptide to form peptide/protein complex.	Systemic aSyn injection trigger selective neuronal pathology analogous to PD patients	Kuan et al., 2019

Intramuscular (biceps femoris)	4, 8, and 12 m.p.i.	2-month-old M83 mice and M20 mice	10 µg of mouse PFFs, human 21–140 aSyn PFFs or Δ71–82 aSyn (Only mouse PFFs and human 21-140 aSyn PFFs are amyloidogenic)	M83 Tg mice developed widespread aSyn inclusions. Astrogliosis, microgliosis and motor impairments. WT mice, aSyn inclusion pathology in spinal cord, motor function remained intact. Transection of sciatic nerve in M83 Tg mice delayed spreading of aSyn pathology and motor symptoms.	Sacino et al. 2014
Duodenal and pyloric muscularis layer		C57BL.6J mice and aSyn knockout mice	2.5µl/ul, total 2.5µl/location (total of 12.5µg)	Gut injection converted endogenous form of aSyn to pathological species and spreading into the brain. Vagotomy and aSyn KO prevented neuropathology and neurobehavioral phenotypes.	Kim et al. 2019
Intramuscular, intravenous and intraperitoneal	180 d.p.i. and 210 d.p.i.	M83 Tg and M20 Tg mice (human aSyn A53T mutation and WT human aSyn, driven by prion promoter)	20µg for intramuscular, 20µg for intravenous and 50 µg for intraperitoneal	The efficiency of aSyn PFF to invade the CNS differs via multiple routes of peripheral administration. All induce robust pathological aSyn, some led to paralysis phenotype.	Ayers et al. 2018
Muscle	1,2,3, and 4 m.p.i.	2-month-old M83+/- mice	2,5, or 10 µg of mouse aSyn fibrils	aSyn induced phenotype is largely dose-independent. Motor neuron cell death and aSyn pathology occur within 2 months, astrogliosis appears at a later time point. Neuroinflammation is thought of a consequence rather than trigger. At 3mpi, immune activation dominates revealed by transcriptome analysis.	Sorrentino et al. 2018

Sciatic nerve (unilateral)	1,2,4, m.p.i.	M83 Tg and M20 Tg mice (human aSyn A53T mutation and WT human aSyn, driven by prion promoter)	2 µL of 2 mg/mL mouse WT or human Δ71–82 aSyn PFFs	Injection site is efficient in triggering the spreading of pathological aSyn and leading to paralytic symptoms. Axonal transport is a mechanism of spread and seeding. Human aSyn PFFs containing E46K mutation exhibited reduced ability to undergo aggregation.	Ayers et al. 2018
Enteric neurons of the descending colon	1, 6, 12 m.p.i. 12 m.p.i. (normal human primates)	6 weeks old male Sprague Dawley rats and Non-human primates (Macaca fascicularis)	6×5 µl of 2 µg/µl mouse or human aSyn PFFs or 10 injections of 10 µL (2 µg/µL)	Minor aSyn pathology was observed in the brainstem at 1 mpi but not at later time points, in rats. Enteric aSyn pathology correlated with decreased gastrointestinal motility in both rats and non-human primates. ENs inoculations led to persistent aSyn pathology in both models. aSyn pathology in the enteric nervous system in the colon correlated with transient aSyn pathology in brainstem in rats. Induction of enteric aSyn pathology is insufficient to induce sustained brain pathology in both models.	Manfredsson et al. 2018
Vein	12 h.p.i.	2-month-old C57BL/6 mice	5 µg of Atto 488-labeled aSyn fibrils or ribbons	Intraperitoneal LPS injection prior to system intravenous delivery aSyn PFFs in WT mice led to increase brain resident microglia and leukocytes towards the spinal cord and brain aSyn can be internalised by LPS primed inflammatory monocytes. A differential recruitment of CD4+ and CD8+ T cells after LPS priming was noted compared to control mice.	Peralta Ramos et al. 2019

Gastric Wall	45 d.p.i.	2-month-old male C57BL/6J mice	3 µL of 2 µg/µL mouse aSyn PFFs	No cell type specificity in neurons containing aSyn inclusions. Inoculation of aSyn PFFs into gastric wall triggers LB like aggregates in brainstem via vague nerve.	Uemura et al., 2018
Olfactory Bulb	1,2,3,6,9,12,18 and 23 m.p.i.	3-month-old female C57BL/6J mice	0.8 µl of 5 mg/ml WT mouse or human aSyn PFFs	aSyn PFFs associated with early neuronal loss. At longer time points, lack of continual progression, speculate due to compromised neuronal circuitry or, activation of proteolytic mechanism to counterbalance the spread and seeding by degradation of pathogenic aSyn.	Rey et al., 2018
Peritoneum, tongue	13 m.p.i.	Tg (M83+/−:Gfap-luc+/−) and (Gfap-luc+/−) mice (A53T mutant human of aSyn and firefly luciferase)	5 µl (intraglossal) or 50 µl (intraperitoneal) of 1 ug/ul aSyn PFFs	Intraperitoneal: mice developed sarkosyl insoluble aSyn aggregates in brain and spinal cord, colocalised with p62 ubiquitin, accompanied by gliosis. Intraglossal: 1 of 5 developed aSyn pathology in CNS	Breid et al., 2016

Table 1.3 Summary of α–synuclein PFF animal studies, since 2012. Information shown, authors who conducted the study, the site of injection, the time point and duration of experiments, the species of animal, background strain and age of the rodent used. The main findings of the studies are also summarised. SN= substantia nigra, ST, striatum. h.p.i = hours post injection d.p.i. = days post injection, w.p.i. = weeks post injection, m.p.i=months post injection, aSyn=alpha synuclein, pSyn=phosphorylated α–synuclein. M83 Tg mice express human α–synuclein with the A53T mutation, M20 Tg mice express WT human α–synuclein driven by the mouse prion protein promoter. G2019S leucine-rich repeat kinase (LRRK2) is a risk factor for PD. Where known, age of rodents is stated. Studies which are particularly relevant to the work conducted in this thesis are shaded as yellow.

1.7 Aims and objectives of my thesis work

My hypothesis is that despite α–synuclein being a critical factor in PD pathogenesis, α–synuclein alone is not sufficient to trigger neurodegeneration at early stages of disease. Rather, additional factors such as oxidative stress are required to promote synapse and neuronal degeneration, compounded by α-synuclein spread from damaged synaptic terminals.

In order to address my hypothesis, I have carefully planned my study into two specific aims. **Aim 1** is to investigate the consequences of α–synuclein PFFs in triggering neurodegenerative changes when injected into the MFB of Sprague Dawley (SD) rats. This allows understanding of the consequences of α–synuclein spread in the absence of any other neurodegenerative disease-associated factors. This extends previous work in this area since injection into the MFB allows study of α–synuclein spread following its injection into a fibre tract consisting of both axons and fibres, and that has direct and indirect connections to many areas affected in PD, including those important for executive dysfunction. Previous reports have shown that injection of α-synuclein PFFs into rodent brain can trigger mild behavioural phenotypes characteristic of PD, including motor impairments that are associated with dopaminergic neuron loss (Luk et al., 2012a).

Here, behaviour tests such as the asymmetric cylinder test were used to detect asymmetric motor impairments, while the Morris water maze (MWM) and 5-choice serial reaction time task (5-CSRTT) were used to monitor visuospatial and executive cognitive impairments, respectively. Tissues were collected at 60 d.p.i., 90 d.p.i. and 120 d.p.i. and were used to investigate the consequences of α-synuclein PFFs on key neurodegenerative changes

associated with PD in regions connected to the MFB, including the distribution and abundance of phosphorylated α-synuclein and tau, synaptic proteins, oxidative stress and astrocyte reactivity.

In Aim 2, the classic neurotoxin 6-OHDA was injected into rat MFB to allow further understanding of how rapid neuron loss may allow widespread oxidative stress-mediated neurodegenerative changes in MFB-connected regions. This includes the emergence of protein and cellular changes in regions connected to the MFB and SN including the frontal cortex and hippocampus, and the consequences for cognitive and behavioural abnormalities.

The significance of aim two is to understand if high levels of neuron death affect connected brain regions to facilitate the neurodegenerative cascade by mediating changes associated with neurodegeneration such as α-synuclein and tau phosphorylation and synapse synaptic, thus promoting cognitive and behavioural changes.

I administered 6-OHDA by stereotaxic injection into the MFB of SD rats. 6-OHDA lesion in the MFB of rodents is a common approach to experimental model PD, in which oxidative stress responses cause degeneration of dopaminergic neurons in the SN, damage to key cellular pathways, and enable a damaging bidirectional interaction with pathogenic proteins. This could induce release and spread of α–synuclein from damaged terminals. This results in a vicious cycle whereby more ROS are produced to promote disease progression (Dias et al., 2013). Similarly, to the experimental approach to the α–synuclein PFF injected rats, 6-OHDA-lesioned rats underwent behaviour tests at 3 w.p.i. to confirm dopaminergic loss within the SN. This was followed by additional behaviour tests for motor and cognitive impairment.

Immunohistochemical staining was performed to detect the presence of oxidative stress and changes in tau and α–synuclein proteins. Subsequent changes in synaptic proteins were monitored using biochemical techniques.

The significance of these experiments is that this work will elucidate the relationship between α–synuclein and oxidative stress in PD pathogenesis. Specifically, it may be that rapid neuronal loss, induced in these studies by oxidative stress, is necessary for cognitive decline in PD.

Chapter 2 Materials and methods

2.1 Materials

Unless stated otherwise, reagents for the experiments performed in the UK were purchased from Thermo Fisher Scientific (Paisley, UK) and all other chemicals and reagents were purchased from Sigma-Aldrich (Dorset, UK). Stock solutions and buffers were prepared using ultrapure water from an Elga Maxima Purification System, Veolia Water, (London, UK). A full list of primary and secondary antibodies used in this thesis can be found in Table 2.2 and Table 2.3.

2.1.1 General buffers and reagents

1 x Phosphate-buffered saline (PBS)

140 mM NaCl, 2.689 mM KCL, 12.54 mM Na_2HPO_4, 1.98 mM KH_2 PO_4 in ultrapure H_2O, adjusted to pH 7.4

1 x PBS-tween (PBS-T)

PBS with 0.05% (v/v) Tween-20, National diagnostics (Hull, UK)

1 x tris-buffered saline (TBS)

50 mM Tris-HCl, 150 mM NaCl in ultrapure water, adjusted to pH 7.4

0.9% Saline solution

NaCl in ultrapure water

4% fixation agent

16% (w/v) paraformaldehyde, diluted 1:3 in PBS to give a 4% (v/v) working solution

Bovine serum albumin (BSA) protein standard 2 mg/mL albumin in 0.9% saline,

Thermo Fisher Scientific (Waltham, MA, USA)

Ethylenediaminetetraacetic acid (EDTA)

500 mM EDTA in ultrapure water, pH 8.0 stock solution

Protease inhibitor cocktail

cOmplete™, Mini, EDTA-free Protease Inhibitor Cocktail Roche (Basel, Switzerland)

Phosphatase inhibitor cocktail

Phos-Stop™ tablets, Roche (Basel, Switzerland)

Sarkosyl N-Lauroylsarcosine

(sarkosyl) sodium salt solution, 20% (w/v)

2x Sample buffer

2x Protein loading buffer blue National Diagnostics (Hull, UK)

Precision Plus Protein™ All blue prestained proteins standards, Biorad Hercules (CA, USA)

Or

Precision Plus protein™ Dual colour standards, Biorad Hercules (CA, USA)

TBS-tween (TBS-T)

TBS with 0.05% (v/v) Tween-20, National diagnostics (Hull, UK)

2.1.2 Human Brain Tissues

Postmortem human brain samples from control and clinically and pathologically confirmed and staged cases of Alzheimer's disease and Parkinson's disease, according to BrainNet Europe (BNE) protocol for assessment (Braak and Braak, 1991; Alafuzoff et al., 2008; Alafuzoff et al., 2009), were obtained from the Medical Research Council Neurodegenerative Diseases Brain Bank, King's College London. All tissue collection and processing procedures were carried out under the regulations and licensing of the Human Tissue Authority, in accordance with the UK Human Tissue Act (2004), and following ethical approval (Research Ethics Committee reference: 08/MRE09/38 + 5).

Tissue sections were from 10% (v/v) formalin-fixed, paraffin-embedded brain sections, 7 µm thick, were from the temporal cortex region of Braak stage VI AD cases. Frozen human brain tissue (200 mg) was obtained from the frontal cortex of Parkinson's disease dementia cases, see Table 2.1 for further information.

ID	Age (years)	Gender	PMD (hours)	Pathological diagnosis
Ctrl-1	74	M	72	Very mild ageing changes according to BrainNetwork Europe (BNE), stage 1
Ctrl-1	73	F	27	Early ageing changes, BNE stage 1
PDD-1	85	M	29.5	Diffuse Lewy body disease, BNE Braak VI
AD-2	79	M	31	Alzheimer's disease BNE Braak stage VI
AD-2	73	M	30	Alzheimer's disease BNE modified Braak stage VI, and severe cerebral amyloid angiopathy.

Table 2.1 Human brain samples used in this study. Samples of control, AD and PDD brain were obtained from Brains for Dementia Research/The Medical Research Council London Neurodegenerative Disease Brain Bank at King's College London. Pathological assessment was according the BrainNet Europe (BNE) protocol. Tissue sections were from the temporal cortex region of control and AD cases, while frozen tissue samples were from the frontal cortex region from PDD cases. Age, gender, and postmortem delay (PMD), and pathological diagnosis are shown.

2.1.3 Synthesis of α–synuclein preformed fibrils

α-Synuclein was subcloned into the NdeI and HindIII restriction sites of bacterial expression vector pRK172 (1-1304). Respective proteins were then expressed in *Escherichia coli* BL21 (DE3) cells, Thermo Fisher Scientific (Waltham, MA,USA). The protocol for the synthesis of α–synuclein preformed fibrils was as mentioned from Volpicelli-Daley et al. (2014). Other studies have also successfully synthesised recombinant α-synuclein using the same protocol (Patterson et al., 2019). The choice of using *Escherichia coli* BL21 (DE3) cells to expression has several advantages; a high protein concentration can be obtained (up to 30 mg/ml), the choice of final buffer can be controlled, and purification of α–synuclein can be prepared in the absence of a tag that may interfere with fibrillisation. This protocol can successfully and equally purify both recombinant human and mouse α–synuclein. In cell culture, the resultant pathology from these α–synuclein PFFs are strikingly similar to those found in human synucleinopathies. The aggregates initially form within axons, sequestering endogenous α–synuclein from pre-synaptic terminals, followed by propagation into the somata and eventually the formation of the α–synuclein aggregates lead to selective alterations in synaptic protein, compromised of neuronal excitability and eventually neuronal death (Volpicelli-Daley, 2017; (Volpicelli-Daley et al., 2011).

S.O.C. medium

2% tryptone, 0.5% yeast extract,

10 mM NaCl, 2.5 mM KCl, 10 mM $MgCl_2$, 10 mM $MgSO_4$ and 20 mM glucose

Terrific broth (TB)

12 g/L bacto-tryptone, 24 g/L yeast extract, 4% (v/v) glycerol,

17 mM KH_2PO_4 and 72 mM K_2HPO_4

1x Phosphate-buffered saline

137 mM NaCl, 2.7 mM KCl, 8 mM Na_2HPO_4, 2 mM KH_2PO_4.

High Salt buffer

750 mM NaCl, 10 mM Tris pH 7.6, 1 mM EDTA, 1 mM PMSF,

Dialysis buffer

10 mM Tris pH 7.6, with 50 mM NaCl, 1 mM EDTA, 1 mM PMSF

Dialysis tubing

SpectrumLabs, Spectra/Por molecular porous membrane tubing 12-l4 kDa

Gel Filtration Buffer

10 mM Tris, pH 7.6 with 50 mM NaCl, 1 mM EDTA

Amicon Ultra Centrifugal Filter devices

Amicon Ultra 15 3.5K molecular weight cut-off (MWCO)

Buffer A

10 mM Tris pH 7.6, 25mM NaCl, 1 mM EDTA, 1 mM PMSF

Buffer B

10 mM Tris, 1M NaCl pH 7.6, 1 mM EDTA, 1 mM PMSF

Dialysis buffer

10 mM Tris pH 7.6, with 50 mM NaCl

2.1.4 Quality control assays for α–synuclein preformed fibrils

2.1.4.1 Thioflavin T assay

1 mM Thioflavine T in ultrapure water

100 mM Glycine pH 8.5

384-well Black polystyrene (PS) assay plate (NUNC 262260)

2.1.4.2 Sedimentation assay

α–Synuclein monomer in 10 mM Tris pH 7.6, 50 mM NaCl or tissue culture grade sterile filtered Dulbeccos PBS without Mg^{2+} or Ca^{2+} pH 7.0

1.5 mL eppendorf tubes or Axigen PCR tubes

2.1.5 Cell culture and treatment of rat primary neurons with α–synuclein PFFs

Coating substrate

25μg/mL poly-L-lysine, Sigma-Aldrich (Missouri, USA)

Dissection solution

1xPBS with 18 mM glucose

Complete Neurobasal medium Gibco, (Waltham, Massachusetts, USA)

Neurobasal medium containing 2mM glutamax, 25 μM β-mercaptoenthanol, 50 U/ml penicillin 50 μg/ml streptomycin and 2% B-27 serum-free supplement.

Supplemented minimal essential medium (SMEM) Gibco, (Waltham, Massachusetts, USA) supplemented with 18 mM glucose, 2 mM L-glutamine, 25 μM β-mercaptoenthanol, 50 U/ml penicillin, 50 μg/ml streptomycin, 30% glucose (w/v), 5% heat inactivated fetal bovine serum

2.1.6 Stereotaxic Injections

Injection needle

Hamilton syringe, 10 μl, 33G needle, 701 SN, Hamilton (Reno, USA)

Anaesthetic agent

Ketamine, Xylazine and sodium pentobarbital, Alfasan International (Worerden, Holland)

Local analgesic

Lidocaine

Stereotaxic frame

Narishige Scientific Instruments Lab, (Japan)

Sutures

Ethilon © size 4-0, polyamide

Pain relief

Metacam ®, Meloxicam, (Boehringer, Ingelheim, Germany)

6-hydroxydopamine (6-OHDA)

L-Ascorbic acid

Chicago Skyblue dye, Sigma-Aldrich (Missouri, USA)

2.1.7 Immunohistochemistry

Microscope slides

SuperFrost Plus, Menzel Glaser microscope slides, Thermo Fisher Scientific, (Gerhard Menzel, Saarbruckener, Germany).

Or

PCS-13, Positive Charged Adhesion microscope slides, Ground Edge

(Lab'IN Co, Tsuen Wan, N.T, Hong Kong)

Blocking solution

3% (w/v) BSA, 2% (v/v) Foetal Bovine Serum (FBS), 1% (v/v) triton-x-100 in 0.1M Tris,

OR

10% (w/v) normal goat serum in PBS containing 0.3% (v/v) Triton-x-100

Peroxidase blocking solution

3% (v/v) H_2O_2 in TBS

Antigen retrieval solution

Antigen unmasking solution, citric acid based, Vector Laboratories (Peterborough UK) in ultrapure water, pH 6.0

OR

0.01 M sodium citric, pH 6.0

OR

EDTA 1 mM, pH 9.0

Immunohistochemical (IHC) diluent

0.3% (v/v) Triton-x-100 in PBS

Avidin-biotin peroxidase

Vectastain ABC kit, Vector Laboratories (Peterborough UK)

Cytoseal 60

Cytoseal mountant for histology, Thermo Fisher Scientific (Waltham, MA, USA)

Fluoromount-G™, with DAPI

Clear liquid medium containing fluorescent nuclear stain, Thermo Fisher Scientific, (Waltham, MA, USA)

Glass coverslips

24 x 50 mm, borosilicate glass coverslips, VWR (Leighton Buzzard, UK)

3,3'-diaminobenzidine (DAB solution)

DAB Peroxidase (HRP) Substrate Kit, Vector Laboratories (Peterborough, UK)

100% ethanol, Fisher Chemical (Loughborough, UK)

90% ethanol

100% ethanol diluted 9:1 in ultrapure water

70% ethanol

100% ethanol diluted 7:3 in ultrapure water

Xylene solution, Fisher Chemical (Loughborough, UK)

Sudan black solution

1% (w/v) of Sudan Black B in 70% ethanol, Fisher Chemical (Loughborough, UK)

2.1.8 Synaptoneurosome isolation

Glass-teflon tissue grinder

OR

Omni Tissue Master 125 homogenizer (Kennesaw, USA)

Easy Pressure Filter Holder 25 mm, PALL (Portsmouth, UK)

Nylon Filter 80 um, 25 mm, Merck Millipore (Watford, UK)

Acrodisc filter, 32 mm, Supor membrane with 5 um pores, PALL (Portsmouth, UK)

Tube adapters (303313) 6.5ml, PALL (Portsmouth, UK)

Beckman polycarbonate tubes, 2-2.5 ml, Fisher scientific (Rockford, IL, USA)

Buffer A

25 mM HEPES pH 7.5

120 mM NaCl

5 mM KCl

1 mM $MgCl_2$

2 mM $CalCl_2$

in ultrapure H_20

plus

cOmplete™, Mini, EDTA-free Protease Inhibitor Cocktail

Phos-Stop™ tablets, Roche (Basel, Switzerland)

Buffer B

50 mM Tris pH7.5

1.5% (w/v) SDS

2 mM DTT

in ultrapure H_20

2.1.9 Isolation of proteins using sarkosyl

Beckman polycarbonate tubes, 2-2.5 ml, Fisher scientific, (Rockford, IL, USA)

1x PBS

Tris buffer

50 mM Tris-HCl pH 7.4, 10 mM NaF, 5 mM EDTA

High salt buffer (HS)

50 mM Tris-HCl pH 7.4, 750 mM NaCl, 10 mM NaF, 5 mM EDTA

HS-Triton-x (Tx) 100 buffer

Nine parts HS buffer, 1 part 10% (v/v) Triton-x

HS-Sarkosyl (Sark) buffer

Nineteen parts HS buffer, 1 part 20% (v/v) Sarkosyl

2.1.10 SDS - polyacrylamide gel electrophoresis (SDS-PAGE)

Resolving buffer

4x ProtoGel resolving buffer (1.5M Tris-HCL, 0.4% (w/v) SDS, pH = 8.8,

National Diagnostics (Hull, UK)

Stacking buffer

4x ProtoGel stacking buffer (500mM Tris-HCL, 0.4% (w/v) SDS, pH = 6.8,

National Diagnostics (Hull, UK)

Acrylamide

ProtoGel (30% (w/v) acrylamide/methylene bisacrylamide solution,

National Diagnostics, (Hull, UK)

N, N, N' N'- TEMED-ultra pure water

Tetramethylethylenediamine (TEMED), National Diagnostics (Hull, UK)

Ammonium persulphate (APS)

10% (w/v) APS in ultrapure water

10% resolving gel

10% (v/v) acrylamide, 25% (v/v) resolving buffer, 0.1% (v/v) TEMED, 1% (w/v) APS

in ultrapure water

12% resolving gel

12% (v/v) acrylamide, 25% (v/v) resolving buffer, 0.1% (v/v) TEMED, 1% (w/v) APS

in ultrapure water

4% Stacking gel

4% (v/v) acrylamide, 25% (v/v) stacking buffer, 0.1% (v/v) TEMED, 0.1% (w/v) APS

Pre-cast gels

NuPage® 10%, 4-12% or 4-20% bis-tris 1.0 mm x 15 well gels

Thermo Fisher Scientific (Paisley, UK)

Running buffer

10X tris-glycine-SDS PAGE buffer National Diagnostics, (Hull, UK), diluted to 1X in ultrapure water

Or

20x Bolt™ MES SDS running buffer, Thermo Fisher Scientific (Paisley, UK)

Transfer buffer

10x tris-glycine electroblotting buffer National Diagnostics, (Hull, UK), diluted to 1x in 20% (v/v) methanol and ultrapure water.

Blocking buffers

Odyssey Blocking Buffer, Li-Cor Biotechnology, (Cambridge, UK) diluted 1:1 in TBS

Or

5% (w/v) skimmed milk powder in TBS

Washing buffers

TBS-T

Coommassie blue stain Bio-Rad, (Biorad Hercules, CA, USA)

2.1.11 Enzyme-linked immunosorbent assay (ELISA)

ELISA buffer

50 mM TBS (pH 7.4), 2 mM EGTA, 1 mM PMSF, 10 mM NaF, 1 mM Na_3VO_4

cOmplete™, Mini, EDTA-free Protease Inhibitor Cocktail

Phos-Stop™ tablets, Roche (Basel, Switzerland)

Blocking buffer

2.5% (w/v) BSA in 1x TBS

Antibody diluent

5% (w/v) BSA in 1x TBS

Chromagen substrate solution

1-Step™ Ultra TMB-ELISA substrate solution, Thermo Fisher Scientific, (Rockford, IL, USA)

Stop solution

1 N Hydrochloric acid

ELISA Washing buffer

TBS, 0.05% Tween-20

Antibody	Specificity	Host	Clonality	Immunogen	Dilution	Source (product code)	Pretreatment
β-actin	Mouse, rat, rabbit, horse, chicken, cow, dog, human, pig and zebrafish	Rat (Rb)	Polyclonal	Mouse, rat and human beta-actin (amino acids 1-100, exact sequence is proprietary)	1:5000 (WB)	Abcam Plc., Cambridge, UK (ab8227)	N/A
β-actin	Mouse, rat, rabbit, horse, chicken, cow, dog, human, pig and zebrafish	Mouse (M)	Monoclonal	Mouse, rat and human beta-actin (amino acids 1-100, exact sequence is proprietary)	1:5000 (WB)	Abcam Plc., Cambridge, UK (ab8226)	N/A
α– synuclein	Phosphorylated and non-phosphorylated α–synuclein. Rat (QC testing), Human, Mouse	Mouse (M)	Monoclonal	Rat Synuclein-1 aa. 15-123	1:1000 (WB)	BD Transduction laboratories (610787)	N/A

α–synuclein (pSer129)	Human	Mouse (M)	Monoclonal	Raised against a synthetic peptide corresponding to amino acids 124-134 of α–synuclein, phosphorylated at Serine 129	1:10,0000 (IHC)	Virginia Lee, Centre of neurodegenerative diseases, University of Pennsylvania, USA.	Microwave (medium heat) 10 min 0.01M sodium citrate buffer (pH 6)
4-hydroxynonenal (4HNE)	Species independent	Mouse (Ms)	Monoclonal	Chemical/small molecule [HNE-J-2] to 4 hydroxynonenal	1:50 (IHC)	Abcam Plc., Cambridge, UK. (ab138501)	N/A
8-Hydroxy-2-deoxyguanosine	Species dependent,	Mouse (M)	Monoclonal	Chemical/ Small Molecule corresponding to DNA/RNA Damage. 8-hydroxy-guanosine-BSA and -casein conjugates.	1:150 (IHC)	Abcam Plc., Cambridge, UK. (ab62623)	N/A
AT8	Tau phosphorylated at Ser 202, Thr205. Reacts	Mouse (M)	Monoclonal	Partially purified human PHF-Tau	1:500 (WB) 1:50 (IHC)	Thermo Fisher Scientific, Waltham, Massachusetts, USA (MN1020)	Microwave (medium heat) 10 min

	with human tau, but published species *include;* chicken, dog, fruit fly, hamster, human, mouse, non-human primate, rabbit and rat.						0.01M sodium citrate buffer (pH 6)
BT2	Bovine, primate (various, human, rat	Mouse (Ms)	Monoclonal	Recognises tau between amino acids 194-198 but not PHF tau	1:1000 (WB)	Pierce Thermo Scientific (MN-1010B)	N/A
CP13	Human, mouse, rat	Mouse (Ms)	Monoclonal	Epitope around phosphoserine 202	1:1000 (WB)	Peter Davies, Department of pathology, Albert Einstein College of Medicine, The Feinstein institute for Medical Research, USA	N/A
DA31	Human, mouse, rat	Mouse (Ms)	Monoclonal	Pan-tau antibody, maps amino acid region 150-190 of tau	1:1000 (WB)	Peter Davies, Department of pathology, Albert Einstein College of Medicine, The Feinstein institute for	N/A

						Medical Research, USA	
DAKO total-tau	Mouse, rat and human total (phosphorylated and non-phosphorylated) tau (amino acids 243-441)	Rabbit (Rb)	Polyclonal	Recombinant human tau protein expressed in E. coli, corresponding to the C-terminal part (amino acids 243-441) containing the four repeated sequences involved in microtubule binding	1:5000 (WB) 1:500 (ELISA)	DAKO/Agilent Technologies, Santa Clara, CA, USA. (A0024)	N/A
Glial fibrillary acidic protein (GFAP)	Mouse, rat and human glial fibrillary acidic protein (GFAP)	Rabbit (Rb)	Polyclonal	GFAP isolated from cow spinal cord	1:200 (IHC) 1:1000 (WB)	DAKO/Agilent Technologies, Santa Clara, CA, USA. (Z0334)	N/A
GSK-3β	Mouse, rat, human and xenopus	Mouse (Ms)	Monoclonal	Produced in mouse against recombinant Xenopus laevis protein	1:1000 (WB)	Thermo Fisher Scientific, Waltham, Massachusetts, USA (44-610)	N/A

Phosphorylated GSK-3β	Mouse, Rat and Human	Rabbit (Rb)	Polyclonal	Immunising animals with a synthetic phosphopeptide corresponding to the sequence of human GSK-3β	1:1000 (WB)	Cell Signalling #9336, Hamilton House Mabledon Place London	
MJF-R 1	Mouse, Rat and Human	Rabbit (Rb)	Monoclonal	Recombinant full length protein within human α–synuclein aggregate aa 1 to the C-terminus. The exact sequence is proprietary	1:1000	Abcam Plc., Cambridge, UK (ab138501)	N/A
Neuronal nuclei (NeuN)	Avian, chicken, ferret, human, mouse, pig, rat and salamander	Mouse (M)	Monoclonal	Purified cell nuclei from mouse brain	1:500 (IHC)	Merck Millipore, Billerica MA, MUSA (MAB377)	N/A
Nitrotyrosine	Chemical, Human	Rabbit (Rb)	Polyclonal	Keyhole limpet hemocyanin (KLH) containing nitrated tyrosines	1:500	Thermo Fisher Scientific, Waltham, Massachusetts, USA. (A212-85)	Microwave (medium heat) 10 min 0.01M sodium

							citrate buffer (pH 6)
Ubiquitin	Mouse, human, yeast, crab-eating monkey	Rabbit (Rb)	Polyclonal	Ubiquitin isolated from cow erythrocytes and conjungated to chicken gammaglobulins with glutaraldehyde.	1:400 (ICC)	DAKO/Agilent Technologies, Santa Clara, CA, USA (Z0458)	N/A
Paired helical filament 1 (PHF1)	Human, epitope around phosphorylated Ser396 and Ser 404 of human tau.	Mouse (M)	Monoclonal	Epitope around Ser396 and Ser404 phosphorylated sites	1:100 (IHC)	Peter Davies, The Feinstein institute for Medical Research, USA	Microwave (medium heat) 10 min 0.01M sodium citrate buffer (pH 6)
Postsynaptic density protein (PSD-95)	Human, mouse and rat	Rabbit (Rb)	Polyclonal	Synthetic peptide corresponding to residues of human PSD95.	1:1000 (WB)	Cell signalling, MA, USA (2507S)	N/A
Synaptophysin (SYP D4)	Mouse, rat and human	Mouse (M)	Monoclonal	raised against amino acids 221-	1:1000 (WB)	Santa Cruz Biotechnologies Inc.,	N/A

				313 of SYP of human origin		Santa Cruz, CA, USA (sc-17750)	
Tau (phospho S396)	Human, mouse, rat, bovine	Rabbit (Rb)	Polyclonal	Antiserum produced against a chemically synthesized phosphopeptide derived from the region of human tau that contains serine 396.	1:100 (IHC) 1:100 (ELISA)	Thermo Fisher Scientific, Waltham, Massachusetts, USA. (44-752G)	Microwave (medium heat) 10 min 0.01M sodium citrate buffer (pH 6)
Tau (phospho S404)	Tau phosphorylated at serine 404	Rabbit (Rb)	Polyclonal	Antiserum produced against a chemically synthesized phosphopeptide derived from the region of human Tau that contains serine 404.	1:20 (IHC)	Thermo Fisher Scientific, Waltham, Massachusetts, USA. (44758G)	Microwave (medium heat) 10 min 0.01M sodium citrate buffer (pH 6)
Tyrosine hydroxylase (TH)	Human, rat, mouse Ferret, Squid, Feline, drosophila and mollusk	Rabbit (Rb)	Polyclonal	Denatured tyrosine hydroxylase from rat pheochromocytoa	1:1000 (IHC)	Millipore, Billerica, USA (AB152)	Microwave (medium heat) 10 min 0.01M sodium

							citrate buffer (pH 6)

Table 2.2 Details of the primary antibodies used in this thesis. Table provides information about host, clonality, specificity (sequence information is given when available), concentration used, pretreatment and source.

Antibody	Dilution (application)	Source
Goat anti-Mouse IgG (H+L) AlexaFluor® 488	1:400 (IHC)	Thermo Fisher Scientific, Paisley, UK
Goat anti-Mouse IgG (H+L) AlexaFluor® 568	1:400 (IHC)	Thermo Fisher Scientific, Paisley, UK
Goat anti-Mouse IgG IRDye® 800CW	1:5000 (WB)	Li-Cor Biotechnologies Inc., Lincoln, NE, USA
Goat anti-Mouse IgG IRDye® 680CW	1:5000 (WB)	Li-Cor Biotechnologies Inc., Lincoln, NE, USA
Goat anti-Rabbit IgG IRDye® 800CW	1:5000 (WB)	Li-Cor Biotechnologies Inc., Lincoln, NE, USA
Goat anti-Rabbit IgG IRDye® 680CW	1:5000 (WB)	Li-Cor Biotechnologies Inc., Lincoln, NE, USA
Goat anti-Rabbit IgG (H+L) AlexFluor® 568	1:400 (IHC)	Thermo Fisher Scientific, Paisley, UK
Biotinylated Goat Anti-Rabbit IgG Antibody	1:400 (IHC)	Vector Laboratories, Peterborough, UK
Biotinylated Goat Anti-Mouse IgG Antibody	1:400 (IHC)	Vector Laboratories, Peterborough, UK
Goat anti-rabbit IgG-HRP Antibody	1:500 (ELISA)	Thermo Fisher Scientific, Paisley, UK

Table 2.3 Details of the secondary antibodies used in this thesis. Table provides information about clone name, specificity (sequence information is given when available), concentration used and source.

2.2 Methods

2.2.1 Synthesis of α–synuclein preformed fibrils (PFFs)

2.2.1.1 Transformation, expression in *Escherichia coli*

WT mouse α–synuclein was cloned into the ampicillin resistant bacterial expression vector, pRK172 (bp 1-1304). Next, plasmids were transformed into BL21 (DE3) RIL-competent E.coli (Thermo Fisher Scientific, Waltham, MA, USA, (230245) which were streaked onto LB-agar plates containing ampicillin. A single colony was picked and transferred to 4 ml of SOC medium, which was incubated with shaking for 1-2 h at 37°C to initiate a starter culture. After shaking, 0.5 ml of starter culture was added into each of two 4 litre flasks containing ampicillin and 500 ml of Terrific Broth (12 g per litre of Bacto-tryptone, 24 g per litre of yeast extract, 4% (v/v) glycerol, 17 mM KH_2PO_4 and 72 mM K_2HPO_4). Cultures were incubated at 37°C overnight with shaking.

2.2.1.2 Harvesting cells

Bacteria were pelleted by centrifugation of cultures at 6,000 g, for 10 min at 4°C (Beckman Coulter rotor JA-10, California, USA). The pellet was collected and resuspended in high salt buffer containing protease inhibitors and 1 mM PMSF. The pellet was sonicated using a probe tip of at least 0.25 inch and at 60% power, for a total time of 5 min (in a sequence of 30 s pulse on, 30 s pulse off). To precipitate unwanted proteins, the samples were boiled for 15 min, followed by immediate cooling on ice. The suspension was centrifuged at 6,000 g for 20 min at 4 °C, the supernatant containing α–synuclein was collected and dialysed, as described by (Luk et al., 2016).

2.2.1.3 Purification

Recombinant α–synuclein was purified according to methods described in (Luk et al., 2016). Briefly, using 3.5 kDa molecular weight cut-off Amicon ultra centrifuge filter devices, α–synuclein protein was concentrated, and the concentrated protein filtered through a 0.22 µm syringe filter, before loading onto a Superdex 200 gel filtration column. Approximately 30 1mL fractions were collected. 10 µl of 2x Laemmli buffer was added to 10 µl of each fraction to allow analysis by SDS-PAGE using 4-20% (w/v) acrylamide gradient gels. Proteins in the resulting gels were stained with Coomassie blue. Samples yielding bands that corresponded to the predicted molecular weight of pure α–synuclein (approximately 15 kDa) were re-dialysed and the purified protein applied to Hi-Trap Q HP anion-exchange columns (GE Healthcare Life Sciences) and run along a linear gradient ranging from 25 mM NaCl to 1 M NaCl. α–Synuclein was eluted at approximately 300 mM NaCl. Approximately 50 fractions, each of 2 mL were collected, and 10 µl of each fraction was combined with 10 µl of 2x Laemmli buffer prior to SDS-PAGE using 4-20% polyacrylamide gradient gels and Coomassie staining of proteins. Samples yielding bands of approximately 15 kDa were again dialysed, and concentrated to 30 mg/ml. These samples, containing monomeric α–synuclein, were aliquotted and stored at -80°C until required.

2.2.1.4 α–Synuclein

As a native protein, α–synuclein exists as a monomer, but for reasons still unclear the native protein can misfold, leading to the formation of oligomers and eventually protofibrils/fibrils, which are deemed to be toxic (Jucker and Walker, 2013). α–Synuclein monomers were added to sterile-filtered dPBS (without Ca^{2+} or Mg^{2+}) to a final concentration of 5 mg/ml. α–synuclein PFFS were made from pure recombinant monomeric α–synuclein that was shaken on an orbital shaker (Eppendorf ThermoMixer ®, Enfield, USA) at 100 rpm for 7 days at 37°C. Samples were then vortexed to reduce turgidity.

2.2.1.5 Quality check assays; Thioflavin and Sedimentation

Thioflavin T (ThT) and sedimentation assays are commonly used to characterize the assembly of fibrils from monomer. Results of ThT assays fluctuate with time and do not measure the direct amount of amyloid structures present, but do detect the presence of cross beta-sheet structures within the sample (Patterson et al., 2019). The binding of ThT to tertiary protein structures leads to increased fluorescence. Briefly, samples were diluted 1:50 in glycine and 10 µl of each diluted sample was added to 384-well black PS assay plates in triplicate. 1mM of ThT solution was added to each well and incubated for 1 h, before any resulting fluorescence changes were detected on a SpectraMax M50 spectrophotometer at 450 nm excitation and 510 nm emission.

Sedimentation assays were also used to detect the proportion of α–synuclein that has been fibrillised. In this assay, monomers are found in the supernatant whereas fibrils sediment in the pellet. Briefly, α–synuclein PFF stocks were diluted ten-fold in dPBS (without Ca^{2+} or Mg^{2+}) and centrifuged at 45,000 g (Beckman Coulter rotor JA-10, California, USA) for 30 min at 23°C. The supernatant was collected as the soluble fraction and the pellet was immediately resuspended in an equal volume of dPBS. Samples of supernatant and pellet were mixed with 2X sample buffer and loaded onto a 4-20% SDS gel, which was electrophoresed until the dye front reached the bottom of the gel. Proteins in the gel were detected by staining with Coomassie blue.

2.2.2. Rat primary hippocampal neuron culture

Experimental procedures in Section 2.2.2 and Section 2.2.2.1 were conducted by final year project student, Mr Cyrus Liu. Experimental procedures followed the guidelines of the Committee on the Use of Live Animals in Teaching and Research, at the University of Hong Kong. Sprague-Dawley (SD) rats were used to prepare primary cultures of hippocampal neurons. Pregnant rats underwent euthanasia with carbon dioxide. Embryos at embryonic day 18 (E18) were collected and transferred to a class I tissue culture hood (Edgegard EG-5252, Stanford, Maine, US). Using a Leica MZ8 microscope (Leica, Germany), the hippocampi of the embryos were isolated and dissected in medium consisting of 1xPBS with 18 mM glucose. Hippocampal tissues were minced and then centrifuged for 5 min at 300 g (Rotofix 32A, Hettich, Germany). Following centrifugation tissues were dissociated using supplemented Minimum Essential Medium (Gibco, Waltham, Massachusetts, USA). Hippocampal neuronal cells were seeded at a cell density of 1 x 10^5 onto 15 mm coverslips (Thermo Scientific, Waltham, Massachusetts, USA) pre-coated with poly-L-lysine (Sigma-Aldrich, St. Louis, Missouri, USA) at a concentration of 25 μg/ml. Neurons were maintained in Neurobasal medium (Gibco, Waltham, Massachusetts, USA) supplemented with Minimum Essential Medium, at a ratio of 2:1. Neurobasal medium was supplemented with 2% B-27 supplement (Thermo Fisher Scientific, Waltham, Massachusetts, USA) and Minimum Essential Medium was supplemented with 5% heat inactivated foetal bovine serum (Gibco, Waltham, Massachusetts, USA). To inhibit non-neuronal cell growth 5'-deoxy-5'-fluorouridine (dFUR) (2 μM) was added into neuronal cultures one day after seeding.

2.2.2.1 Rat primary neuron treatment, incubation of α–synuclein PFFs

To confirm that the α–synuclein PFFs prepared were able to induce seeding and aggregation of native α–synuclein, PFFs were incubated with primary hippocampal neurons according to previously published protocols (Volpicelli-Daley et al., 2014b). Briefly, primary hippocampal neurons were treated with either α-synuclein PFFs at a concentration of 2 μg / cover slip at 7 days in vitro (DIV 7). α-Synuclein PFFs were added into cell culture medium in a 6-well plate where cells were seeded on coverslips. The control group was treated with PBS (Gibco, Waltham, Massachusetts, USA) at 2μL / cover slip. Cells were fixed at DIV 21 for immunostaining.

2.2.3 Rodent studies

Animal experiments were conducted according to National Institute of Health (USA) standards and were approved by the Committee for the Use of Live Animals in Teaching and Research (CULATAR) in the University of Hong Kong's Laboratory Animal Unit (LAU). CULATAR license reference numbers: 4479-17.

Male SD rats (Outbred; Charles River Lab, USA) weighing 230 - 250 g were obtained from the LAU, University of Hong Kong. Rats were housed in cages with no more than three animals per cage and were kept in a 12 h light/dark cycle at 22 ºC, with water and food available *ad libitum* throughout the study. For CULATAR under the reference number 4551-17, a subset of rats underwent food restriction for 3-7 days, until the target weight was reached (85-95% of free-feeding weight) prior to a 5-choice serial reaction time task (5-CSRTT). Food restriction was necessary for the group of animals that underwent 5-CSRTT task as the task was dependent on the rat's motivational behaviour and rats tend to comply better with diet restriction, as indicated in previous literature (Mar et al., 2013)

2.2.3.1 Accuracy of stereotaxic injection into the medial forebrain bundle (MFB) of rats

The medial forebrain bundle (MFB) was chosen as the site of injection primarily due to its relatively accessible location and its connectivity to a wide range of structures that are affected in PD. The MFB has direct projections with the striatum and substantia nigra (SN), and is part of the nigrostriatal pathway. Additional regions of interest include the fronto-striatal network, where the striatum has connectivity to the frontal lobe (Gratwicke et al., 2015). Connectivity between the hippocampus and MFB is not fully elucidated. However, previous studies have shown outputs to the hippocampus from the rat MFB (Nieuwenhuys et al., 1982) (Figure 2.6).

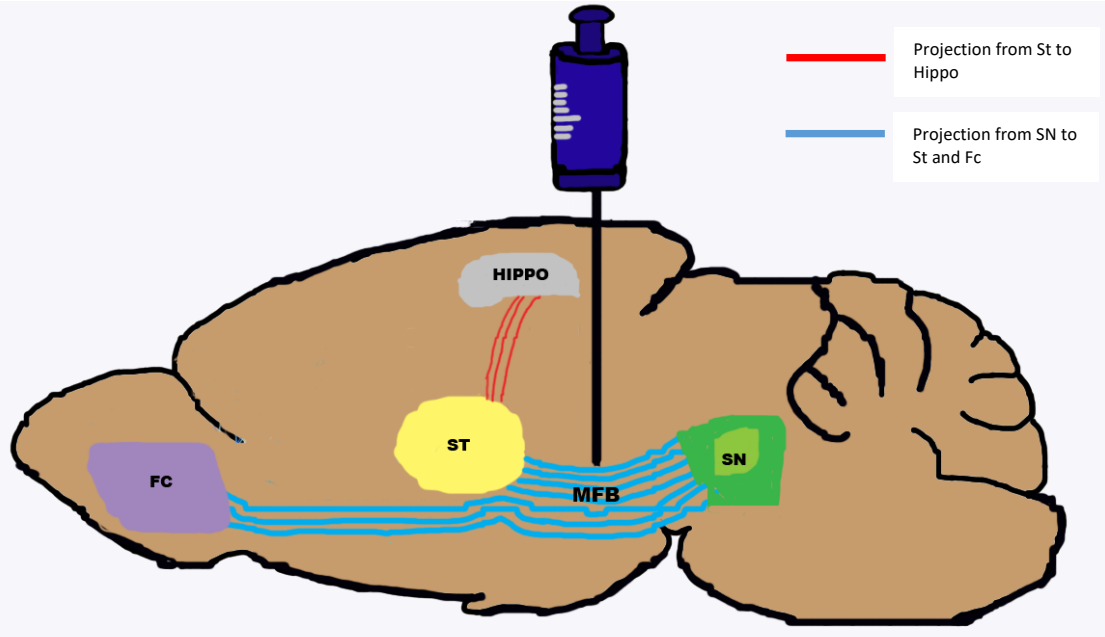

Figure 2.2. Illustration depicting the location of the MFB and the key regions of interest. Direct and indirect innervations between anatomical regions are shown. Blue tracts indicate direct projections from the MFB and red tracts indicate indirect inputs to regions of interest. Frontal cortex (FC), striatum (ST), hippocampus (HIPPO) and substantia nigra (SN).

The MFB is a relatively expansive structure and there is some variation in the literature concerning precise injection sites (Lehmkuhle et al., 2009; Goren et al., 2009; Mertens et al., 2009). Utilising the rat brain atlas (Paxinos and Watson, 7th Ed) co-ordinates were selected for injection: AP-4, ML-1.2, DV +7.5 and nose bar at 3.3 mm below interaural line from bregma. To verify that the injection co-ordinates were correct, 2.5 µl of Chicago sky blue dye was injected into the MFB using a 10 µl Hamilton syringe. Following injection the rat was immediately sacrificed. The brain removed from the skull and sections were prepared at AP-4 based on the rat atlas (Paxinos and Watson, 7th Ed) using a rat brain matrix. The lesion site was apparent from Chicago blue staining and was found to be consistent (Figure 2.7). These parameters were then used for injection of 30 µg of 6 µg/µl of α–synuclein PFFs into 230 – 250 g rats. An equivalent volume of PBS was used as a vehicle control. For 6-OHDA, previous studies within the lab group established a total dosage of 12 µg was sufficient to induce significant nigrostriatal dopaminergic loss within 3 weeks after injection (Shah et al., 2019). The amount of α–synuclein PFFs injected was guided by previous literature governed by the site of injection and animal species. A total of 60 µg was injected into 6 weeks old SD rats (Manfredsson et al., 2018) into the enteric neurons of the descending colon. A total of 8 µg was injected into unilateral striatum (Paumier et al., 2015) although this quantity of PFFs was deemed insufficient given the increase in size of the rat brain compared to a mouse brain. Therefore, given the relative size of the rat brain and delicate structure of the MFB, also taking into consideration the time of the experimental design, a total of 30 µg α–synuclein PFFs was injected unilaterally into the rat MFB.

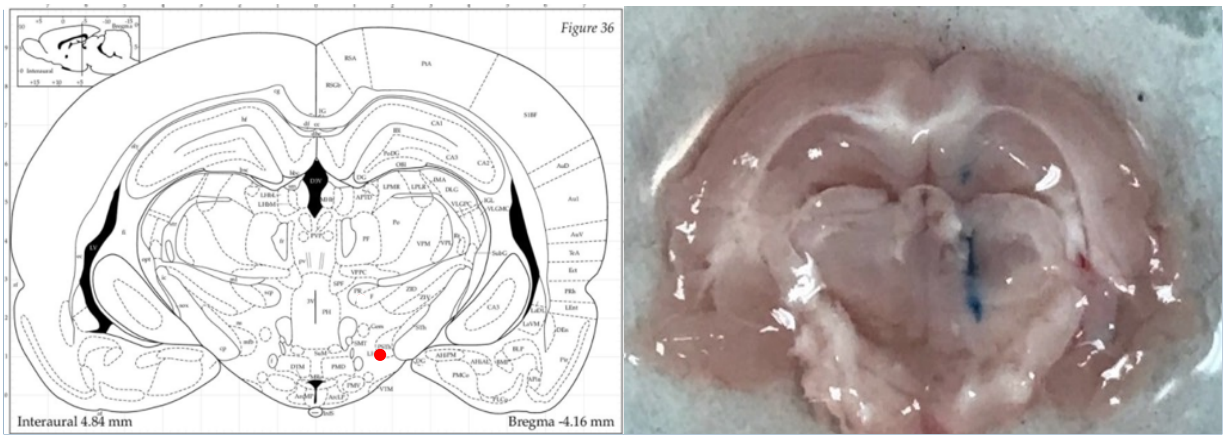

Figure 2.2 Verification of stereotaxic injection into rat MFB. Left: coronal section of rat brain, at AP -4, adapted from rat brain atlas (Watson and Paxinos, 2007). The red dot represents the site of injection into the MFB. Right: Representative image showing Chicago blue dye at the site of injection and along the injection track (AP-4, ML-1.2, (from bregma), DV +7.5 (from dura) and nose bar 3.3 mm below interaural line). Adult rats weighing approximately 230 - 250 g were used.

2.2.4 Stereotaxic lesioning of the medial forebrain bundle (MFB) in rats with α–synuclein PFFs or 6-hydroxydopamine

Adult male SD wild type rats, 230 – 250 g at the time of surgery, were used. Animals were obtained from Centre for Comparative Medicine Research (an AAALAC member), LKS Faculty of Medicine, The University of Hong Kong. On the day of surgery, PFFs were thawed, sonicated as previously described (Polinski et al., 2018; Luk et al., 2012a) and kept at room temperature during surgical procedures. 6-Hydroxydopamine (6-OHDA) was made up with 0.02% mg of L-ascorbic acid and kept in the dark on ice to prevent oxidation prior to the surgical procedure. Surgical procedures were adapted from (Zhang et al., 2019) for PFFs and (Shah et al., 2019) for 6-OHDA. After aseptic procedures such as shaving and disinfecting surgical regions, rats were deeply anaesthetised with ketamine hydrocholoride (100 mg/kg, i.p) and xylazine (10 mg/kg, i.p). Only when the animal showed no response to the tail pinch reflex test was it immobilised onto the stereotaxic frame (Narishige Scientific Instruments Lab, Japan). Rats were aseptically stereotaxically injected in one hemisphere of the MFB: AP-4, ML -1.2 and DV 7.5, relative to the bregma and from dura *either* with recombinant α–synuclein PFFs (6 μg/μl; 30 μg) *or* 6-OHDA (3 μg/μl; 12μg) or an equivalent volume of PBS containing 0.02% of ascorbic acid as control. A total of 5 μl PBS was injected into the α–synuclein PFF control group and 4 μl of PBS was injected for the 6-OHDA control group. Injections were performed using a 10 μL syringe, gauge 33 (Hamilton, NV) at a rate of 2 μl/min. The needle was left in situ for a further 5 min to allow for diffusion before retraction of the needle and suturing of the wound with non-absorbent Ethilon© size 4-0, polyamide sutures. During surgery rats received subcutaneous injections of 3 mL of saline solution and post-surgery rats received Metacam® (Meloxicam, Boehringer, Ingelheim, Germany) at 1 mg/kg into their drinking water as analgesia. Animals were monitored regularly, and were provided wet palatable food.

2.2.5 Behavioural testing

Behavioural testing of rats was assisted by research assistants Ms Becky Stell and Ms Maja Sorenseng from the Laboratory of Neurodegenerative Diseases. All members involved in the behavioural testing were blinded to the groups wherever possible.

2.2.5.1 Open field test

After injections of either α–synuclein PFFs (at time points of either 60 d.p.i., 90 d.p.i., or 120 d.p.i.) or 6-OHDA (3 w.p.i.), locomotor activity and anxiety like behaviour was assessed using the open field test using a protocol adapted from (He et al., 2018). After habituation for 30 min, rats were placed individually into the centre of the square arena with a floor area of 100 cm x 100 cm and black opaque walls of 30 cm in height. Movement of rats was recorded immediately after animals were placed in the open-field arena. Each trial lasted for 10 min with a total of three trials. The open field arena was divided into two zones, outer and inner. The percentage of time spent within the inner zone and the total distance travelled during the behaviour test was quantified. Trials were recorded using Panlab Smart 3.0 software (Shenzhen, China).

2.2.5.2 Apomorphine induced rotation test

Apomorphine hydrochloride at 0.2 mg/kg was intraperitoneally injected. Following the injection, the rat was placed inside a 30 cm diameter cylindrical container and were allowed 10 min to acclimatize. Contralateral rotation activity of the rat was recorded for 30 min. The total number of full (360°) contralateral rotations were counted during the 30 min period of testing.

2.2.5.2. Asymmetric cylinder test

Rats were tested for forelimb use asymmetry by the cylinder test according to previously published protocols (Heuer et al., 2013). Rats were placed in a glass cylinder of 30 cm in height and 20 cm diameter. A total of 10 forepaw touches (or the number of forepaw touches within a maximum time of three min) were recorded. Exploration activity such as wall touching, push- off and landing were also counted. To enable analysis of the forelimb movement when the animal was rearing with its back facing the camera, two mirrors angled at approximately 120° was placed behind the cylinder. The total percentage of left (contralateral) paw usage was determined using the following equation:

[*Number of contralateral forelimb use + ½ number of simultaneous forelimb use/ number of ipsilateral forelimb use + number of contralateral forelimb use + number of simultaneous forelimb use] x 100.*

2.2.5.3. Rotarod test

Rotarod analysis was performed on an accelerating rotarod (IITC Life science, USA California). The protocol was adapted from Animal Models of Movement Disorders (Hickey and Chesselet, 2012). All rats received an initial training session of three days, and rats were tested after their recovery from surgery. An average of three readings of their latency to fall from the rotarod were recorded. Data was analysed using one-way ANOVA.

2.2.5.4. Morris water maze (MWM)

Protocol was adapted from (You et al., 2019). A pool of 150 cm in diameter was filled with water and care was taken to ensure it was maintained at an ambient temperature of 21 ºC at all times. Surgical curtains were used to surround the tank to minimise distraction, and spatial cues were positioned on the curtains. Coloured tapes were stuck on the floor to divide the tank into four quadrants. A platform of 10 - 15 cm in width was secured to one of the quadrants. Training for the Morris water took five days with four trials per day. Rats were placed facing in each quadrant facing the edge of the tank. Each training day had a randomised order. The time taken for each animal to reach the platform was recorded and timed. On the 6th day, a probe test was conducted where the platform was removed from the water tank and rats were given 1 min in which the time spent in the target quadrant and the number of crossings of where the platform was placed, were recorded. Spatial learning for the Morris water maze was analysed using repeated measures, one-way ANOVA while the number of platform crossing and percentage of time spent in the target was analysed using t-test.

2.2.5.5 5-choice serial reaction time task (5-CSRTT)

The 5-choice serial reaction time task (5-CSRTT) can be tailored to probe for different aspects such as visual attention processing, working memory, pattern separation and executive function. For the purpose of this investigation, the protocol was adapted from (Mar et al., 2013) for assessing executive function in rodents. Schematic diagram shown in Figure 2.3.

Preparation of rats

Rats were acclimatised for seven days, and the weight of the rats four days after acclimatisation were recorded for three consecutive days. During this period, rats received food and water *ad libitum*. During this period, the mean weight of the free-feeding rats was determined. Food restriction followed over three to seven days, until the target weight of 85-95% of free-feeding weight, (7 g food per 100 g of body weight) was reached. Solid rewards (banana/tropical flavoured food pellets) were scattered onto the cage floor, and the rats were further habituated for 1 - 3 days.

Pre-training

Rats were placed into their assigned chambers for 30 min (stage 1) with rewards for two consecutive days. When rewards were consumed, training moved to the next stage. Stages 2-5 of pre-training are shown in Figure 2.8. In brief, for stages 2-4, sessions were only considered as completed after 60 min or when 100 trials were reached. Only when rats completed all 60 trials within the 60 min time period were they moved to the next stage. For stage 5, only rats that completed all trials with a score greater than 60% accuracy within 60 min for two consecutive trials were allowed to proceed to the training phase of this test.

Training

Training was carried out once daily for 5 - 7 days per week. The following parameters were set up for the training procedure. A stimulation is shown for 8 seconds. This is followed by an intertrial interval (ITI) of 5 s where the rat can respond and select the correct illuminated screen. If the rat does not select anything, all options will be illuminated for a further 5 s

followed by a time out of 5 s to signify the end of that particular trial. Each rat was assigned a chamber and the session was initiated, where the duration of the task was set for 60 min (or completion of 100 trials). Once a rat reached the criterion of completing all trials with ≥ 60% response accuracy and ≤ 20% trial omissions (with 8 s stimulus duration), training continued with a gradual reduction of stimulus from 4 s to 2 s. As different subjects reached this criterion at different rates, a hybrid approach was used, whereby animals were "rested" followed by reminder sessions until the entire group had attained the desired pre-training criterion.

Probe test

The probe test was conducted following recovery from surgery. Various stimulus durations were applied ranging from 2 s to 1.5 s, 1 s, 0.8 s, 0.6 s, 0.4 s or 0.2 s. Data relating to executive function, including accuracy, omission, premature responses was obtained.

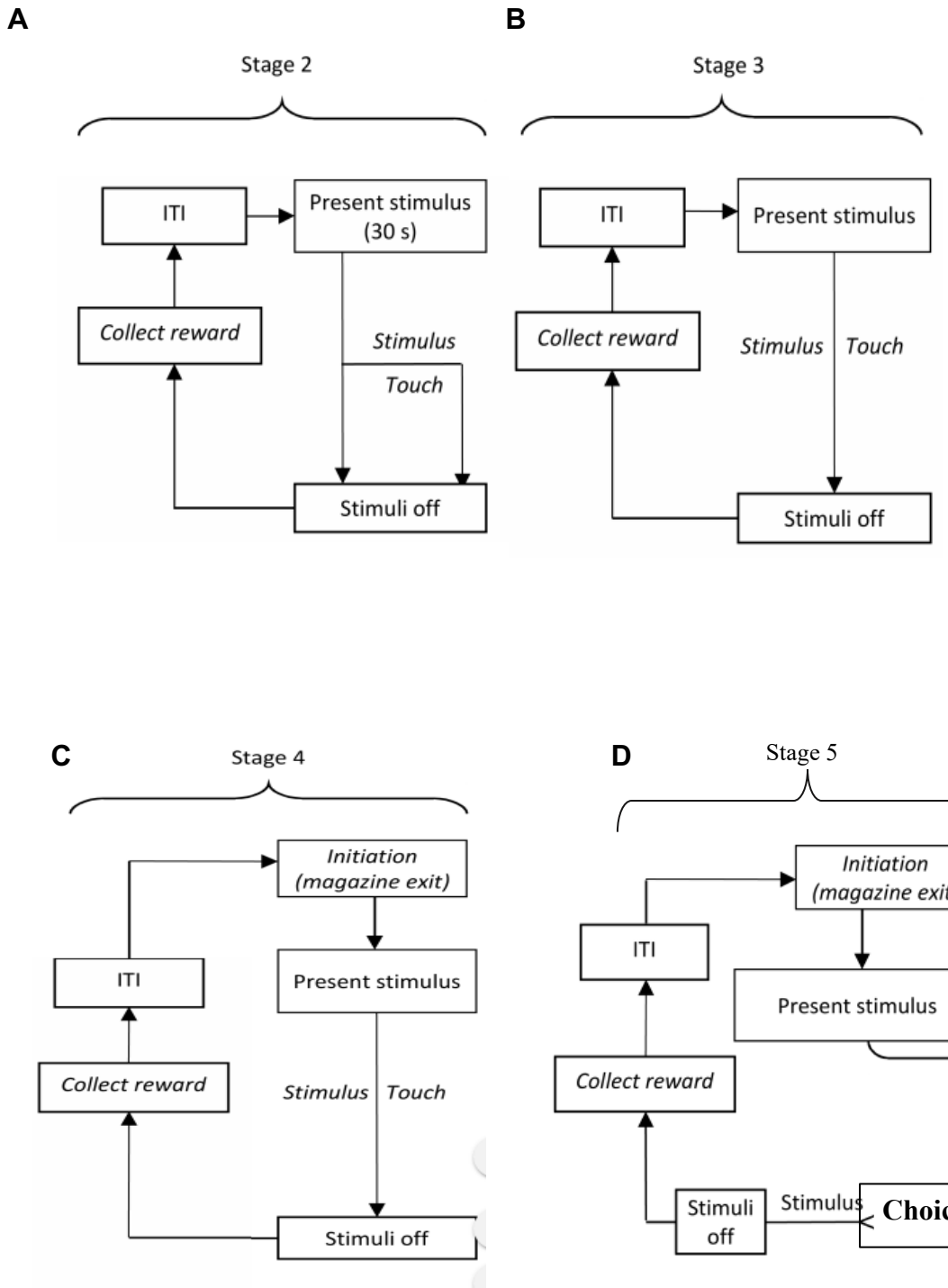
A
Stage 2
ITI
Present stimulus (30 s)
Collect reward
Stimulus
Touch
Stimuli off
B
Stage 3
ITI
Present stimulus
Collect reward
Stimulus
Touch
Stimuli off
C
Stage 4
Initiation (magazine exit)
ITI
Present stimulus
Collect reward
Stimulus
Touch
Stimuli off
D
Stage 5
Initiation (magazine exit)
ITI
Present stimulus
Collect reward
Stimuli off
Stimulus
Choice

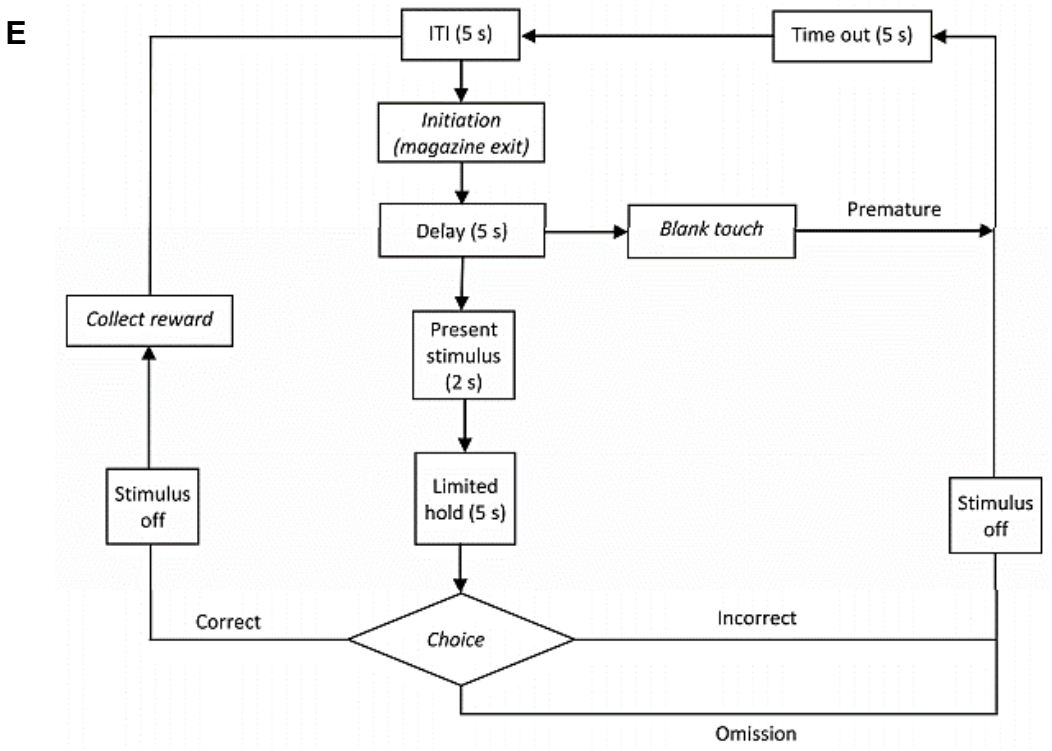

Figure 2.4 5-choice serial reaction time task (5-CSRTT) training flow chart. **A)** In stage 2, rats are placed into the chamber with a stimulus presented to them for 30 seconds. Once they respond to the stimulus, the stimuli are switched off and a reward (flavoured pellet) is released from the magazine followed by ITI to signify the end of trial. **B,C)** In stages 3 and 4, a stimulus is again presented to the animal inside the chamber. Following a correct response, a reward pellet is released from the magazine. **D)** In stage 5, rats must complete all trials and score above 60% in accuracy within 60 min and for 2 consecutive trials before proceeding onto the official training. **E)** During the training period, a stimulus is presented for 2 s and rats have 5 s to respond (limited hold) before making a choice. If the choice is incorrect, the stimulus is stopped, are given a time out of 5 s (black out) before the procedure is repeated. Should the rat make a choice before the presentation of the stimulus, it is regarded as a premature response. When the rat selects the correct stimulus, a reward is given through the magazine. Diagram adapted from (Mar et al., 2013).

2.2.6 Htau and wild-type (WT) mouse lysates

All animal housekeeping and procedures were carried out in accordance with the UK Scientific Procedures (Animals) Act (1986) under the authority of Project and Personal Licences.

Human tau (htau) mice were purchased from The Jackson Laboratory, Bar Harbor, ME, USA and bred and maintained at the Institute of Psychiatry, Psychology and Neuroscience. Htau mice were generated by mating 8c mice (Duff et al., 2000) with tau knockout (KO) mice (Tucker et al., 2001). The former express the full human tau gene (*MAPT*) under control of the *MAPT* promoter, whilst the latter were generated by upon targeted disruption of the mouse tau gene *Mapt* gene by insertion of cDNA for enhanced green fluorescent protein (EGFP) into exon one of *Mapt*. The resulting offspring, known as htau mice, are hemizygous for the full-length human tau gene and express all six tau isoforms of human tau in the absence of endogenous tau. Htau mice progressively develop hyperphosphorylated and aggregated tau, alongside synaptic and cognitive deficits (Kelleher et al., 2007; Polydoro et al., 2009). WT mice of an identical background strain (C57Bl/6J) were used as controls.

Brain tissue from Htau and WT mice was homogenised at 100 mg/ml in extra strong lysis buffer (100 mM Tris-HCl (pH 7.5), 0.5% (w/v) sodium dodecyl sulphate (SDS), 0.5% (w/v) sodium deoxycholate, 1% (v/v) Triton X-100, 75 mM sodium chloride, 10 mM ethylenediaminetetraacetic acid, 2 mM sodium orthovanadate, 1.25 mM sodium fluoride and protease inhibitor cocktail for mammalian tissues), prior to centrifugation at 16 000 g for 20 min at 4 °C. The protein concentration of supernatants was measured using a BCA protein assay kit (Pierce Endogen, Rockford, IL, USA) and samples were standardised to equal protein concentration before being used for western blotting.

2.2.7 Preparation of formalin fixed paraffin embedded rodent brain

Rats were euthanised by an overdose of sodium pentobarbitol (120 mg/kg body weight, i.p.), with a tail-pinch test used to confirm depth of anaesthesia. Rats were transcardially perfused with first 0.9% (v/v) saline to remove remaining blood, and then with 4% (v/v) paraformaldehyde (PFA) at a steady flow rate, until the brain was sufficiently fixed. The brain was carefully extracted and immersed in 4% (v/v) PFA overnight at 4°C to ensure full brain fixation. 6 cm coronal sections through the entire brain were taken using a rat brain matrix (Zivic Instruments, Pittsburgh, USA). Sections were immersed in PBS for at least 5 h to ensure the removal of excess PFA. Sections were then immersed in a graded series of ethanol (30% (v/v), 30% (v/v), 50% (v/v), 50% (v/v)) for 1 h each at room temperature (RT), and were stored in 70% (v/v) ethanol overnight at 4 °C. The following day brain slices were immersed into an increasing concentration of ethanol (80% (v/v), 90% (v/v), 95% (v/v), 95% (v/v), 100%, 100%, 100%, all for 1 h each at RT) on a shaker (Stuart Scientific, Essex, London). This was followed by immersion in xylene (15 min, 15 min, 30 min) and then tissues were placed into molten wax (Fisher Scientific, MA, USA) in an oven (Memmert, Shanghai, China) set at 60°C for 1 h, followed by 2 x 1 h with vacuum (Memmert, Shanghai, China). Finally, tissues were manually embedded into paraffin blocks, using a Leica (HistoCare Arcadia H) embedding machine/system. Blocks were cooled on ice for approximately 3 min, prior to being sectioned at 7 μm using a Leica (RM2125 RTS) microtome and floated into a 40 – 43°C water bath. Sections were collected and mounted on SuperFrost microscope slides and air dried in a 37°C oven.

2.2.8 Histological staining

Dewaxing and coverslipping

Tissues sections were dewaxed in xylene (2 x 5 min), rehydrated through a series of decreasing concentrations of ethanol (100%, 100%, 90% (v/v), 70% (v/v); 3 min each) and rinsed in ultrapure water (5 min) and tap water (5 min). Following labelling, tissues were dehydrated and cleared in increasing concentrations of ethanol (70% (v/v), 90% (v/v), 100%, 100%; 5 min each) and xylene (2 x 5 min), before cover-slipping with either Distrene-Plasticiser-Xylene (DPX) or Cytoseal™.

2.2.8.1 Immunohistochemistry

For immunohistochemistry of phosphorylated of α-synuclein, a 1:20 series of sections was used for each brain and quantification was for the entire brain. For all other immunohistological and immunofluorescence staining 3 consecutive sections per region were quantified. The area of quantification was 500 mm^2 and counter were performed manually. Tissue sections were dewaxed and rehydrated as above. To quench endogenous peroxidase activity, sections were immersed into 1% (v/v) hydrogen peroxide in PBS (pH 7.4) for 30 min at RT, followed by washing with ultrapure water for 5 min. When required (Table 2.2), antigen retrieval was performed. Tissue sections were immersed in the appropriate antigen retrieval solution and underwent heat treatment of approximately 95°C for 10 min.

Sections were cooled and rinsed with ultrapure water (5 min) and PBS (3 x 5 min), before incubation with primary antibody at 4°C overnight. Antibodies were all diluted in immunohistochemical (IHC) diluent consisting of PBS containing 0.3% (v/v) Triton-X-100 and

2% -10% (v/v) species-appropriate serum. Primary antibody was removed and sections were washed in PBS (3 x 5 min; RT), followed by incubation with the appropriate species of biotinylated secondary antibodies, diluted in IHC diluent for 1 hr at RT. After a further 3 x 5 min washes in 1x PBS, sections were incubated with VECTASTAIN Elite ABC kit reagents according to the manufacturers' instructions, mixed with immunohistochemical diluent (PK-6100; Vector Laboratories, UK) for 1 hr at RT. Subsequently, tissues were washed in PBS (3 x 5 min) and developed with DAB for approximately 5 min (developing times varied depending on the antibody).

2.2.8.2 Immunofluorescence

Immunofluorescence labelling was performed as described above, except the appropriate species of AlexaFluor coupled secondary antibodies were added for 1 hr at RT. In some cases, autofluorescence was quenched by dipping slides in Sudan black solution for 20 s followed by 3x washes in PBS. Once slides had no residues of Sudan black remaining, coverslips were mounted using mounting media containing the DNA dye DAPI to stain nuclei (Thermo Fisher Scientific, Paisley, UK*).*

2.2.9 Isolation of proteins with sarkosyl

Insoluble proteins were isolated from brain tissue using a protocol adapted from Peng *et al.* (2018) (Peng et al., 2018) for rat tissue. Four parts volume (vols) of cold HS buffer containing protease inhibitors and phosphatase was used to homogenise brain tissue in Beckman ultracentrifuge tubes (Rockford, USA) with an Omni Tissue Master 125 homogenizer (Kennesaw, USA). Samples were incubated on ice for 20 min, followed by centrifugation at 126, 000 g or 30 min at 4°C using a Beckman Optima MAX-XP benchtop ultracentrifuge and

TLA55 centrifuge rotor. The supernatant is collected as the high salt (HS) fraction. The remaining sample was re-homogenised and centrifuged as before, and the supernatant/wash discarded. Next, the pellet was homogenised in 4 vols of HS-Tx buffer and centrifuged at 126,000 g for 30 min at 4°C. The supernatant is collected and labelled as HS-Tx fraction. The pellet was homogenised in 4 vols of cold HS-Tx buffer containing 30% (w/v) sucrose, and centrifuge as described above. Following centrifugation, the floating myelin was removed. The pellet was then homogenized in 4 vols of 1% (v/v) sarkosyl buffer and samples nutated at RT for 1 hr. Samples were then centrifuged at 20°C for 30 min at 100,000 g, the supernatant was collected as the sarkosyl-soluble fraction. The pellet was washed by adding 1% (v/v) sarkosyl buffer and centrifugation for 10 min at 100,000 g. The supernatant was discarded and the resulting pellet (sarkosyl-insoluble fraction) was collected and resuspended in 2 x sample buffer.

2.2.10 Synaptoneurosome isolation

Prior to homogenisation, filter holders assembled with two layers of 80 µm nylon filters were precooled. All materials were kept at 4°C throughout the procedure to inhibit phosphatase and protease activities. Brain tissue was homogenised according to weight (200 mg/ml) in 1.5 ml ice cold buffer A with 2 mL glass-teflon homogenisers, with a rotor setting of 40% for seven strokes. The samples were then loaded into 3 ml syringes, and an additional 0.6 ml of Buffer A was added to reduce dead volume. Filters and holders were added and the samples filtered. 200 µl of each homogenate was collected. To this, 200 µl of ultra-pure water and 70 µl of 10% (w/v) SDS was added and the sample passed through a 27G needle three times to shear DNA. Samples were boiled for 5 min and centrifuged at 15,000 g for 15 min. A sample of the supernatant was collected as total extract. The remaining homogenate was centrifuged at

5000 g for 3 min to remove nuclei and the supernatant was loaded in syringes with 5 µm filters, and another 0.6 ml of Buffer A was added to reduce dead volume. The samples were passed through the 5 µm filters. The filtrates were centrifuged for 10 min at 1000 g, the pellet collected and labelled as P1 and the supernatant as S1. The P1 pellets were resuspended in 1 ml of buffer A, split into two tubes and each was centrifuged at 1000 g for 10 min giving rise to two P1' synaptoneurosome pellets. The supernatant was discarded. One of the P1' pellets was resuspended in 200 µl buffer B, boiled for 5 min, centrifuged at 15,000 g for 15 min, and the supernatant saved as the SNS fraction. The remaining P1' pellet was frozen in liquid nitrogen and stored at -80°C as a back-up. To generate the cytosolic fraction, the S1 fraction was centrifuged at 100,000 g for 45 min to remove organelles/microsomes. The supernatant was collected, 70 µl of 10% (w/v) SDS was added for each 400 µl, and samples boiled for 5 min. Samples were mixed with an equal volume of 2x SB for biochemical analysis. To check the purity of fractions, samples were western blotted using synaptic markers such as PSD-95 or synaptophysin. Figure 2.9 shows a schematic diagram of this method.

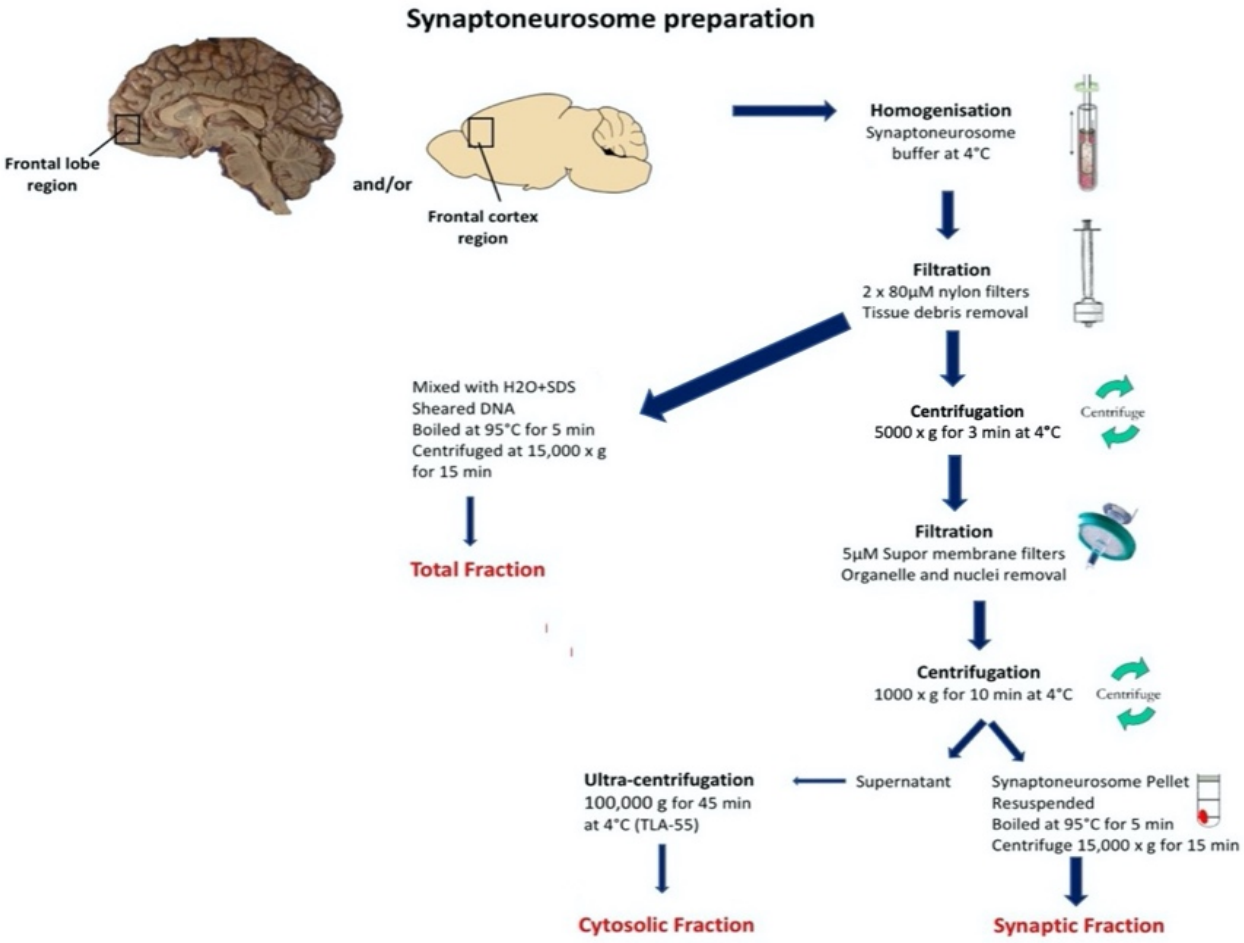

Figure 2.5 Schematic diagram of the synaptoneurosome isolation methods used to isolate synaptic fractions from human postmortem or rat brain tissue. Three fractions were obtained using this protocol, referred to as the total fraction, cytosolic fraction and synaptic fraction. After homogenisation of the tissue, to obtain the total fraction, samples are mixed with H_2O and SDS. To obtain the cytosolic fraction or synaptic fraction, homogenised tissue undergoes multiple filtration and centrifugation steps.

2.2.11 Protein Assay

To determine the concentration of protein present in samples the BCA assay kit (Thermo Fisher Scientific, Paisley, UK) was used according to the manufacturer's instructions. Briefly, BSA standards were diluted in the same buffer as that used to homogenise/lyse samples. A total of eight concentrations of BSA standards (including blank standard) were produced ranging from 0-2 mg/mL. Samples were diluted 1:4 in homogenisation buffers, and 25 μl of sample or standard was pipetted into a 96-well plate (Thermo Nunc, Roskilde, Denmark) in duplicate. The BCA reagent was prepared according to the manufacturer's instructions and 200 µl was added into each well, followed by a 30 min incubation in the dark at RT. The absorbance of the purple reaction product was determined using a Wallac 1420 Victor3TM plate reader (Perkin Elmer, Waltham, MA, USA) or FluoStar Omega plate reader (BMG LabTech, Aylesbury, UK) at 562 nm. The absorbencies of the protein standards were used to construct a standard curve from which the protein concentrations of the samples could be verified using the equation $y=mx+b$ where y is the absorbance. The samples were then standardised to equal protein concentration following dilution using the appropriate buffer.

2.2.12 SDS-PAGE and Western Blotting

Samples were mixed with an equal volume of 2x sample buffer and heated to 85°C on a digital heat block, followed a brief centrifugation at 16,300 x g with a Spectrafuge 24D centrifuge (Jencons PLS, East Grinstead, UK) for 15 seconds.

1.0 mm or 1.5 mm 10% or 12% (w/v) polyacrylamide gels were cast using glass plates (Biorad Hercules, CA, USA). Compositions of gels are described in Section 2.1.10. Gels were inserted into Mini-PROTEAN®TGX™ tanks (Biorad Hercules, CA, USA) and the buffer reservoir filled

with running buffer. At least one lane was retained for loading an appropriate volume (usually 2.5 µl) of protein ladder. Proteins were electrophoresed at 90 V for 15 min using a Bio-rad PowerPac™ (Biorad Hercules, CA, USA). Once the dye had stacked in a straight line, the voltage was increased to 120 V for 60-90 min, until the dye front reached the bottom of the gel.

Gels were placed onto Protran® nitrocellulose membranes of pore size 0.45 µm (Whatman, Maidstone, UK) sandwiched between Grade 1 filter paper (Whatman) and immunoblotting sponges (Thermo Fisher Scientific, Paisley, UK) in a Mini Trans-Blot cell (Biorad Hercules, CA, USA). The electrode assembly was inserted into the Mini Trans-blot cell electrophoresis system and immersed in 1 x Transfer buffer. Proteins were transferred onto nitrocellulose membrane. Depending on the protein of interest, transfer times varied but all proteins examined in the thesis with the exception of phosphorylated α–synuclein (transfer time of 45 min) were transferred over a 90 min period under a constant 230A. To reduce the effects of heating, an ice pack was inserted inside the Mini Trans-Blot cell.

Once the transfer was finished, the membrane was collected and to reduce non-specific binding of antibodies, the membrane was incubated with blocking buffer for 60 min at RT. This was followed by incubation with primary antibody overnight at 4°C with rocking on a SSL4 see-saw rocker (Cole- Palmer, Straffordshire, UK). The membrane was washed three times with washing buffer, followed by incubation with the appropriate species of fluorescently-tagged secondary Infra-Red Detection System antibodies (Li-Cor Biotechnologies Inc., Lincoln, NE, USE). 800 nm and 680 nm channels were used to detect infrared- and green-fluorescent antibodies respectively. Intensity of individual bands were

determined using ImageStudio Lite version 5.0 software (Li-Cor), subtracting background as necessary.

2.2.12.1 Alternative apparatus

The procedure was identical to the above, except that pre-cast gels were used, in combination with 1x NuPAGE® MES SDS running buffer diluted in ultrapure water from 20x stock. Proteins were transferred from the gel to the membrane using XCell II™ blot module (Thermo Fisher Scientific, Paisley, UK).

2.2.13 Semi-quantitative ELISA

To quantify tau protein amounts in total and synaptoneurosome fractions, semi-quantitative ELISA was used. Samples were diluted to equal protein concentration in ELISA buffer (802 µg/µL for total lysates and 373 µg/µL for synaptoneurosomes*).* 50 µg/µL of each sample or ELISA buffer only (as control) were loaded onto 96-well Nunc™ MaxiSorp™ plates (BioLegend, UK) in duplicate. Plates were incubated in 60 °C oven, uncovered and in a non-humidified environment for 2 hr - 4 hr to allow proteins to adsorb onto the substrate of the plate. A blocking solution of 2.5% (w/v) BSA in TBS was applied to each well for 1 hr at RT. Blocking buffer was removed and primary antibody diluted in blocking solution added overnight at 4°C with shaking (SSL4 see-saw rocker, Cole-Palmer, Straffordshire, UK). The antibody was removed by washing five times with ELISA washing buffer. Secondary anti-rabbit or anti-mouse-IgG HRP-conjugated antibodies, diluted in 2.5% BSA blocking solution were added for 2 hr at RT with rocking (SSL4 see-saw rocker, Cole-Palmer, Straffordshire, UK). Secondary antibodies were removed, followed by further washing (5 x TBS-T). TMB chromogen solution (Thermo Fisher Scientific, MA, USA) was added into each well, and the reaction developed

until a blue colour appeared (approximately 1 - 2 min) at which point stop solution (IN HCl) was added. The absorbance of each well was then read at 450 nm on a Wallac 1420 Victor3™ plate reader (Perkin Elmer, Waltham, MA, USA).

2.2.14 Statistical analysis

The number of samples or animals analysed per experiment and the statistical analysis performed, including the p values for all results, are stated within the figure legends. The reported n represents the number of animals. Data was first tested for normality tests; D'agostino-pearson. For comparisons between two groups such as control and α–synuclein PFF, or control and 6-OHDA, a t-test was used for parametric data, otherwise a Mann-Whitney U test was used for non-parametric data (e.g. number of platform crossing from Morris water maze, total distance travelled as a measure of locomotor activity). Unpaired t-test was also used for the difference between pre-post post groups of control and PFF or 6-OHDA (rotarod), and for the difference between contralateral and ipsilateral hemisphere between control, PFF or 6-OHDA treated groups (immunoblot analysis and immunohistochemical analysis). For IHC quantification Table 2.4 consists all actual values of cell counts use for statistical analysis within control and α-synuclein PFF animals. Repeated measures two-way ANOVA was used for data with two variables and when data was obtained from the same the subjects with repeated measures (e.g. learning curve during the Morris water maze task). Sidak's multiple comparisons test followed as post-hoc test. Statistical analysis was performed using Prism V6.0 (GraphPad Software, Inc., USA). All data is presented as mean ± SEM. The level of significance was set at $p < 0.05$.

Fc	60 d.p.i			90 d.p.i			120 d.p.i		
Contra	7	7	3	21	21	6	8	31	24
Ipsi	4	14	11	65	45	7	21	10	16
ST									
Contra	2	2	2	9	14	1	17	10	0
Ipsi	3	2	1	11	8	1	7	8	7
Hippo									
Contra	3	0	0	9	5	2	3	1	0
Ipsi	1	0	0	12	9	2	0	0	1
Crtx									
Contra	2	1	0	13	6	19	0	2	2
Ipsi	2	3	3	8	4	20	0	0	1
SN									
Contra	1	0	0	1	3	0	0	2	0
Ipsi	0	2	0	5	8	0	0	2	2

Time point: 90 d.p.i Marker: 8OHG, FC	Contralateral			Ipsilateral		
Control	2.6	1,7	3.4	1.4	1.1	1.6
PFFS	2.9	1.5	4.2	3.7	1.8	2.1
Time point: 90 d.p.i Marker: 8OHG, CA1	Contralateral			Ipsilateral		
Control	3.8	3.1	5.2	4.5	4.8	5.9
PFFS	5.4	6.4	9.5	6.3	6.0	7.6
Time point: 90 d.p.i Marker: 8OHG, CA3	Contralateral			Ipsilateral		
Control	3.6	5.4	3	8.3	2.8	4.6
PFFS	6.8	4.3	11.3	2.7	1.6	8.31

Time point: 60 d.p.i Marker: GFAP, FC	Contralateral			Ipsilateral		
Control	3.4	1.3	4.7	1.4	0.5	5.1
PFFS	1.8	5.8	1.6	0.6	5.3	0.7
Time point: 90 d.p.i Marker: GFAP, FC	Contralateral			Ipsilateral		
Control	4.0	3.1	4.3	4.3	5.10	4.10
PFFS	1.2	8.3	11.4	0.38	13	8
Time point: 120 d.p.i Marker: GFAP, FC	Contralateral			Ipsilateral		
Control	0.89	4.30	2.4	5.5	7.6	1.5
PFFS	1.70	3.20	3.10	0.8	4.6	12.2
Time point: 120 d.p.i Marker: TH, SN	Contralateral			Ipsilateral		
Control	57	55	50	51	55	59
PFFS	60	57	50	30	25	28

Table 2.4 a)Values of actual cell counts in control and α-synuclein PFF animal groups, used for statistical analysis through the thesis.

Fc	FC			ST			Hippo			Crtx		
Control	0	0	0	0	0	0	0	0	0	0	0	0
6-OHDA	38	23	27	7	17	7	37	6	8	20	6	14

Marker: pTau404, FC	Contralateral			Ipsilateral		
Control	10	12.7	19	13.3	14.7	12.3
6-OHDA	42.7	25.7	11.7	50	18.7	17.7
Marker: pTau404, CA1	Contralateral			Ipsilateral		
Control	0.3	0.7	2.7	2.3	0	2.3
6-OHDA	16.3	29	25.3	2.7	12.7	5.7
Marker: pTau404,CA3	Contralateral			Ipsilateral		
Control	4.3	4.3	4.3	2.7	5	14.3
6-OHDA	13.3	23	24.3	21.7	9.3	6.3
Marker: PHF1, FC	Contralateral			Ipsilateral		
Control	7.0	2.7	3	6	0	3.7
6-OHDA	71	23.7	0	62	0	7.3
Marker: PHF1, CA1	Contralateral			Ipsilateral		
Control	4.3	2.7	0.7	3.7	1.7	3.0
6-OHDA	14	7.7	2.0	11.3	2.3	2.0
Marker: PHF1,CA3	Contralateral			Ipsilateral		
Control	25.3	2	0.3	5.7	4	6.7
6-OHDA	19.3	4.3	2	10	7.3	3.7
Marker: 8OHG, FC	Contralateral			Ipsilateral		
Control	7.8	4.8	2	9	4	2
6-OHDA	9.5	9.5	12.9	13	7	13
Marker: 8OHG, CA1	Contralateral			Ipsilateral		
Control	3.8	3.1	5.2	4.5	4.8	5.9
6-OHDA	5.4	6.4	9.5	6.3	6	7.6
Marker: 8OHG,CA3	Contralateral			Ipsilateral		
Control	4.2	5	8.8	6.6	5.2	6.3
6-OHDA	11.6	5.5	9.4	10.5	6.1	13.9
Marker: NIT, FC	Contralateral			Ipsilateral		
Control	7.8	4.8	2	9	3.6	1.9

6-OHDA	5.4	6.4	9.5	6.3	6	7.6
Marker: NIT, CA1	Contralateral			Ipsilateral		
Control	3.8	3.1	5.2	4.5	4.8	5.9
6-OHDA	11.6	5.5	12.9	10.5	6.1	9.4
Marker: NIT,CA3	Contralateral			Ipsilateral		
Control	4	5	8	6	6	6
6-OHDA	9.5	9.5	12.6	13	7	13
Marker: TH,SN	Contralateral			Ipsilateral		
Control	128	102	102	146	75	103
6-OHDA	116	89	89	29	14	30

Table 2.4 b) Values of actual cell counts in control and 6-OHDA animal groups, used for statistical analysis through the thesis.

Chapter 3- Alpha synuclein preformed fibrils (PFFs)

3.1 Introduction

One of the most extensively studied proteins is the 140 amino acid protein, α–synuclein (Spillantini et al., 1997; Spillantini et al., 1998a). Misfolding and aggregation of α–synuclein is the main culprit responsible for Parkinson's disease (PD) (Spillantini et al., 1997; Trojanowski and Lee, 1998), and abnormal aggregation of α–synuclein can trigger downstream cascades leading to neuroinflammation and neurodegeneration (Duffy et al., 2018a).

Cell-to-cell propagation is a key underlying mechanism of disease-related pathological protein transfer in neurodegeneration (Peng et al., 2020) (Luk et al., 2009; Luk et al., 2012a). The pathological seeds act as templates to induce normal endogenous proteins to misfold leading to an amplification of the pathological protein (Guo and Lee, 2011) (also referred to as "templated amplification") (Peng et al., 2020). Recently, the spreading phenomenon has been successfully modelled using synthesised α–synuclein preformed fibrils (PFFs). PFFs can sufficiently induce the conversion of normal proteins into insoluble aggregates, even when used in small quantities. The α–synuclein PFFs also induce Lewy-like pathology that is strikingly similar to that observed in post mortem PD brain (Duffy et al., 2018b). Spreading (cell to cell transmission) of pathological seeds is a sequential via neural connections that can be observed throughout the brain and is dominated by 1) the endogenous expression of α–synuclein and 2) anatomical connectivity (Henderson et al., 2019a; Okuzumi et al., 2018), mimicking the natural progression of the disease (Braak et al., 2003). Unlike transgenic rodents which typically over-express wild-type or mutant α–synuclein in widespread brain

regions and are prone to overexpression artefacts, injection of α–synuclein PFFs into the olfactory bulb of mice has been demonstrated to induce accumulation of misfolded or aggregated α–synuclein with ageing (Rey et al., 2018). Thus, α–synuclein PFFs are thought to represent a more physiological approach to modelling PD (Duffy et al., 2018a).

The non-motor components, particularly cognitive deficits are difficult to replicate in animal models. In a model of synucleinopathy, to test the role of tau in mediating cognitive deficits, transgenic TgA53T mice were mated with tau knockout mice to generate TgA53T/mTau–/– mice. Post-synaptic deficits and memory deficits were ameliorated in TgA53T/mTau–/– mice compared to TgA53T mice; suggesting that both synaptic abnormality and memory impairment are mechanistically linked via tau. Tau also plays a critical role as the mediator in A53T α–synuclein-mediated abnormalities (Singh et al., 2019). The contribution of α–synuclein to cognition has also been evaluated extensively. The deletion of either γ or α–synuclein in mice was not sufficient to impair cognition. Only the inhibition of both forms of synuclein was enough to impair cognitive function on the T-maze task (Senior et al., 2008). Similarly, when the importance of α–synuclein was examined in a spatial learning task using mice with α–synuclein deficiency (α–synuclein -/-), no notable differences were found in the Morris water maze (MWM) task at 6 months (Chen et al., 2002) compared to wild type (WT) mice. Therefore, the absence of α–synuclein is not considered a critical contributor for cognition. In contrast, findings based on overexpression models of either mutated or WT human α–synuclein under different promoters describe progressive worsening of cognitive deficits (Freichel et al., 2007; Chen et al., 2002; Masliah et al., 2011). These studies suggest that α–synuclein has a role in triggering and contributing to cognitive deficits, though the relationship between the two remains poorly understood.

Synaptic disturbance is detected in early PD (Picconi et al., 2012) and alterations in synapse functions in response to the accumulation of abnormal α–synuclein have been proposed to underlie cognitive and behavioural changes in PD (Bridi and Hirth, 2018). In a mouse line overexpressing human WT α–synuclein under the platelet-derived growth factor (PDGF) promotor, the mice display intraneuronal inclusions that are positive for α–synuclein and ubiquitin in olfactory bulb and neocortex (Freichel et al., 2007). These mice exhibit impaired MWM performance compared to WT by 12 months of age. The cognitive deficit was accompanied by notable decreases in both post-synaptic densities and pre-synaptic terminals in the temporal cortex (Masliah et al., 2011). Using a conditional model of mutant A53T α–synuclein under the calmodulin kinase II (CaMKII) promoter, mice displayed a progressive impairment in contextual fear memory that was accompanied by synaptic structural deficits in the hippocampus. The deficit was reversed once the transgene was turned off, further implying a link between α–synuclein, synaptic disruption and memory impairment (Lim et al., 2011).

This association between α–synuclein and synapse alteration has been mimicked in cell models. For example, the addition of exogenous α–synuclein PFFs to cultured neurons causes Lewy-like pathology along with synaptic dysfunctions that ultimately result in neuronal death (Volpicelli-Daley et al., 2011). Similarly, infusion of α–synuclein PFFs into single primary hippocampal mouse neurons caused a widespread accumulation of phosphorylated α–synuclein and a reduction in synaptic activity within 10 min (Wu et al., 2019). The findings demonstrate the detrimental effects of α–synuclein on synapse functions in cell models is convincing. However, it is important to better understand the consequences of other

α–synuclein-induced changes, including the phosphorylation of α–synuclein, changes in oxidative stress, tau proteins and synaptic proteins, in contributing to behavioural deficits. This can only be achieved using animal models. To decipher potential changes triggered by α–synuclein PFFs at pre-established time points of 60 days post injection (d.p.i.), 90 d.p.i. and 120 d.p.i., α–synuclein PFFs were prepared and intracerebrally injected into the medial forebrain bundles (MFB) of rats.

3.2. Aims and Objectives

The specific goal of this chapter is to evaluate the consequences for key PD-like features, including spreading and transmission of α–synuclein, leading to cognitive and motor phenotype after α–synuclein PFF injections into the MFB of rats.

Key objectives are to evaluate any behavioural phenotypes relevant to PD that are apparent at 60, 90, and 120 d.p.i. of α–synuclein PFFs, including impairment of executive functions and/or visuospatial memory impairment. Following behavioural analysis, further analysis was carried out to determine if endogenous α–synuclein was modified and α–synuclein PFFs induced phosphorylation of α–synuclein at the site of injection in the MFB and in anatomically associated regions, i.e. spreading and transmission of phosphorylated α–synuclein. Next, the assessment of changes in key PD-associated events including tau phosphorylation, oxidative stress, and changes in synaptic proteins indicating synaptic dysfunction, with attention to frontal cortex and hippocampus regions. The consequences of α–synuclein PFFs on cellular interactions were explored by observing astrogliosis within the frontal cortex region.

3.2 Methods

A total of 198 (66 per time point) male Sprague-Dawley (SD) rats weighing between 230 – 250 g aged 7-8 weeks, were used for the experiments described in this chapter. Male rats were used to limit the effects of hormonal interplay. All rats were handled and kept in accordance with international ethical guidelines at The University of Hong Kong, which are based on National Institutes of Health (USA) animal ethics and British Society of Animal Science - Ethical guidelines for research in animal science: the three R reduction guidelines (replacement, reduction and refinement). Rats were grouped randomly according to their designated behaviour tests: Morris water maze, *n = 7*; cylinder test, *n = 10*; Rotarod, *n= 10* (same group as cylinder animal), 5-choice serial reaction time task, *n = 6* and open field test, *n = 10*. Due to the nature of some behaviour tests, separate groups of animals were required to prevent conditioning and prior influence/exposure that would potentially affect the overall results. In the case where some behavioural tests do not have the same number of animals, this is either due to death during surgical procedure or that the animal did not comply with the task and had to be omitted. Tables 3.1-3.3 provide further details. After pre-training and stereotaxic injection, rats were tested according to predetermined time points, followed by tissue collection (Figure 3.1A). Immunohistochemical staining was performed on 3 - 4 rats per control and α–synuclein PFFs group, and biochemical analysis were conducted on 5 - 6 rats per control and α–synuclein PFFs group. Table 3.1 shows the compilation of animal groupings, weight prior surgery and at time of sacrifice after final behavioural tests. Only valid behavioural tests were included in the table., the 5-CSRTT and rotarod tests were excluded. The methods and materials, such as stereotaxic injections, immunohistochemistry, sarkosyl extraction methods and immunoblotting methods have been described in Chapter 2.

Behaviour at 60 d.p.i.	Rat ID	Weight at surgery (g)	Weight at sacrifice (g)	Comments
Morris Water Maze	1	230	430	
	2	230	410	
	3	240	470	
	4	250	460	
	5	250	460	
	6	250	550	
	7	250	530	
	8	230	430	
	9	230	520	
	10	230	540	
	11	250	440	
	12	250	480	
	11	235	480	
	13	250	460	
	14	240	510	
Cylinder	1	240	620	
	2	240	490	
	3	240	480	
	4	245	460	
	5	250	470	
	6	235	410	
	7	235	460	
	8	235	490	
	9	235	410	
	10	235	480	Didn’t comply
	11	230	490	
	12	240	400	
	13	245	470	
	14	245	510	
	15	250	460	
	16	240	400	
	17	250	500	Didn’t comply
	18	235	480	
	19	320	470	
	20	240	460	
Open field test	5	250	560	
	2	240	460	
	3	245	490	
	4	233	400	
	7	240	500	
	8	250	410	
	9	235	480	
	10	245	420	

	11	250	400	
	12	240	500	
	13	230	490	
	14	235	480	
	15	250	470	Froze in test
	16	250	490	
	17	235	480	
	18	230	510	
	19	245	460	
	20	250	410	
	21	245	400	
	22	235	400	
	23	230	410	

Table 3.1 A compilation of α-synuclein PFFs and control injected animals organised according to animal behavioural testing at 60 d.p.i. Information on exclusion criteria, animal ID and animal's weight at time of surgery and at end of final behaviour test prior to sacrifice. Orange= α-synuclein PFFs, Blue=Control

Behaviour at 90 d.p.i	Rat ID	Weight at surgery (g)	Weight at sacrifice (g)	Comments
Morris Water Maze	1	250	500	
	2	250	570	
	3	255	490	
	4	250	530	
	5	235	539	
	6	235	546	
	7	230	530	
	8	230	630	
	9	235	570	
	10	340	530	
	11	240	560	
	12	250	560	
	11	245	530	
	13	240	540	
	14	245	650	
Cylinder	1	255	600	Didn't perform
	2	235	620	Didn't perform
	3	230	570	
	4	230	650	
	5	235	640	Didn't perform
	6	235	655	
	7	235	600	
	8	240	640	
	9	250	600	
	10	250	570	
	11	235	650	
	12	230	505	
	13	230	570	
	14	235	480	Didn't perform
	15	250	600	
	16	250	570	Died during surgery
	17	245	500	
	18	245	530	
	19	245	520	
	20	240	490	
Open field test	5	250	620	
	2	230	600	
	3	230	610	
	4	235	530	
	7	230	620	
	8	250	640	
	9	255	580	
	10	240	500	

	13	245	600	
	14	245	560	
	15	240	540	
	16	240	490	
	17	250	560	
	18	250	580	

Table 3.2 A compilation of α-synuclein PFFs and control injected animals organised according to animal behavioural testing at 90 d.p.i. Information on exclusion criteria, animal ID and animal's weight at time of surgery and at end of final behaviour test prior to sacrifice. Orange= α-synuclein PFFs, Blue=Control

Behaviour at 120 d.p.i	Rat ID	Weight at surgery (g)	Weight at sacrifice (g)	Comments
Morris Water Maze	1	235	570	
	2	255	590	
	3	240	650	
	4	250	640	
	5	250	600	
	6	250	640	
	7	230	600	
	8	235	680	
	9	230	700	Died in surgery
	10	240	700	
	11	240	815	
	12	250	700	
	11	250	650	
	13	230	735	
	14	240	610	
Cylinder	1	240	640	
	2	240	650	
	3	240	660	
	4	230	700	
	5	230	640	
	6	245	735	Didn’t perform
	7	250	570	
	8	250	620	
	9	255	640	
	10	230	730	
	11	230	650	
	12	230	800	
	13	235	700	
	14	245	815	
	15	245	630	
	16	230	650	Didn’t perform
	17	255	600	
	18	235	630	
	19	255	650	
	20	235	800	
Open field test	5	245	700	
	2	240	720	
	3	240	730	
	4	250	810	
	7	250	800	
	8	240	690	
	9	250	650	
	10	250	800	
	13	240	720	

	14	230	700	Died in surgery
	15	235	800	
	16	235	790	
	17	235	700	
	18	255	760	

Table 3.3 A compilation of α–synuclein PFFs and control injected animals organised according to animal behavioural testing at 120 d.p.i. Information on exclusion criteria, animal ID and animal's weight at time of surgery and at end of final behaviour test prior to sacrifice. Orange= α-synuclein PFFs, Blue=Control

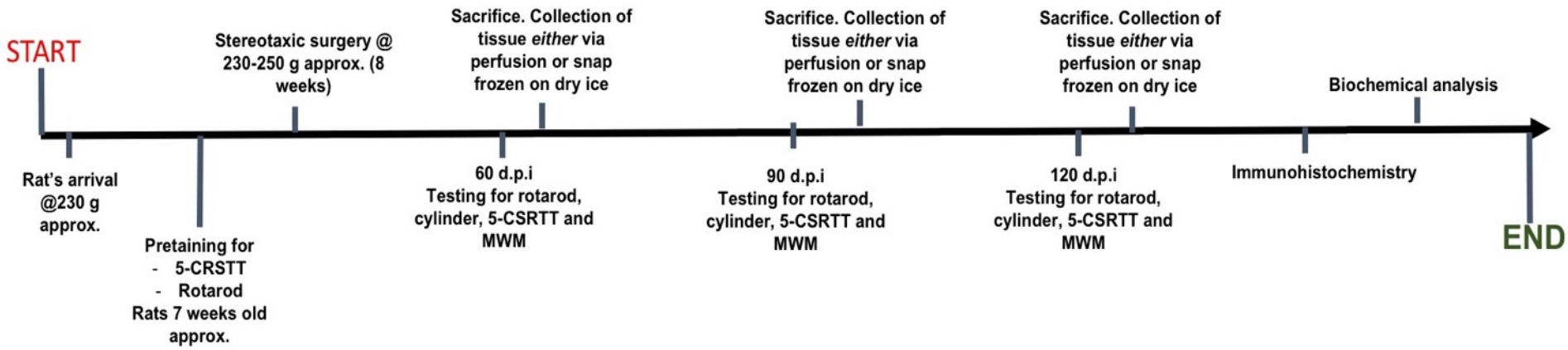

Figure 3.1 Timeline of experimental design for α–synuclein PFF and control rats. **A)** Rats arrived at approximately 230 g in weight and were allowed to acclimatise prior to behavioural pre-training. Pre-training began when animals were 7 weeks old. Depending on the behavioural group allocation, rats underwent pre-training for rotarod, 5-choice serial reaction time task (5-CSRTT). For tests that do not require pre-training, they were directly tested at predetermined time points of 60 days post injection (d.p.i.), 90 d.p.i. and 120 d.p.i. Collection of rat brain tissue followed, immunohistochemistry and biochemical analysis were performed on collected rat brain tissues.

3.4 Results: Characterisation of α–synuclein PFFs

α-Synuclein PFFs were made using recombinant WT mouse α-synuclein following previously established protocols (Volpicelli-Daley et al., 2011; Luk et al., 2016) as described in further detail in Chapter 2, 2.2 Methods. Upon transformation procedures using BL21 (DE3) RIL-competent E.coli, recombinant α-synuclein was purified, firstly according to size using a fast protein liquid chromatography (FPLC) column, then later according to charge using a high performance liquid chromatography (HPLC) column according to methods described in Luk et al. (2016) to obtain pure α-synuclein monomer. The amount of recombinant protein purified from total protein loaded into columns is dependent on previous trial and error attempts. To increase purity a second day of fractionation is needed to achieve >90% purity where majority of C-terminal is removed. For this batch (originally from 1L, 30mg were produced).

Figure 3.2 shows a schematic diagram of the initial purification step using fast protein liquid chromatography (FPLC). Fractions eluted from the FPLC column according to size; due to α–synuclein being a relatively small protein, larger proteins were eluted off and were not collected. Figure 3.3 shows a schematic diagram for the second step of purification using high performance liquid chromatography (HPLC). Here, fractions were eluted through the HPLC column according to charge. Using a range of buffers with increasing salt concentrations, fractions containing α–synuclein were isolated.

α–Synuclein monomers underwent a fibrillisation procedure and to ensure the success of fibrillisation Thioflavin and sedimentation assays were utilised to confirm the presence of fibrils. Thioflavin can detect the presence of amyloid structure and sedimentation will provide

information on the amount of materials fibrilised. Analysis of the PFFs generated for this project are shown in Figure 3.4. Monomeric mouse α–synuclein gave readings of 40 a.u., similar to that of glycine, which was used here as a control. α–Synuclein PFFs showed increased ThT reactivity and a reading of approximately 70 a.u., demonstrating that predominantly α–synuclein fibrils with high beta-sheet structure are present. Monomeric α–synuclein has an absorbance value lower than fibrillised material (Luk et al., 2016). Although not performed here, it would have been useful to determine the proportion of PFF generated relative to monomer. The sedimentation assay was used only to check for the presence of fibrils. Results from the sedimentation assay (Figure 3.5) demonstrate that the monomeric form of α–synuclein PFFs (15 kDa) is predominantly found in the supernatant fraction and α–synuclein PFFs are predominantly distributed in the pellet. Of the total sample loaded, >60% of α–synuclein PFFs was found to be present in the pellet fraction relative to the supernatant. Thus, this assay further indicates efficient fibrillisation of mouse WT α–synuclein.

Finally, the last quality check assay to ensure the α–synuclein fibrils at hand were are able to induce seeding, propagation and aggregation as demonstrated in current literature, (Volpicelli-Daley et al., 2014b), α–synuclein fibrils were incubated with primary hippocampal neurons. In brief, primary hippocampal neurons were treated with either α-synuclein PFFs at a concentration of 2 μg / cover slip at 7 days in vitro (DIV 7). The control group was treated with PBS (Gibco, Waltham, Massachusetts, USA) at 2μL / cover slip. Cells were fixed at DIV 21 for immunostaining. Protocol was adapted from (Volpicelli-Daley et al., 2014b), and further detail of this protocol is further described in Chapter 2, Section 2.2.2.1.

To detect α–synuclein aggregates, neurons were immunolabelled with antibodies against α–synuclein phosphorylated at Ser129 and ubiquitin, features of α–synuclein observed in Lewy pathology (Gomez-Tortosa et al., 2000). Neurons were able to efficiently internalize and accumulate α–synuclein PFFs and Figure 3.6A shows this qualitatively. Thus, α–synuclein PFFs with seeding capacity have been successfully synthesised. To quantitate the number of α-synuclein puncta internalised by cells, fluorescent imaging could be used to calculate the intensity of a-synuclein pS129 puncta relative to cell area in comparison to vehicle-treated cells, in a minimum of three biological replicates.

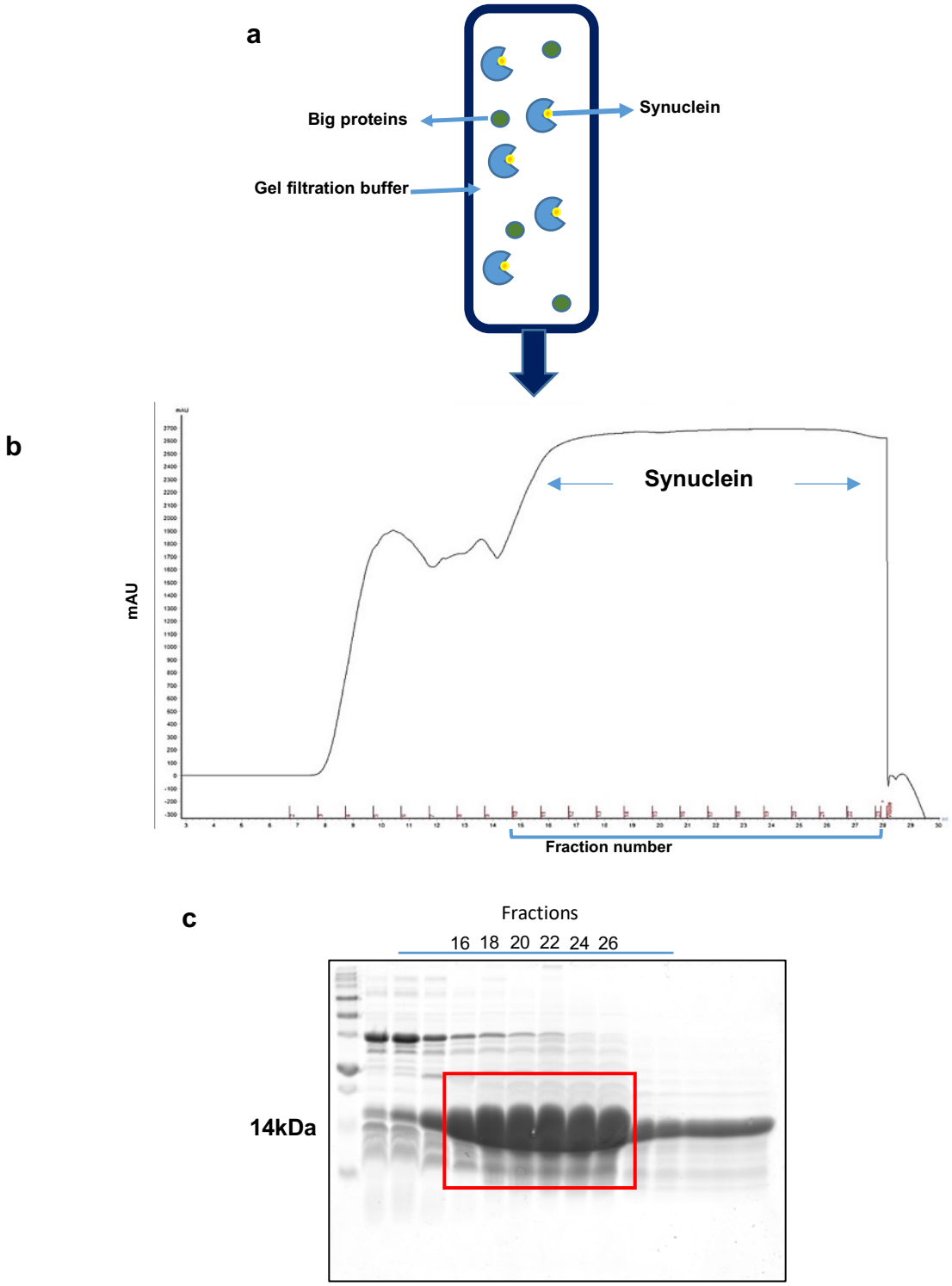

Figure 3.2 a) Schematic diagram of fast protein liquid chromatography (FPLC) column. In the first purification step, α–synuclein underwent gel filtration according to size. Larger proteins will elute first, followed by relatively small α–synuclein. **b)** Once peaks that correspond to α–synuclein were identified, the corresponding fractions were loaded onto a 4-20% gradient gel. **c)** Samples from fractions corresponding to monomeric α–synuclein in size (approximately 15 kDa). Fractions outlined by the red box were selected for input into FPLC columns for filtration according to affinity. Alternate eluted fractions from 10-28 were loaded onto gel as indicated by blue line.

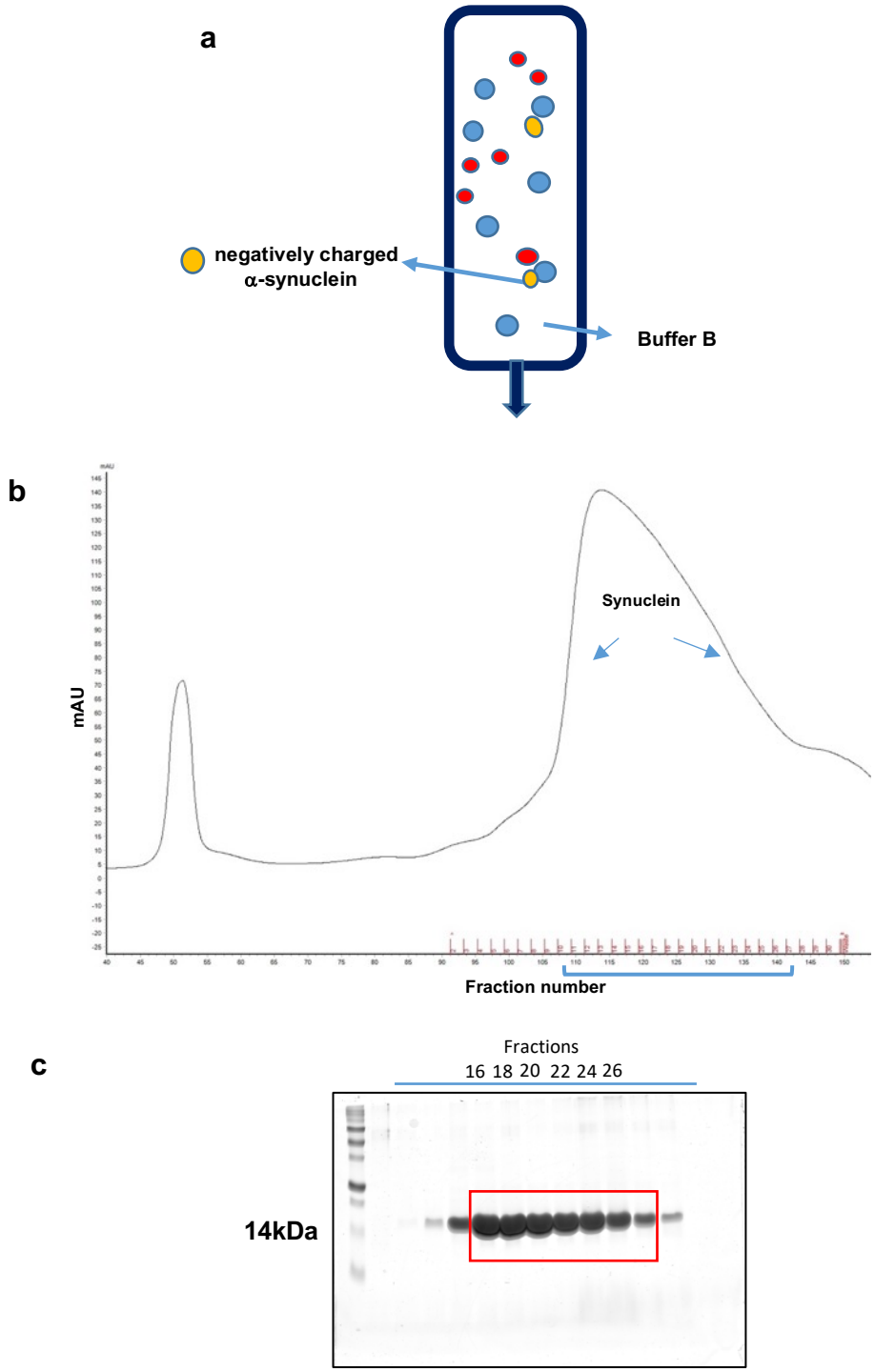

Figure 3.3 a) Schematic diagram of high performance liquid chromatography (HPLC) column. The second purification step filters α–synuclein according to charge. α–synuclein is a negatively charged protein, therefore will bind to column beads and as the buffer salt concentration increases, α–synuclein is eluted. **b**) Peaks that correspond to α–synuclein are identified and the corresponding samples are loaded onto a 4-20% gradient gel for verification. Bands that correspond to α–synuclein are then selected to input into the HPLC column for a final round to polish content. **c**) Immunoblot of α–synuclein-containing fractions, highlighted by red box. Alternate eluted fractions from 10-28 were loaded onto gel as indicated by blue line.

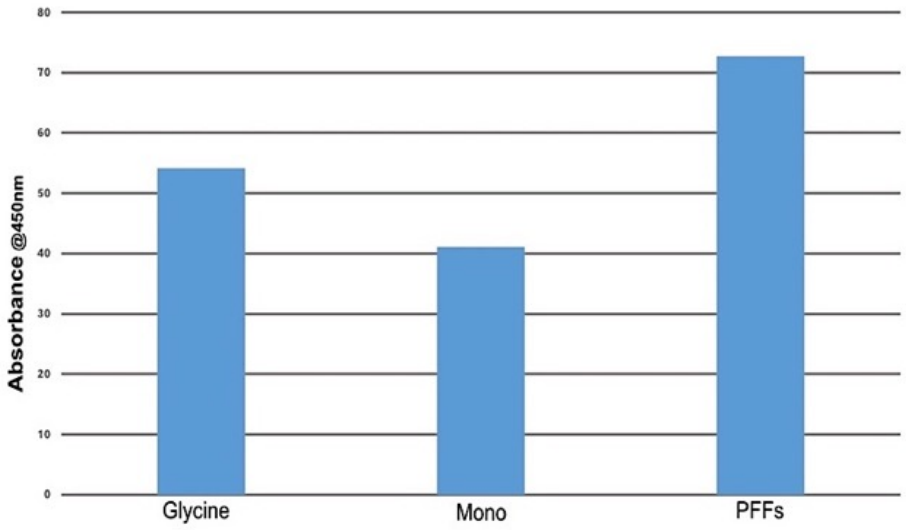

Figure 3.4 Example of ThioflavinT assay results. Graph shows absorbance at 450 nm in arbitrary units (a.u) for glycine (control), mouse α–synuclein monomers (mono), and mouse α–synuclein PFFs (PFFs), demonstrating efficient fibrillisation of α–synuclein monomers into beta-sheet containing filaments. Samples were run in triplicate.

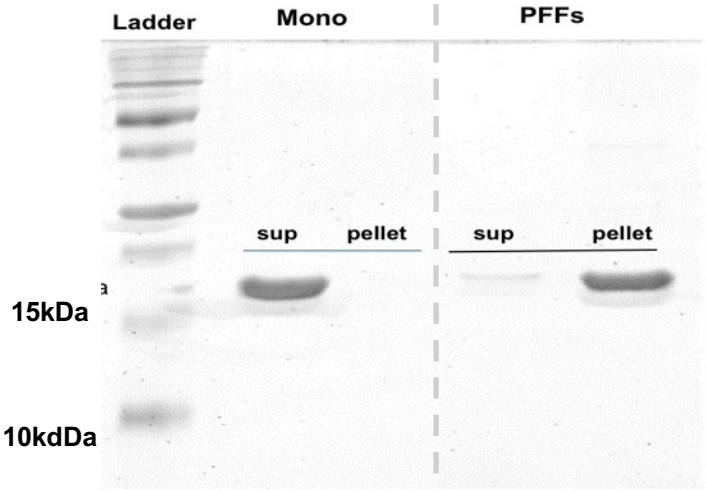

Figure 3.5 Example of a Coomassie-stained gel from a sedimentation assay. Supernatants and pellets from a sedimentation assay were electrophoresed, alongside a protein ladder. Soluble monomeric (mono) α–synuclein is mostly retained in the supernatant (sup) (15 kDa), whereas fibrillised α–synuclein (PFFs) sediments in pellets (15 kDa). Image shows two sections from the same gel.

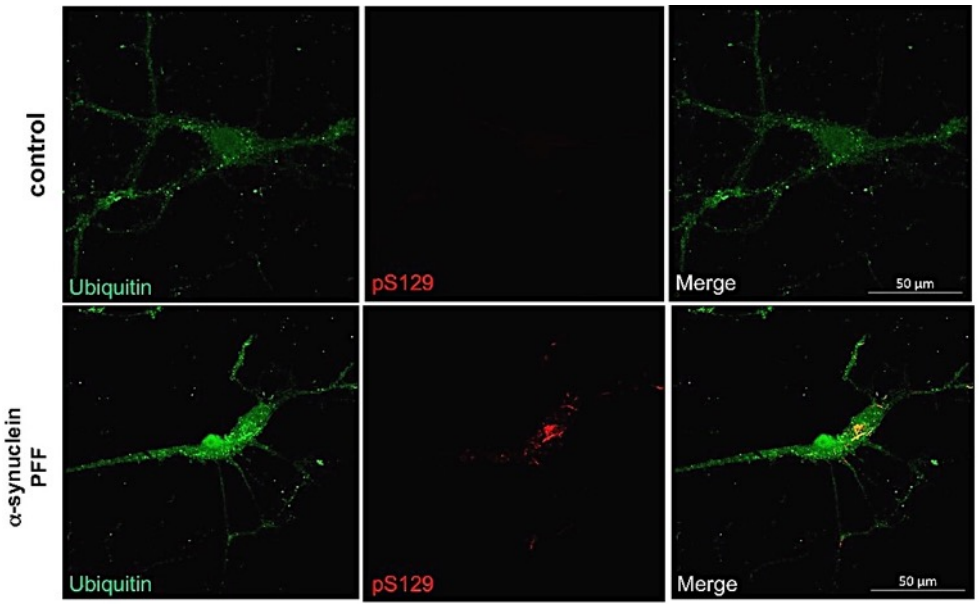

Figure 3.6 Internalisation of α–synuclein PFFs by primary cultured hippocampal neurons. Representative images of primary hippocampal neurons treated with α–synuclein PFFs or control for 14 days, fixed and immunolabelled with antibodies against α–synuclein phosphorylated at serine 129 (pS129) and ubiquitin (green). Images were obtained using a 40x oil objective on a Carl Zeiss LSM 700 confocal microscope. Scale bar is 50 µm. Accumulation of phosphorylated α–synuclein was indicated by immunoreactivity for both phosphorylated α–synuclein (pS129) and ubiquitin following addition of PFFs, but not in control cultures (no PFF treatment). Image adapted from the project thesis of final year project student, Mr Cyrus Liu, submitted in 2017.

3.5. Results: Behavioural characterisation of α–synuclein PFF-injected rats

A total of 30μg of α–synuclein PFFs at 5 μg/μL were injected unilaterally into the medial forebrain bundle (MFB) of randomly assigned SD rats aged 7-8 weeks, 230-250 g. The dosage was chosen on the basis of use in previous literature (Table 1.3) with the size of the rat brain taken into consideration, compared to a mouse brain. Due to the significant increase in structure size, the quantity of α–synuclein PFFs was adjusted as suggested by Paumier et al. (2015). Unilateral injection was chosen as this allowed assessment of spreading of α–synuclein PFFs from one side of the brain. The MFB site of injection has not previously been extensively studied. It was used as the site of injection here since it connects the nigrostriatal pathway, mesolimbic and fronto-striatal pathways and allows study of spread from the MFB bundle to anatomically connected regions that are affected in PD and that regulate executive functions. Rats were aged for 60, 90, and 120 d.p.i. Rats underwent a battery of behavioural tests prior to tissue collection to determine any consequences of presumed α–synuclein spread.

3.5.1 α–Synuclein PFFs did not affect gait imbalance on the rotarod

Firstly, to explore if injection of α–synuclein PFFs into the MFB induced any motor co-ordination deficits, the rotarod test was used. Previous work in which α–synuclein PFFs were injected into mouse dorsal striatum found a progressive motor impairment from 60 d.p.i. through to 180 d.p.i. when tested with the rotarod (Luk et al., 2012a). Using a protocol similar to that described by Luk et al. (2012), rats were trained prior to surgery at 230 g, approximately 7 weeks of age, and were then assessed at 60, 90, and 120 d.p.i.

Rotarod gives an indication of motor ability by allowing measurement of how long an animal can remain on a spinning rod. Animals with a motor impairment perform less well than healthy animals. Here, there were no significant differences between pre-post surgery for control or PFF groups at any of the time points. The results indicate that α–synuclein PFFs injected into the MFB were not sufficient to induce any motor deficits within the time frame investigated. It should be noted that technical difficulties were encountered during this experiment. The reduced latency of both control and PFF pre-treated groups at 90 d.p.i. and at 120 d.p.i. post-surgery was due to the significant increase in weight with age which meant animals were performed poorly on the rotarod test. It should be noted that rats did not receive re-training between the initial injection till the desired time-point and in hindsight it may have been beneficial for the animals to have had to re-training session to familiarise them with the rotarod procedure. Still, the significant increase in weight of the animals rendered them unable to perform on the rotarod test.

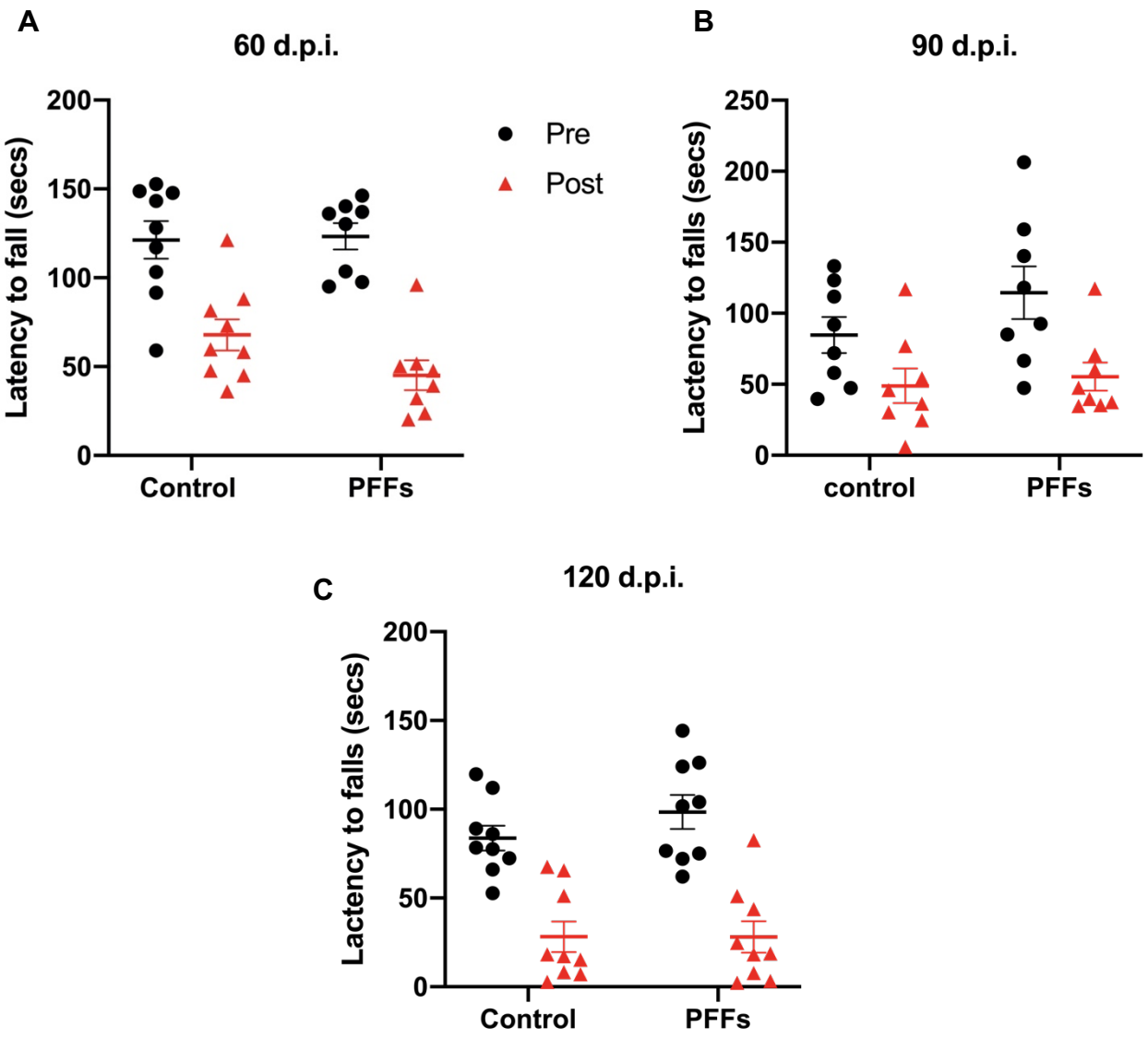

Figure 3.7. Motor function was not altered after α–synuclein PFF injections into rat MFB. A rotarod was used to determine if there are changes in motor function/gait following injection of rat MFB with α–synuclein PFFs. Rats were tested pre-surgery (pre) at 7 weeks and at 60, 90, and 120 d.p.i. (post) relative to controls. The speed of the rotarod was gradually increased from 0 rpm to 40 rpm over a 5 min period. Bar graphs show mean latency to fall (s) of total three trials for pre- and post-surgery for α–synuclein PFF and control-injected rats at **A)** 60 d.p.i. (control n = 9; PFFs n= 8) **B)** 90 d.p.i. (n = 8 for control and PFFs) and **C)** 120 d.p.i. (n = 9 or control and PFFs). Analysis with unpaired t-test on the difference between pre and post-surgery between control and PFF groups did not indicate any statistical significance for any time points.

3.5.2 A transient asymmetric deficit was observed at 90 days post injection only

In addition to rotarod, I further examined motor functions by cylinder asymmetric test. The results showed subtle reductions in the use of the contralateral forepaw in α–synuclein PFF injected rats at all time points. These were found not to be statistically significant at 60 and 120 d.p.i. but PFF injected rats showed significantly reduced contralateral forepaw usage at 90 d.p.i. relative to control group (**$p < 0.001$). Thus,α–synuclein PFFs might cause a transient motor impairment (Figure 3.8A-C).

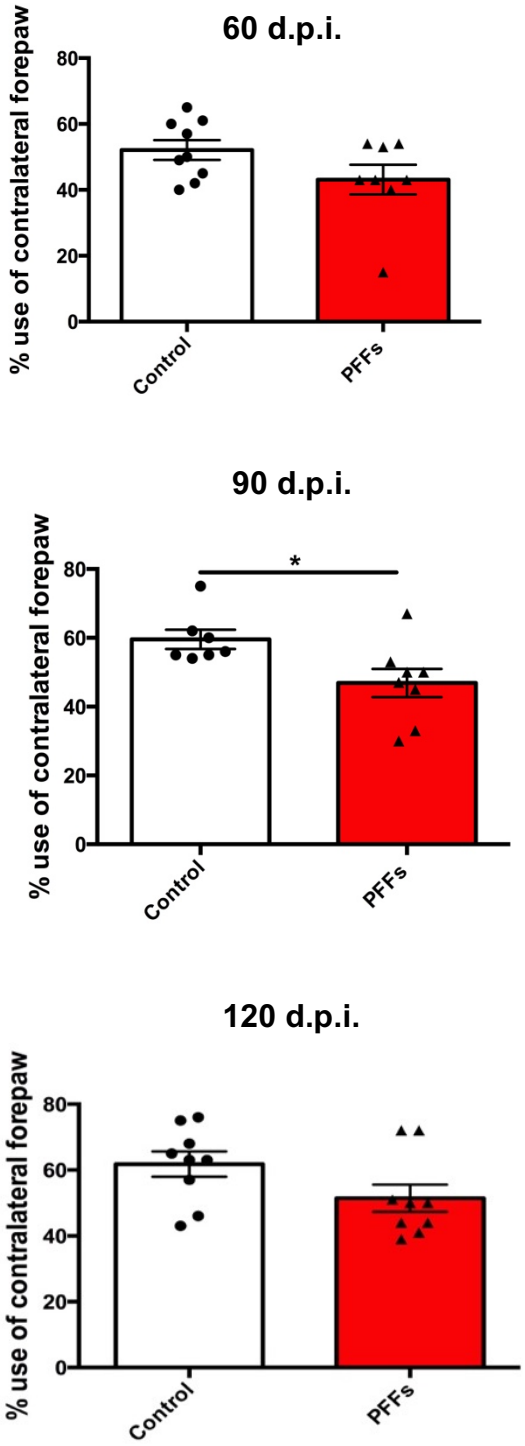

Figure 3.8. Transient asymmetric forelimb deficits in α–synuclein PFF injected rats. An asymmetric cylinder test was used to determine if there are changes in contralateral forelimb usage following injection of rat MFB with α–synuclein PFFs. Rats were tested post-surgery at 60, 90, and 120 d.p.i. Bar charts show percentage of contralateral forepaw usage at **A)** 60 d.p.i. control n = 9, PFF, n = 9, **B**) 90 d.p.i. control n = 7, PFF n = 8 and **C**) 120 d.p.i. (n = 9) Data are shown as mean ± SEM, ** $p < 0.05$*. Statistical analysis used was unpaired t-test.

3.5.3 α–Synuclein PFFs did not induce deficits in executive functions

Rats were tested according to predetermined time points with pre-established testing parameters (Table 3.1). A protocol adapted from (Horner et al., 2013) and (Mar et al., 2013), as described in Chapter 2 was used. Results from the test is shown in Figure 3.9

Executive function domain	Activity tested	Readout from 5-CSRTT
Global attention processing	Attention Spatially divided attention	Accuracy (number of correct responses)
Inhibitory control	Sensitivity	Premature responses (response before stimulus onset)
Motivation	Processing	Time taken (seconds) (time taken to complete the pre-set task)

Table 3.4. The range of executive deficits that can be tested using the 5-choice serial reaction time task (5-CSRTT). Table shows the activities used to assess the α–synuclein PFF injected and control rats, with readouts associated with specific executive functions. Stimulus was presented as an illuminated square inside the 5-choice chamber. The activities were set prior to training and testing.

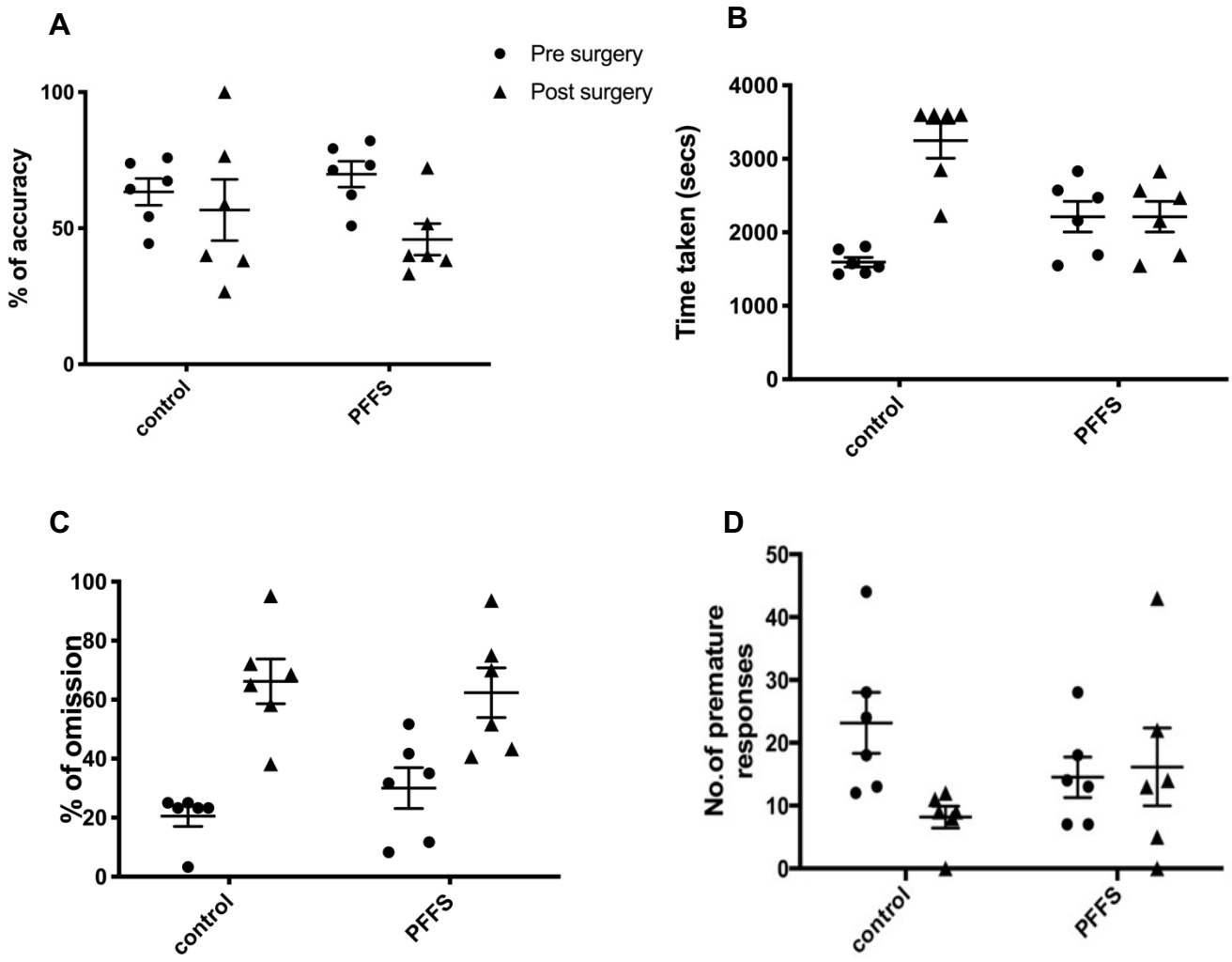

Figure 3.9. The 5-CSRTT at 90 d.p.i. as a means of assessing executive dysfunction in α–synuclein PFF injected rats. Rats were tested prior to surgery at 7-8 weeks of age (pre-surgery) and again following injection of control- or α–synuclein PFFs (post-surgery). Bar charts show **A)** percentage of accuracy during the training and testing phase for control and α–synuclein PFF injected rats. **B)** Time taken in seconds (s) during the training and testing phase for control and α–synuclein PFF injected rats. **C)** Percentage of omission during the training and testing phase for control and α–synuclein PFF injected rats. **D**) Premature responses during the training and testing phases for control and α–synuclein PFF injected rats. Analysis with unpaired t-test on the difference between pre-post-surgery for control and PFF group did not indicate a statistical significance **(A-D).**

Analysis of these measures indicated no significant effects of α–synuclein PFF relative to control at 60, 90 and 120 d.p.i. Sample data for 90 d.p.i. is shown in Figure. 3.9. There was no significant difference in task accuracy, a measure of attention, before or after surgery or between α–synuclein PFF and vehicle-treated groups (Figure 3.9A). The time taken to complete the task, which required rats to travel back and forth within their "chambers", showed slight increase after surgery (Figure 3.9B). Omission was defined as lack of response during a trial and indicates spatially divided attention and global attention. Both control and α–synuclein PFF injected animals exhibited a similar baseline reading prior to surgery, and no effect of treatment. However, there were significant differences following surgery in both PFF and control-injected rats, again indicating an effect of the surgical procedures (Figure 3.9C) or alternatively the age of the rats may also be an additional factor for the reduction in speed of completing the task particularly in control animals. Premature responses are responses detected before stimulus onset, part of inhibitory control. There were no significant changes in the number of premature responses before or after surgery, or in response to treatment (Figure 3.9D).

These data did not show any significant effect on frontal cortex-associated executive functions following α–synuclein PFF injection into rat MFB. It should, however, be noted that although the 5-choice serial reaction time task (5-CSRTT) is a very informative behaviour task, it is a very complex protocol to follow for inexperienced users. Subsequently, some technical errors meant the behavioural task would benefit from being repeated when these technical errors are able to be resolved.

3.5.4 No sustained impairment in spatial learning and memory were induced by α–synuclein PFFs

Rats were trained and tested according to a previously established protocol (You et al., 2019). Testing was conducted at previously established time points (Figure 3.10). Spatial learning of α–synuclein PFF injected and control rats was assessed throughout the 5-day training protocol, and reference memory was tested on the probe test day (6^{th} day), where the platform was removed. In the probe trial, the number of times the platform location was crossed and time spent in the target quadrant were measured. α–Synuclein PFF and control injected rats showed improvements in latency to escape the maze (time taken to find the platform) across the 5 training days. α–Synuclein PFF injected rats did not exhibit any deficits in spatial learning at 60, 90 or 120 d.p.i. relative to controls. Indeed, the control and α–synuclein PFF groups showed a similar learning curve throughout the 5-day training protocol (Figure 3.10A-C). Similarly, there were no significant differences in the number of platform crossings during the probe trial, indicating no deficits in reference memory following α–synuclein PFF injection (Figure 3.10D-F), or proportion of time spent in the target quadrant (Figure 3.10 G-I). Therefore, when injected into rat MFB α–synuclein PFFs were not sufficient to induce deficits in visuospatial learning or reference memory.

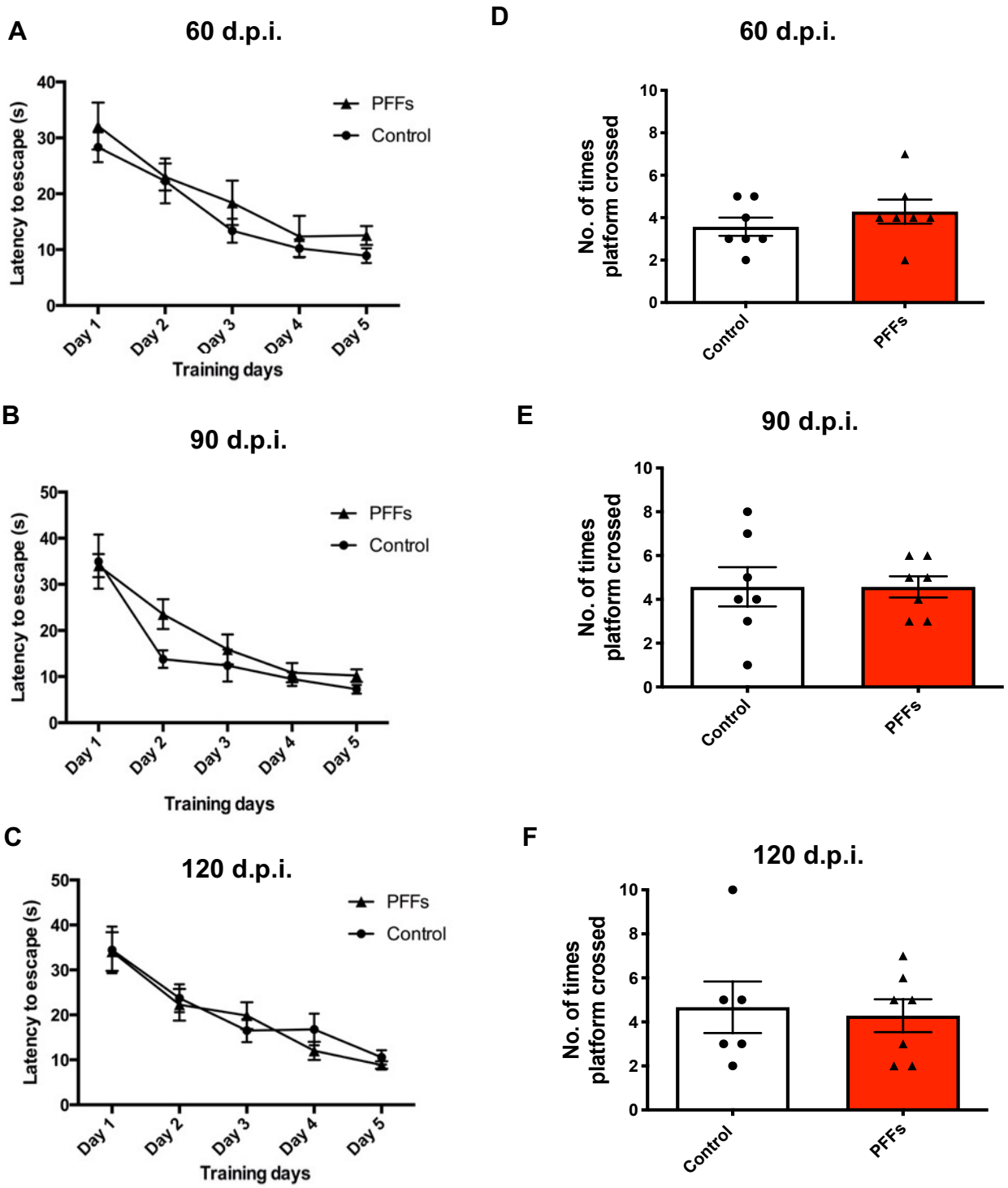
A
60 d.p.i.
Latency to escape (s)
PFFs
Control
Day 1
Day 2
Day 3
Day 4
Day 5
Training days
D
60 d.p.i.
No. of times platform crossed
Control
PFFs
B
90 d.p.i.
Latency to escape (s)
PFFs
Control
Training days
E
90 d.p.i.
No. of times platform crossed
Control
PFFs
C
120 d.p.i.
Latency to escape (s)
PFFs
Control
Training days
F
120 d.p.i.
No. of times platform crossed
Control
PFFs

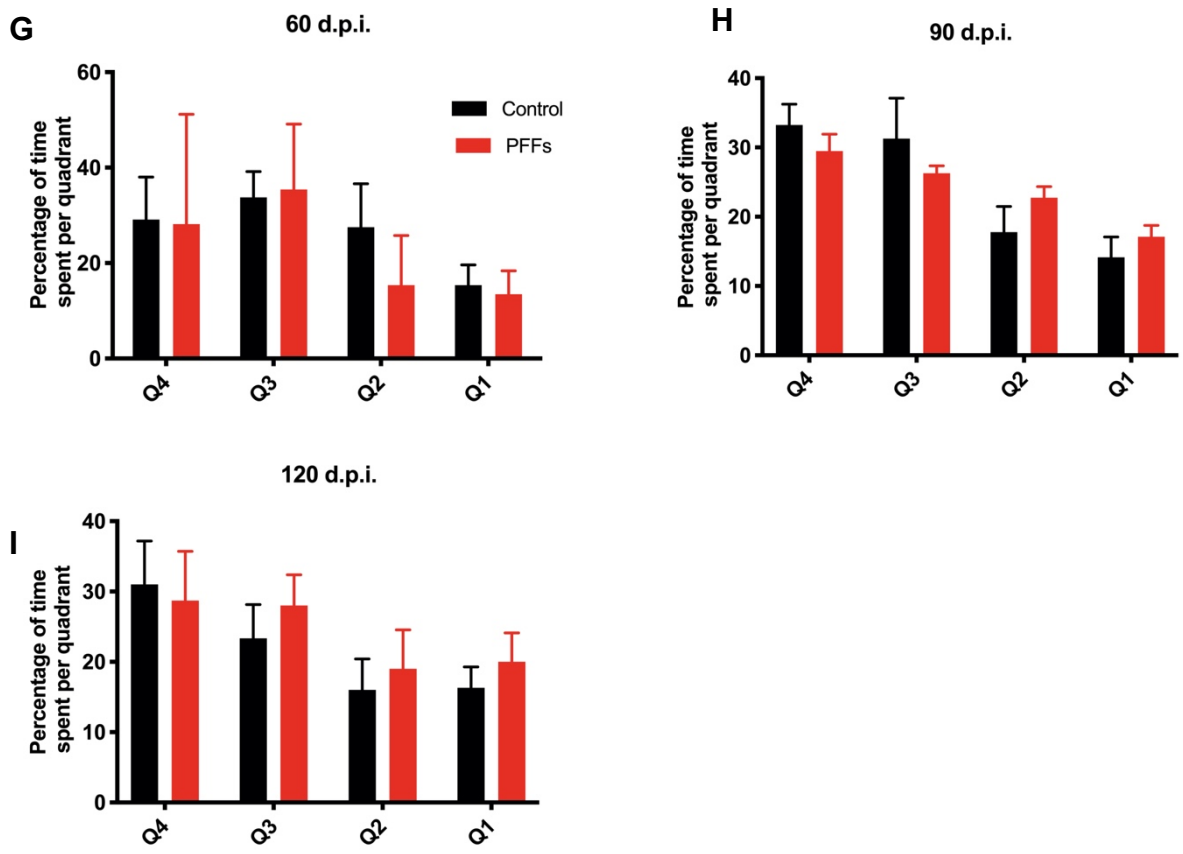

Figure 3.10. α-Synuclein PFFs did not result in cognitive impairment using the MWM task, at any of the time points investigated. The learning curve during the MWM task. Rats injected with α-synuclein PFFs at **A)** 60 d.p.i. **B)** 90 d.p.i. and **C)** 120 d.p.i. show no impairment in their learning ability on the MWM task compared to control rats as determined when the latency to escape the water maze was measured on each of the five days of training. The number of times that rats cross the area from which the platform was removed was determined as a measure of visuospatial memory during the probe test, **D)** 60 d.p.i. (n = 7), **E)** 90 d.p.i. (n = 7) or **F)** 120 d.p.i., control n = 6, PFF n = 7. **G-I)** The time spent in each quadrant during the probe trial at **G)** 60 d.p.i. (n = 7), **H)** 90 d.p.i. (n = 7) or **I)** 120 d.p.i. (control n = 6, PFF n = 7). Analysis with repeated 2-way ANOVA (A,B,C) indicated a significant effect of training days on visuospatial impairment at all time points and no effect of treatment or a training days x treatment interaction (Appendix 1). Analysis with repeated 2-way ANOVA (G,H,I) did not indicate a significant effect of training days on visuospatial impairment at all time points and no effect of treatment, surgery or a surgery x treatment interaction (Appendix 1). Analysis for (**A, B, C and G, H, I**) repeated 2-way ANOVA, unpaired t-test (**D,E,F**). Data shown as mean ± SEM.

3.5.5 α–Synuclein PFF animals did not trigger anxiety-like behaviour

Results from the open field test showed that α–synuclein PFFs did not cause any changes in anxiety-like behaviour at 60, 90, or 120 d.p.i. since 60, 90, and 120 d.p.i. control and α–synuclein PFF injected groups spent equal amounts of time within the centre zone (Figure 3.11A-C) and no significant alterations in trajectory/path (Fig. 3.11D). 120 d.p.i. animals spend a much longer period of time within the centre zone compared to 60 d.p.i. and 90 d.p.i. animals likely due to age since older animals are less anxious (Denenberg, 1969). Overall, the data suggested that α–synuclein PFFs do not induce any anxiety-like behaviour up to 120 d.p.i. in rats.

3.4.6 α–Synuclein PFFs did not result in land-based locomotor deficits

The open field test can also be used to test overall locomotion and motor activity (Chung et al., 2019). The distance travelled in 10 min was measured. The results showed that α–synuclein PFF injected rats travelled similar distances to controls at 60, 90, and 120 d.p.i. and therefore, they did not exhibit any locomotor deficit when compared to controls at any of the time points investigated (Figure 3.12A-C). The results here agree with previous studies where open field test measurements showed no significant alterations in locomotor activity caused by α–synuclein PFFs (Luk et al., 2012a; Masuda-Suzukake et al., 2013).

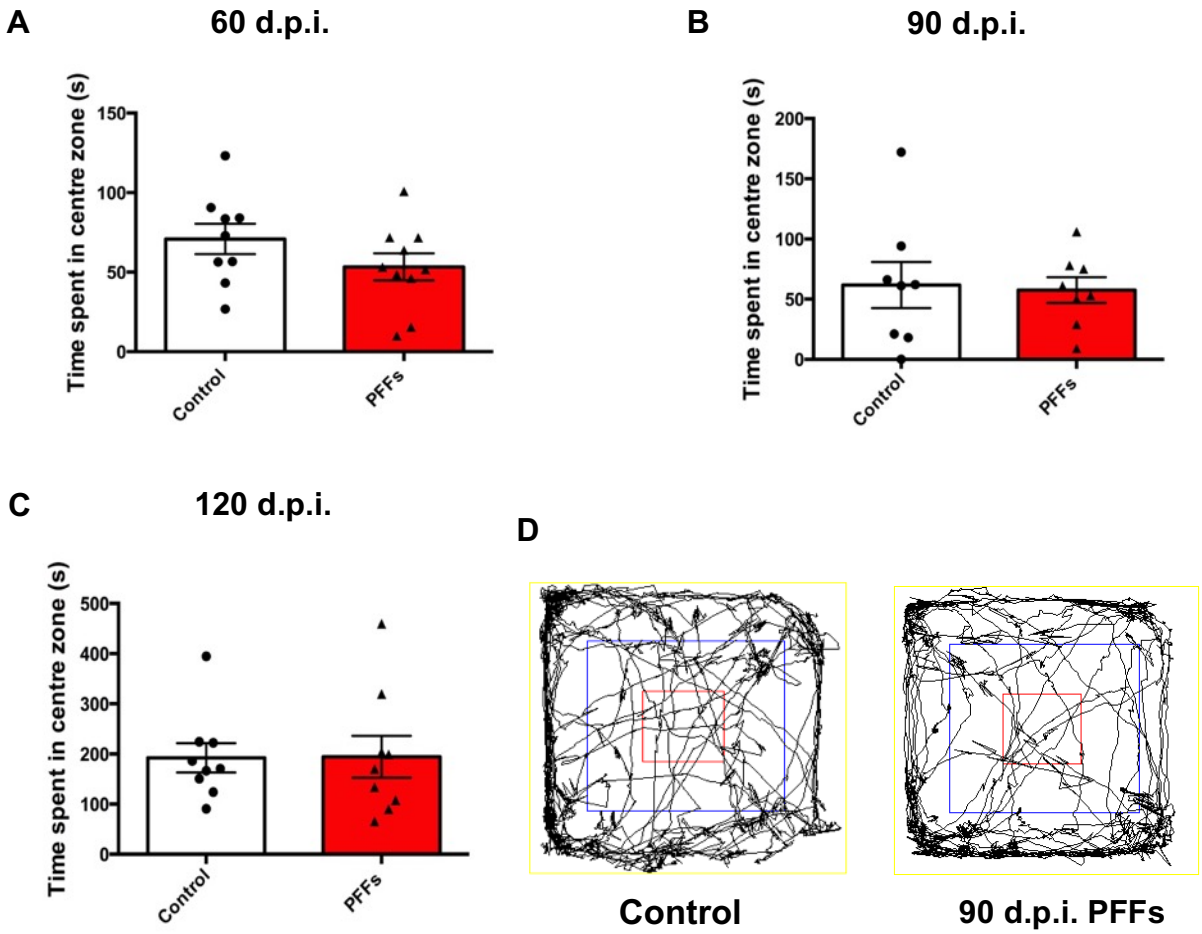

Figure 3.11. No significant alterations in anxiety-like behaviour following α-synuclein PFF injection into MFB. Open field tests were conducted to determine if control and α-synuclein PFF-injected rats show any alterations in anxiety-like behaviour. The bar-charts show the amount of time in seconds (s) spent in the centre zone for control and PFF-injected rats at **A**) 60 d.p.i., control n = 9, PFF n =10, **B**) 90 d.p.i. (n = 8), **C**) 120 d.p.i., control n = 9, PFF n = 10. Data represents mean ± SEM, statistical analysis used was two-tailed unpaired t-test. **D)** Representative tracings of the trajectory of control and α-synuclein PFF injected rats at 90 d.p.i. The centre zone is bounded by red, and the outer edge of the arena is coloured yellow. Both groups spent approximately equal amounts of time in the centre zone of the arena.

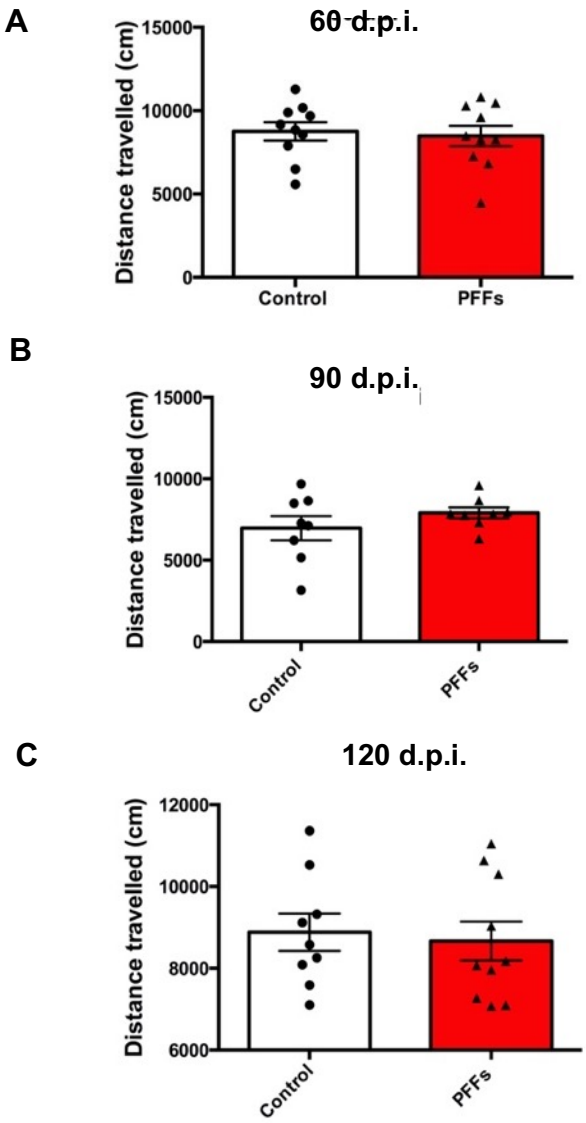

Figure 3.12. No significant alterations in locomotor activity following α-synuclein PFF injection into rat MFB. Distance travelled (cm) in 10 min by control and PFF-injected rats was measured as an indicator of locomotor activity using the open field test. Graphs show no significant difference between groups at **A)** 60 d.p.i. (n = 10), **B)** 90 d.p.i. (n = 8) and **C)** 120 d.p.i., control n = 9, PFF n = 10. Data represents mean ± SEM, statistical test used, unpaired t-test.

3.6 Results: Intracellular changes elicited by α–synuclein PFFs

Despite the lack of sustained behavioural alterations, it was unclear if any other pathological factors in neurons had been stimulated by α–synuclein PFFs. Therefore, both immunohistochemistry and biochemical techniques were used to examine change in protein solubility within the frontal cortex, specifically by examining tau and α–synuclein at the three pre-established time points. Furthermore, the spreading of phosphorylated α–synuclein into regions distant from the initial injection site and the ability to trigger changes in tau phosphorylation, was investigated. Detailed description of immunohistochemistry and the sarkosyl extraction technique can be found in Chapter 2.

3.6.1 Spreading of phosphorylated α–synuclein PFFs to anatomically connected brain regions from the MFB.

Previous publications were used to guide this work (Luk et al., 2012a; Duffy et al., 2018c). Sections throughout the brain from rats at 60, 90, and 120 d.p.i. were subjected to immunohistochemical staining using an antibody against α–synuclein phosphorylated at Ser129 (see Methods section 2.2.7.1). Sections were also briefly immersed in haematoxylin to stain cell nuclei. Positively labelled cells were apparent throughout the brain at all time points, including in the cortex, hippocampus, striatum and substantia nigra (SN). All these brain regions are either directly or indirectly connected to the MFB. The labelling was relatively mild compared to other reports (Duffy et al., 2018c; Rey et al., 2018), and displayed as faint cytoplasmic accumulations, or compact, globular perinuclear-like inclusions (Figure

3.13A). The immunolabelling appeared to be most dense at 90 d.p.i. relative to the 60 d.p.i. and 120 d.p.i. groups. No positively labelled cells were found in control-injected rats at any time point (Figure 3.13A).

A schematic diagram was created to allow visualisation of the extent of phosphorylated α–synuclein immunoreactivity at each time point throughout the brain. Immunolabelling was apparent both contralateral and ipsilateral to the injection site, in agreement with previous reports (Luk et al., 2012a; Paumier et al., 2015). This analysis showed the apparent spread of phosphorylated α–synuclein throughout most brain regions from the MFB. The number of immunoreactive cells increased from 60 d.p.i. to 90 d.p.i. after which time the load of positively labelled cells was reduced (Figure 3.13B). These data indicated that α–synuclein PFF injection into rat MFB induces prion-like spread of phosphorylated α–synuclein from the injection site. Taken together, the results also showed that the presence of abnormal α–synuclein in the hippocampus and cortex was not sufficient to induce any sustained behavioural deficits in rats.

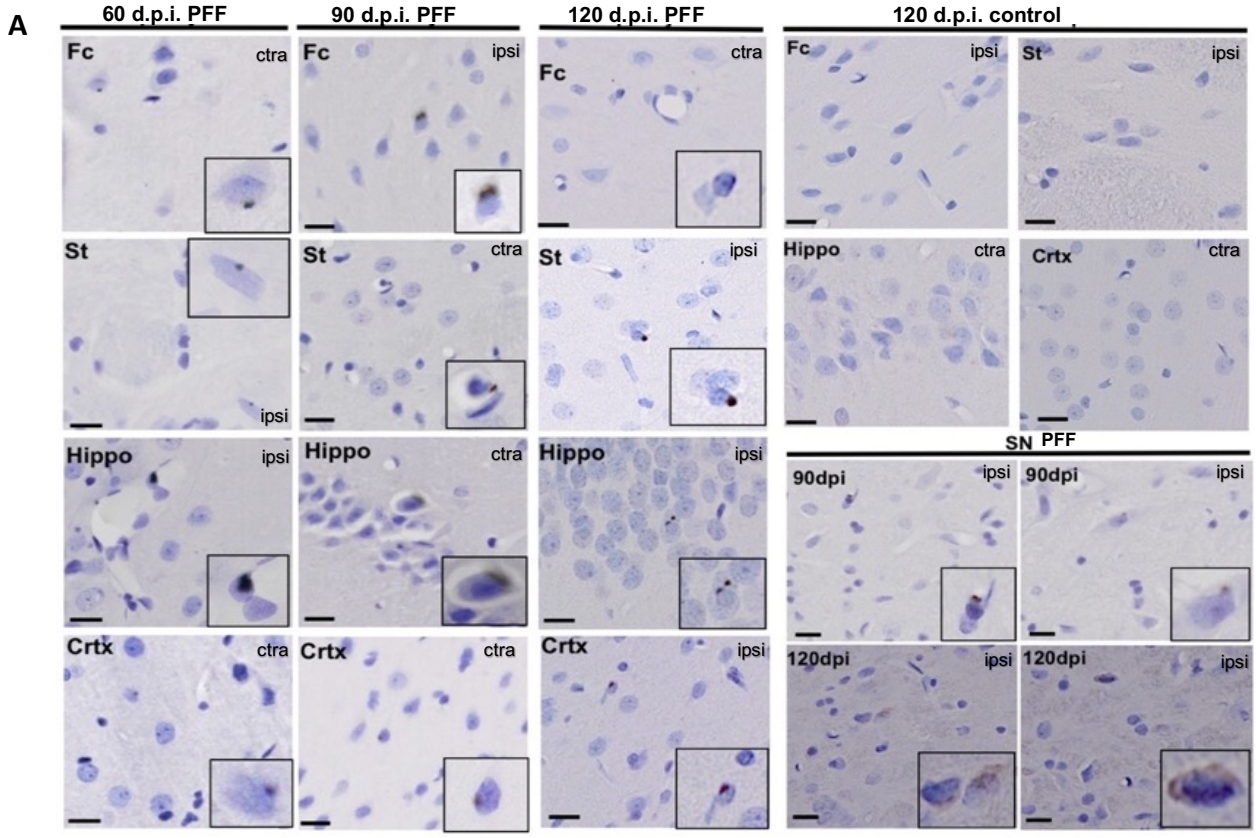
A
60 d.p.i. PFF
90 d.p.i. PFF
120 d.p.i. PFF
120 d.p.i. control
Fc
ctra
ipsi
St
Hippo
Crtx
SN PFF
90dpi
120dpi

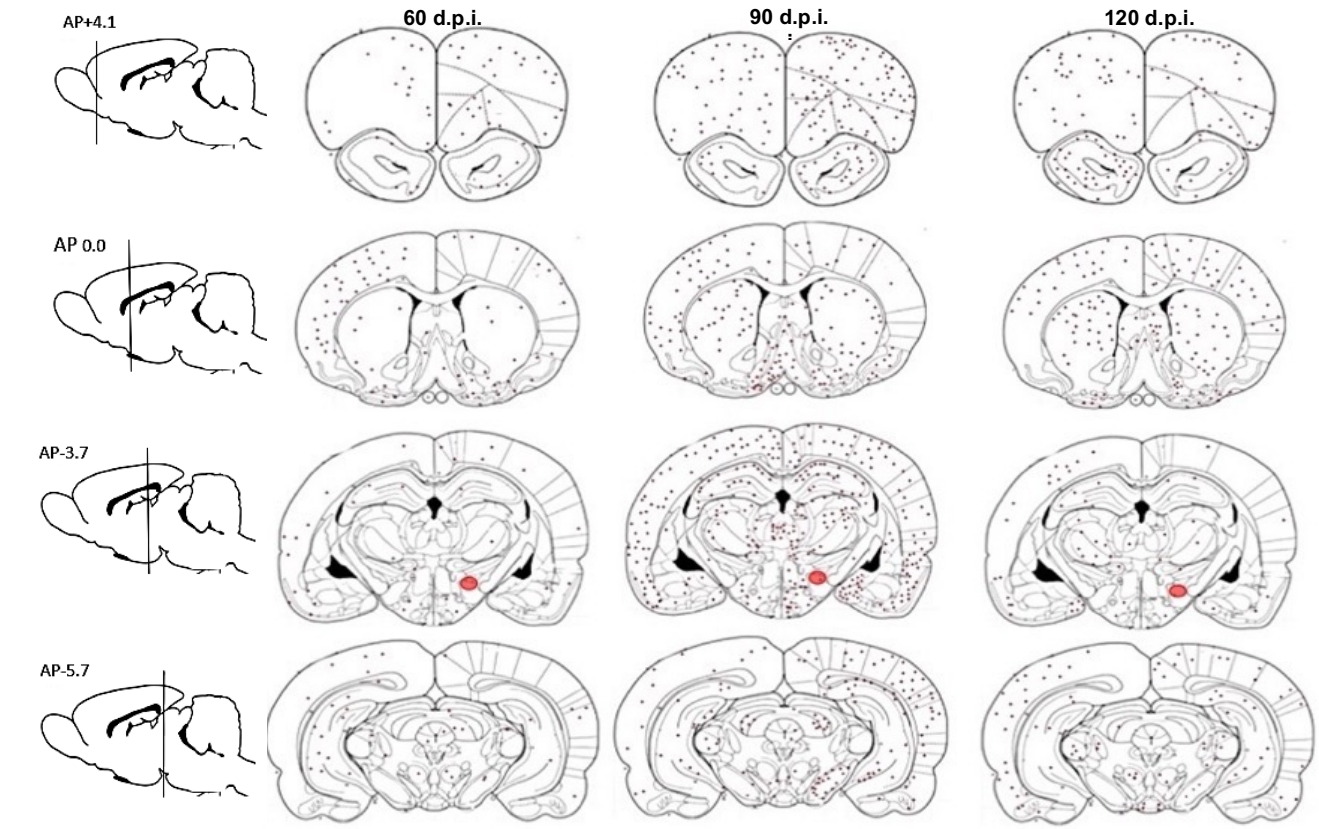
B
AP+4.1
AP 0.0
AP-3.7
AP-5.7
60 d.p.i.
90 d.p.i.
120 d.p.i.

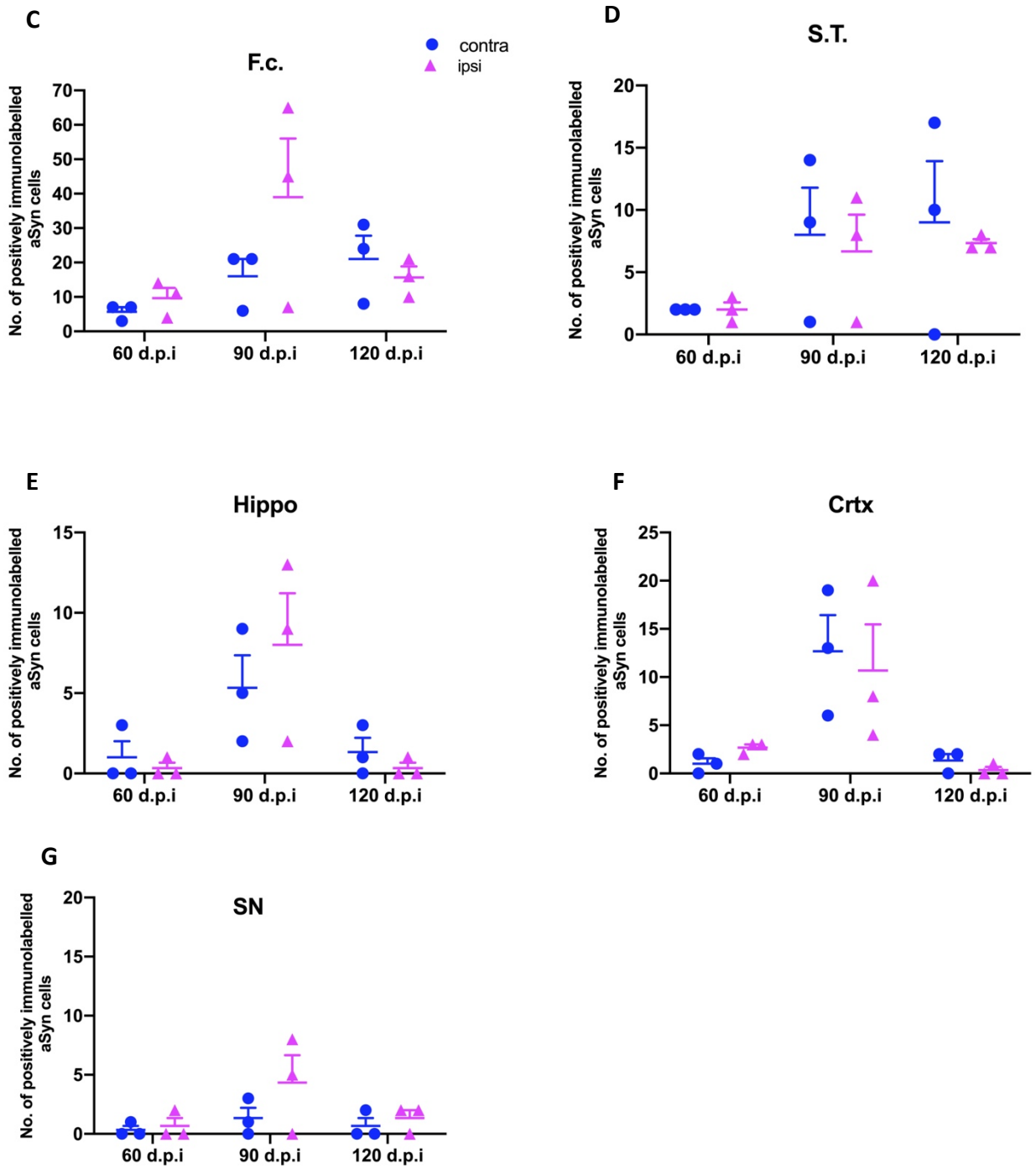
C
F.c.
contra
ipsi
No. of positively immunolabelled aSyn cells
70
60
50
40
30
20
10
0
60 d.p.i
90 d.p.i
120 d.p.i
D
S.T.
No. of positively immunolabelled aSyn cells
20
15
10
5
0
60 d.p.i
90 d.p.i
120 d.p.i
E
Hippo
No. of positively immunolabelled aSyn cells
15
10
5
0
60 d.p.i
90 d.p.i
120 d.p.i
F
Crtx
No. of positively immunolabelled aSyn cells
25
20
15
10
5
0
60 d.p.i
90 d.p.i
120 d.p.i
G
SN
No. of positively immunolabelled aSyn cells
20
15
10
5
0
60 d.p.i
90 d.p.i
120 d.p.i

Figure 3.13 Injection of α–synuclein PFFs into rat brain induced phosphorylated α–synuclein. **A)** Using a stereological approach a 1 in 20 sequence of 7 μm coronal sections was taken from the entire brain from both hemisphere, contralateral and ipsilateral of animals injected with α–synuclein PFFs for 60, 90, and 120 d.p.i. and control (vehicle) for 120 d.p.i. Representative images are shown. Sections were immunolabelled with an antibody against α–synuclein phosphorylated at Ser129 and counterstained with haematoxylin to label nuclei. Phosphorylated α–synuclein inclusions appeared as faint cytoplasmic and denser perinuclear inclusions in the frontal cortex (Fc), Striatum (St), Hippocampus (Hippo), Cortex (Crtx) and Substantia nigra (SN), and appeared to peak at 90 d.p.i. Control animals did not show any positive labelling. Scale bars = 10 μm, n = 3. **B)** The total number of positively immunolabelled cells in three animals of each group were counted and the positions marked on coronal brain tracings. Cells positive for phosphorylated α–synuclein were observed in many regions including those directly and indirectly connected to the MFB, and appeared to peak at 90 d.p.i. The red circle indicates the site of injection MFB. Regions proximal to the injection site appeared to show the most abundant phosphorylated α–synuclein positive cells. C-G) Quantification of the number of positively immunolabelled α–synuclein cell in different brain regions; Fc, St, Hippo, Crtx and SN for the three time points on both contralateral and ipsilateral hemispheres. Analysis using unpaired t-test on the difference between hemispheres did not indicate a significant effect across all time points, in any of the regions. However, there was a trend where the most abundant phosphorylated α–synuclein appeared at 90 d.p.i. Data shown as mean ± SEM, n=3.

3.5.2 Progressive reduction of dopaminergic cells in the SN after α–synuclein PFFs

α-Synuclein PFFs can induce progressive dopaminergic cell death within the SN upon intracerebral injection into the striatum (Luk et al., 2012a) (Duffy et al., 2018c). However, it is unclear whether injection of α–synuclein PFFs into the MFB can also induce death of dopaminergic cells within the SN. Therefore, using immunohistochemical methods and an antibody against tyrosine hydroxylase (TH), coronal brain sections containing the SN taken from rats at the three experimental time points, 60, 90 and 120 d.p.i., were investigated for the extent of TH cell loss within the SN. Due to technical problems, no control tissues at 60 d.p.i. were available, and an insufficient sample size meant that no comparisons between control and PFF injected rats at 90 d.p.i. could be made.

However, at 120 d.p.i., a significant reduction in the number of TH cells within the ipsilateral SN of PFF injected rats relative to controls was noted (Figure 3.14B). Lastly, although not analysed due to insufficient n number, comparison of all data suggested a time -dependent reduction in TH-expressing cells in the ipsilateral SN following α–synuclein PFF injection, whereas in the contralateral hemisphere, TH cell count remained fairly consistent across the time points (Figure 3.14C).

These findings reflect results shown by others that α–synuclein PFFs can lead to progressive dopaminergic neuron loss (Luk et al., 2012a) (Duffy et al., 2018c).

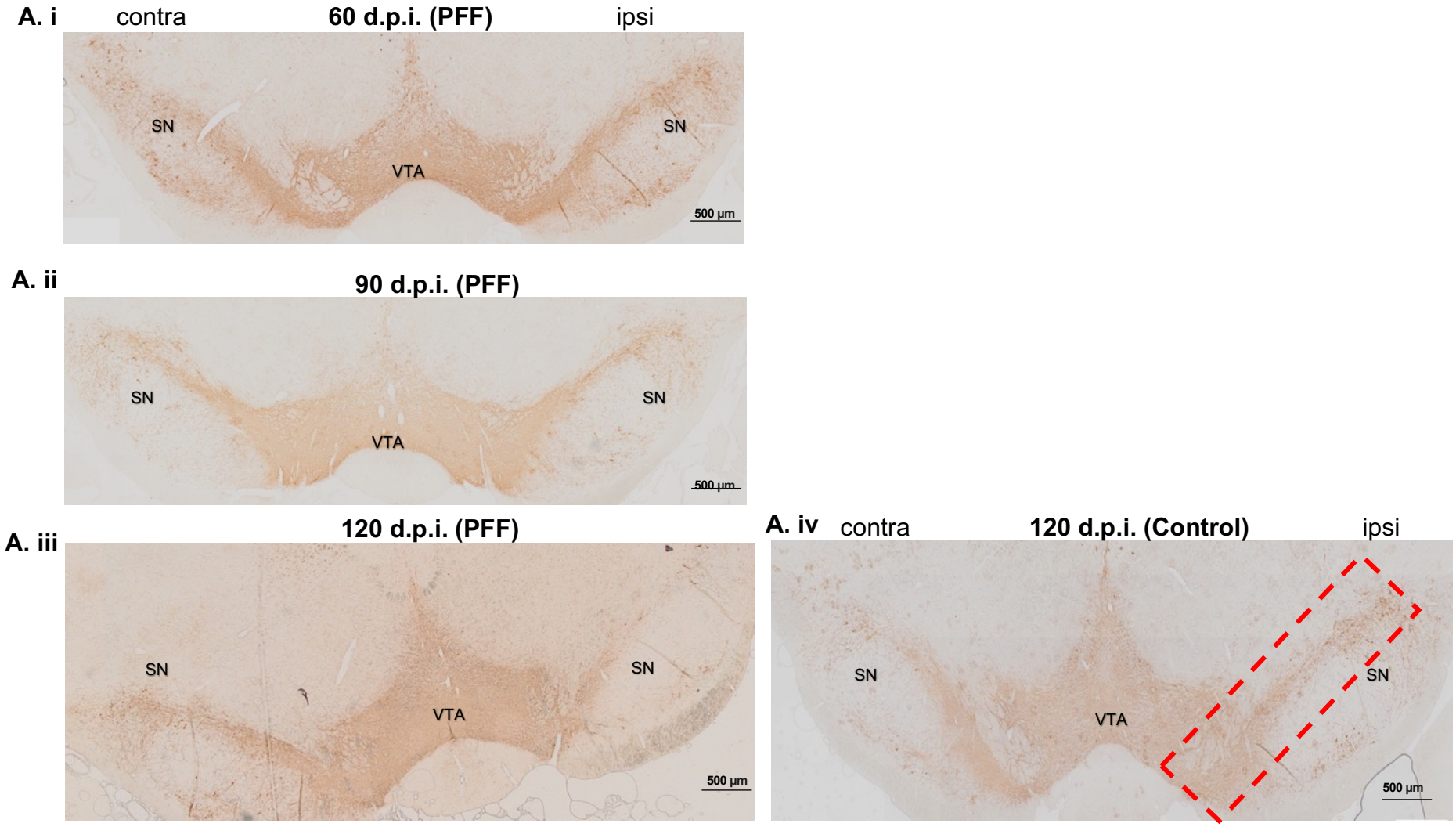
A. i
contra
60 d.p.i. (PFF)
ipsi
SN
SN
VTA
500 µm
A. ii
90 d.p.i. (PFF)
SN
SN
VTA
500 µm
A. iii
120 d.p.i. (PFF)
SN
SN
VTA
500 µm
A. iv
contra
120 d.p.i. (Control)
ipsi
SN
SN
VTA
500 µm

B

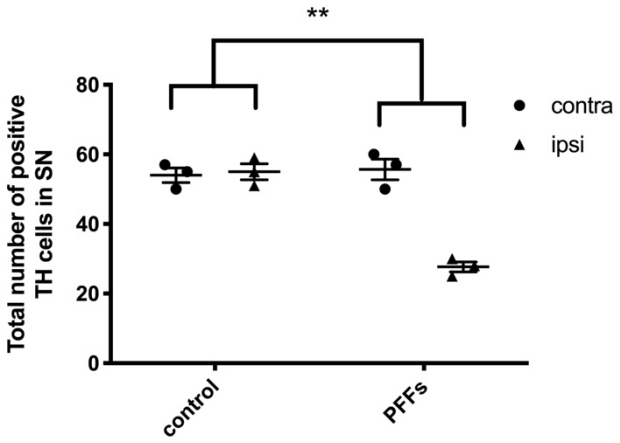

C

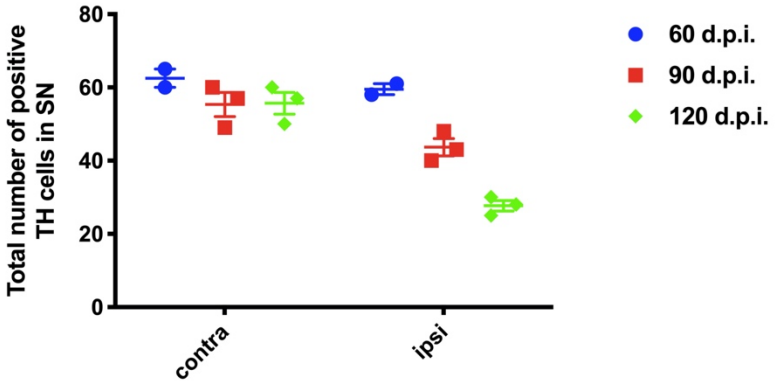

Figure 3.14 Quantification of tyrosine hydroxylase (TH) positive cells in the SN of α-synuclein PFF injected rats. **A.i-iv)** 7 µm coronal sections from control and PFF injected rats at 120 d.p.i, and PFF injected rats at 60 d.p.i, 90 d.p.i were immunolabelled using an antibody raised against TH. Representative images are shown. Red box identifies region of interest used for actual quantification **B)** Quantification of TH cell count for 120 d.p.i tissues. Analysis with unpaired t-test on the difference between pre and post-surgery showed a statistical difference between control and PFF groups. Levels of significance are denoted by *** p < 0.01.* Data shown as mean ± SEM, n=3. **C)** Preliminary data showing TH-positive cell counts in the SN of PFF-injected rats at 60 d.p.i (n= 2), 90 d.p.i (n= 3) and 120 d.p.i (n= 3), showing a trend of reduced number of TH-positive cells in the ipsilateral SN with increasing time post-injection. TH-positive cell numbers remained consistent across the three time points in the contralateral hemisphere. Statistical analysis was not performed due to insufficient n number. Scale bar is 500 µm.

3.6.3 α–Synuclein PFFs did not lead to major changes in α–synuclein solubility

To gain a better understanding of changes to endogenous α–synuclein induced by α–synuclein PFFs, biochemical techniques were employed to explore changes in protein solubility. Many neurodegenerative disorders are characterized by the gradual accumulation of detergent-insoluble protein aggregates in the brain (Diner et al., 2017; Haass and Selkoe, 2007). The aggregates consist of amyloid fibers composed of repeating units of misfolded proteins (Haass and Selkoe, 2007; Taylor et al., 2002) (Diner et al., 2017). There has been much controversy in the field about which "species" of neurodegenerative disease-associated proteins are most toxic, ranging from monomers, dimers, oligomers, soluble and insoluble aggregates and fibrils (Jucker and Walker, 2013). Biochemical approaches can be used to isolate different types of protein on the basis of their insolubility in high salt conditions or in the presence of detergents.

Brain regions were homogenised according to the method described in Chapter 2, Section 2.2.8 to yield HS, Tx, SS and SI fractions. Postmortem control and PDD brain were processed in parallel for comparison. Samples were then immunoblotted using an antibody against α–synuclein (Figure 3.15A). To detect any changes in total α–synuclein, HS, Tx, SS and SI fractions from α–synuclein PFF injected and control rats were immunoblotted at each of the 3 time points (60 d.p.i., 90 d.p.i. and 120 d.p.i.).

From Figure 3.15A, it appeared that α–synuclein monomers were present in all of the fractions from the ipsilateral α–synuclein PFF injected, frontal cortex region at 120 d.p.i. and in the HS, Tx and SS of the human control sample, but only within the HS and Tx sample of the PDD sample. Only the contralateral hemisphere SI fraction was shown for the rat sample

as it was not expected that contralateral hemisphere would develop insoluble material given that that such low amount of insoluble material was present in the injected hemisphere. Some oligomers were detected within the HS fraction of α–synuclein PFF injected rats, human control and PDD sample. Surprisingly, there was no oligomeric α–synuclein detected within the Tx, SI or SS fraction of the PDD sample. This is likely due to the individual variability of the case as the amount of monomers, oligomers and aggregated α–synuclein are reflective of the LB burden (Bandopadhyay, 2016). The total α–synuclein protein content in the brains of control PBS injected and α–synuclein PFF injected rats at all 3 time points were compared. No notable differences were observed between control and PFF injected group at any of the time points (Figure 3.15B). A band for monomeric α–synuclein was detected in both HS and Tx fraction at 60 d.p.i. but by 90 d.p.i. it seemed that small amounts of monomeric α–synuclein were also detected within the SS fraction. The band intensity within the SS fraction was further increased by 120 d.p.i. for both control and PFF injected rats. The changes observed were similar for control and PFF injected rats; and therefore, there appeared to be no effect of PFF injection on global α–synuclein solubility.

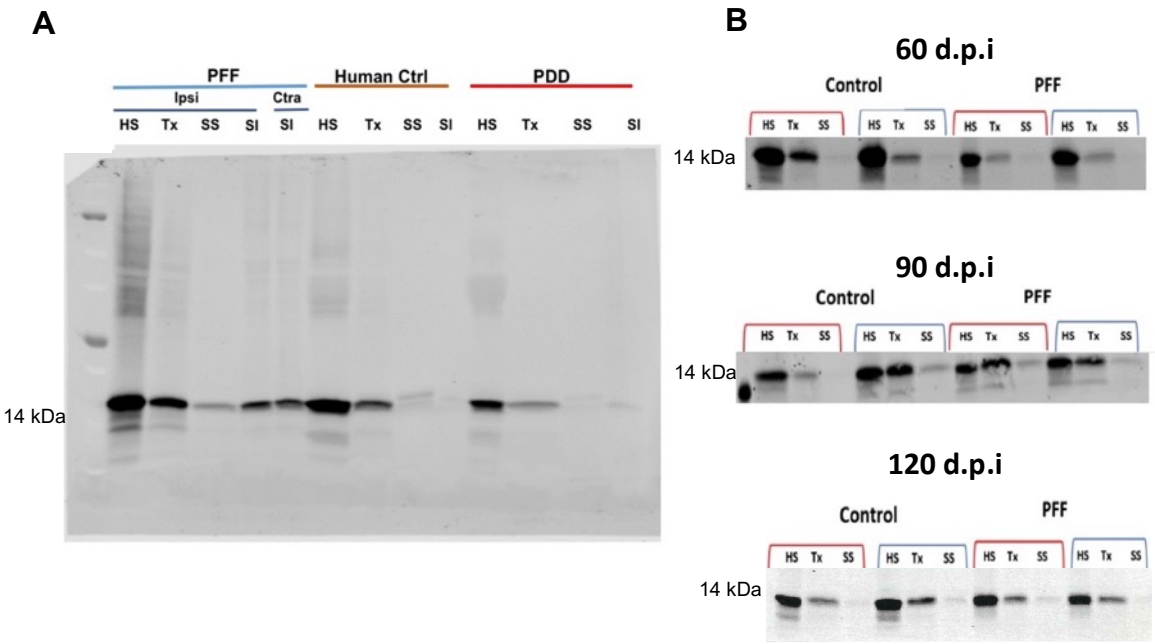
A
PFF
Ipsi
Ctra
Human Ctrl
PDD
HS Tx SS SI SI HS Tx SS SI HS Tx SS SI
14 kDa
B
60 d.p.i
Control
PFF
14 kDa
90 d.p.i
Control
PFF
14 kDa
120 d.p.i
Control
PFF
14 kDa

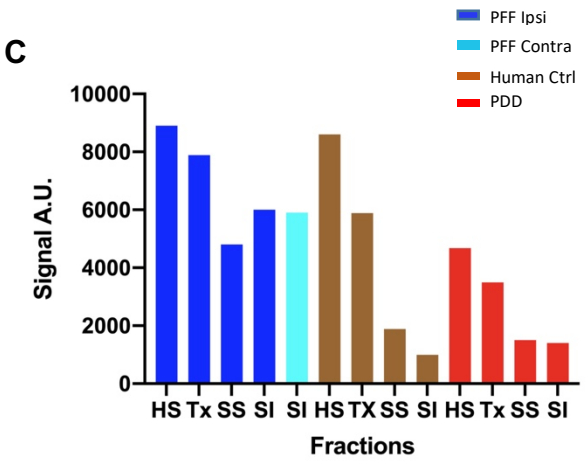
C
PFF Ipsi
PFF Contra
Human Ctrl
PDD
Signal A.U.
10000
8000
6000
4000
2000
0
HS Tx SS SI SI HS TX SS SI HS Tx SS SI
Fractions

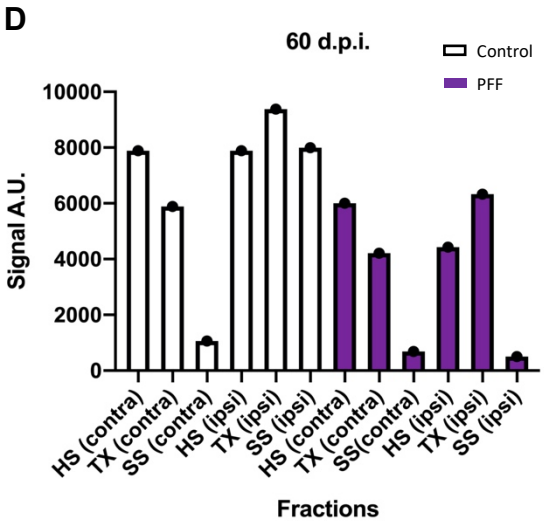
D
60 d.p.i.
Control
PFF
Signal A.U.
10000
8000
6000
4000
2000
0
HS (contra)
TX (contra)
SS (contra)
HS (ipsi)
TX (ipsi)
SS (ipsi)
HS (contra)
TX (contra)
SS(contra)
HS (ipsi)
TX (ipsi)
SS (ipsi)
Fractions

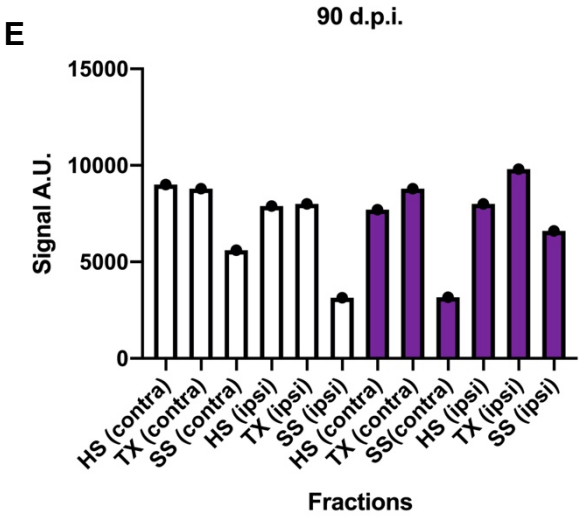
E
90 d.p.i.
Signal A.U.
15000
10000
5000
0
HS (contra)
TX (contra)
SS (contra)
HS (ipsi)
TX (ipsi)
SS (ipsi)
HS (contra)
TX (contra)
SS(contra)
HS (ipsi)
TX (ipsi)
SS (ipsi)
Fractions

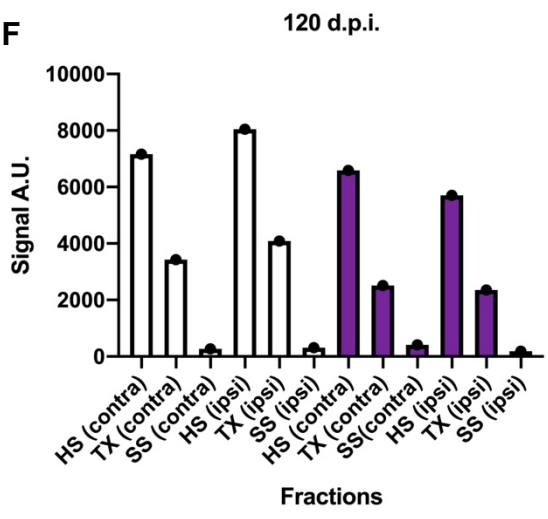
F
120 d.p.i.
Signal A.U.
10000
8000
6000
4000
2000
0
HS (contra)
TX (contra)
SS (contra)
HS (ipsi)
TX (ipsi)
SS (ipsi)
HS (contra)
TX (contra)
SS(contra)
HS (ipsi)
TX (ipsi)
SS (ipsi)
Fractions

Figure 3.15. α–Synuclein PFFs did not induce changes in α–synuclein solubility. **A)** ipsilateral and contralateral frontal cortex of a 120 d.p.i. PFF injected rat, postmortem control and PDD brain were biochemically fractionated to yield high salt (HS), high salt-triton (Tx), and sarkosyl –soluble (SS) and sarkosyl insoluble (SI) fractions. Samples were immunoblotted with an antibody against total α–synuclein (19 kDa). Dark blue lines indicate the hemisphere from the PFF injected rat, ipsi = ipsilateral and ctra = contralateral. **B)** Frontal cortex from contralateral (indicted by red lines) and ipsilateral (indicated by blue lines) hemispheres of control- and α–synuclein PFF injected rats at **B)** 60 d.p.i. **C)** 90 d.p.i. and **D)** 120 d.p.i. were also immunoblotted with an antibody against total α–synuclein. The α–Synuclein content was mostly within the HS and HS-Tx fraction at 60 d.p.i. and progressively increased into the SS fraction from 90 d.p.i. to 120 d.p.i. **C-F)** Quantification of the immunoblots to show the intensity of each fraction for **C)** α-synuclein PPFF injected animals, human post mortem samples and PDD case, **D-F)** show quantification of 60 d.p.i to 120 d.p.i respectively. Due to insufficient *n number* statistical analysis was not performed.

3.6.4. α–Synuclein PFFs did not cause marked alterations in tau protein solubility

Oligomers composed of one misfolded protein capable of promoting the aggregation of another protein is referred to as "cross-seeding" (Morales et al., 2013). When exogenous α–synuclein PFFs were used to promote the aggregation of endogenous α–synuclein, distinct strains of synthetic α–synuclein PFFs were discovered. Different strains were shown to exhibit differential cross-seeding ability with tau in both primary neuron cultures and PS19 mice (Guo et al., 2013).

Since abnormal (phosphorylated) α–synuclein was found to accumulate in rat brain following α–synuclein PFF injection, it was important to determine if this resulted in changes to tau proteins. Tau is normally a highly soluble protein, but it becomes hyperphosphorylated and aggregates in Alzheimer's disease (AD) and related tauopathies (Guo et al., 2017) (Simic et al., 2016). Solubility of tau was therefore examined in the same fractions as described above for α–synuclein.

Tau exists as six major isoforms in human and rat brain, ranging from approximately 46-68 kDa (Guo et al., 2017). Tau bands, detected following immunoblotting with an antibody that detects total (phosphorylated and non-phosphorylated) tau, were apparent primarily in the high salt and high salt-triton fractions (HS) in control rat brain, control and Parkinson's disease dementia (PDD) human brain. This is to be expected since the majority of tau proteins in physiological conditions are soluble. Only trace amounts of tau were visible in the sarkosyl-soluble and sarkosyl-insoluble fractions of all tissues, the latter suggesting that tau aggregation was limited in these samples (Figure 3.16A).

The frontal cortex from the contralateral and ipsilateral hemispheres of α–synuclein PFF and control-injected rats at 60, 90, and 120 d.p.i. were next examined by immunoblotting with the same tau antibody. For these samples, no tau was found in the sarkosyl-insoluble (SI) fraction (data not shown) and therefore only the HS, high salt-Triton (Tx) and sarkosyl-soluble (SS) fractions were shown. No apparent differences in tau amounts in the different fractions between hemisphere, or with treatment (Figure 3.16B-D) were noted. These data indicate that injecting α–synuclein PFF into the MFB did not induce any major changes in either α–synuclein or tau solubility.

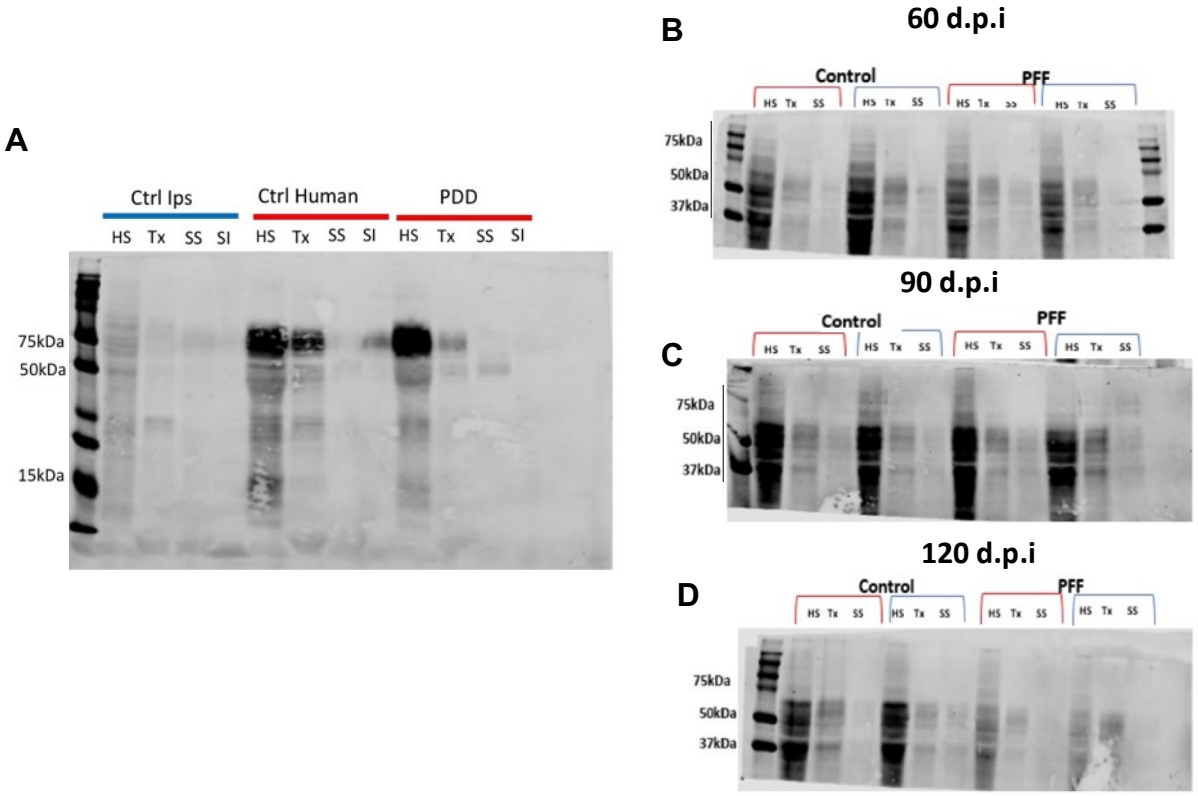
A
Ctrl Ips
Ctrl Human
PDD
HS Tx SS SI HS Tx SS SI HS Tx SS SI
75kDa
50kDa
15kDa
B
60 d.p.i
Control
PFF
HS Tx SS HS Tx SS HS Tx SS HS Tx SS
75kDa
50kDa
37kDa
C
90 d.p.i
Control
PFF
HS Tx SS HS Tx SS HS Tx SS HS Tx SS
75kDa
50kDa
37kDa
D
120 d.p.i
Control
PFF
HS Tx SS HS Tx SS HS Tx SS HS Tx SS
75kDa
50kDa
37kDa

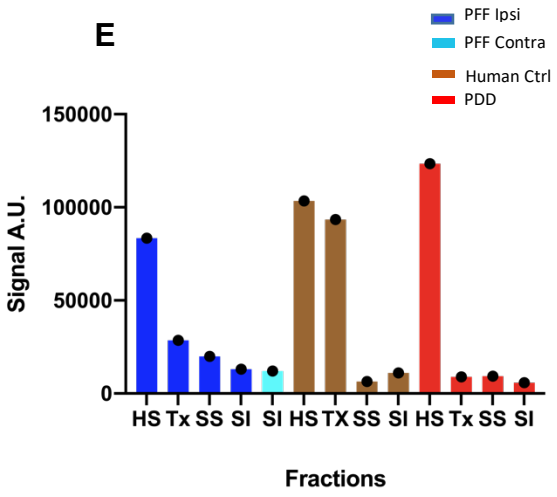
E
PFF Ipsi
PFF Contra
Human Ctrl
PDD
Signal A.U.
150000
100000
50000
0
HS Tx SS SI SI HS TX SS SI HS Tx SS SI
Fractions

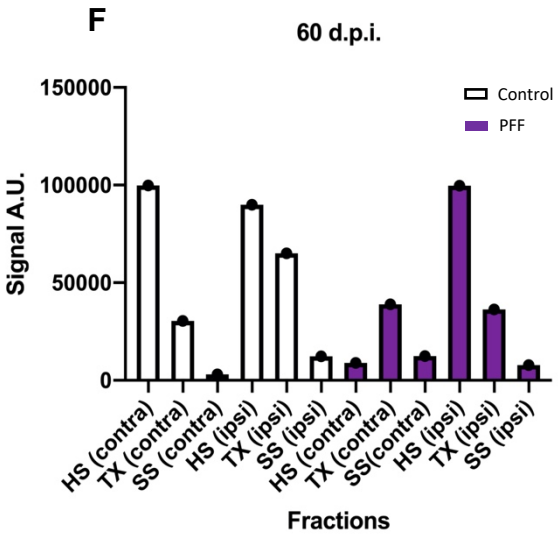
F
60 d.p.i.
Control
PFF
Signal A.U.
150000
100000
50000
0
HS (contra)
TX (contra)
SS (contra)
HS (ipsi)
TX (ipsi)
SS (ipsi)
HS (contra)
TX (contra)
SS(contra)
HS (ipsi)
TX (ipsi)
SS (ipsi)
Fractions

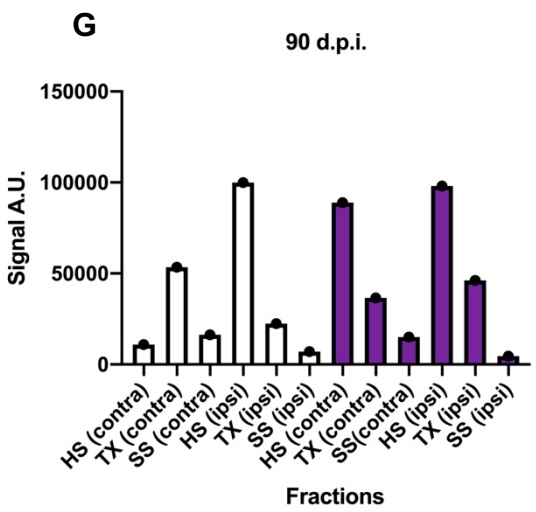
G
90 d.p.i.
Signal A.U.
150000
100000
50000
0
HS (contra)
TX (contra)
SS (contra)
HS (ipsi)
TX (ipsi)
SS (ipsi)
HS (contra)
TX (contra)
SS(contra)
HS (ipsi)
TX (ipsi)
SS (ipsi)
Fractions

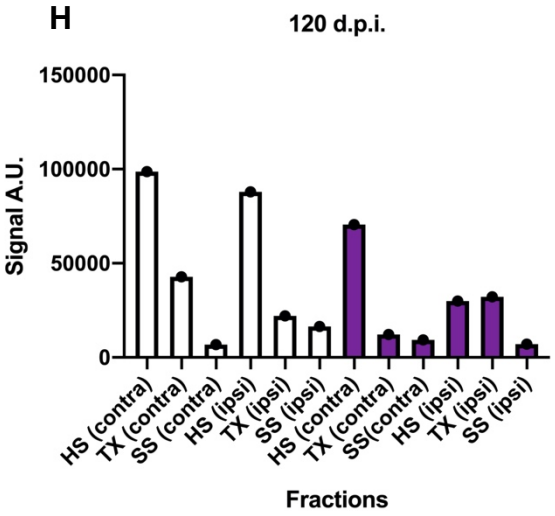
H
120 d.p.i.
Signal A.U.
150000
100000
50000
0
HS (contra)
TX (contra)
SS (contra)
HS (ipsi)
TX (ipsi)
SS (ipsi)
HS (contra)
TX (contra)
SS(contra)
HS (ipsi)
TX (ipsi)
SS (ipsi)
Fractions

Figure 3.16. Injection of α–synuclein PFFs into rat MFB did not cause changes in tau solubility. **A)** ipsilateral frontal cortex of a control-injected rat, postmortem control and PDD brain were biochemically fractionated to yield high salt (HS), high salt-triton (Tx), sarkosyl (SS)-soluble, and sarkosyl-insoluble (SI) fractions. Samples were immunoblotted with an antibody against total tau (46 - 68 kDa). Frontal cortex from contralateral (indicted by red lines) and ipsilateral (indicated by blue lines) hemispheres of control- and α–synuclein PFF-injected rats at **B)** 60 d.p.i. **C)** 90 d.p.i. and **D)** 120 d.p.i. were also immunoblotted with an antibody against total tau. The majority of the tau content was observed in the HS fraction and the HS-Tx fraction. **E-H)** Quantification tau in corresponding immunoblots after α-synuclein PFF and control injected animals. **E)** PFF, human and PDD samples, **F)** 60 d.p.i, **G)** 90 d.p.i., **H)** 120 d.p.i. Due to insufficient *n number,* statistical analysis was not performed.

3.6.5 α–Synuclein PFF injections in rat MFB did not lead to increase in phosphorylated tau-immunoreactivity throughout the brain

Results from immunoblots showed that total tau protein was not significantly altered due to α–synuclein PFFs. To investigate if there was any change in phosphorylated tau, I used immunohistochemical methods to detect different epitopes of phosphorylated tau. Immunohistochemical staining reflected the results from immunoblots and minimal immunoreactivity was detected in α–synuclein PFF injected and control brains (Figure 3.17A, B). This is not unexpected, as despite profound evidence of a synergistic relationship between α–synuclein and tau in Lewy body dementias (LBD) (Irwin and Hurtig, 2018; Moussaud et al., 2014; Vasili et al., 2019), tau pathology has only been observed in very few studies within animal models of PD (Haggerty et al., 2011). Induction of tau phosphorylation is dependant due to both the strain of α–synuclein PFFs (Guo et al., 2013) and model system. Stereotaxic injection of α–synuclein PFFs into WT mice did not trigger changes in tau phosphorylation (Bassil et al., 2020), therefore it is not expected for tau to be phosphorylated within this model, firstly given the short timepoint investigated and the mild synuclein pathology observed across all time points thus only an *n= 1* was performed. In contrast, α–synuclein PFFs can facilitate the spreading of other pathological proteins such as β-amyloid peptide (Aβ) (Bassil et al., 2020). Subsequently, using immunohistochemistry with antibodies against phosphorylated tau at various epitopes (pS404; PHF1: pS396/404), no substantial immunoreactivity for either epitope was noted within the frontal cortex or hippocampus of α–synuclein PFF and control-injected groups at 90 d.p.i. However, it would be beneficial to have additional studies to confirm this.

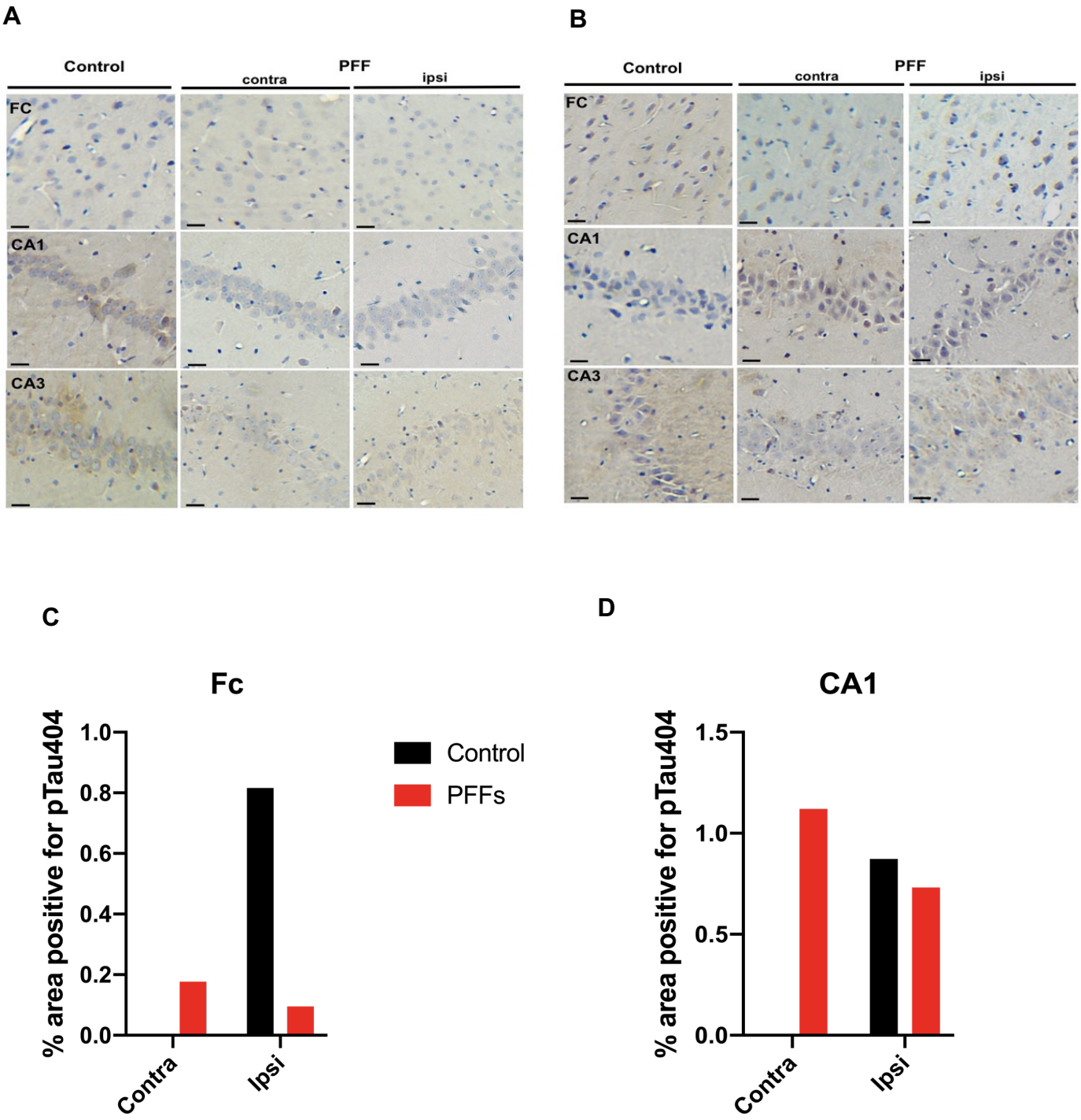
A
Control
PFF
contra
ipsi
FC
CA1
CA3
B
Control
PFF
contra
ipsi
FC
CA1
CA3
C
Fc
% area positive for pTau404
1.0
0.8
0.6
0.4
0.2
0.0
Contra
Ipsi
Control
PFFs
D
CA1
% area positive for pTau404
1.5
1.0
0.5
0.0
Contra
Ipsi

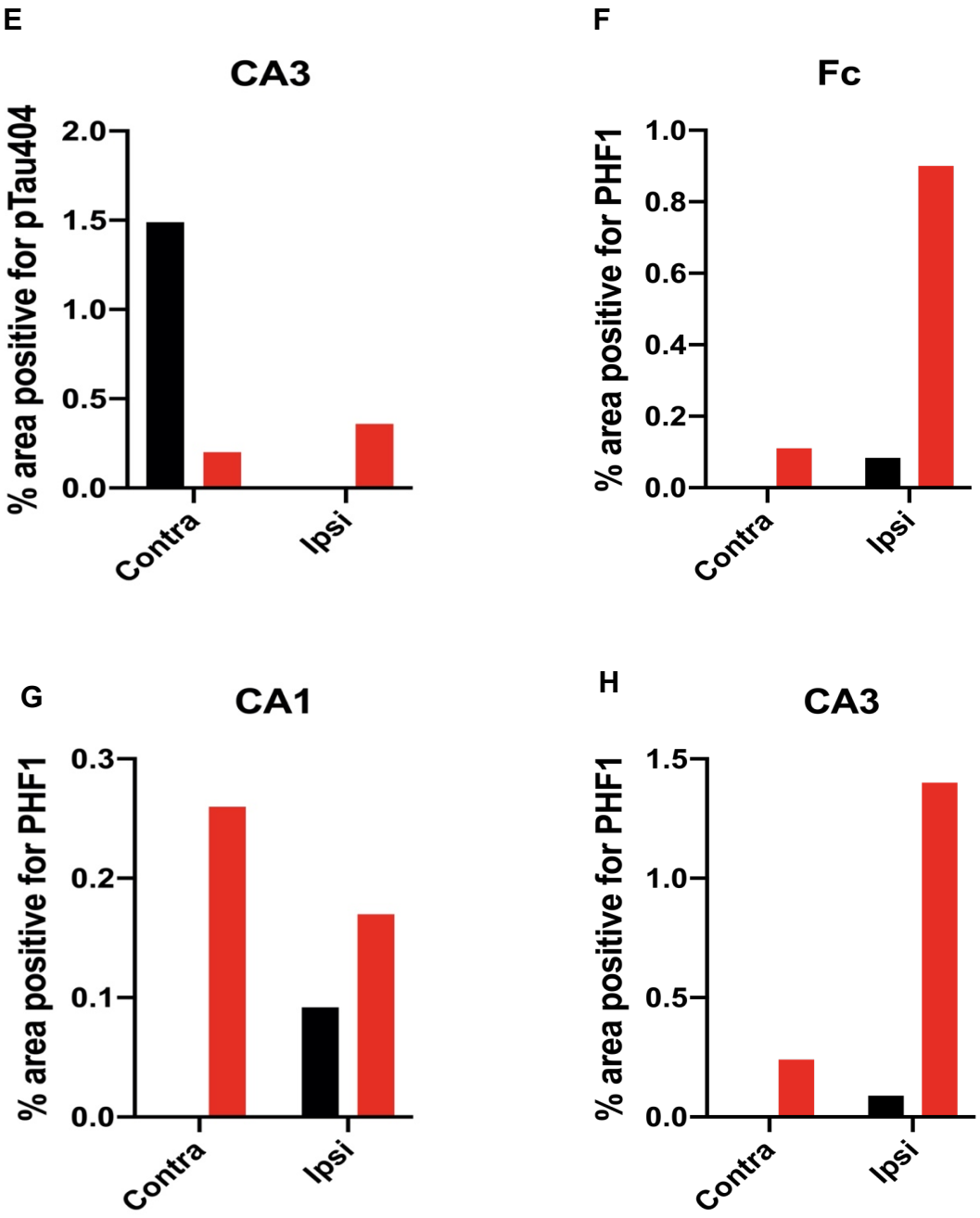
E
CA3
% area positive for pTau404
2.0
1.5
1.0
0.5
0.0
Contra
Ipsi
F
Fc
% area positive for PHF1
1.0
0.8
0.6
0.4
0.2
0.0
Contra
Ipsi
G
CA1
% area positive for PHF1
0.3
0.2
0.1
0.0
Contra
Ipsi
H
CA3
% area positive for PHF1
1.5
1.0
0.5
0.0
Contra
Ipsi

Figure 3.17 A) Immunolabelling of tau phosphorylated at Ser404 (pTau404). Sections were counterstained with haematoxylin in 7 µm paraffin embedded sections of the frontal cortex (Fc), hippocampal subfields CA1 and CA3. α–Synuclein PFFs did not cause an increase in pTau404 immunoreactivity compared to control rats. Images shown are from control and PFF-injected rats, contralateral (contra) and ipsilateral (ipsi) hemisphere. Scale bars are 20 µm. **B)** Immunolabelling of PHF1 (pTau396/pTau404) and counterstain with haematoxylin in 7 µm paraffin embedded sections of the frontal cortex (Fc), hippocampal subfields CA1 and CA3. α–Synuclein PFFs did not show a significant difference with an increase in PHF1 immunoreactivity compared to control. Images shown are from control and PFF-injected rats, contralateral (contra) and ipsilateral (ipsi) hemisphere. Scale bars are 20 µm, n = 1. **C-H**) Quantification of percentage area positive for pTau404 in control and PFF-injected rats, in the frontal cortex (Fc), **D-E)** hippocampal subfields CA1 and CA3 regions (CA1 and CA3). **F)** Quantification of percentage area positive for PHF1 in control and PFF-injected rats, in the frontal cortex (Fc), **G-H)** hippocampal subfields CA1 and CA3 regions (CA1 and CA3). Statistical analysis was not performed due to insufficient *n* number of samples per group stained.

3.7 Results: Effects of α–synuclein PFFs on synaptic proteins

3.7.1 α–Synuclein PFFs did not affect levels of synaptic proteins

The accumulation of pathological α–synuclein following addition of α–synuclein PFFs to mouse primary cultures leads to selective loss of synaptic proteins (Volpicelli-Daley et al., 2011; Wu et al., 2019). Representative blots from the frontal cortex of rats injected with control and α–synuclein PFFs at 90 d.p.i are shown (Figure 3.18A). Protein bands were detected at their expected molecular weights of N-methyl-D-aspartate receptor subunit (NR2B) (150 kDa), post-synaptic density protein (PSD-95) (95 kDa), synaptotagmin (60 kDa) and synaptophysin (38 kDa). An antibody against β-actin was used as a loading control. There were no apparent differences in the intensity of bands in lysates from control and PFF injected brains. The amount of each synaptic protein was quantified following normalization to the amount of β-actin in the same sample. For ease of comparison, the results were plotted as percentage average control, where control refers to the ipsilateral cortex of control-injected rats. Results showed no significant differences in the amounts of NR2B (Figure 3.18C), PSD-95 (Figure 3.18E), synaptotagmin (Figure 3.18G) and synaptophysin (Figure 3.18I) in tissue from α–synuclein PFF injected rats relative to controls, or between hemispheres.

Similarly, in the hippocampus (Figure 3.13B) although levels appeared more variable than in the frontal cortex, there were no significant changes in either of the postsynaptic proteins (NR2B, PSD-95) or presynaptic proteins (synaptotagmin, synaptophysin) between lysates from control and α–synuclein PFF injected brains in either hemisphere (Figure 3.18D, F H, J).

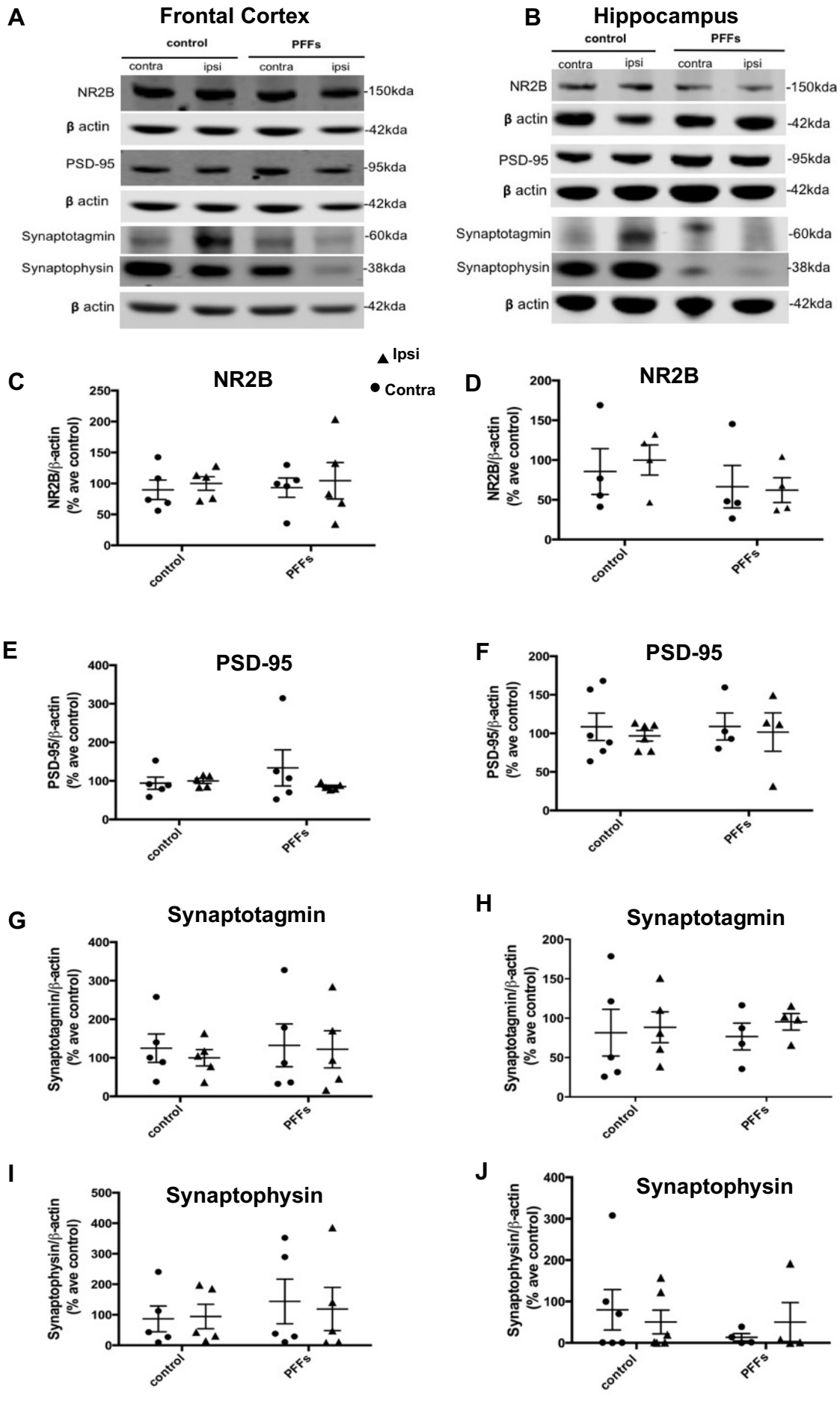
A
Frontal Cortex
control
PFFs
contra
ipsi
contra
ipsi
NR2B
-150kda
β actin
-42kda
PSD-95
-95kda
β actin
-42kda
Synaptotagmin
-60kda
Synaptophysin
-38kda
β actin
-42kda
B
Hippocampus
control
PFFs
contra
ipsi
contra
ipsi
NR2B
-150kda
β actin
-42kda
PSD-95
-95kda
β actin
-42kda
Synaptotagmin
-60kda
Synaptophysin
-38kda
β actin
-42kda
▲ Ipsi
● Contra
C
NR2B
NR2B/β-actin (% ave control)
control
PFFs
D
NR2B
NR2B/β-actin (% ave control)
control
PFFs
E
PSD-95
PSD-95/β-actin (% ave control)
control
PFFs
F
PSD-95
PSD-95/β-actin (% ave control)
control
PFFs
G
Synaptotagmin
Synaptotagmin/β-actin (% ave control)
control
PFFs
H
Synaptotagmin
Synaptotagmin/β-actin (% ave control)
control
PFFs
I
Synaptophysin
Synaptophysin/β-actin (% ave control)
control
PFFs
J
Synaptophysin
Synaptophysin/β-actin (% ave control)
control
PFFs

Figure 3.18 A) Immunoblots conducted on high salt fractions of contralateral (contra) and ipsilateral (ipsi) frontal cortex and hippocampus of control and α–synuclein PFF treated rats at 90 d.p.i were probed for post- and pre-synaptic proteins. Blots are of representative control and α–synuclein PFF treated rats in frontal cortex region, n = 5 for all. No changes in pre- or post- synaptic markers within the frontal cortex or hippocampal region were found for **C**) NR2B, **E)** PSD-95, **G)** Synaptotagmin or **I)** Synaptophysin. **B)** Immunoblots conducted on high salt fractions of contra and ipsi hippocampus from control and α–synuclein PFF injected animals probed for post- and pre-synaptic proteins. Blots are of representative control and α–synuclein PFF injected rat hippocampus, **D**) NR2B (n = 4), **F)** PSD-95 (n = 6), **H)** Synaptotagmin (n = 5) and **J)** Synaptophysin (n = 4 - 6). Analysis using unpaired t-test on the difference between contralateral and ipsilateral hemispheres of control and PFF groups did not indicate any significant effect on synaptic proteins **(C - J).** Data is mean +/- SEM presented as % average control where control is the ipsilateral hemisphere of control-injected rats.

The lack of changes to synaptic protein levels in the frontal cortex and hippocampus suggests that α–synuclein PFFs were not sufficient to perturb synaptic proteins, despite the presence of phosphorylated α–synuclein-positive neurons in these regions.

3.7.2 α–Synuclein PFF injected rats did not induce any mislocalisation of tau

Results shown above (Section 3.6.2) demonstrated that α–synuclein PFFs were not sufficient to induce increased tau phosphorylation in regions to which phosphorylated α–synuclein was found to spread, or to cause any effects on synaptic protein levels (Section 3.7.1). To confirm these findings, tau content in synaptic fractions were examined, since the mislocalisation of tau to synapses causes synaptotoxicity (Ittner et al., 2010; Glennon et al., 2020; Zhou et al., 2017; Hoover et al., 2010).

Antibodies against total tau and phosphorylated tau were used in the (Enzyme-linked immunosorbent assay) ELISA. In the total homogenate fraction, the results did not indicate a reduction in total tau amounts in this fraction of ipsilateral hemisphere in PFF injected relative to control-injected rats, (Figure 3.19A). The amount of phosphorylated tau in this fraction in PFF injected rats relative to controls was not found to be significantly elevated either (Figure 3.19B).

Lastly, using the same ELISA methods, the abundance of total and phosphorylated tau was measured in synaptoneurosome fractions isolated from the hippocampus of control and α–synuclein PFF groups (Figure 3.19C-D). Quantification of these data showed no statistical differences in the amounts of synaptic tau in control versus α–synuclein PFF injected rats, in either hemisphere (Figure 3.19C-D).

Taken together, my results indicate that there was no mislocalisation of tau following α–synuclein PFF injection into the MFB. This is in agreement with the analysis of synaptic proteins and behaviour, which indicates no evidence of synaptic perturbations.

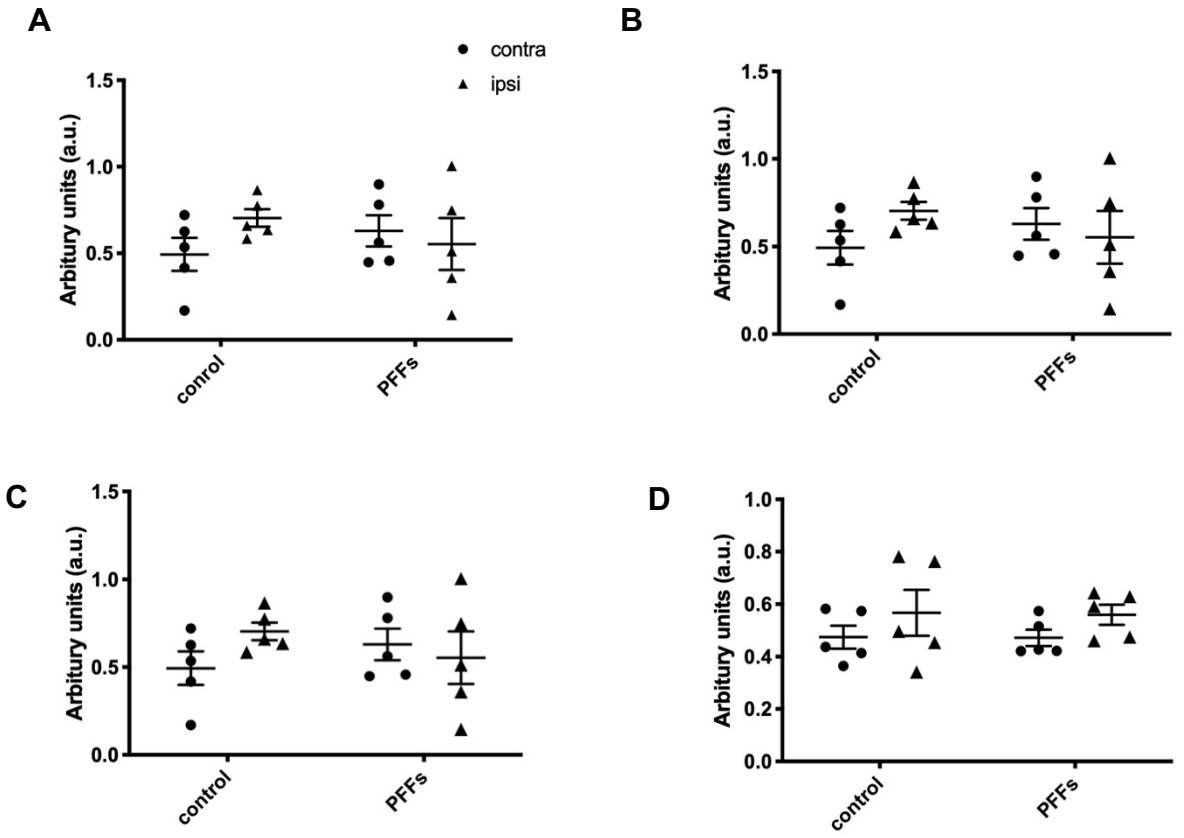

Figure 3.19 Semi-quantitative ELISA on hippocampal homogenates following α–synuclein PFF injection and control rats. Semi-quantitative tau ELISA was used to determine **A)** total tau and **B)** phosphorylated tau at Serine 396 (pTau396) amounts in the total homogenate fraction derived from a synaptoneurosome preparation of contralateral (contra) and ipsilateral (ipsi) cortex. Absorbance was read at 450nm, and data shown is mean ± SEM absorbance units (a.u.). No significant difference *(n.s)* was noted in total tau or phosphorylated tau, in either control or PFF groups in either hemisphere (n= 5). Total and tau phosphorylated at pTau396 within the synaptoneurosome fraction were detected by ELISA. **C)** ELISA graphs of the synaptoneurosome fraction detecting for total tau, no statistical difference was noted between control and α–synuclein PFF rats in in either hemisphere, n = 5. **D)** Synaptoneurosome fraction of contralateral and ipsilateral hemispheres from control and α–synuclein PFF rats were assessed. *n.s* was found between groups (n = 5) for phosphorylated tau at pTau396. Total and tau phosphorylated at pTau396 within the synaptoneurosome fraction were detected by ELISA. Analysis with unpaired t-test on the difference between contralateral and ipsilateral hemisphere of control and PFF groups did not indicate any statistical difference **(A -D).** Data presented as mean ± SEM, contra. = contralateral, ipsi. = ipsilateral.

3.8 Results: α–Synuclein PFFs and oxidative stress

3.8.1 Oxidative stress markers were not elevated in α–synuclein PFF injected rats

Cells immunoreactive for 8-hydroxyguanosine (8OHG) were found throughout the frontal cortex in both control and PFF injected rats (Figure 3.20A). Quantification of the percentage area positive for 8OHG-positive cells per 100 mm^2 in contralateral and ipsilateral hemispheres, black arrows point to cells positive for 8OHG immunoreactivity. Quantification showed no overall significant increase in the % area positive for 8OHG immunoreactivity cells in PFF injected rats compared to controls at 90 d.p.i. in either hemisphere (Figure 3.20 B,C,D). This suggests that DNA/RNA oxidative stress damage was not induced due to α–synuclein PFFs at this particular time point, within the frontal cortex region. In the hippocampus, 8OHG labelling appeared to be mainly cytoplasmic, in agreement with previous reports (Zhang et al., 1999). Labelling was also apparent in the pyramidal cell layer throughout the hippocampal formation. The number of 8OHG-positive cells was quantified in the CA1 and CA3 regions of the hippocampus. These results also did not show an overall significant increase in the number of 8OHG-positive cells at 90 d.p.i. in response to α–synuclein PFFs. Taken together, these finding suggests that oxidative stress levels are not increased in α–synuclein PFF injected rats, within the time frame examined here. To further confirm the results, nitrotyrosine, an alternative marker for probing oxidative stress was used. A similar result was also noted with nitrotyrosine labelling in the frontal cortex and hippocampal subfields CA1 and CA2 of PFF injected rats. No evident immunoreactivity was detected in the α–synuclein PFF injected brain at 90 d.p.i. (Figure 3.20E). A later time point will need to be investigated to gain a better understanding of the relationship between α–synuclein and oxidative stress as oxidative stress build up is common during aging (Liguori et al., 2018) and α–synuclein PFFs may potentially induce an additive effect, further increasing oxidative stress levels.

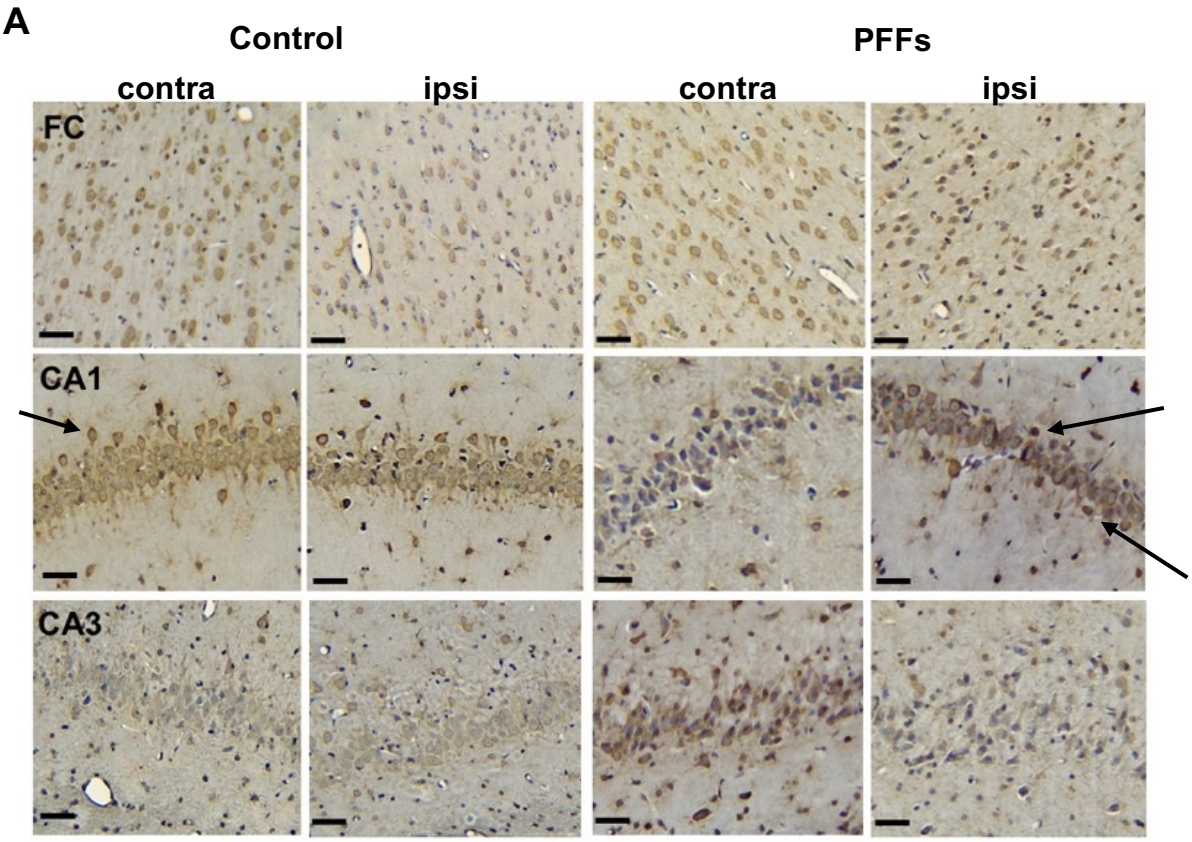
A
Control
PFFs
contra
ipsi
contra
ipsi
FC
CA1
CA3

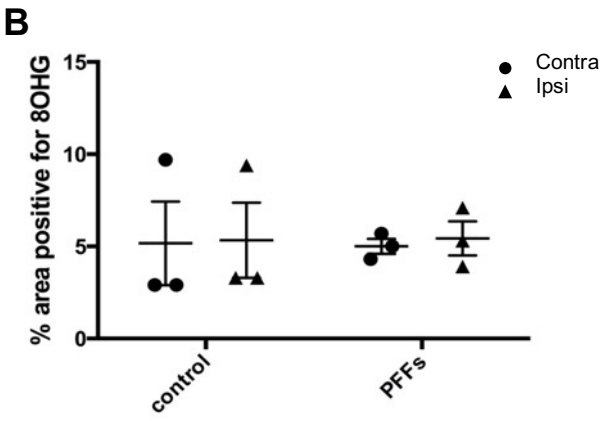
B
% area positive for 8OHG
15
10
5
0
Contra
Ipsi
control
PFFs

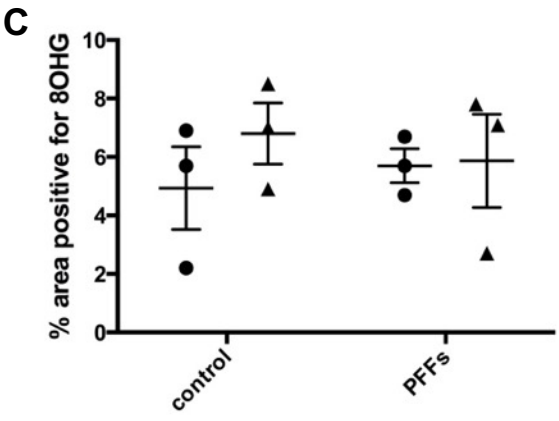
C
% area positive for 8OHG
10
8
6
4
2
0
control
PFFs

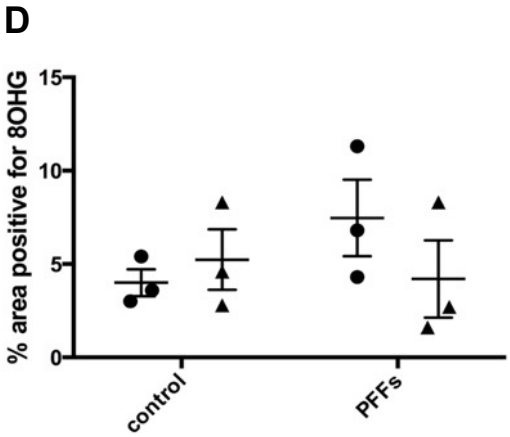
D
% area positive for 8OHG
15
10
5
0
control
PFFs

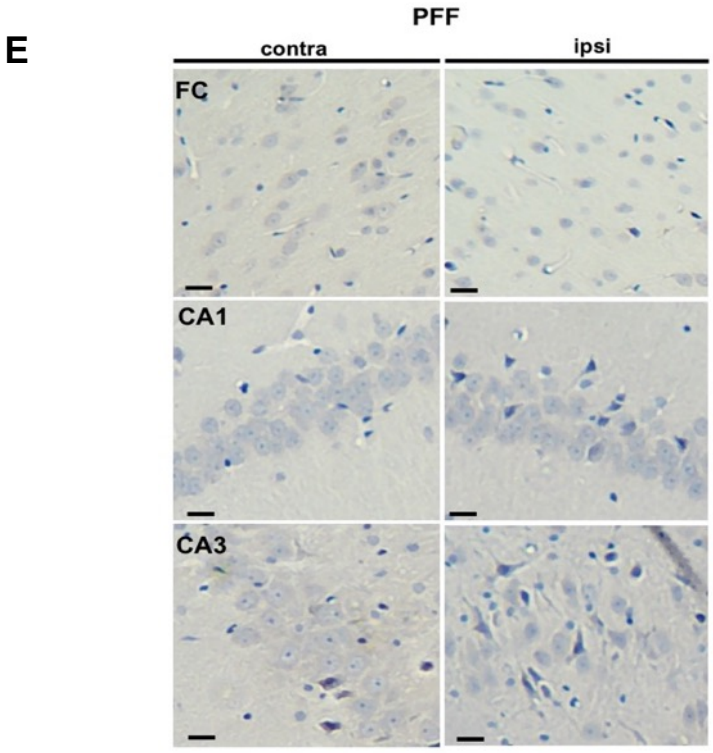

Figure 3.20. Oxidative stress was not increased in the frontal cortex and hippocampal subfields in response to α–synuclein PFFs. **A)** Immunolabelling of 8-hydroxyguanosine (8OHG) to detect for the presence of oxidative DNA/RNA damage in 7 µm paraffin embedded sections of the frontal cortex (Fc), hippocampal subfields CA1 and CA3 from α–synuclein PFF and control injected rats. Black arrows indicate labelled cells **B**) Quantification of the percentage area of positive 8OHG cells within the frontal cortex of control and α–synuclein PFF injected rats. No significant difference *(n.s)* was found between either treatment groups, or either hemispheres, ipsilateral (ipsi), contralateral (contra). **C)** Quantification of the percentage area of positive 8OHG cells within the hippocampal subfield, CA1, of control and α–synuclein PFF injected rats. *n.s* was noted between treatment groups, and hemisphere, ipsi, contra. **D)** Quantification of the percentage area of positive 8OHG cells within hippocampal area, CA3 of control and α–synuclein PFF injected rats. *n.s* was noted between treatment groups and hemisphere, ipsi, contra. **E)** Immunolabelling of nitrotyrosine positive cells to detect for cell damage and inflammation, on 7 µm paraffin embedded sections from the frontal and hippocampal subfield CA1 and CA3 regions. α–synuclein PFF injected rats did not show any positive nitrotyrosine cells in the frontal cortex or hippocampal subfields (CA1) and (CA3), in either ipsi or contra hemisphere. Control rats not shown. Scale bar 20 µm. Analysis with unpaired t-test on the difference between contralateral and ipsilateral hemisphere of control and PFF group did not indicate any statistical significance. Data presented as mean ± standard error of the mean (SEM), n=3.

3.9 Results: Non-neuronal effects of α–synuclein PFFs

3.9.1 α–Synuclein PFFs did not induce the activation of astrocytes

To gain insights into any activation of glia stimulated by α–synuclein PFF, activation states of astrocytes were examined in the frontal cortex and hippocampus by immunohistochemical analysis. These regions were selected since they show accumulation of phosphorylated α–synuclein and are associated with executive dysfunction and visuospatial impairments.

Coronal rat brain sections of 7 μm were immunolabelled using an antibody against glial fibrillary acidic protein (GFAP), and nuclei were stained with 4'6-diamidinio-2-phenylindole (DAPI). Qualitative analysis suggested that GFAP was somewhat upregulated in tissue from PFF-injected rats relative to controls. Furthermore, while astrocytic morphology appeared similar between 60 d.p.i. and 90 d.p.i. there was a thickening of processes and increased number of processes at 120 d.p.i. suggestive of reactive astrocytes (Figure 3.21A). Quantification of GFAP signals as percentage area of positively labelled cells indicated no significant difference between treatment groups or across hemispheres (Figure 3.21C, D, E). To gain a clearer understanding of the reactive state of astrocytes, it would be beneficial to examine additional markers of reactive astrocytes and to quantify the number of primary processes leaving the soma (Wilhelmsson et al., 2006). However, due to restrictions imposed by COVID-19, this was not feasible. This preliminary data was used for power calculations to determine the sample size required to generate robust data about astrocyte reactivity in these samples. These calculations show that at a 5% significance level and a statistical power of 80%, we will require a sample size of 33.

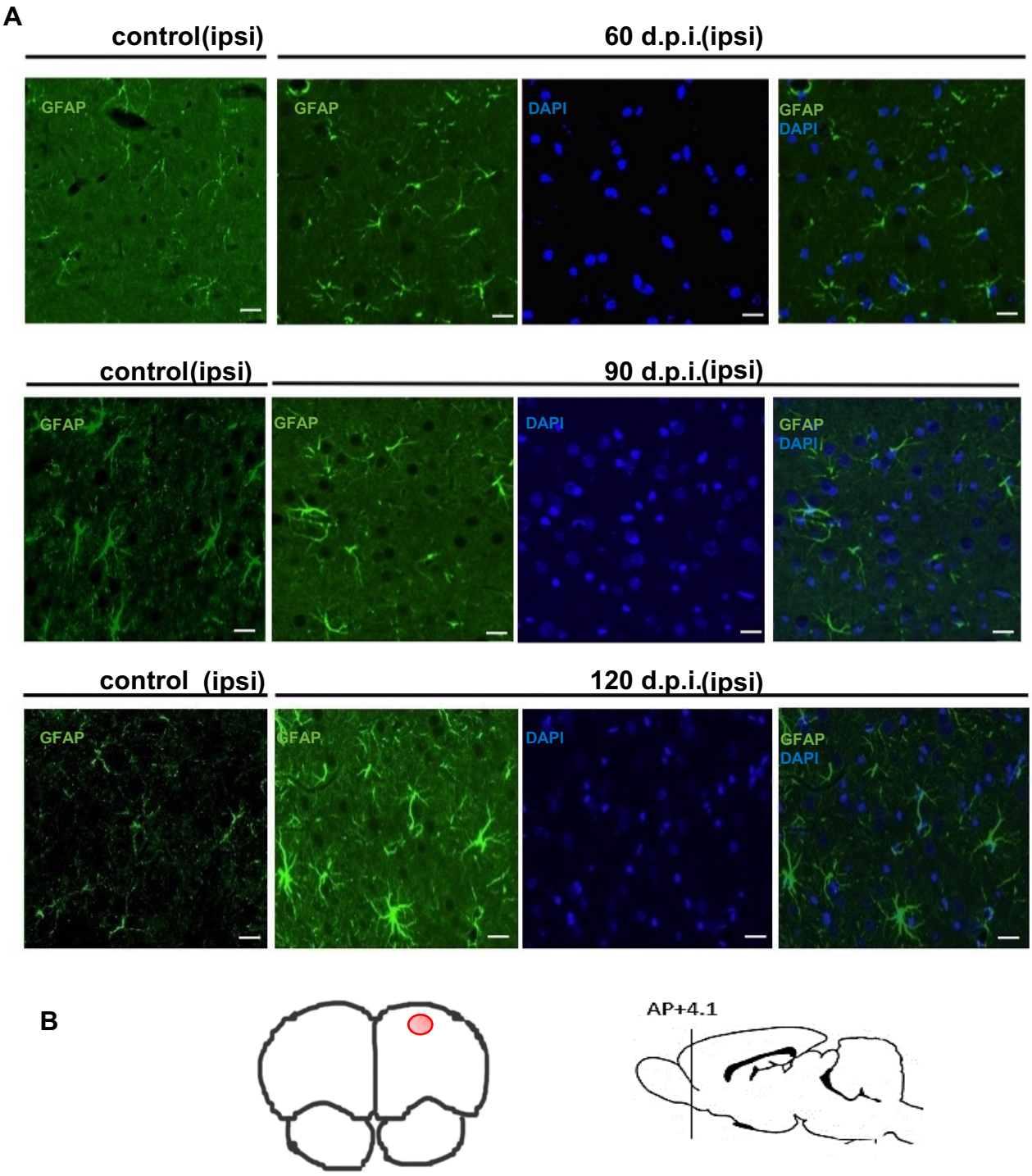
A
control(ipsi)
60 d.p.i.(ipsi)
GFAP
GFAP
DAPI
GFAP
DAPI
control(ipsi)
90 d.p.i.(ipsi)
GFAP
GFAP
DAPI
GFAP
DAPI
control (ipsi)
120 d.p.i.(ipsi)
GFAP
GFAP
DAPI
GFAP
DAPI
B
AP+4.1

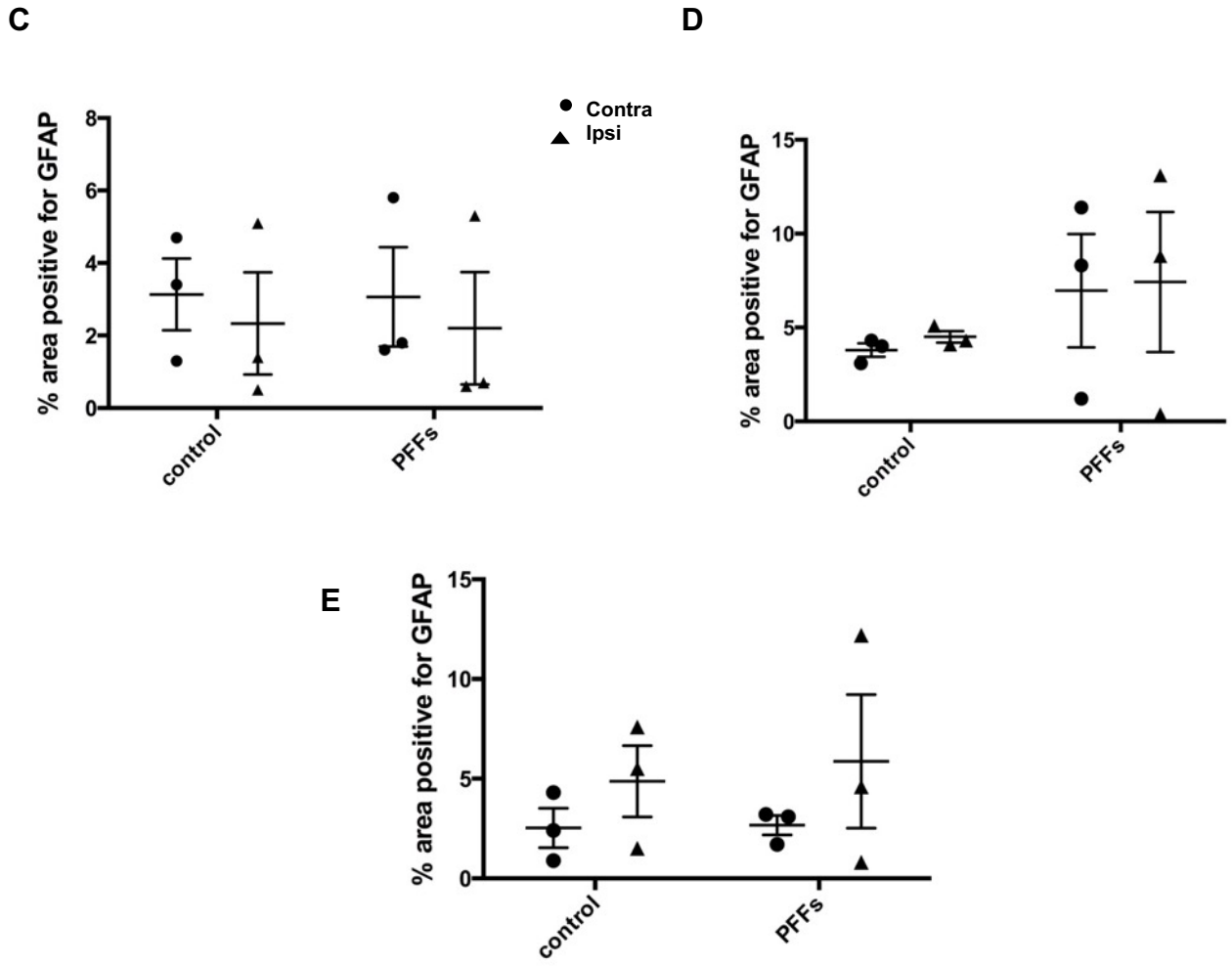

Figure 3.21. Altered astrocyte features following α–synuclein PFF injection into rat MFB. **A**) 7 µm thick coronal sections of frontal cortex from control or α–synuclein PFF injected rats at 60, 90, and 120 d.p.i. were immunolabelled with an antibody against GFAP to detect activated astrocytes (green). Nuclei were stained with DAPI (blue). Sections were imaged using an Olympus VS120 slide scanner. GFAP labelling appeared more intense in PFF injected rats, and altered morphology suggested that astrocytes are more reactive at 120 d.p.i. of α–synuclein PFFs. Only ipsilateral hemisphere is shown. Scale bar = 20 µm. **B)** Diagrams showing the region from which sections were taken in coronal and sagittal views. Quantification of the percentage area of GFAP-positive cells in control and α–synuclein PFF injected frontal cortex at **C)** 60 d.p.i. **D)** 90 d.p.i. and **E)** 120 d.p.i. Analysis using unpaired t-test on the difference between contralateral and ipsilateral hemisphere for control and PFFS groups did not indicate any statistical significance. Data presented as mean ± standard error of the mean (SEM), n=3.

3.10 Discussion

The goal of this chapter was to explore the effects of α–synuclein PFFs when injected into the MFB, at three pre-established time points. Different behavioural tests were used to detect for any behavioural phenotypes relating to motor and cognitive impairments. Secondly, I aimed to investigate α–synuclein spreading after α–synuclein PFFs were introduced into the MFB, including intracellular and non-neuronal changes.

α–Synuclein PFFs injection into the MFB was insufficient to trigger marked behavioural phenotypes, with no cognitive impairment noted at any of the time points investigated.

Due to the significant weight gain of older rats (90 d.p.i and 120 d.p.i), these animals performed poorly on the rotarod test as rats were unable to maintain themselves on the rotating bar. However, rats from all time points were able to participate in the asymmetric cylinder task as this task was not restricted by their weight. A statistically significant transient change in asymmetric deficit was detected in this test at 90 d.p.i., which also coincided with the highest load of phosphorylated α–synuclein. Therefore, it is possible that the accumulating phosphorylated α–synuclein induced the transient changes leading to a mild motor impairment. However, results from immunohistochemical findings suggest that the accumulation of phosphorylated α-synuclein did not further increase from 90 d.p.i to 120 d.p.i therefore, it is feasible that a self-repairing mechanism may exist to reduce such damage which may have, for example, facilitated clearing of phosphorylated α–synuclein.

Executive function is regarded as the ability to plan, organise and regulate goal-directed behaviour and general cognitive flexibility (Emre, 2003; Gratwicke et al., 2015) and is known to be disrupted in PD/PDD (Halliday et al., 2014; Aarsland et al., 2017). The 5-CSRTT has been used to measure alterations in executive function in mice (Horner et al., 2013; Mar et al., 2013). In the absence of better available alternatives for use with rats, this test was used here to examine any impact on executive functions of α–synuclein PFF injection into rat MFB. However, due to inexperience coupled with technical issues, robust data was not obtained. Additional executive behaviour tasks include the puzzle box which tests for higher order functioning and problem solving measures with varying levels (Ben Abdallah et al., 2011). However, due to the intricacy of the behaviour task, it was deemed more suitable for mice than rats.

Future suitable alternatives for detecting attentional deficit could include indirect measures such as immunohistochemical staining for changes in parvalbumin interneurons (White et al., 2018b) as data from a TAR DNA binding protein-43 (TDP-43) mouse model, RNASeq revealed a downregulation in parvalbumin gene expression which was positively correlated with the number of parvalbumin interneurons and attentional deficits or measuring the electrophysiology recordings (Kim et al., 2016) as data from chronic electrophysiological recordings in mice revealed that parvalbumin interneurons within the prefrontal cortex region were highly active and showed increased activity during attentional and goal-driven processing during the 5-CSRTT (Kim et al., 2016).

The lack of visuospatial memory impairment observed at all three time points after α–synuclein PFF injection into rat MFB differed to findings reported by Durante et al. (2019),

where visuospatial impairment was noted following striatal injection of human PFFs. The differences are possibly because Durante et al. (2019) performed the injections bilaterally whereas in this study injections were unilateral which may result in slower onset of behavioural impairment. Secondly, Durante et al. (2019) used a novel object recognition test to detect short term memory impairment, whereas alternative tests were used here. Furthermore, despite the presence of phosphorylated α–synuclein within hippocampal regions it suggests in this instance that phosphorylated α–synuclein was not sufficient to impair spatial memory. This coincides with findings from (Kasongo et al., 2020) where chronic administration of α–synuclein PFFS led to phosphorylated α–synuclein, but without direct impairment to spatial memory when examined with the Morris water maze (MWM). This further implies that neuropathology requires an extended period of time to induce detrimental effects leading to cognitive impairment.

Using immunohistochemical analysis, the ability of α–synuclein PFFs to convert nearby endogenous α–synuclein to a phosphorylated form was investigated in regions that are known to have afferent and efferent projections to and from the MFB, including but not limited to; septal nuclei, anterior olfactory nucleus, nucleus of the diagonal band of broca and caudatoputamen (Nieuwenhuys et al., 1982; Veening et al., 1982), septal septum, amygdala, substantia inominata and nucleus accumbens (Millhouse, 1969; Troiano and Siegel, 1978a; Troiano and Siegel, 1978b). Despite the vast number of studies on α–synuclein PFFs inoculations and injections into various sites including the striatum in rats (Paumier et al., 2015), and in mice the striatum (Luk et al., 2012a; Luk et al., 2012b; Okuzumi et al., 2018), hippocampus (Luna et al., 2018; Bassil et al., 2020), olfactory bulb (Rey et al., 2018) and gut (Kim et al., 2019), this is the first time α–synuclein PFFs have been stereotaxically injected

into the MFB. The MFB is an intricate bundle structure composed of a descending and ascending system of fibres that connect medial and basal forebrain structures (Nieuwenhuys et al., 1982; McMullen et al.., 1981). Ascending axons from dopaminergic, serotonergic and noradrenergic neurons located in the lower brain stem also pass through the MFB structure (Nieuwenhuys et al., 1982, Kollensperger et al., 2007). The MFB is best known for its connectivity between the ST and SN, therefore making it a relevant injection site for investigating PD-like features in animal models. In rats, the MFB has both output and input projections to and from a diverse range of regions including the locus coeruleus, neocortex, hypothalamus, septum, thalamus and cerebellum. Injection of material into MFB therefore allows study of effects in projection regions such as the frontal cortex that control executive function.

Results from the immunohistochemical staining showed that in accordance with previous literature (Henderson et al., 2019a), α–synuclein PFFs induce the conversion of endogenous α–synuclein to a phosphorylated form, and it does so according to anatomical connectivity. Although the phosphorylated α–synuclein detected here appeared weaker compared to findings reported by others (Duffy et al., 2018c), a possible explanation for this could be due to the difference in injection site and time frame. The MFB is a fibre system, interspersed with numerous neurons connecting to a diverse range of structures (McMullen and Almli, 1981; Shiosaka et al., 1980). In contrast, conventional injection sites have been in sites consisting of soma and dendrites which facilitate the uptake and spread of α–synuclein PFFs through multiple cellular processes including direct interactions with plasma membrane proteins and receptors, trafficking along the endo-lysosomal pathway (Wu et al., 2019). Furthermore, upon quantification there was also no statistical significance in the load of phosphorylated α-

synuclein between injected animals and control animals. However, by qualitative observation (Figure 3.13 C-G) there was a trend at 90 d.p.i. where phosphorylated α-synuclein was the most abundance in all brain regions. This peak was followed by a decrease by 120 d.p.i. The phosphorylated α-synuclein load therefore may not be high enough to result in synapse damage and other neurodegenerative changes, but had time permitted, α-synuclein load may reach a sufficient threshold enabling such damage to occur.

Another determinant of the spreading ability of phosphorylated α–synuclein is time; spread occurs in a dose-dependent and time-dependent manner. The results gathered from this chapter reflect this; the increase in phosphorylated α–synuclein load from 60 d.p.i. to 90 d.p.i. The plateau of phosphorylated synuclein at 90 d.p.i. is somewhat surprising. The system responsible for the clearance of α–synuclein accumulations is not fully understood in this model. Evidence has suggested a possible role of internal clearing mechanisms involving the ubiquitin-proteasome system or the autophagy-lysosomal system (Xilouri et al., 2013). The partial degradation of α–synuclein by either of these two systems can prevent further spreading and accumulation of phosphorylated α–synuclein. Glial cells may also participate in clearing of excess phosphorylated α–synuclein, as cell cultures studies have shown that astrocytes can degrade α–synuclein aggregates (Loria et al., 2017), while microglia are known to clear protein aggregates, debris and dead cells (Burke et al., 2016). Lastly, neuronal death may lead to a reduction of available endogenous α–synuclein, therefore perturbing the spread of phosphorylated α–synuclein (Rey et al., 2018)

Intracerebral α–synuclein PFF inclusion were found to correlate with dopaminergic neurodegeneration (Abdelmotilib et al., 2017). Progressive TH reduction within the SN in mice

after α–synuclein PFF injections at 180 d.p.i. (Duffy et al., 2018c; Luk et al., 2012a) and in rats at 5-6 months post injection (Duffy et al., 2018). However, it was not known whether α–synuclein PFFs into the MFB would induce similar dopaminergic cell loss in the SN within the time frame investigated. Results from immunohistochemical findings found that at 120 d.p.i. injection, PFFs induced a statistically significant dopaminergic cell loss within the ipsilateral SN compared to controls, and there was a progressive reduction in TH immunopositive cells from 60 d.p.i. through to 120 d.p.i. in the ipsilateral SN of PFF-injected rats, while contralateral hemisphere did not show any significant cell loss. Previous reports have shown TH cell loss is detected typically 5 months post injection. An explanation for the early TH cell loss observed here (by 120 d.p.i.) could be the location of injection. The MFB is in closer proximity to the SN than the striatum and secondly the dosage used within this model is substantially higher than those reported in existing literature (Paumier et al., 2015; Duffy et al., 2018b). There was variability in TH positive cell loss between hemispheres. Although Paumier et al. (2015) reported a bilateral nigral loss post-unilateral injection, Duffy et al. (2018b) have shown nigral loss as being restricted to one hemisphere only after unilateral injection. The reasons for this variability remains unclear, however several factors may have influenced this phenomenon including neurofinflammation as the severity of neuroinflammation could potentially influence the degree of TH cell loss. An alternative possibility could be due to intrahemispheric imbalance where differing levels of dopamine can lead to subset of neuronal overactivity subsequently resulting in cell death. These contributors may not be exclusive but act synergistically towards unilateral TH positive cell loss while the contralateral hemisphere is relatively well preserved (Paumier et al., 2015). Furthermore, Paumier et al. (2015) noted that although α-synuclein pathology was present in both hemispheres of the SN, degeneration only occurred in the contralateral hemisphere

suggesting that dopaminergic degeneration may be mediated by a mechanism other than α-synuclein. Due to insufficient sample size, data for control animals for all the three time points could not be obtained, limiting the value of the findings presented here.

Results from both immunohistochemical and biochemical methods show that there are limited changes to protein solubility and minimal overall changes to tau or synuclein in response to α–synuclein PFFs in this model. Sarkosyl is a mild detergent that is commonly used to isolate insoluble (filamentous) proteins from postmortem neurodegenerative disease brain and rodent models of neurodegenerative diseases (Peng et al., 2018). Sarkosyl is preferred over other detergents such as urea for permeabilising cells and extracting proteins in isolation. It is stringent enough to solubilise the majority of natively folded proteins in the brain but does not solubilize the misfolded protein aggregates composed of α–synuclein, tau and other proteins relevant to neurodegeneration including Aβ , scrapie prion proteins (PrP^{Sc}) and TDP-43. Other detergents of increasing stringency can also be used to partition soluble and insoluble proteins (Diner et al., 2017). The non-ionic detergent used here was Triton-x which serves as a mild surfactant to break protein-lipid and lipid-lipid associations, though not protein-protein interactions. Non-ionic detergent generally do not denature proteins and so many membrane proteins can be solubilised in their native and active forms while retaining their protein interactors (Tao et al., 2010; Rabilloud, 2009). No changes in the solubility of tau or α–synuclein were detected here is in-keeping with previous observations.

Although α–synuclein can successfully promote tau fibrillisation in a synergistic manner in a cell culture system (Waxman and Giasson, 2011; Giasson et al., 2003), the type and strain of pathological seed is a critical determinant in the ability of α–synuclein and tau to cross-seed

(Guo et al., 2013; Castillo-Carranza et al., 2018; Strohaker et al., 2019). Phosphorylation of tau is generally assumed to occur prior to, and to promote, tau aggregation into insoluble forms (Narasimhan et al., 2017). Therefore, it is perhaps not surprising that no significant changes in tau phosphorylation were found here in response to α–synuclein PFFs. These findings are also in concordance with previous results who showing that α–synuclein PFF injection into WT mice at various time points also did not induce major changes in tau phosphorylation (Bassil et al., 2020). However, as only two tau phosphorylation sites were investigated here, it could be of interest to explore additional sites in the future.

α–Synuclein PPFs are able to compromise synaptic activity and enhance synapse loss in cell culture studies (Volpicelli-Daley, 2017; Volpicelli-Daley et al., 2011; Wu et al., 2019). However, the contribution of α–synuclein PFFs to synapse loss in animal studies is poorly understood. Results from immunoblots of synaptic proteins did not show any loss of synaptic proteins following α–synuclein PFF injection into rat MFB. This may be a consequence of the relatively early time points studied here, the relatively mild accumulation of phosphorylated α–synuclein that resulted, or other factors such as age at time of injection, injection site and/or model system. Future studies could examine additional changes in synaptic proteins and structure including in regions more proximal to the MFB. A wider range of synaptic markers could be examined, or synaptic morphology examined following Golgi staining for example, or by electron microscopy.

Several studies suggest that oxidative stress is a key underlying mechanism in neurodegeneration (Hwang, 2013; Blesa et al., 2015). An abundance of findings suggests a bidirectional relationship between α–synuclein and oxidative stress, cell culture studies (Luna

et al., 2018; Musgrove et al., 2019) and in rodent studies, where upon intrastriatal α–synuclein PFF injection, DNA damage was evident, involving oxidative stress and mitochondrial dysfunction (Milanese et al., 2018). However, immunohistochemistry results did not show any effect of α–synuclein PFFs on common markers of oxidative stress. Further studies are necessary to investigate this difference between the animal and cell culture system.

Oxidative stress responses are largely mediated by alterations in glial cells, and astrocytes in particular. To begin to determine if there are changes in astrocytes in response to α–synuclein PFF injection in areas local to the injection site and distally, immunohistochemical staining with an antibody against GFAP was performed. GFAP is a type III intermediate filament forming part of the cytoskeleton of mature astrocytes and upon activation, an upregulation of GFAP is detected making it a suitable candidate for distinguishing activated astrocytes (Yang and Wang, 2015), although additional and more sensitive markers of reactive astrocytes have been described (Zamanian et al., 2012).

Despite the appearance of alterations in astrocyte morphology in the 120 d.p.i. group, suggestive that astrocytes become more reactive following α–synuclein injections, results from immunohistochemistry did not indicate any major changes in the percentage area of GFAP-positive labelling in the frontal cortex of control and α–synuclein PFF rats.

Overall, these data are considered somewhat inconclusive. The findings from the immunohistochemical staining were variable particularly for the α–synuclein PFF groups due

to the limited number of astrocytic markers used and insufficient *n* number. Additional experiments will be necessary to extend these findings, including additional immunohistochemistry and immunoblotting using astrocytic markers such as aldehyde dehydrogenase 1 family member L1 (AldhL1) to detect total numbers of astrocytes as all astrocytes express the AldhL1 protein (Cahoy et al., 2008), and markers of reactive astrocytes including Lipocalin (LCN2), Serpin Family A Member 3 (SerpinA3) and Complement 3 (Liddelow and Barres, 2017) (Liddelow et al., 2017; Zamanian et al., 2012). It would also be of interest to study additional brain regions, particularly with respect to the accumulation of phosphorylated α–synuclein. A similar approach could be applied for microglia given that reactive microglia are frequently present around α–synuclein positive LBs in PD and DLB, particularly within the proximity of dying neurons (Croisier et al., 2005).

3.11 Summary

The main findings described in this chapter are that injection of α–synuclein PFFs into rat MFB led to the appearance of phosphorylated synuclein in anatomically connected brain regions from as early on as 60 d.p.i., right through to 120 d.p.i. with a peak of phosphorylated α–synuclein at 90 d.p.i. observed. A trend of positive TH cell loss correlated with progressed time points within the ipsilateral SN. And, despite the presence of phosphorylated α–synuclein in various brain regions (frontal cortex, striatum, hippocampus, cortex and substantia nigra), no changes in tau and α–synuclein protein solubility were detected within the time frame investigated. No disruption to synaptic proteins were noted, including no evidence of damaging tau mislocalisation to synapses. These data indicate that α–synuclein PFFs are insufficient to induce damage, via changes in tau in rats. Oxidative stress levels were also unchanged following α–synuclein PFF injections into the MFB at 90 d.p.i. and there were

no marked changes in astrocytes, however further experimental studies are needed to provide further clarification. Data from behavioural studies also showed no sustained alterations in motor or cognitive functions as a result of α–synuclein PFFs.

To conclude, these data suggest that despite evidence of phosphorylated α–synuclein spread to anatomically connected regions from the site of injection, these modifications to α–synuclein *per se* are not sufficient to induce further neurodegenerative features of PD, at least not at the time points studied here. Alternatively, the lack of phosphorylated α-synuclein induced at by the dosage of α-synuclein PFFs and site of injection led to relatively low quantities of phosphorylated α-synuclein throughout the brain, therefore may not be sufficient to induce any neurodegenerative changes, therefore longer time points may be required for any effects to occur.

Chapter 4-Effects of 6-hydroxydopamine (6-OHDA) on cognitive dysfunctions and pathological spreading of α–synuclein

4.1 Introduction

6-Hydroxydopamine (6-OHDA) has been one of the most common neurotoxins used to study Parkinson's disease (PD) since its initial description (Ungerstedt, 1968). It was deemed particularly attractive for many years as investigators thought PD to be a single system disorder. Therefore, targeting the dopaminergic system alone was thought to lead to a solution for the disease despite evidence from histological studies demonstrating alterations in non-dopaminergic structures (Agid et al., 1987; Cash et al., 1987). With this in mind, 6-OHDA had clear advantages as it was able to cause nigrostriatal dopamine depletion upon injection in a predictable and stable manner. Other notable benefits of 6-OHDA include its utility for studying symptomatic therapies, understanding L-3,4-dihydroxyphenylamin (L-dopa) induced dyskinesia and in motor fluctuation models (Duty and Jenner, 2011).

6-OHDA itself is structurally similar to catecholamines (Figure 4.1) and due to its high affinity for catecholamine transporters, it is able to induce damage to catecholaminergic neurons (Luthman et al., 1989). Since 6-OHDA targets both noradrenergic neurons and dopaminergic neurons, researchers often use 6-OHDA in conjunction with the noradrenaline reuptake inhibitor desipramine to allow selective targeting of dopaminergic neurons (Bove and Perier, 2012). Owing to its hydrophilic properties, 6-OHDA cannot pass the blood brain barrier (BBB). 6-OHDA can be injected intraventricularly, intracisternally or most commonly intracerebrally to induce damage to the central catecholaminergic systems (Jonsson, 1983). Bilateral injections are not commonly used because of high mortality rates due to complications such

as adipsia, aphagia and seizures (Smith and Young, 1974). Unilateral intracerebral injections therefore became a regular protocol for 6-OHDA administration. Once the researcher has grasped the techniques of intracerebral injection, the rate of dopamine neuron degeneration can be manipulated through different dosages and alternate sites of injection.

For complete and immediate degeneration of the substantia nigra (SN) resulting in full motor and neurobiological consequences, common sites of injection include the medial forebrain bundle (MFB) (Perese et al., 1989) and SN (Stanic et al., 2003; Park et al., 2018). The SN neurons tend to die within 12 h of 6-OHDA injection, accompanied by reduction in striatal dopaminergic terminals and dopamine depletion within 2-3 days (Deumens et al., 2002), with complete loss of dopamine content apparent in the striatum by 3 weeks (Sarre et al., 2004). The number of dopaminergic neurons in the SN also decreases over time with a near complete lesion (>90%) achieved approximately 5 w.p.i. In addition to the dopaminergic cell and fibre loss in both the ipsilateral SN and striatum (Park et al., 2018), cognitive and motor impairments have also been reported upon MFB lesion (Ma et al., 2014).

In contrast, for a partial and progressive approach, intrastriatal 6-OHDA lesion is preferred. From the striatum, the toxin reaches the SN via retrograde transport along the striatal terminals in a progressive manner, often referred to as “dying back mechanism” (Winkler et al., 2002). Overall, intrastriatal injections lead to a milder pathology with low levels of tyrosine hydroxylase (TH) neuronal loss in the SN compared to injections into the MFB site (Sauer and Oertel, 1994). The prolonged rate of progressive dopaminergic depletion of approximately 1-3 weeks (Heuer et al., 2012), allows therapeutic strategies to be tested during the degenerative process due to an accessible therapeutic window.

The extent of dopaminergic neuron depletion in response to 6-OHDA injection also varies with species and dosage. The efficacy of 6-OHDA in dogs, cats and monkeys has been evaluated although the rat remains the most common choice of experimental animal (Bezard and Przedborski, 2011).

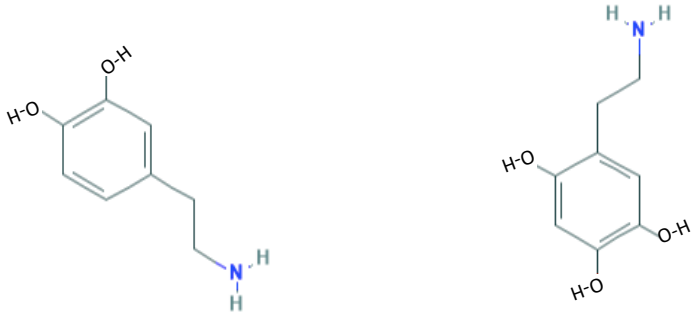

Dopamine **6-OHDA**

Figure 4.1 Chemical structure of dopamine and 6-hydroxydopamine (6-OHDA). Comparison of the chemical structure of dopamine and 6-OHDA. Images adapted from Pubchem.com.

The neuronal damage induced by 6-OHDA is mainly due to oxidative stress caused by the toxin. Due to its high affinity for the dopamine transporter (DAT), 6-OHDA is transferred via DAT into dopaminergic neurons. Once inside the neuron, 6-OHDA accumulates in the cytosol and undergoes auto-oxidation or metabolic degradation producing at high rate such free radicals includes hydrogen peroxide, superoxide, and hydroxyl radicals (Hwang, 2013). Additionally, 6-OHDA can also cause mitochondrial dysfunction within dopaminergic neurons in the SN by accumulating within the mitochondria and inhibiting mitochondrial respiratory chain complex I activity (Glinka et al., 1996) and decreasing mitochondrial membrane potential (Prajapati et al., 2017). Dopamine itself is also an unstable molecule that will undergo auto-oxidative leading to the formation of dopamine quiones and additional free radicals. The reaction is catalysed by oxygen, metals and enzymes such as tyrosinase, MAO and catechol O-methyl transferase (COMT). Together they are involved in dopamine metabolism. MAO-A and MAO-B, located in the outer mitochondrial membrane also degrade excess dopamine in the cytosol by catalysing it's oxidative deamination (Munoz et al., 2012; Jenner and Langston, 2011)

Together, the two mechanisms of 6-OHDA toxicity result in lipid peroxidation, protein oxidation and DNA oxidation (Hwang, 2013) that ultimately further exacerbate oxidative stress and mitochondrial dysfunction (Hwang, 2013).

In PD, evidence from post mortem brain demonstrated the presence of oxidative stress products such as 4-hydroxyl-2-nonenal (HNE) (Yoritaka et al., 1996), a by-product of lipid peroxidation, and 8-hydroxy-deoxyguanosine (8OHG) (Zhang, 1999), a DNA/RNA oxidation production as well as the reactive nitrogen species nitrotyrosine (Duda et al., 2000) in affected

brain regions. Although it is evident that oxidative stress is associated with PD, the mechanisms linking oxidative stress to neurodegeneration and cognitive decline have not been fully worked out.

In models of Alzheimer's disease (AD), oxidative stress has been shown to mediate changes in tau phosphorylation and synapses, ultimately resulting in cognitive decline (Chen and Zhong, 2014) (Zhao and Zhao, 2013). Therefore, a similar mechanism may be occurring in PD. The previous chapter focused predominantly on α–synuclein preformed fibrils (PFFs) induced neurodegenerative pathways. In this chapter, the primary focus is on 6-OHDA induced oxidative stress and SN neuron loss, and the downstream consequences of these events including phosphorylated α-synuclein spread, tau phosphorylation and loss of synaptic proteins that are associated with behavioural outcomes following 6-OHDA injection into rat MFB.

4.2 Aims and objectives

Oxidative stress has long been regarded as a key underlying mechanism across several neurodegenerative disorders. However, the precise association between oxidative stress, cognitive impairment and neurodegeneration remains poorly understood. We propose that substantial and rapid loss of SN neurons in a primed environment of elevated oxidative stress resulting from 6-OHDA injection allows rapid release of α-synuclein from damaged nerve terminals, subsequent α–synuclein spread and the rapid development of neurodegeneration resulting in cognitive and behavioural abnormalities. The objective of this chapter is therefore to elucidate the effects of rapid neuronal loss in the presence of increased oxidative stress levels, in regions that extend beyond the initial MFB injection site and site of neuron loss in

the SN. Changes in tau and α–synuclein phosphorylation were examined via immunohistochemical and biochemical techniques. Changes in synaptic protein amounts were measured as an indicator of synapse function, and behavioural phenotypes resulting from 6-OHDA injection were also investigated. The main objectives were to investigate the following.

Firstly, behavioural tests such as rotarod and Morris water maze (MWM) were used to assess any alterations in motor behaviour and cognition. To further understand the causes of the behavioural phenotype, neuropathological analysis was conducted to examine markers of oxidative stress, changes in tau and α–synuclein phosphorylation and extent of α–synuclein spread. Biochemical techniques were used to examine intracellular changes in protein solubility and phosphorylation. Finally, synaptic proteins were examined as an indicator of alterations in synapse structure.

4.3 Methods

A total of 82 male Sprague-Dawley (SD) rats weighing between 230 - 250 g were used for the experiments described in this chapter. Male rats were used to limit the effects of hormonal interplay. All rats were handled and kept in accordance with the international ethical guidelines at The University of Hong Kong, which are based on National Institutes of Health (USA) animal ethics and British Society of Animal Science - Ethical guidelines for research in animal science: the three R reduction guidelines (replacement, reduction and refinement). Experimental rats were injected unilaterally with 6-OHDA into the MFB. Control and experimental rats were grouped randomly for behavioural tests: induced rotational

behaviour, n = 9; Morris water maze, n = 10; rotarod and cylinder, n = 10; 5-choice serial reaction time task, n = 6 and lastly open field test, n = 6. Immunohistochemical studies were performed on 3-4 rats per control and 6-OHDA group and a designated area of 100mm² was quantified. Furthermore unless stated quantification were conducted as cell counts, otherwise expressed as % area positive of marker of interest. Biochemical analyses were conducted on 5-6 rats per control and 6-OHDA group. A table with information regarding animal ID, groupings and weight can be found in Table 4.1.

Full methods for all experimental procedures described in this chapter can be found in Chapter 2. Experimental timeline for this chapter is shown is (Figure 4.2).

Behaviour	Rat ID	Weight at surgery (g)	Weight at sacrifice (g)	Comments
Apomorphine	40	239	260	
	42	237	263	
	53	230	250	
	54	225	239	
	57	236	241	
	70	358	270	
	93	250	270	
	94	250	271	
	60	233	240	
	62	230	240	
	47	240	250	
	71	245	255	
	73	246	260	
	90	242	250	
	179	232	240	
	43	250	263	
	41	250	267	
	91	250	260	
Rotarod and cylinder test	1	240	260	
	2	250	260	
	3	245	259	
	4	247	260	
	5	244	260	
	70	242	260	
	72	250	269	
	57	230	265	
	58	235	240	
	59	244	250	Didn’t perform
	6	242	250	
	7	241	258	
	8	257	268	
	9	230	234	
	10	250	265	
	11	251	260	
	12	230	245	
	51	233	258	
	71	245	250	
	47	250	260	
	40	234	250	
	42	246	260	
	44	241	260	
	46	241	260	
	70	246	263	
	72	240	246	

Morris water maze	75	240	260	
	76	234	255	
	78	243	260	
	84	245	262	
	81	245	269	
	41	250	270	
	43	241	265	
	45	240	260	
	47	246	261	
	71	248	260	
	73	250	265	
	77	249	270	
	79	239	247	
	80	240	261	
	82	243	268	
5- Choice serial reaction time task (5-CSRTT)	1	240	261	Didn't perform
	2	230	255	
	3	239	252	
	4	240	261	
	5	241	262	
	6	247	268	
	7	250	266	
	1	250	271	
	2	250	267	
	3	250	273	
	4	241	260	
	5	243	264	
	6	244	260	
	7	250	271	
Open field test	1	240	264	
	2	247	270	
	3	249	276	Didn't move
	4	225	240	
	5	225	246	
	6	227	247	
	7	230	250	
	8	231	255	
	9	232	250	
	10	230	250	
	11	230	254	
	12	250	253	

Table 4.1 A compilation of 6-OHDA and control injected animals organised according to animal behavioural testing. Information on exclusion criteria, animal ID and animal's weight at time of surgery and at end of final behaviour test prior to sacrifice. Orange=6-OHDA, Blue=Control

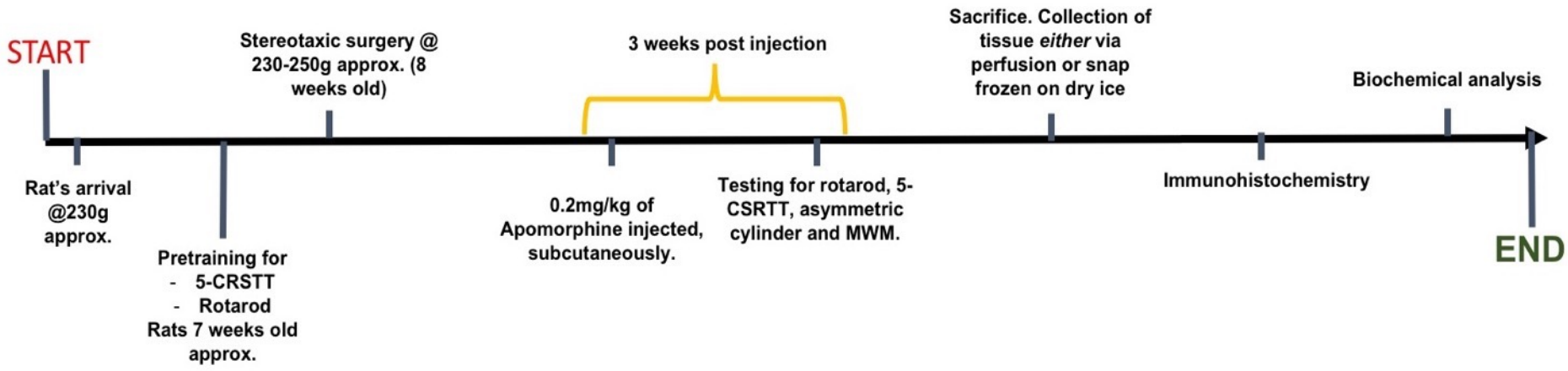

Figure 4.2 Timeline of experimental design for 6-OHDA and control rats. Rats arrived at approximately 230 g in weight and were allowed to acclimatise prior to behavioural pre-training. Pre-training began when animals were 7 weeks old. Depending on the behavioural group allocation, rats underwent pre-training for rotarod or 5-choice serial reaction time task (5-CSRTT). For tests that do not require pre-training, they were directly tested at 3 weeks post injection (w.p.i.). Collection of rat brain tissue followed by, immunohistochemical analysis and biochemical analysis were performed on those collected rat brain tissues.

4.4 Results: Validation of 6-OHDA neurotoxin model at 3 weeks post injection

4.4.1 6-OHDA led to induced rotational behaviour

Control and 6-OHDA rats at 3 w.p.i. received a subcutaneous injection of the dopamine agonist, apomorphine (0.2 mg/kg) according to a previously established protocol (Shah et al., 2019). 6-OHDA-injected rats exhibited an increase in contralateral rotations within the 30 min testing period compared to control (PBS injected) rats. Figure 4.3 indicates marked sensitivity towards apomorphine due to the reduction in dopamine in 6-OHDA-injected rats.

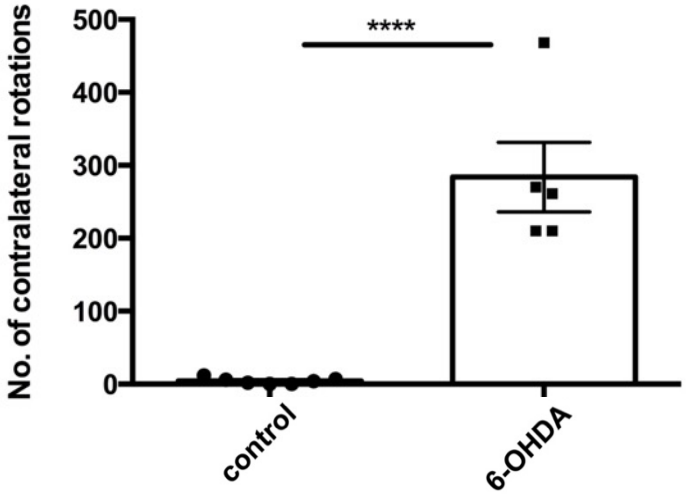

Figure 4.3 6-OHDA injected animals exhibited an increase in contralateral rotations in a drug induced rotational test following injection with apomorphine. The bar chart shows the number of contralateral rotations within a 30 min time frame. The number of rotations is proportional to dopamine loss. 6-OHDA-injected rats showed significantly more rotations than control rats. Error bar denotes mean ± standard error of mean (SEM), control, n = 7, 6-OHDA, n = 5, *****p<0.0001,* statistical test used unpaired, t-test**.**

4.4.2 6-OHDA caused dopaminergic neuron depletion within the SN

Immunohistochemical analysis using an antibody against TH was performed to assess the severity of dopaminergic loss within the SN resulting from 6-OHDA injection.

Previously (Shah et al., 2019) observed that at 3 weeks after unilateral 6-OHDA injection into rat MFB only approximately 28% TH immunoreactivity remained on the ipsilateral side compared to the contralateral side in the SN of 6-OHDA-injected rats. Similarly, in this work substantial reduction of TH-positive cells was found in the ipsilateral SN of 6-OHDA-injected rats compared to the contralateral side, and relative to control rats (Figure 4.4A). A significant difference was noted in total TH cell count between control and 6-OHDA treated rats.

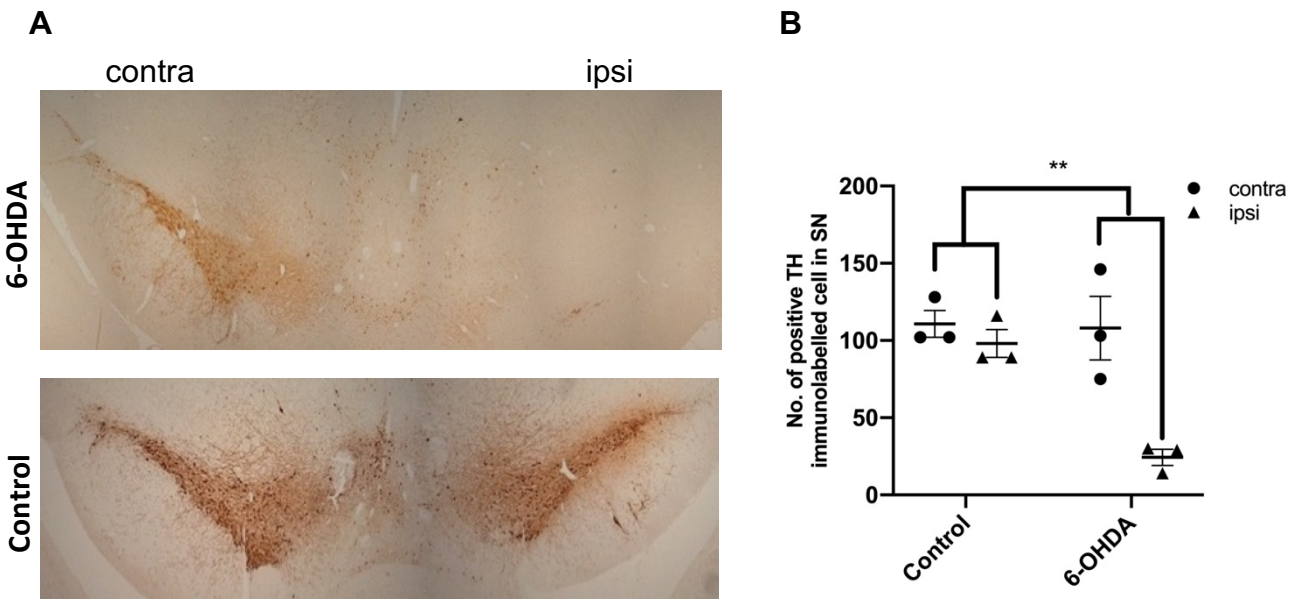

Figure 4.4. Reduction of tyrosine hydroxylase (TH) immunopositivity in 6-OHDA-injected rats. A) 7 µm sections from control and 6-OHDA-injected rats, 3 weeks post-injection, were immunolabelled using an antibody raised against TH. 6-OHDA injected animals demonstrated an ipsilateral loss of TH +ve cells in the substantia nigra compared to control animals. Red box indicates region of interest for counting TH positive cells. B) Graph shows the quantification of the number of TH positive total cell count in control and 6-OHDA animals, in contralateral and ipsilateral. Analysis using unpaired t-test on the difference between pre and post-surgery of control and 6-OHDA indicated a statistical significance, and demonstrated a substantial reduction in positive TH cells within the ipsilateral hemisphere of 6-OHDA rats compared to control. Levels of significance are denoted by ** $p < 0.01$ Data presented as mean ± standard error of the mean (SEM), n=3.

4.5 Results: Behavioural deficits due to 6-OHDA

The primary manifestations of PD include abnormalities in movement, difficulties with gait and imbalance, slowness in movement and a resting tremor (Mazzoni et al., 2012). The cause of such motor symptoms in PD is due to the loss of nigral dopaminergic neurons and dopamine depletion in the basal ganglia (Alexander, 2004). PD patients are also at higher risk of developing dementia-related symptoms compared to the general population (Aarsland et al., 2003) with approximately 80% of longitudinally tracked patients with PD eventually developing dementia during the course of disease (Hely et al., 2008).

To assess for motor impairments within this model, rotarod and asymmetric cylinder tests were used and the MWM test with the 5-choice serial reaction time task (5-CSRTT) was used to assess cognitive deficits.

4.5.1 6-OHDA induced motor deficit

The rotarod test was adapted from a previously established protocol (Iancu et al., 2005). Consistent with findings from the drug-induced apomorphine rotation test, 6-OHDA injected rats clearly demonstrated reduced latency on the spinning rotarod at 3 w.p.i. compared to control group (Figure 4.5A).

A

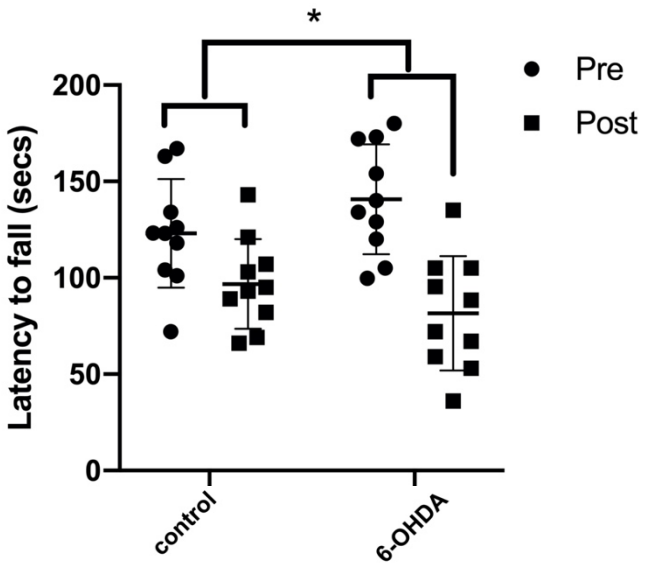

Figure 4.5 Rotarod test for control and 6-OHDA injected rats. A reduction in latency to fall following 6-OHDA injection (post) compared to the initial baseline measures obtained during training (pre), demonstrates that 6-OHDA injection induces a motor deficit. Control and 6-OHDA groups showed similar baseline measurements during training. Analysis with unpaired t-test on the difference between pre and post-surgery of control and 6-OHDA indicated a statistical significance. Levels of significance are denoted by ** $p < 0.05$,* data is mean ± SEM, n = 10.

4.5.2 6-OHDA induced asymmetric deficits

Rats that received unilateral 6-OHDA lesions exhibited marked preferential use of the ipsilateral forepaw, and thus reduction in the usage of the contralateral (impaired) forepaw relative to control animals (Figure 4.6A). Activities including pushing off, touching and landing were also noted within the time frame (Figure 4.6B). Due to variances in animal behaviour tasks, 1 rat did not comply with the asymmetric cylinder test therefore had to be excluded from the task.

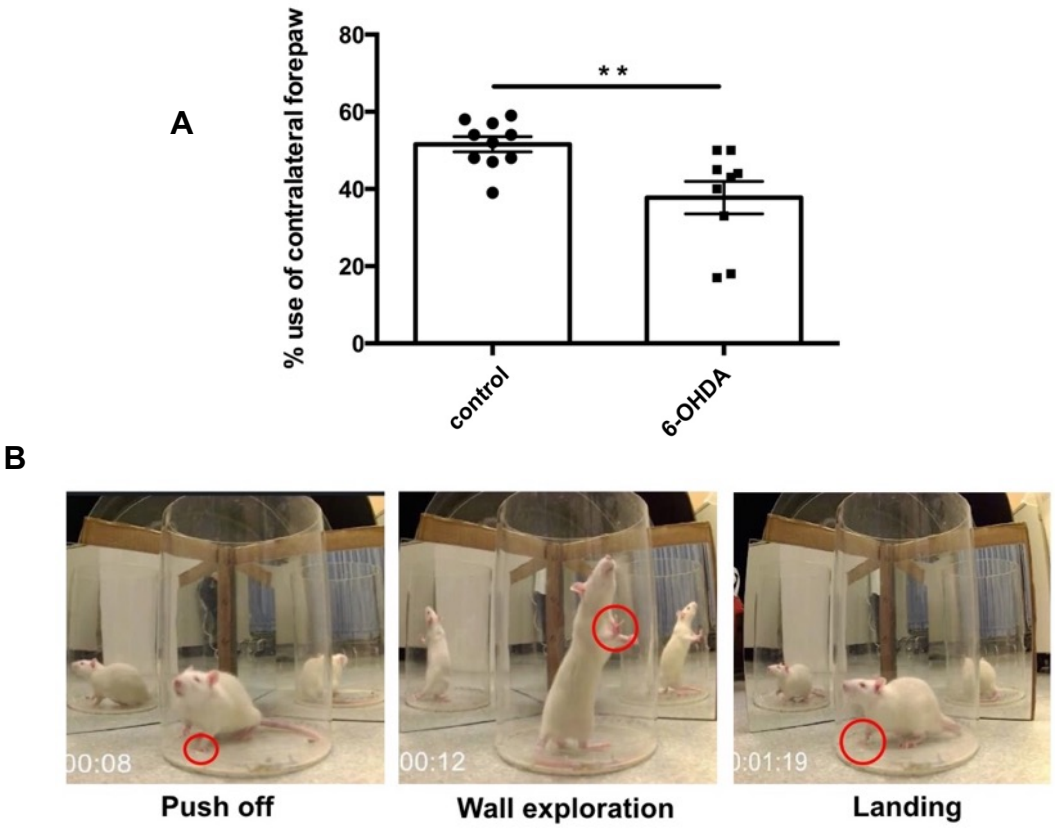

Figure 4.6 6-OHDA injected rats show reduced use of contralateral paws. **A)** Graph shows that 6-OHDA injected animals show a contralateral forepaw impairment, with significantly reduced use of the contralateral forepaw compared to control animals during the asymmetric cylinder test, signifying a fine motor deficit. Data is mean ± SEM, control, n = 10, 6-OHDA, n = 9. ***p<0.01,* statistical test used, unpaired t-test. **B)** Snap shots from the asymmetric cylinder task from a representative rat. Activities including push off, wall exploration and landing were noted within the 5 min time frame or 10 total touches.

The results from the two motor tasks are consistent with findings reported in previous literature, whereby unilateral injection of 6-OHDA into the MFB can induce motor deficits and a asymmetric forepaw impairment (Rozas et al., 1997) (Iancu et al., 2005; Heuer et al., 2012).

4.5.3 6-OHDA-injected rats did not exhibit executive dysfunction

Results for the percentage of accuracy and premature responses obtained from the 5-CSRTT are shown in Figure 4.7A-B. The percentage of accuracy reflects the attention maintained throughout the task, while premature responses detect responses before stimulus onset and is part of inhibitory control. The percentage of accuracy depicts the attention.

The percentage of accuracy measured in control and 6-OHDA groups prior to surgery were very similar. Three weeks post-surgery, the control and 6-OHDA rats showed similar increase in the percentage of accuracy measure, and there were no significant differences between groups. Prior to surgery, control rats showed a slightly higher premature response compared to 6-OHDA pre-surgery animals. However this did not reach statistical significance, and both groups showed only a minor reduction is this measure post-surgery.

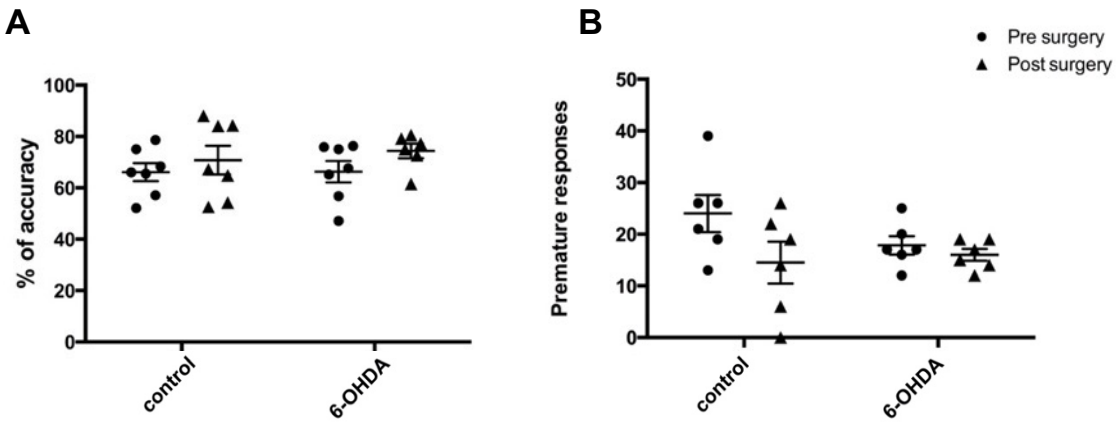

Figure 4.7. The 5-CSRTT was used to assess executive dysfunction in control and 6-OHDA rats. **A)** Graphs show percentage of accuracy during the training and testing phases for control and 6-OHDA-injected rats. 6-OHDA post-surgery rats showed a slight, but non-significant, increase in the percentage of accuracy compared to control post-surgery rats. Overall there were no significant differences between pre-and post-surgery measures for either group, or when comparing groups, n = 7. **B)** Graphs for the number of premature responses measured during training and testing phases for control and 6-OHDA-injected rats. Control post-surgery rats exhibited a slight, but non-significant, reduction in the number of premature responses relative to 6-OHDA-injected rats. Analysis using unpaired t-test on the difference between pre and post-surgery of control and 6-OHDA did not indicate any statistical significance **(A,B).** Data is mean ± SEM, n = 6. Pre = pre-surgery, Post =post-surgery.

4.5.4 6-OHDA induced both spatial and memory impairment

Using a similar approach as described in Chapter 3 the MWM was used to test for any spatial learning deficits and/or reference memory impairments. Rats were trained accordingly, using a protocol previously published by (You et al., 2019) as described in Chapter 2, Section 2.2.5.4.

Control rats were able to learn the location of the platform throughout the training days with a progressively shorter latency to escape time, while 6-OHDA injected rats plateaued by day 2 of training and the latency to escape time remained fairly consistent with limited improvement over time (Figure 4.8A). These findings reflected the results shown on the probe test day as 6-OHDA rats also showed reduced number of platform crossings relative to control rats, indicating an impairment in reference memory (Figure 4.8B). Subsequently, the percentage of time spent within the "target quadrant" which is where the platform was located prior to its removal, was reduced by 6-OHDA (Figure 4.8C).

These results demonstrated that similarly to Carvalho et al. (2013) and Ma et al. (2014) unilateral injection of 6-OHDA into the MFB induced cognitive deficits relating to spatial awareness and reference memory within 3 w.p.i. Furthermore, a study looking at reduction of somatostatic like immunoreactivity in cortex and hippocampus of control and rats injected with cysteamine (neurotoxin), noted that despite visuospatial impairment induced by neurotoxin group, there were no notable differences in swim speed between the two groups (Fitzgerald and Dokla, 1989). This suggests that locomotion and visuospatial impairment are mediated differently and locomotion does not impact visual ability. However, for future experiments using the MWM task as a measure for visuospatial awareness, using more sophisticated software capable of detecting the swim speed of animals would be beneficial.

Finally, despite the lack of cognitive impairment demonstrated with the 5-CSRTT, due to inexperience in running the 5-CSRTT task, the effects of 6-OHDA on executive function remained inconclusive and cannot be used to compare with findings from the MWM.

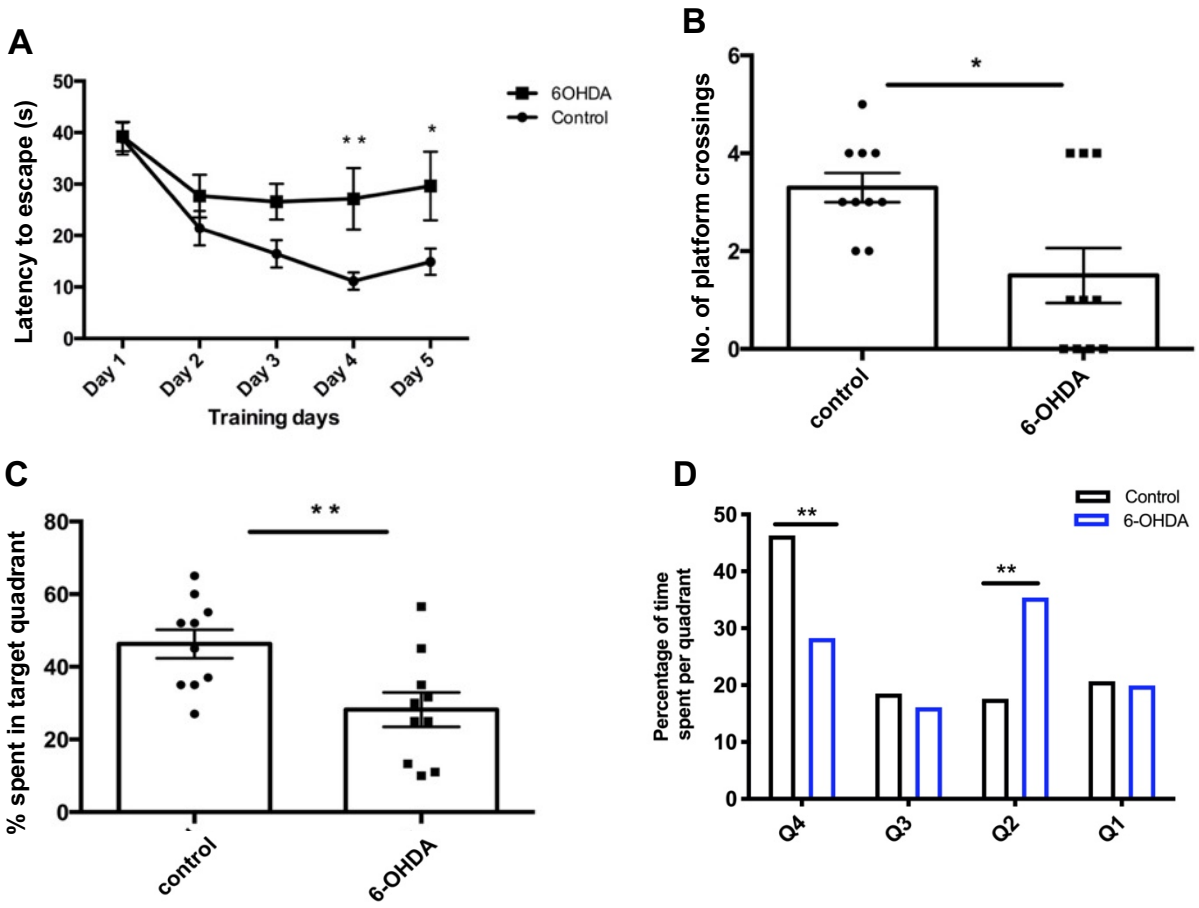

Figure 4.8. 6-OHDA-injected rats show impairments in visuospatial and reference memory in the Morris water maze. **A)** The graph shows the learning curve during training days 1-5. 6-OHDA-injected rats showed a learning deficit throughout the task compared to control animals where there was a reduction in escape latency from the initial training day. 6-OHDA-injected rats took significantly longer than control rats to escape the MWM on days 4 and 5. Analysis with repeated 2-way ANOVA indicated a significant effect of treatment on escape latency but no effect of timepoint or a timepoint x treatment interaction (Appendix 1). Post-hoc analysis by Tukey's multiple comparisons test did show significance in control or 6-OHDA-treated groups on 4th and 5th day of training. Levels of significance are denoted by ** p < 0.05, **p < 0.01.* Data is mean ± SEM, n = 10. **B)** The number of platform crossings during the probe test day indicated that 6-OHDA-injected rats showed a deficit in reference memory compared to PBS-injected controls with fewer numbers of platform crossings. **C)** Percentage spent in the target quadrant during the probe test day of MWM also indicated that 6-OHDA-injected rats spent less time in the target quadrant compared to control animals. D) Percentage of time spent per quadrant during probe test day. Analysis with repeated 2-way ANOVA indicated a significant effect of treatment on quadrant preference but no effect of timepoint or a time point x treatment interaction (Appendix 1). Post-hoc analysis by Sidaks's multiple comparisons test did show significance in control or 6-OHDA-treated groups. Levels of significance are denoted by ***p < 0.01.* Data is mean ± SEM, n = 10.

4.5.5 6-OHDA did not induce anxiety-like behaviour or lead to alterations in land-based locomotor activity

The open field test was conducted using a protocol adapted from (Kim et al., 2019). The results showed that 6-OHDA did not cause any anxiety-like activity as both control and 6-OHDA lesioned rats spent similar amount of time within the centre zone (Figure 4.9A).

Measurement of the total distance travelled throughout the task indicate that although 6-OHDA lesioned rats demonstrated a slightly reduced overall distance travelled there was no significant difference between the two groups (Figure 4.9B). Trajectories obtained from PanLab analysis software also demonstrate the similarity in movement patterns between the two groups of rats (Figure 4.9C-D).

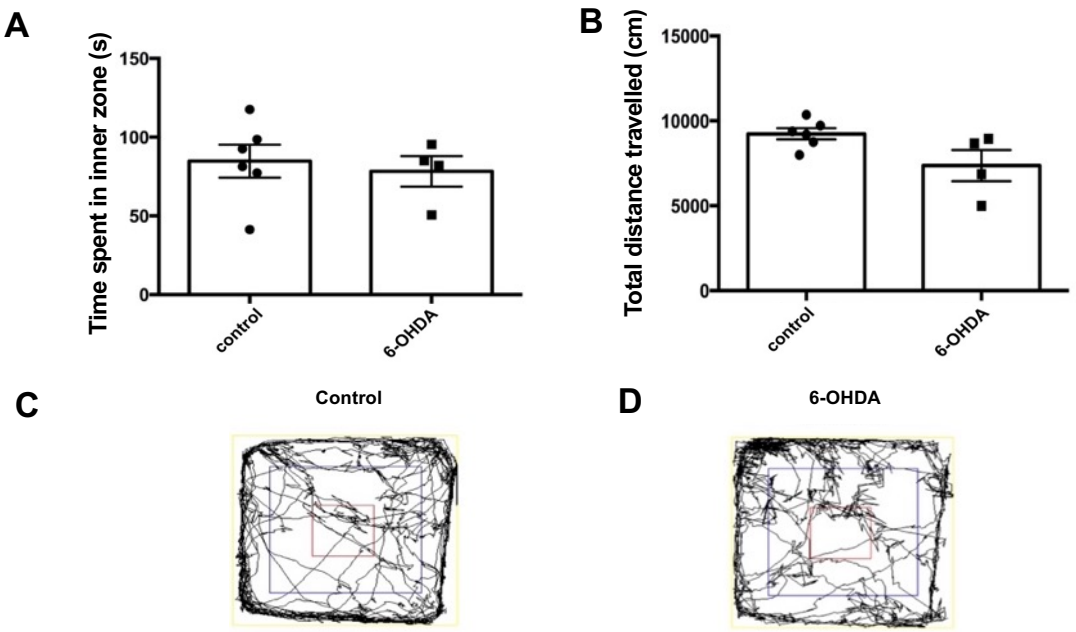

Figure 4.9. 6-OHDA did not-induce alterations in anxiety-like behaviour or land-based locomotor activity in the open field test. **A)** Measures of time spent in seconds inside the centre zone as an indication of anxiety-like behaviour using the open field test shows no difference between control and 6-OHDA groups. **B)** Land-based locomotor activity was measured as total distance travelled in centimetres. Control and 6-OHDA rats travelled similar distances. For **C)** control and **D)** 6-OHDA-treated rats, the black lines show the trajectories of representative animals during the open field task. Yellow box represents outer zone, blue square is the middle zone and the red box indicates the inner zone of the open field arena. Data were expressed as mean ± SEM, control, n = 6, 6-OHDA, n = 4. Statistical test used Mann-Whitney U **(A-B).**

4.6 Results: Changes in oxidative stress and phosphorylation of α–synuclein due to 6-OHDA

Dementia is considered to be resulted from the loss of connectivity within cognitive circuits (Braak et al., 2004; Braak et al., 2003) and the accumulation of pathological factors (Goedert et al., 1998). The presence of LBs and LNs correlate closely with dementia in PD (Irwin et al., 2013). By assessing pathological changes in α–synuclein and neurodegenerative events including tau modifications and oxidative stress, it was hoped that fundamental insights into the causes of the behavioural phenotypes identified in 6-OHDA-injected rats could be elucidated.

4.6.1 6-OHDA induced robust increase in oxidative stress levels

To investigate oxidative stress responses resulting from injection of rat MFB with 6-OHDA, immunohistochemical analysis was performed on brain sections from 6-OHDA-injected rats using antibodies against markers of oxidative stress, 8-hydroxy-deoxyguanosine (8OHG), a DNA/RNA oxidation production, and reactive nitrogen species, nitrotyrosine.

Increased oxidative stress responses in the frontal cortex and hippocampal subfield, CA1 were confirmed using an antibody specific to 8OHG as shown in (Figure 4.10A,C,D). Although hippocampal CA3 also demonstrated an increase in 8OHG labelling, it was not significant when comparing 6-OHDA injected rats to controls (Figure 4.10E). The additional oxidative stress marker nitrotyrosine was also examined and although there was a trend of increase, this was not deemed significant overall (Figure 4.10B,G). These data suggest that 6-OHDA induced a robust increase in oxidative stress levels.

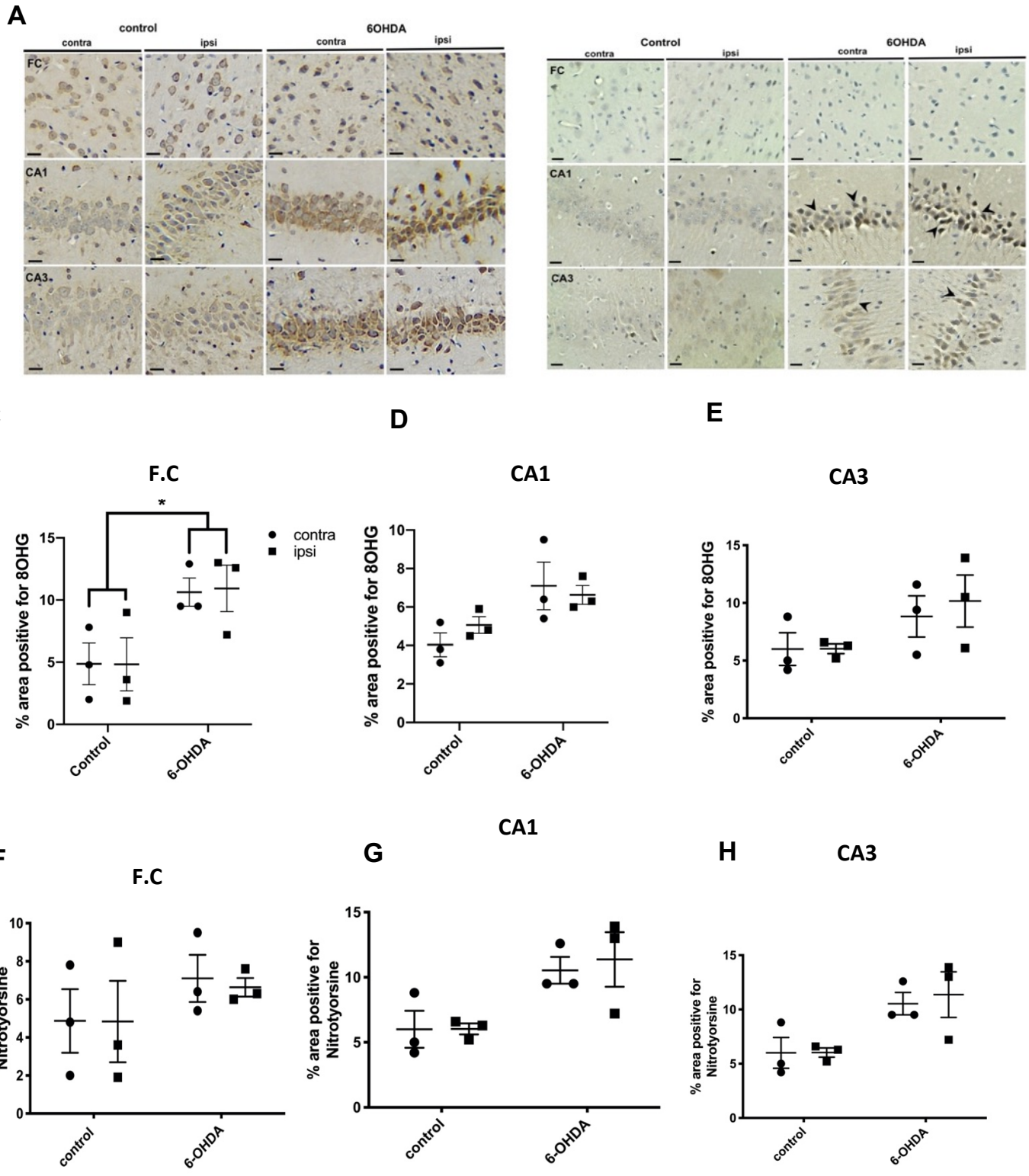
A
control
6OHDA
contra
ipsi
contra
ipsi
FC
CA1
CA3
Control
6OHDA
contra
ipsi
contra
ipsi
FC
CA1
CA3
C
F.C
*
% area positive for 8OHG
contra
ipsi
Control
6-OHDA
D
CA1
% area positive for 8OHG
control
6-OHDA
E
CA3
% area positive for 8OHG
control
6-OHDA
F
F.C
% area positive for Nitrotyorsine
control
6-OHDA
G
CA1
% area positive for Nitrotyorsine
control
6-OHDA
H
CA3
% area positive for Nitrotyorsine
control
6-OHDA

Figure 4.10 6-OHDA induced a robust oxidative stress response. **A)** Using an antibody raised against anti-8-hydroxyguanosine (8OHG) to detect for damage in DNA/RNA, 7 µm paraffin embedded rat brain sections from control and 6-OHDA injected rats were immunolabelled. Regions of the brain shown include frontal cortex and hippocampal subfields, CA1 and CA3, both contralateral (contra) and ipsilateral (ipsi) hemispheres. Scale bar 20 µm. **B)** Using an antibody raised against anti-nitrotyrosine to detect for cell damage and inflammation, 6-OHDA injected animals showed an increase in anti-nitrotyrosine positive cells in both the frontal cortex and hippocampal CA1 and CA3, compared to control animals, *n=1*. Scale bar 20 µm. Analysis with unpaired t-test on the difference between contralateral and ipsilateral hemisphere of control and 6-OHDA showed a statistical significance in Fc region **(C)** while CA1 and CA3 did not indicate any statistical significance **(D,E).** Analysis of the percentage area positive for anti-nitrotyrosine did not show any statistical significance between control and 6-OHDA group in Fc, CA1 or CA3 **(F, G, H).** Data is mean ± SEM, n = 3.

4.6.2 6-OHDA triggered phosphorylation of α–synuclein

To investigate whether the elevated level of oxidative stress induced by 6-OHDA can trigger changes leading to phosphorylation of α–synuclein, immunohistochemistry was performed on 7 µm thick tissues from both control and 6-OHDA injected rats, using an antibody raised against phosphorylated α–synuclein. Line drawings of the frontal cortex, striatum and hippocampal sections are shown in Figure 4.11A, where red circles indicate the regions immunolabelled. Positively labelled cells containing phosphorylated α–synuclein appearing similar to those triggered by α–synuclein PFFs were found in regions of interest including frontal cortex, striatum, hippocampus and cortex (left panel). Immunoreactivity for phosphorylated α–synuclein was not noted in control injected rats that received PBS (right panel, Figure 4.11B). Quantification of total phosphorylated α-synuclein load induced by 6-OHDA injection versus control is shown in Figure 4.11C.

The presence of phosphorylated α–synuclein from 6-OHDA unilateral lesion coincides with existing literature that an environment of elevated oxidative stress can trigger changes in α–synuclein including increased phosphorylation (Musgrove et al., 2019; Scudamore and Ciossek, 2018; Norris and Giasson, 2005).

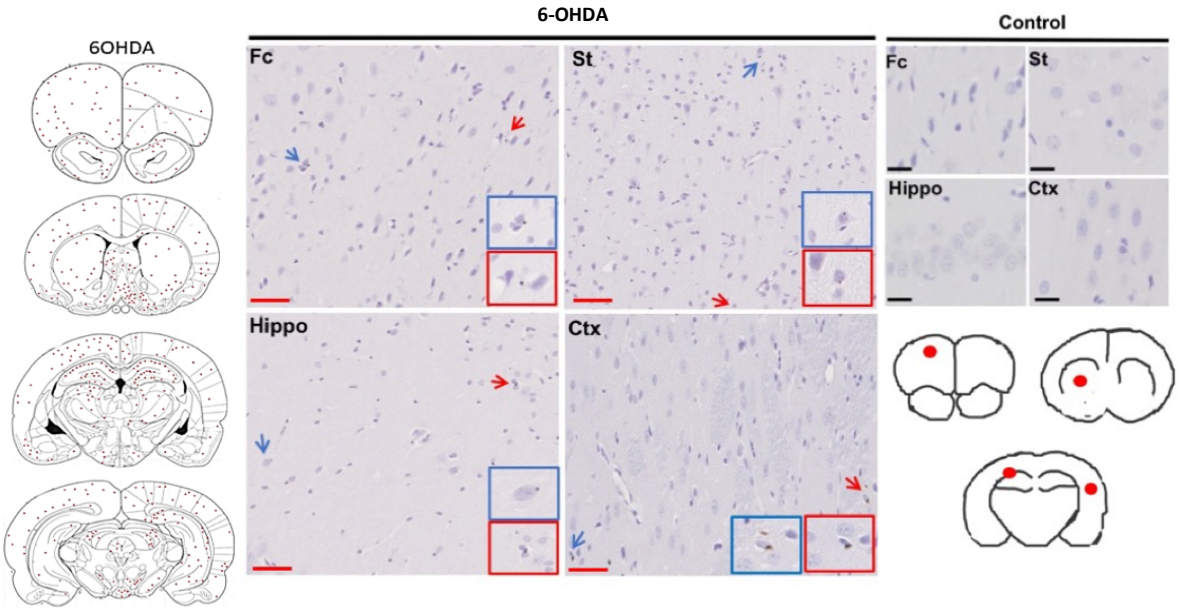
6OHDA
6-OHDA
Control
Fc
St
Hippo
Ctx
Fc
St
Hippo
Ctx

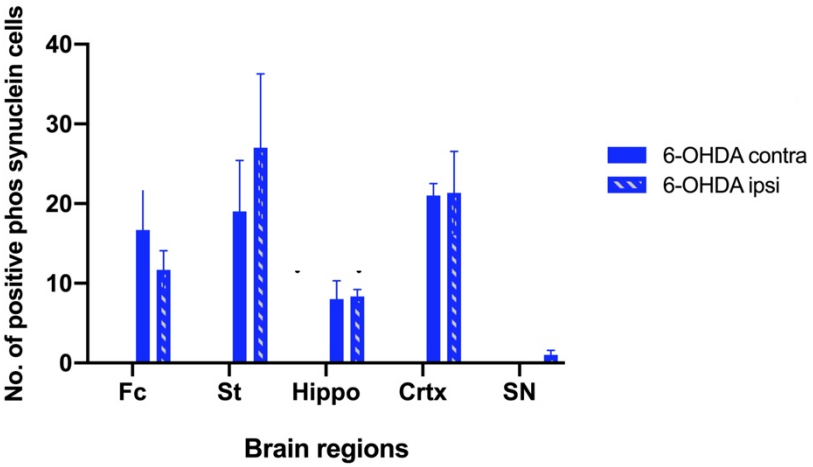
No. of positive phos synuclein cells
40
30
20
10
0
Fc
St
Hippo
Crtx
SN
Brain regions
6-OHDA contra
6-OHDA ipsi

Figure 4.11 A) Immunohistochemistry was performed on 7 µm thick brain tissues from rats unilaterally injected with PBS (control) or 6-OHDA into the MFB. An antibody raised against phosphorylated aSyn at serine 129 (81A) was used to label cells containing phosphorylated α-synuclein. Control rats (right panel) did not show any 81A immunoreactivity, while cells showed faint positive labelling for phosphorylated α-synuclein in Fc, St, Hippo and Crtx in response to 6OHDA. Red scale bar 20 µm, black scale bar, 5 µm n = 3. Blue and red arrows indicate phosphorylated α-synuclein-positive cells. Insets showed higher magnification of cells containing phosphorylated aSyn. Images are from representative rodents. Fc = Frontal cortex, St = Striatum, Hippo = Hippocampus and Crtx = cortex. Representative illustrations showing the Fc, striatum, hippocampus and cortical areas from which sections were obtained and immunolabelled (indicated with red circles). B) The total number of positively immunolabelled cells in three animals of each group were counted and the positions marked on coronal brain traces. Cells positive for phosphorylated α -synuclein were observed in many regions including those directly and indirectly connected to the MFB after 6-OHDA injection. The green circle indicates the MFB site of injection. C) Graph of total phosphorylated α-synuclein load in various brain regions after α-synuclein- PFF injection into the MFB region. Analysis with unpaired t-tests on the difference between pre and post-surgery for control and 6-OHDA did not indicate any statistical significance for each of the regions (Fc, ST, Hippo, Crtx and SN). Results were presented as mean ± SEM, *n=3*.

4.7 Results: Effects of 6-OHDA on protein solubility

Following a protocol based on that published by (Peng et al., 2018), the solubility of α-synuclein and tau proteins in 6-OHDA injected and control brain tissues were analysed. Brain regions were homogenised according to the method described in Section 2.2.8 to generate high salt (HS), high-salt plus Triton-x (Tx), sarkosyl-soluble (SS) and sarkosyl-insoluble (SI) fractions. Samples were then immunoblotted using antibodies against α–synuclein and tau as previously described in Chapter 3.

4.7.1 Sarkosyl extraction: 6-OHDA did not lead to change in the solubility of α-synuclein or tau

To determine if 6-OHDA caused changes in the solubility of α–synuclein or tau, such as would be expected should these proteins aggregate, the amounts of each protein extracted in increasingly stringent buffers were examined. When blots were probed with an antibody against α–synuclein antibody, bands were only observed in both the HS and HS plus Tx fractions; no apparent α–synuclein band was found in the SS fraction (Figure 4.12C) or the SI fraction (Figure 4.12 A,B). There were no differences in α–synuclein amounts in different fractions between hemispheres, or with treatment (Figure 4.12C). Tau was detected using the DAKO total tau antibody. Tau was present primarily in the HS, Tx and SS fractions from the frontal cortex of control and 6-OHDA- injected rats (Figure. 4.12D). No tau band was found in the SI fraction (data not shown). Tau that is insoluble in sarkosyl is aggregated and filamentous (Noble et al., 2003). The absence of sarkosyl-insoluble tau suggests that tau is not aggregated in the control rat brain and that tau aggregation is not induced by 6-OHDA. The results indicated that 6-OHDA did not induce any major changes in either α–synuclein or tau solubility, although these data must be interpreted cautiously.

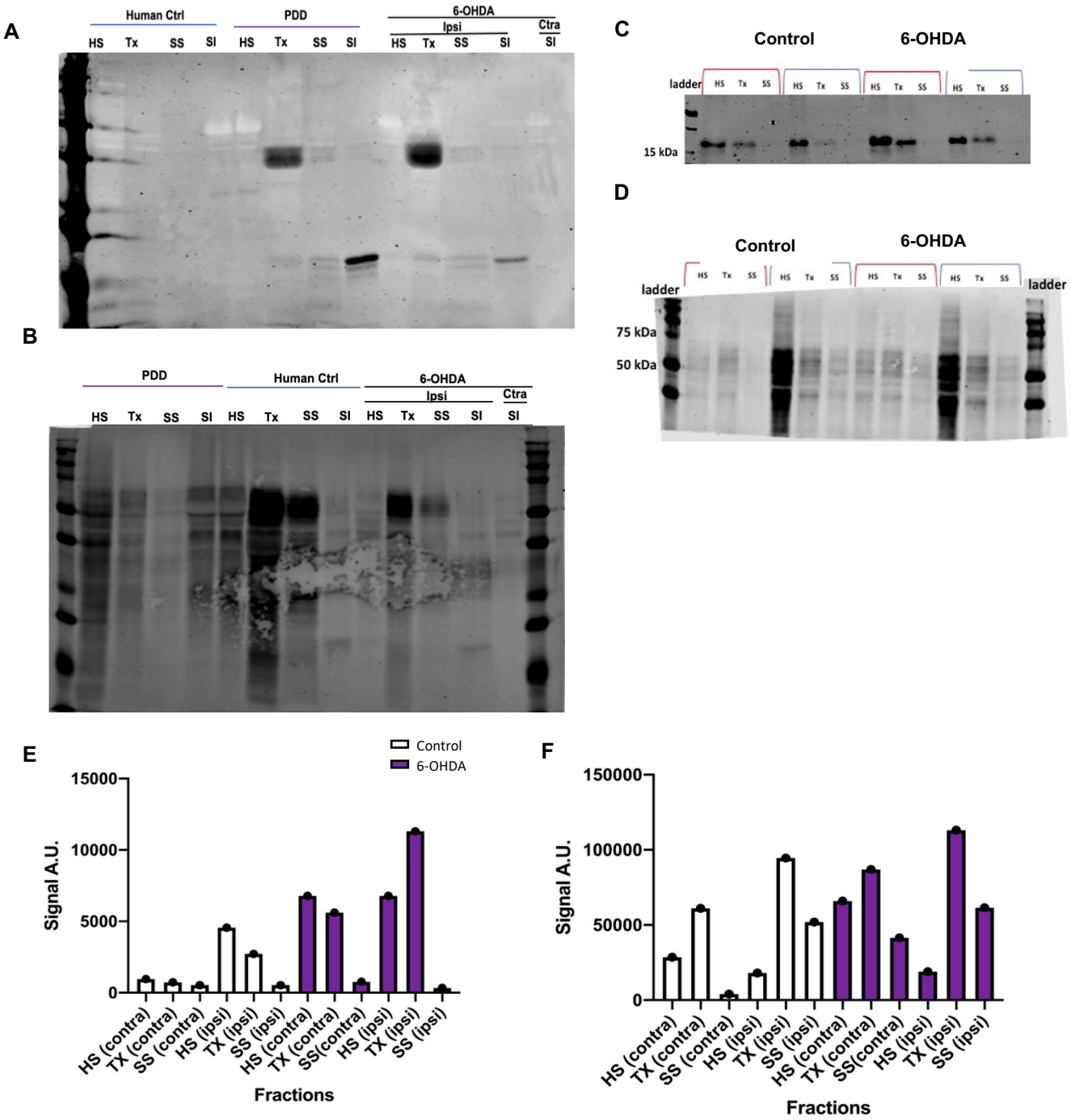

Figure 4.12. A,B) PDD, postmortem brain and ipsilateral and contralateral frontal cortex of 6-OHDA injected rat were biochemically fractionated to yield high salt (HS), high salt-triton (Tx), sarkosyl-soluble (SS) and sarkosyl insoluble (SI) fractions. Samples were immunoblotted with an antibody against α-synuclein and tau. Blots A and B were not quantifiable due to the quality of immunoblots. Injection of 6-OHDA into rat MFB did not cause changes in the solubility of α-synuclein or tau. Proteins from the ipsilateral (blue lines) and contralateral (red lines) hemispheres of frontal cortex from a control-injected and 6-OHDA injected rat were biochemically fractionated using high salt (HS), high salt-Triton x (Tx), and sarkosyl (SS) -soluble fractions. Samples were immunoblotted with an antibody against **C)** total α-synuclein (19 kDa), **D)** total tau (46 kDa-68 kDa), n= 1. The majority of the tau and α-synuclein content was observed in the HS fraction. α-synuclein was also prominent in the Tx fraction. **E,F)** Show the quantification of the corresponding immunoblots, **C)** α-synuclein between control and 6-OHDA samples and **D)** tau between control and 6-OHDA.

4.7.2 Optimisation of antibodies against total and phosphorylated tau

A series of optimisation procedures were conducted to identify suitable tau antibodies for the rat brain tissue and to detect any degradation products. The initial optimisation step was to find compatible antibodies against total tau and phosphorylated tau. Two samples from the HS fraction of the frontal cortex region were immunoblotted with a series of total tau antibodies (Tau-5, BT2 and DA31) (Figure 4.13A) and two antibodies against phosphorylated tau (rabbit polyclonal pTau404 and mouse monoclonal CP13 which detects pSer202) (Figure 4.13B). All three total tau antibodies showed tau bands of the expected molecular weight (46-64 kDa), but also a strong unexpected band of lower molecular weight (green arrows). A similar non-specific band was also apparent when the CP13 antibody was used, suggesting cross reactivity with the secondary anti-mouse IgG antibody. The in question band was still visible, though less intense when the rabbit polyclonal pTau404 antibody was used (black arrow). Furthermore, when the monoclonal DA31 and polyclonal pTau404 antibodies were used together (Figure 4.13C.i), although both antibodies were expected to detect presumed tau bands at 46-64kD, overlap of the additional bands detected was incomplete, suggesting that pTau404 is not detecting only phosphorylated tau. Another brand of secondary anti-mouse IgG antibody (secondary A) was next used (Figure 4.13C.ii.). Under these circumstances, the non-specific bands at 37-50kDa were no longer detectable, but neither were the expected bands around 46-64 kDa; instead only a single strong band was detected at 50 kDa (red arrow).

An antibody against pTau396 was also used, and this detected bands of the expected molecular weight for tau and a strong band of approximately 25 kDa, (pink arrow) (Figure 4.13D.i). The 25 kDa band remained when membranes were incubated with the pTau396

antibody in the absence of secondary antibody, purple arrow (but not vice versa), suggesting cross-reactivity of the primary antibody with the rat samples (Figure 4.13Dii-D.iii.). A blank membrane void of any antibodies was also included as a negative control. No signal was detected, suggesting that the bands in question were probably due to cross reactivity of antibodies or degradation of the samples. The results suggested that neither of the phosphorylated tau antibodies (pTau404 or pTau396) was suitable for further use (Figure 4.13D.iv).

A rabbit polyclonal antibody against total tau was next tested using the high salt fraction. The total tau antibody (DAKO) is raised against the middle of the tau molecule, and identifies full length tau, C and N terminal fragments (Figure 4.14A). The AT8 antibody that recognises the double phosphorylated tau epitope of serine 202 and threonine 205, often regarded as a suitable marker for late stage filamentous tau (Augustinack et al., 2002), was also tested. Blots were incubated sequentially with the total tau and phosphorylated tau antibodies (Figure 4.14B). Due to the secondary antibodies being tagged with different fluorophores, it was possible to detect signals detected by both antibodies simultaneously using a Li-Cor Odyssey scanning system. Both the total tau and phosphorylated tau bands that were detected corresponded in molecular weight, showing bands at sizes predicted for tau, along with the non-specific band at 50 kDa (Figure 4.14C). Samples from wild-type mouse brain and htau mouse brain were run in comparison. Htau mice express the entire wild-type human tau gene on a mouse tau knockout background and so all six tau isoforms present in the adult human central nervous system (CNS) are present in htau brain (Andorfer et al., 2003).

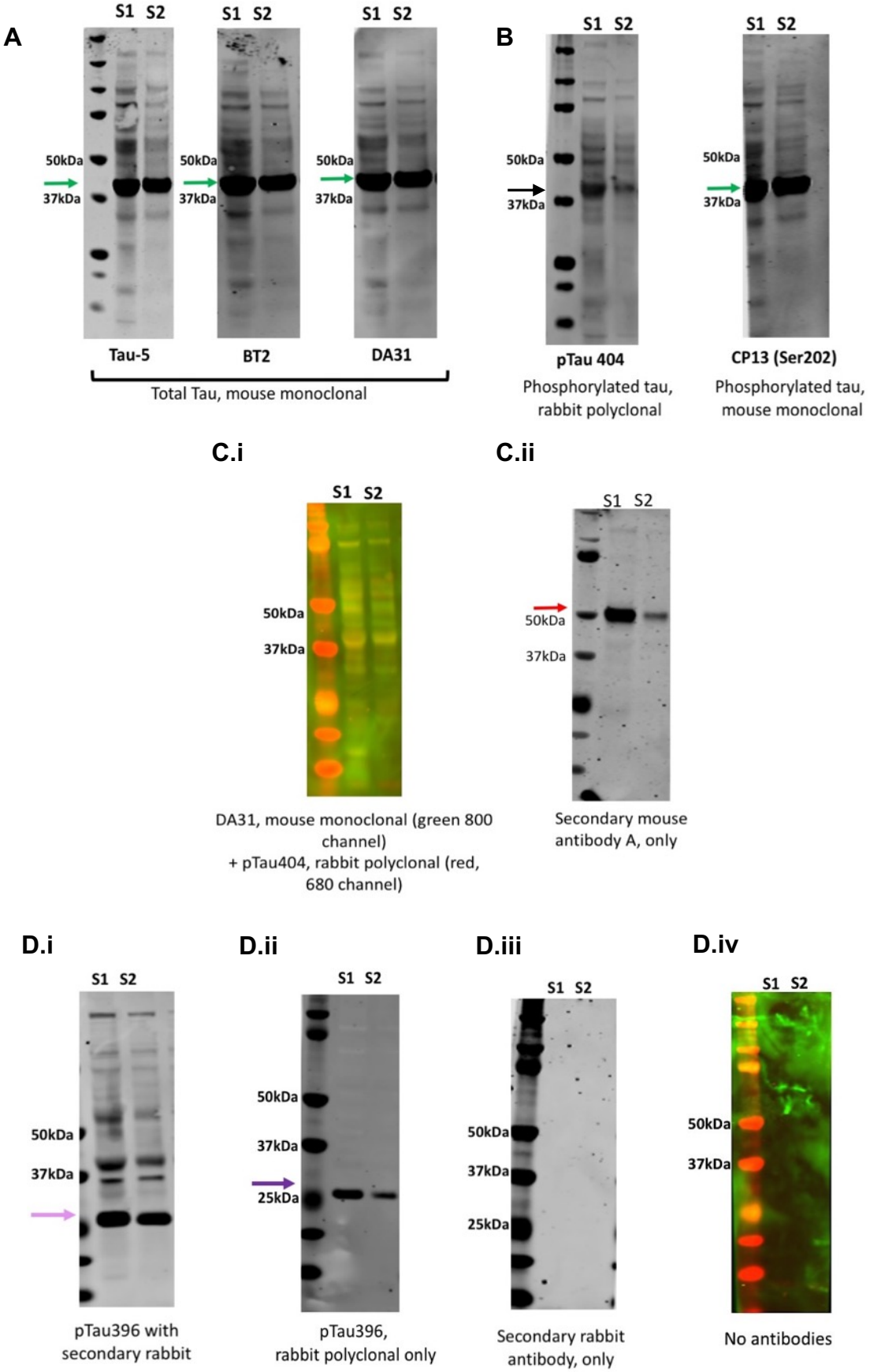
A
S1 S2
S1 S2
S1 S2
50kDa
37kDa
50kDa
37kDa
50kDa
37kDa
Tau-5
BT2
DA31
Total Tau, mouse monoclonal
B
S1 S2
S1 S2
50kDa
37kDa
50kDa
37kDa
pTau 404
Phosphorylated tau, rabbit polyclonal
CP13 (Ser202)
Phosphorylated tau, mouse monoclonal
C.i
C.ii
S1 S2
S1 S2
50kDa
37kDa
50kDa
37kDa
DA31, mouse monoclonal (green 800 channel)
+ pTau404, rabbit polyclonal (red, 680 channel)
Secondary mouse antibody A, only
D.i
D.ii
D.iii
D.iv
S1 S2
S1 S2
S1 S2
S1 S2
50kDa
37kDa
50kDa
37kDa
25kDa
50kDa
37kDa
25kDa
50kDa
37kDa
pTau396 with secondary rabbit
pTau396, rabbit polyclonal only
Secondary rabbit antibody, only
No antibodies

Figure 4.13 Testing of tau antibodies for detection of tau in brain samples from control and 6-OHDA groups. Proteins were isolated from brain tissue samples (S1 and S2) using a high salt (HS) buffer. **A)** Samples were immunoblotted with three antibodies against total tau (Tau-5, BT2 and DA31) (46 kDa-68 kDa). **B)** The same samples were also immunoblotted with two different antibodies against phosphorylated tau (pTau404 and CP13/pTau202). A nonspecific band at approximately 37 kDa was apparent (green arrows) for all mouse monoclonal antibodies, that was also apparent though less intense for the rabbit polyclonal pTau404 antibody (black arrow). **C.i)** Western blot showing signals when mouse monoclonal DA31 antibody against total tau and a rabbit polyclonal, against pTau404 were used. Some bands at the expected molecular weight were detected, but the signals did not appear to be specific for tau. i**i)** When an alternative secondary anti-mouse IgG was used (secondary antibody A), the original nonspecific band was no longer apparent, however a new unidentifiable band was observed at 50 kDa, (red arrow). **D.i)** Samples were incubated with the pTau396 antibody and a rabbit secondary antibody. When the primary and secondary antibodies were both used, tau bands were detected alongside the non-specific 25kDa band (pink arrow). When the membrane was incubated with **ii**) primary or **iii**) secondary antibody only, no tau bands were detected, primary antibody only conditions showed the non-specific band (purple arrow) **iv)** Negative control. No primary or secondary antibodies were incubated with the membrane. No signals were detected.

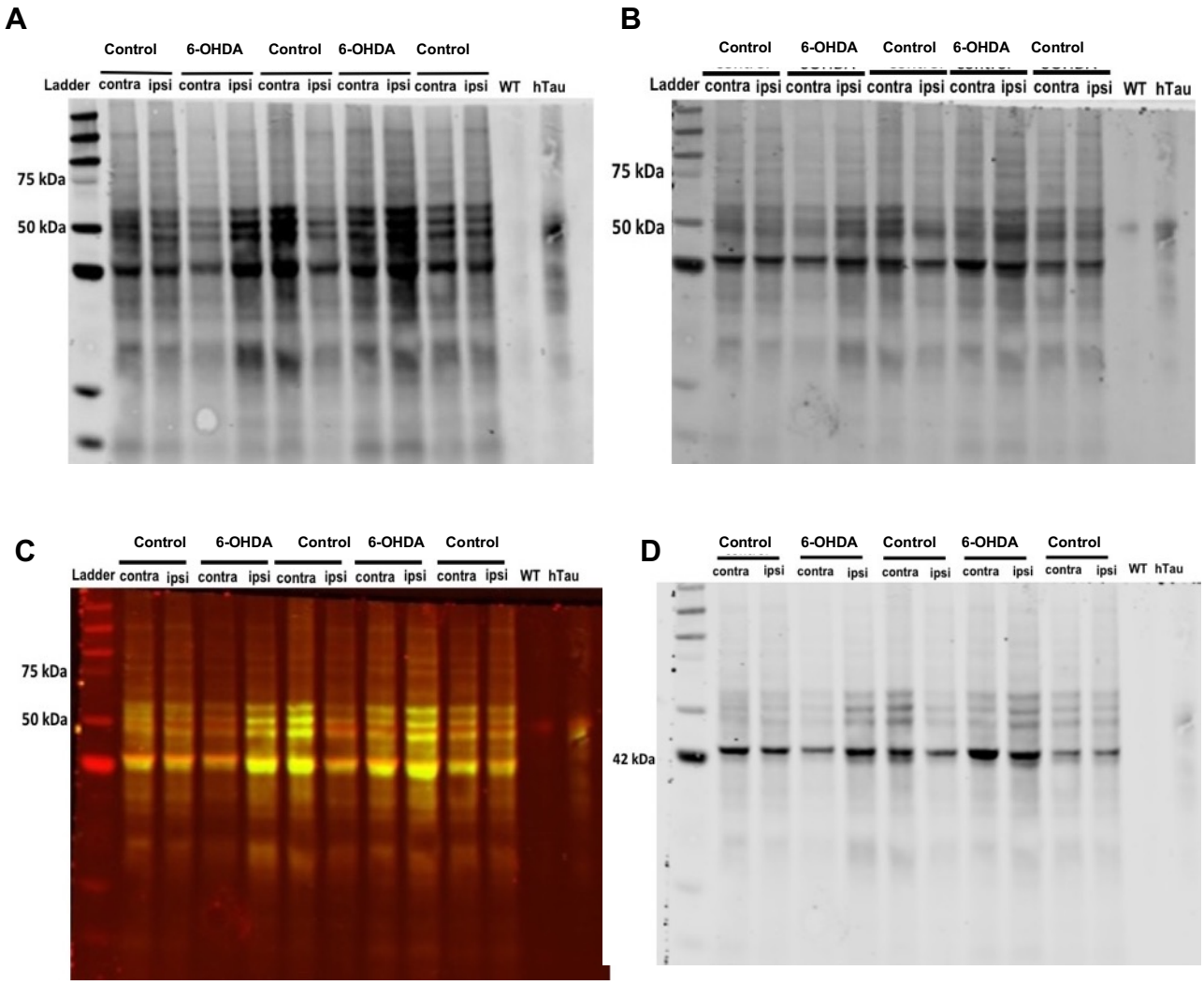

Figure 4.14 Optimisation of tau antibodies, AT8. Proteins from the contralateral (contra) and ipsilateral (ipsi) frontal cortex of a control-injected rat and 6-OHDA injected rat were extracted in high salt (HS) buffer, n= 2. Samples were immunoblotted sequentially with **A)** DAKO total tau antibody (46-68 kDa) and **B)** AT8 antibody against phosphorylated tau (46-68 kDa). **C)** Channel merge shows overlap of bands detected by the total tau (red) and AT8 (green) antibodies, including bands at the predicted molecular weight for tau. Samples of wild-type mouse brain and htau mouse brain were run in parallel for comparison. **D)** β -actin (42 kDa) as loading control.

Sequential immunoblotting with two primary antibodies was then used for the DAKO total tau antibody together with CP13. CP13 detects pTau202, often regarded as a marker for early changes in tau phosphorylation, typically pre-tangles and intracellular neurofibrillary tangles (NFT) (Espinoza et al., 2008). Immunoblots showed tau bands at 46-64 kDa for DAKO, of which some bands were also reactive for CP13 (Figure 4.15A-C). The DAKO total tau antibody also detected some lower molecular weight bands that were not detected by CP13 and which are likely degradation products.

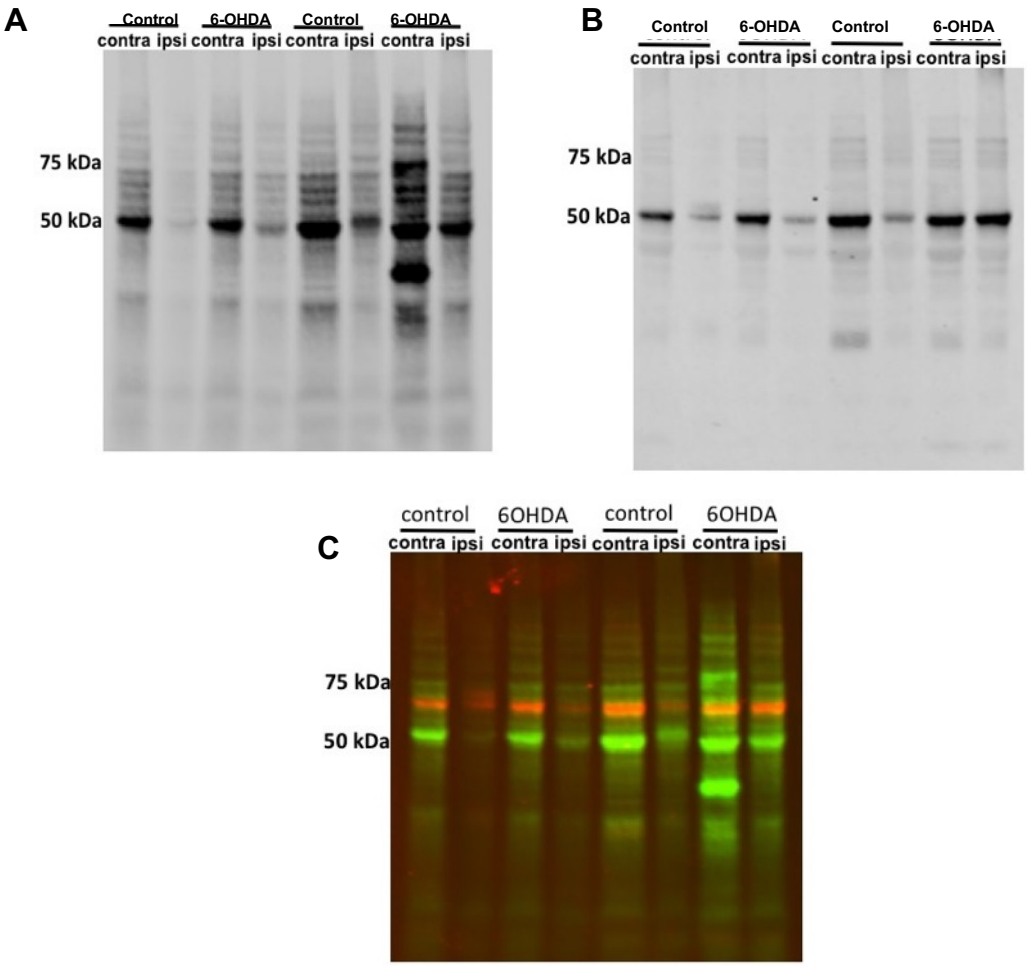

Figure 4.15 Optimisation of tau antibodies, CP13. Proteins from the contralateral (contra) and ipsilateral (ipsi) frontal cortex of a control-injected rat and 6-OHDA injected rat were extracted in high salt (HS) buffer, n = 2. Samples were immunoblotted sequentially with **A)** DAKO total tau antibody (46-68 kDa) followed by **B)** CP13 which detects tau phosphorylated at Ser202. **C)** Channel merge shows overlap of bands detected by the DAKO total tau antibody (green) and CP13 (red). Both antibodies detected a band of the expected molecular weight for tau. DAKO also detected additional bands that represent tau not phosphorylated at Ser202, alongside cleaved/degraded tau.

4.7.3 6-OHDA did not lead to changes in tau phosphorylation as detected by western blot

The HS fraction, in which most tau was extracted, from the frontal cortex (Figure 4.16A) and hippocampus (Figure 4.16B) of control and 6-OHDA injected rats was immunoblotted with antibodies against tau that were previously optimised in these tissues - total tau (DAKO), AT8 pTau205/208 and CP13 (pTau202). Immunodetection of β-actin was used to indicate loading control. Quantification of total tau amounts relative to β-actin in the same sample showed no effect of 6-OHDA treatment in frontal cortex (Figure 4.16C) or hippocampus (Figure 4.16F). Quantification of phosphorylated tau relative to total tau amounts in the same sample showed no effect of 6-OHDA treatment for AT8 in frontal cortex (Figure 4.16D) or hippocampus (Figure 4.16G). Similarly, there was no change in relative intensity of CP13 bands relative to total tau in frontal cortex between groups (Figure 4.16E). These data indicate that 6-OHDA does not cause tau phosphorylation, at least not that is sufficient to be detected when whole brain regions are homogenised and examined by western blot.

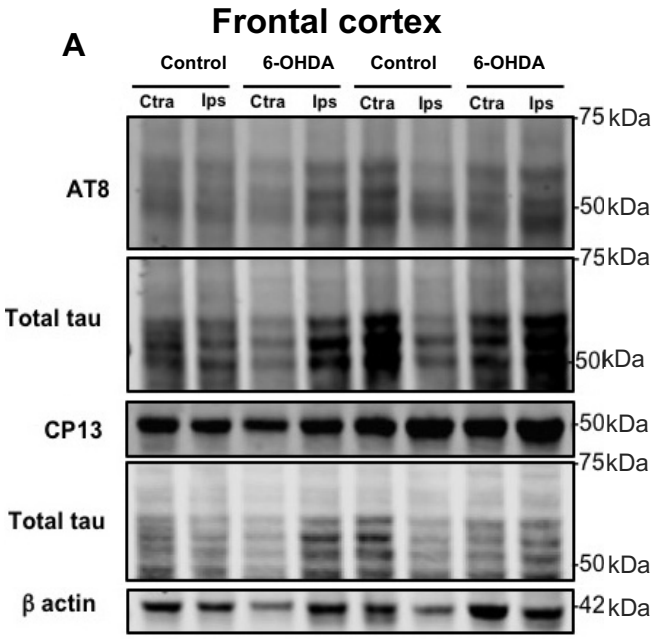
A
Frontal cortex
Control
6-OHDA
Control
6-OHDA
Ctra
Ips
Ctra
Ips
Ctra
Ips
Ctra
Ips
AT8
75 kDa
50kDa
Total tau
75kDa
50kDa
CP13
50kDa
Total tau
75kDa
50 kDa
β actin
42 kDa

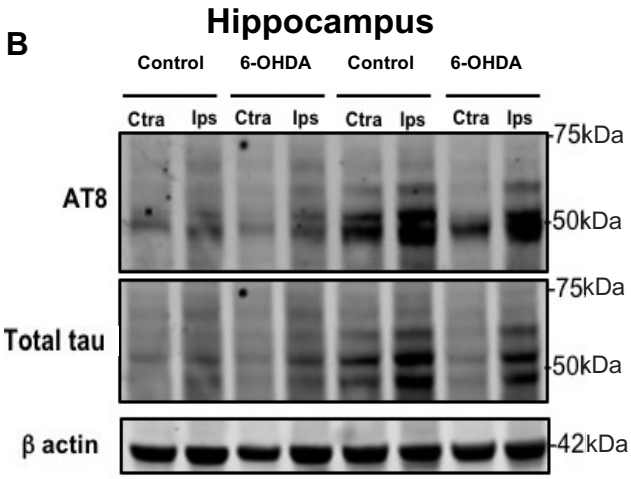
B
Hippocampus
Control
6-OHDA
Control
6-OHDA
Ctra
Ips
Ctra
Ips
Ctra
Ips
Ctra
Ips
AT8
75kDa
50kDa
Total tau
75kDa
50kDa
β actin
42kDa

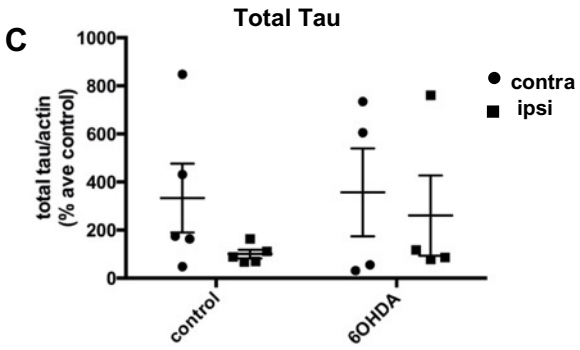
C
Total Tau
total tau/actin
(% ave control)
1000
800
600
400
200
0
contra
ipsi
control
6OHDA

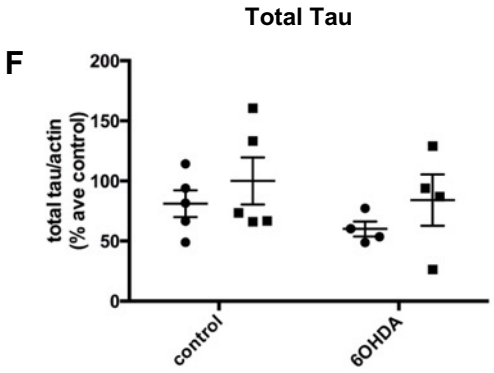
F
Total Tau
total tau/actin
(% ave control)
200
150
100
50
0
control
6OHDA

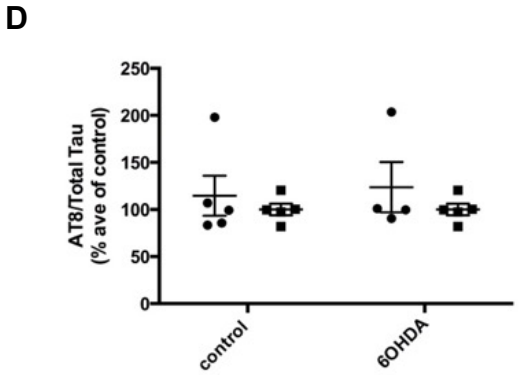
D
AT8/Total Tau
(% ave of control)
250
200
150
100
50
0
control
6OHDA

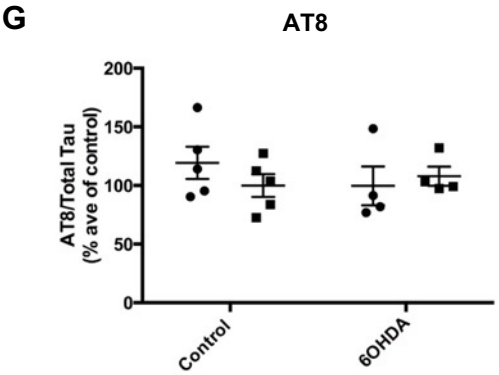
G
AT8
AT8/Total Tau
(% ave of control)
200
150
100
50
0
Control
6OHDA

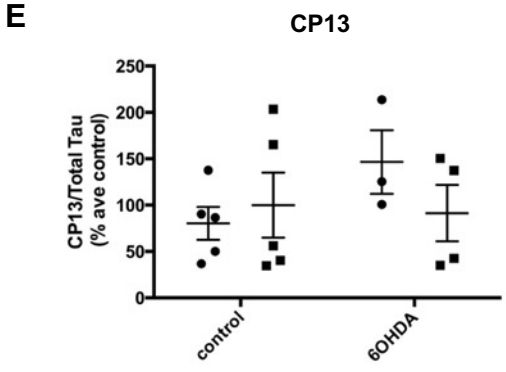
E
CP13
CP13/Total Tau
(% ave control)
250
200
150
100
50
0
control
6OHDA

Figure 4.16 Western blots of total and phosphorylated tau in the high salt fraction from both hemispheres of the frontal cortex and hippocampus of control and 6-OHDA injected rats at 90 d.p.i. **A)** Representative western blots showing AT8, CP13, and total tau (46-68 kDa) in samples of frontal cortex. β-actin (42 kDa) was used as a loading control. **B)** Representative western blots showing AT8, total tau and β-actin in hippocampal samples. Graphs show four frontal cortex samples **B)** AT8/total tau **C)** CP13/total tau and **D)** total tau/ β -actin. Graphs show four hippocampal samples **F)** AT8/total tau and **G)** total tau/ β -actin. Data is shown as percentage average of control, where control is the contralateral hemisphere of control rats. Control, n = 5, 6-OHDA n = 4. Analysis using unpaired t-test on the difference between contralateral and ipsilateral hemisphere of control and 6-OHDA did not indicate any significance for tau proteins. Data is mean +/- SEM presented as % average control where control is the ipsilateral hemisphere of control-injected rats. Contra. = contralateral, ipsi. = ipsilateral.

4.7.4 Increased tau phosphorylation after 6-OHDA injection was detected via immunohistochemical staining

Immunohistochemistry was performed on 7 µm sections of control and 6-OHDA injected rat brain containing the frontal cortex and hippocampus. The antibodies used detected tau phosphorylated at Ser404 and Ser396 (pTau404 and pTau396) or at both of these sites (PHF1). Phosphorylation of tau at pTau396 and pTau404 is found at basal levels in control human brain, but levels are abnormally elevated in AD (Hanger et al., 2007). Figure 4.17A shows the presence of elevated pTau404 levels in human AD postmortem sections, which serves as a positive control for the tau antibody. PHF1 is characteristic of abnormally modified tau in disease (Hanger et al., 2007).

When antibodies against pTau396 and pTau404 were used, immunoreactivity was apparent in hippocampal subfields of both control and 6-OHDA lesioned rats (Figure 4.17B-E and Figure 4.18A-E). When the number of immunoreactive cells were quantified, a statistically significant increase in the abundance of neurons positive for pTau404 was demonstrated in both CA1 and CA3 hippocampal subfields of sections from 6-OHDA injected rats relative to controls (Figure 4.17C). Sections containing the frontal cortex also displayed tau neurons immunoreactive for pTau404. While labelling was denser for 6-OHDA injected rats, there was variability between samples (Figure 4.17D, white arrow) and no significant difference was found between groups or hemispheres (Figure 4.17E), although labelling in the contralateral hemisphere appeared to be more cytoplasmic than the membranous labelling apparent in the ipsilateral cortex.

An increase in pTau396-containing neurons as a result of 6-OHDA stimulation was also noted within the CA1, CA3 subfield of the hippocampus (Figure 4.18B, Figure 4.18C), however this was not deemed significant. The MFB also has indirect projections to the frontal cortex, and immunohistochemistry of sections containing the frontal cortex with an antibody against pTau396 showed an apparent (Figure 4.18D), but not statistically significant increase, in the number of pTau396 immunoreactive neurons in the 6-OHDA injected group compared to controls for both contralateral and ipsilateral sides of the frontal cortex (Figure 4.18E).

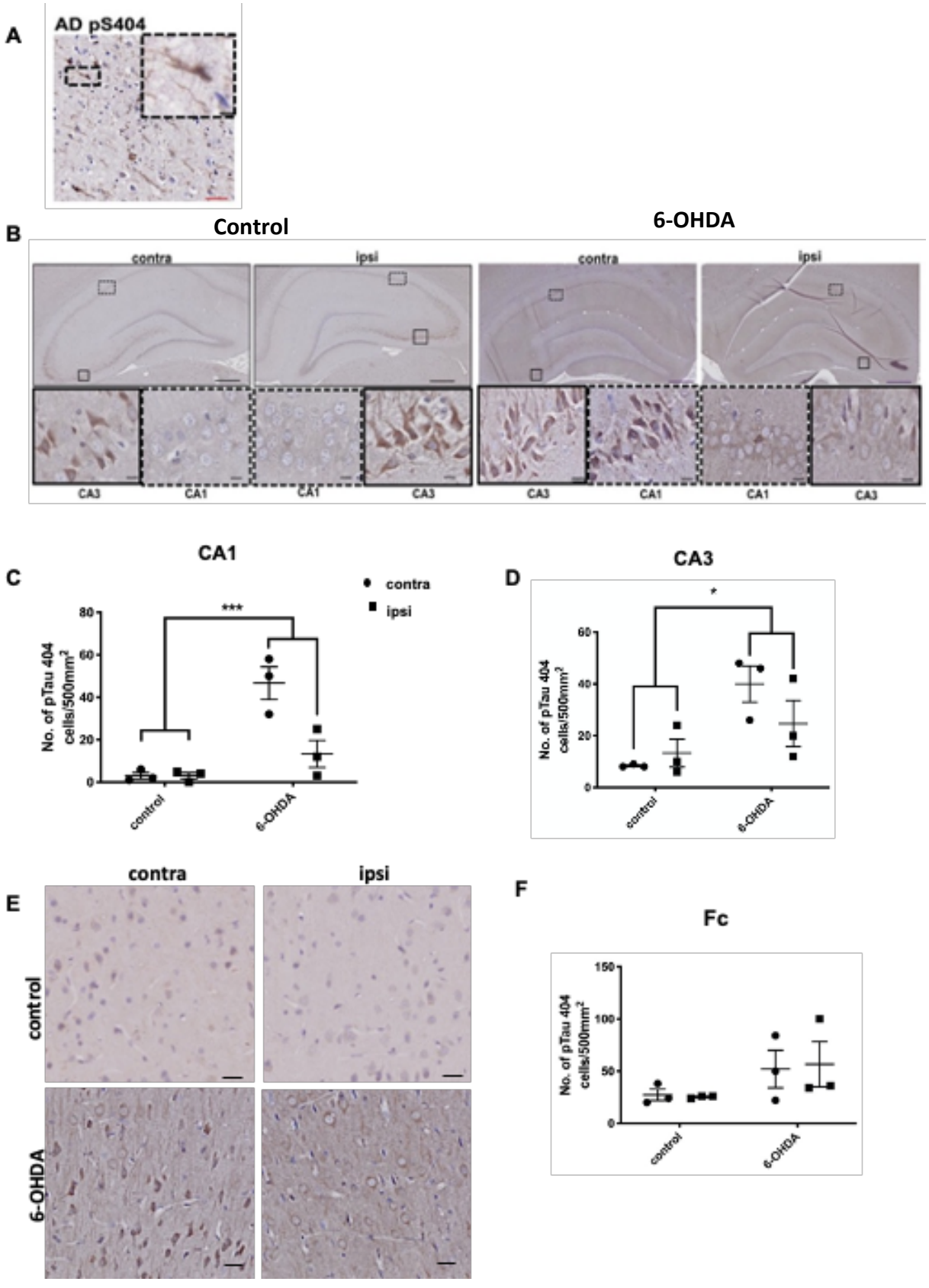
A
AD pS404
B
Control
6-OHDA
contra
ipsi
contra
ipsi
CA3
CA1
CA1
CA3
CA3
CA1
CA1
CA3
C
CA1
contra
ipsi
***
No. of pTau 404 cells/500mm²
0
20
40
60
80
control
6-OHDA
D
CA3
*
No. of pTau 404 cells/500mm²
0
20
40
60
control
6-OHDA
E
contra
ipsi
control
6-OHDA
F
Fc
No. of pTau 404 cells/500mm²
0
50
100
150
control
6-OHDA

Figure 4.17 Immunohistochemical analysis of phosphorylated tau (pTau404) in the frontal cortex and hippocampus in sections from 6-OHDA and control injected rats. **A)** Immunohistochemical staining was performed on 7 µm paraffin embedded sections from the temporal cortex of a postmortem AD brain. Inset shows higher magnification of immunoreactive neurons. For rat brain, 7 µm paraffin embedded sections were labelled with antibodies against pTau404. (**B**) Representative images of pTau404 immunolabelling. Sections were counterstained with haematoxylin. Both control and 6-OHDA injected animals showed labelling of pTau404 in CA3. pTau404 labelling was also apparent in CA1 of 6-OHDA animals, but not control animals. Scale bars in main images are 500 µm, and 5 µm scale bars are used in insets. Graphs show the **C)** CA1 **D)** CA3 **F)** Fc. Analysis with unpaired t-test on the difference between contralateral and ipsilateral hemisphere of control and 6-OHDA demonstrated a statistical significance in CA1 region and CA3 **(C, D).** No statistical differences were noted in Fc region (**F).** Levels of significance denoted by *** $p < 0.001$. Scale bar 20 µm. Data shown is mean ± SEM, n = 3.

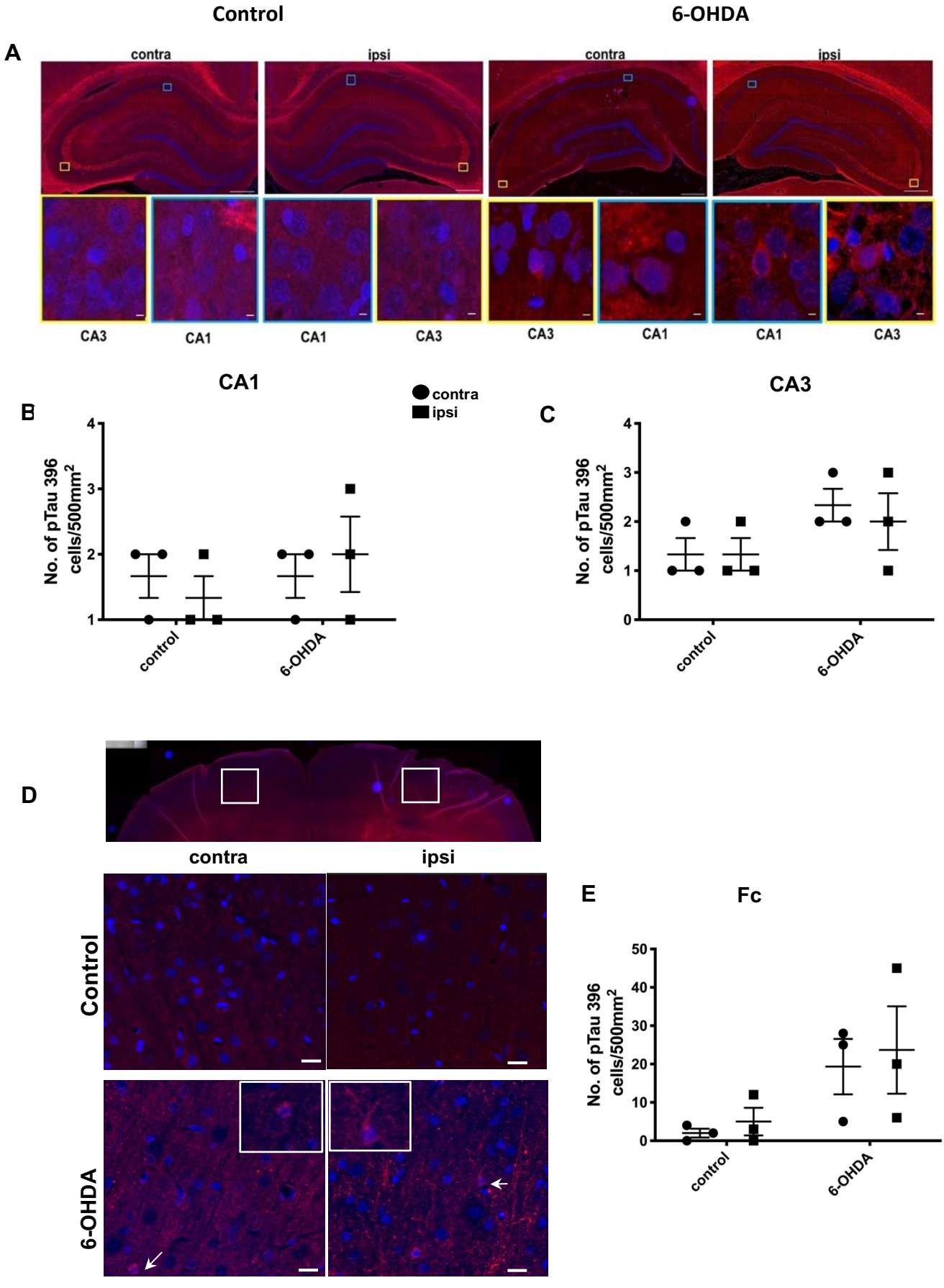
Control
6-OHDA
A
contra
ipsi
contra
ipsi
CA3
CA1
CA1
CA3
CA3
CA1
CA1
CA3
CA1
contra
ipsi
B
No. of pTau 396 cells/500mm2
control
6-OHDA
CA3
C
No. of pTau 396 cells/500mm2
control
6-OHDA
D
contra
ipsi
Control
6-OHDA
E
Fc
No. of pTau 396 cells/500mm2
control
6-OHDA

Figure 4.18 Immunohistochemical analysis of phosphorylated tau (pTau396) in the frontal cortex and hippocampus in sections from 6-OHDA and control injected rats. For rat brain, 7 µm paraffin embedded sections were labelled with antibodies against pTau396. **A)** Representative immunofluorescence labelling of pTau396 with DAPI (blue) used as a nuclear marker. Control rat brain showed less immunoreactivity compared to 6-OHDA-treated rats. Yellow and blue boxes indicate regions of CA3 and CA1, respectively, that are shown at higher magnification in insets. Scale bars in main images are 500 µm, and 5 µm scale bars are used in insets. Graphs show the **B)** number of pTau396 positive cells per mm^2 in the contralateral (contra) and ipsilateral (ipsi) CA1 and **C)** CA3 regions. **D)** Fc, white arrows indicate area shown at higher magnification in insets. Scale bar 20 µm. **E)** Fc quantification. Analysis with unpaired t-test on the difference between contralateral and ipsilateral hemisphere of control and 6-OHDA group did not indicate any statistical significance. Data shown is mean ± SEM, n = 3.

Tau phosphorylated at pS396/404 (PHF1) is characteristic of abnormally modified tau in disease (Hanger et al., 2007) (Figure 4.19A). Faint PHF1 immunoreactivity was observed in the hippocampus of 6-OHDA injected rats, that was mostly absent from control rat hippocampus (Figure 4.19B-C), although no significant difference was found between groups for either CA1 or CA3 (Figure 4.19D-E). Sections containing the frontal cortex also displayed PHF1 immunoreactive neurons. Labelling was not drastically different for 6-OHDA injected rats and controls (Figure 4.19F), therefore despite the slight increase in 6-OHDA group no significant difference was found between groups or hemispheres (Figure 4.19G).

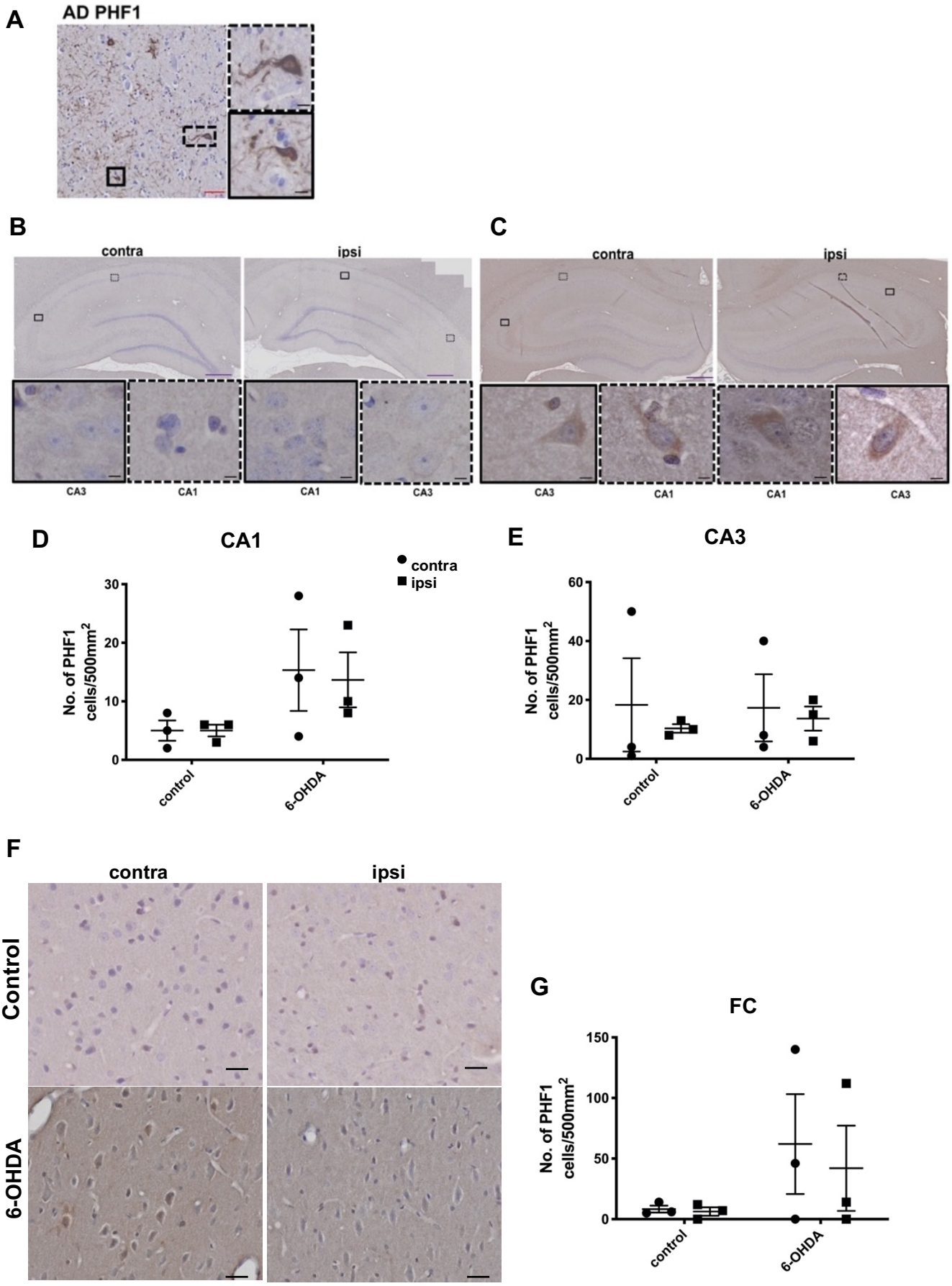
A
AD PHF1
B
contra
ipsi
CA3
CA1
CA1
CA3
C
contra
ipsi
CA3
CA1
CA1
CA3
D
CA1
contra
ipsi
No. of PHF1 cells/500mm2
30
20
10
0
control
6-OHDA
E
CA3
No. of PHF1 cells/500mm2
60
40
20
0
control
6-OHDA
F
contra
ipsi
Control
6-OHDA
G
FC
No. of PHF1 cells/500mm2
150
100
50
0
control
6-OHDA

Figure 4.19 Immunohistochemical staining of rat brains using an antibody against tau phosphorylated at Serine 396/404, PHF1. 7 µm paraffin embedded sections of rat brains using an antibody against tau phosphorylated at Serine 396/404, PHF1. **A)** PHF1 immunolabelling in human AD disease. Inset showed higher magnification of immunoreactive neurons. **B)** Control animals showed limited positivity for PHF1 staining, while **C)** 6-OHDA injected animals showed positive PHF1 staining in both contralateral (contra) and ipsilateral (ipsi) sides. Data presented are of representative animals. All images with a purple scale bar: 5 µm; black scale bars 500 µm. **D)** The number of positive PHF1 cells per mm2 in the CA1 region. **E)** CA3 region **F)** PHF1 immunolabelling of frontal cortex region. **G)** PHF1 quantification. Analysis with unpaired t-test on the difference between contralateral and ipsilateral hemisphere between control and 6OHDA did not indicate any statistical significance**(D,E,G).** Data shown is mean ± SEM, n = 3.

4.7.5 Exploring potential changes in tau kinases in response to 6-OHDA

Several kinases are known to phosphorylate tau, and amongst them, glycogen synthase kinase-3 beta (GSK-3β) is one of the most studied, and is involved in the phosphorylation of tau at the epitopes studied here (Hanger et al., 2009; Lee et al., 2011). Therefore, to understand if the increased tau phosphorylation observed by immunohistochemistry is related to changes in GSK-3β activity, samples of rat brain hippocampus were immunoblotted with antibodies against GSK-3β (Figure 4.20A).

GSK-3β , unlike conventional kinases, is constitutively active and its substrates often require pre-phosphorylation by other kinases to be phosphorylated by GSK-3 (Beurel et al., 2015). GSK-3 activation is determined by its phosphorylation. Phosphorylation at Ser9 is inhibitory, whereas phosphorylation at Tyr216 activates GSK-3β. Immunoblots were incubated with antibodies raised against total GSK-3β and GSK-3β phosphorylated at Ser9 (Figure 4.20A-B). Bands were detected at the expected molecular weight (46 kDa) that overlapped when channels were overlaid (Figure 4.20C). No apparent differences in either total or phosphorylated GSK-3 amounts were apparent in immunoblots, suggesting that 6-OHDA did not affect GSK-3β activity.

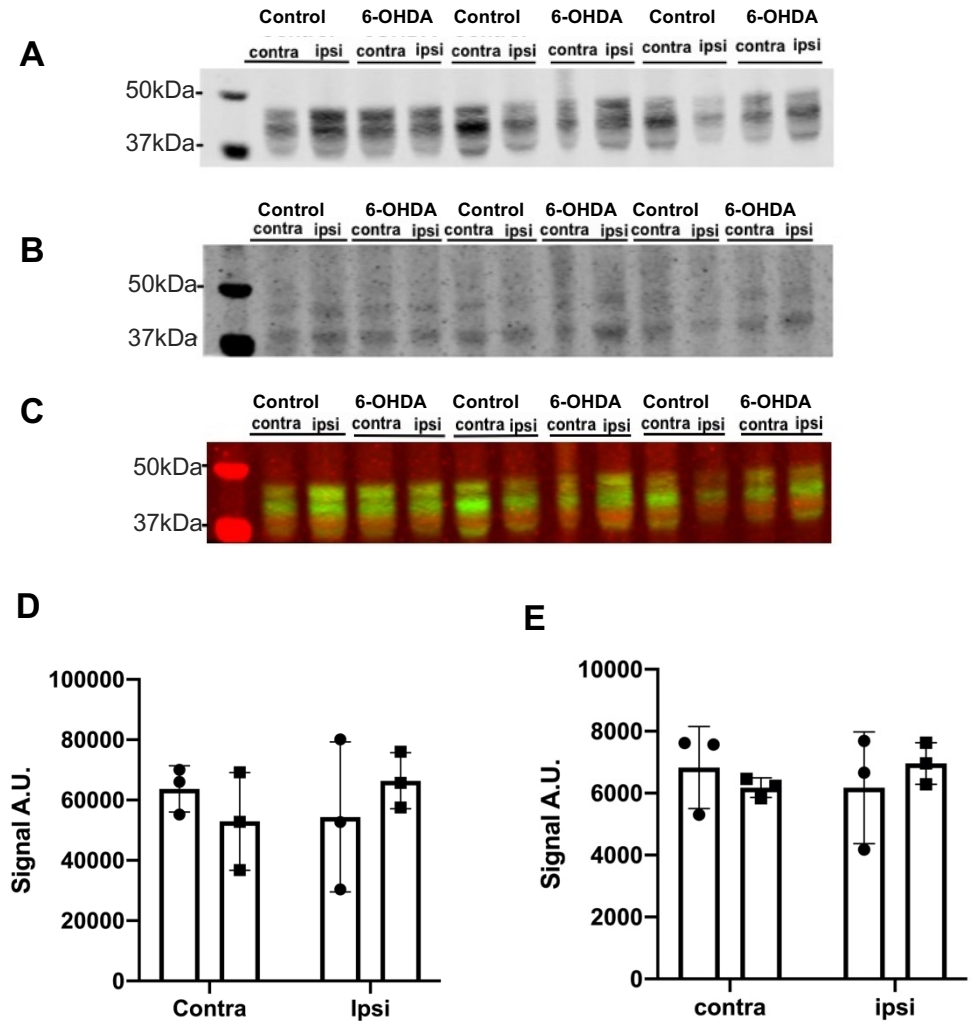

Figure 4.20 Immunoblots of hippocampal samples in high salt buffer were immunoblotted with antibodies against GSK-3β . **A)** Western blot showing total GSK-3β (46 kDa) and **B**) GSK-3 phosphorylated at Ser9 (46 kDa). **C)** Overlap of signals from both total GSK-3β (green) and phosphorylated GSK-3 (red) antibodies. Contra= contralateral, ipsi. =ipsilateral. N= 3. **D-E**) quantification of corresponding immunoblots, **D)** total GSK-3β for control and 6-OHDA, **E)** GSK-3 phosphorylated at Ser9.

4.8 Results: Effects of 6-OHDA on synaptic proteins

4.8.1 Disruption of post-synaptic markers within the frontal cortex is triggered by 6-OHDA

High salt fractions from the frontal cortex and hippocampal regions of 6-OHDA and control injected rats, were immunoblotted with proteins present in pre- and post-synapses, as described in Chapter 3 (Figure 4.21A,B). No changes in the post-synaptic protein, N'methyl D-aspartate receptor subtype 2B (NR2B), or the presynaptic proteins synaptophysin or synaptotagmin, were observed in frontal cortex or hippocampus as a result of 6-OHDA (Figure 4.21 C-I). However, a specific loss of the postsynaptic protein, postsynaptic density protein 95 (PSD-95), was observed in frontal cortex (Figure 4.22 A, B), but not hippocampal (Figure 4.20 B, F), samples as a result of 6-OHDA.

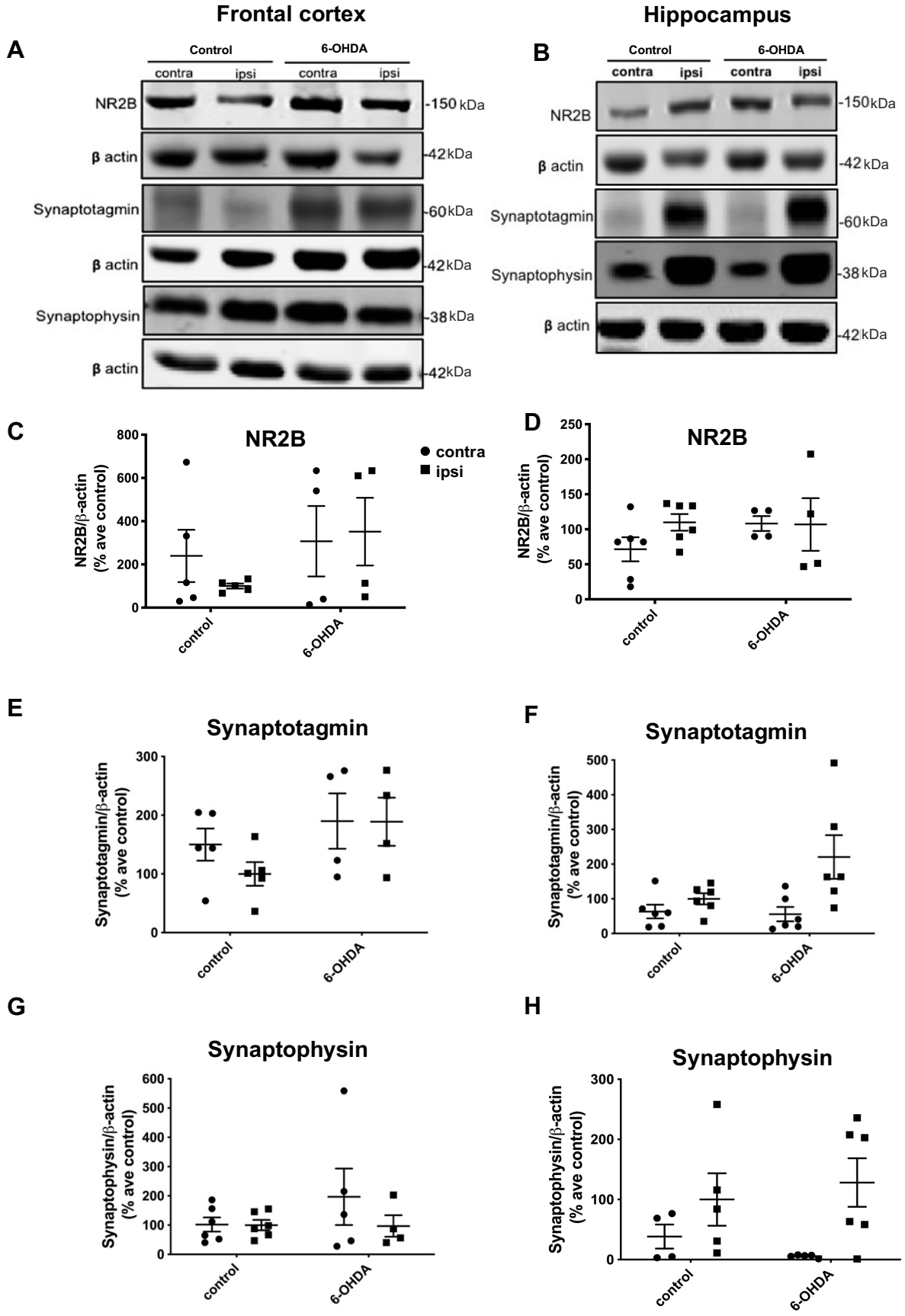
Frontal cortex
Hippocampus
A
B
Control
6-OHDA
contra
ipsi
NR2B
β actin
Synaptotagmin
Synaptophysin
150 kDa
42kDa
60kDa
38 kDa
C
D
NR2B
contra
ipsi
NR2B/β-actin (% ave control)
control
6-OHDA
E
F
Synaptotagmin
Synaptotagmin/β-actin (% ave control)
G
H
Synaptophysin
Synaptophysin/β-actin (% ave control)

Figure 4.21 Immunoblots of pre- and post-synaptic markers in high salt fractions from the frontal cortex and hippocampal regions of 6-OHDA and control injected rats. **A-B)** Representative immunoblots of samples from contralateral (contra) and ipsilateral (ipsi) hemispheres probed with antibodies against NR2B (150 kDa), PSD-95 (95 kDa), synaptophysin (38 kDa) and synaptotagmin (60kDa), with β -actin (42kDa) used as a loading control. Graphs show quantification of frontal cortex synaptic proteins relative to β-actin for **C**) NR2B (control, n = 5, 6-OHDA, n = 5), **E)** Synaptotagmin (control, n = 5, PFF, n = 4) and **G)** Synaptophysin (control, n = 6, 6-OHDA, n = 4). Graphs show quantification of hippocampal synaptic proteins relative to β -actin for **D**) NR2B (control, n = 6, 6-OHDA, n = 4). **F)** Synaptotagmin (n = 6) and **H)** Synaptophysin (control, n = 5, 6-OHDA, n = 6). Analysis using unpaired t-test on the difference between contralateral and ipsilateral hemisphere of control and 6-OHDA groups **(C-H).** Data is mean +/- SEM presented as % average control where control is the ipsilateral hemisphere of control-injected rats.

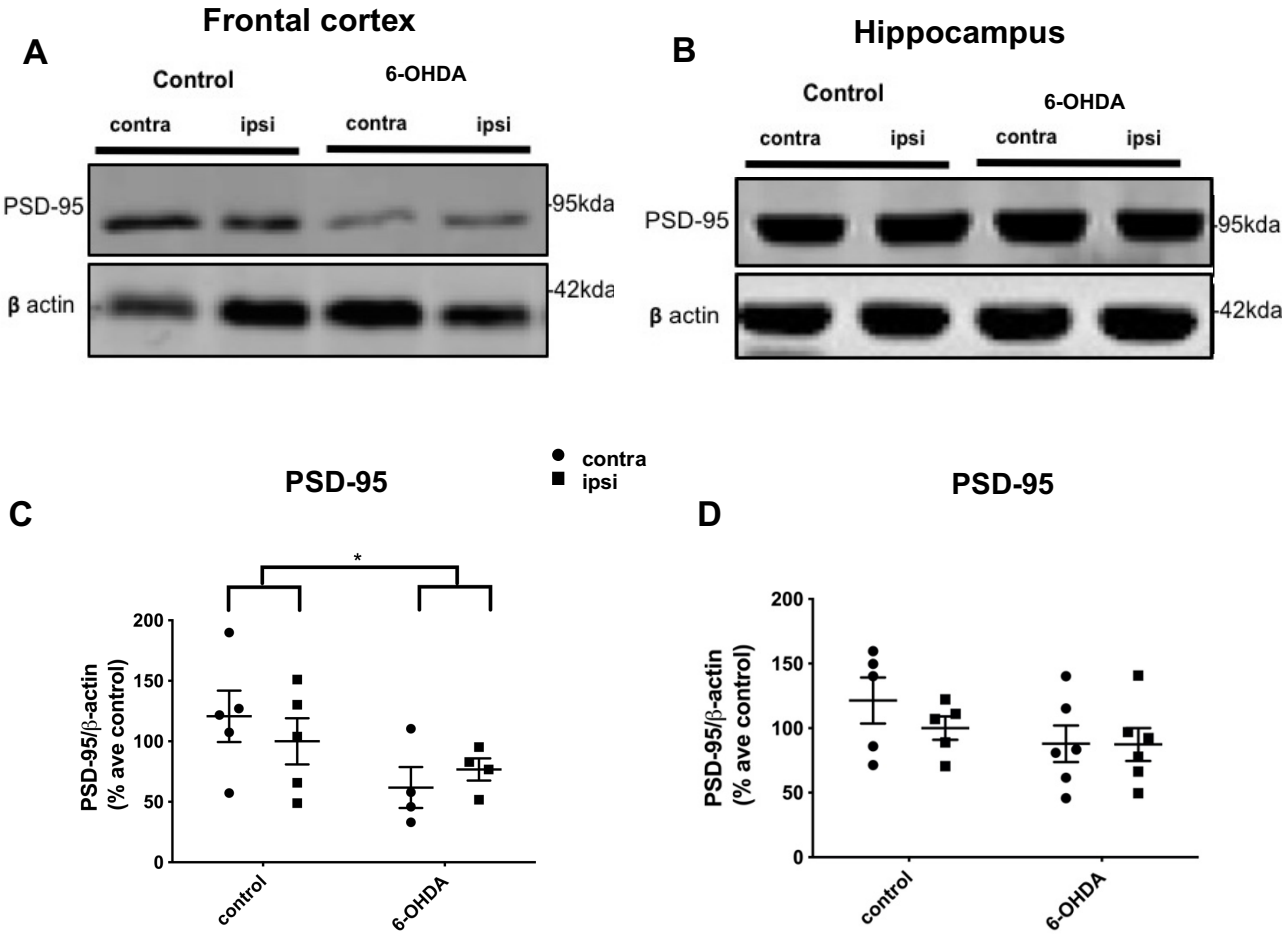

Figure 4.22 Immunoblots of PSD-95 in the high salt fraction of frontal cortex from 6-OHDA and control injected rats. **A)** Representative immunoblots from **A)** frontal cortex **B)** hippocampus, probed with an antibody against the post-synaptic marker, PSD-95 (95 kDa). β-actin was used as a loading control (42 kDa). C) The dot plot shows marked reduction in the amount of PSD-95 relative to β-actin in frontal cortex of 6-OHDA injected rats relative to controls. Control, n = 5, PFF, n = 4. D) the dot plot shows no significant difference found as a result of treatment or between hemispheres in the hippocampus regions, control n = 5, PFF n = 6. Analysis using unpaired t-test on the difference between pre-post did not indicate any statistical significance for PSD-95 in Fc or Hippo **(C,D).** Data is mean +/- SEM presented as % average control where control is the ipsilateral hemisphere of control-injected rats.

4.9 Discussion

The primary aim of this chapter was to investigate the consequences of elevated oxidative stress induced by the 6-OHDA neurotoxin on molecular, histological and cognitive features indicative of PD and Parkinson's disease dementia (PDD). Immunohistochemical analysis together with the induced apomorphine rotation test confirmed the success of the 6-OHDA injection, with results reflecting those established by existing literature (Shah et al., 2019).

Asymmetric circling behaviour correlates with the magnitude of dopaminergic depletion within the nigrostriatal pathway (Grealish et al., 2010; Bove and Perier, 2012). When dopaminergic agonists such as apomorphine or L-dopa are administered, rats typically exhibit contralateral rotational behaviour, away from the lesion site. Apomorphine can induce rotation as this DA receptor agonist can act post-synaptically and as a result of hyperstimulation of supersensitive DA receptors in the denervated striatum will lead to rotation in the opposite contralateral direction (away from the lesioned side) (Bjorklund and Dunnett, 2019). But the drug induced rotation test cannot be used as the sole parameter for detecting dopaminergic loss due to potential misleading results owing to the effects of priming, sensitisation or conditioning (Norman et al., 1993).

To ensure there was dopaminergic depletion due to 6-OHDA toxicity, immunohistochemical methods were also used. Immunohistochemical analysis using an antibody against TH was performed to assess the severity of dopaminergic loss within the SN resulting from 6-OHDA injection. TH is the rate limiting enzyme in dopamine synthesis, and is commonly used as a marker for dopaminergic neurons (Kirik et al., 1998; Morales et al., 2015). Therefore, decrease in the number of TH neurons provides a good indicator of the death of dopaminergic neurons

in the SN (Hernandez-Baltazar et al., 2017; Stanic et al., 2003). These results showed a marked and rapid loss of TH neurons in the SN.

Another typical phenotype of the 6-OHDA model is the presence of motor impairment. The rotarod test is a well-established behavioural deficit test in rat models of hemiparkinsonism, and is a useful mean of evaluating basic motor abilities (Rozas et al., 1997). The rotarod test is also considered one of the most sensitive motor tests to detect deficits resulting from the loss of TH cells within the SN (Iancu et al., 2005), and can help to distinguish rats with severe dopaminergic neuron loss from rats with only partial lesions (Rozas et al., 1997). Results obtained at the 3 w.p.i. time point coincide with previous findings (Carvalho et al., 2013). As a unilateral lesion of the MFB was performed, the asymmetric cylinder test provided an ideal additional motor impairment test to confirm forelimb impairment in 6-OHDA injected rats. Rats are an ideal species for investigating skilled limb movements, and they show very similar motor components to humans (Cenci et al., 2002). The asymmetric cylinder test is a simple yet efficient test of motor function and several research groups have used this as a measure of fine motor impairment (Paumier et al., 2015; Kim et al., 2019; Heuer and Dunnett, 2013).

Although PD is mostly known as a movement disorder, those suffering from PD are at a higher risk of developing dementia related symptoms compared to the general population (Aarsland et al., 2003). Therefore, it was also necessary to investigate if an increased environment of oxidative stress, in which there has been substantial neuron loss in the SN, could result in cognitive impairment. The primary cognitive domains affected in PD include executive function, visuospatial and reference memory (Aarsland et al., 2017). To find if rats would

exhibit such impairments, the MWM test was utilised and an attempt was also made to assess deficits associated with executive function using the 5-CSRTT.

The significant loss of visuospatial and reference memory at 3 w.p.i. of 6-OHDA injection into the MFB echoed findings from Ma et al. (2014). Due to limitations, data concerning the rats swim speed was not recorded during the MWM task, however by gross observation of recordings during the trials, it was noted that there was an obvious deficit in swim speed between groups. Furthermore, a study conducted by Fitzgerald and Dokla (1989) concluded that visuospatial memory is not associated with swim speed as injection of the neurotoxin cysteamine led to reduction of somastatin like immunoreactivity neurons, followed by deficits in spatial learning. However, this memory impairment did not correlate with swimming deficit. Lastly escaping from water was found to be unrelated to activity or body mass. Additionally, land based motor deficits (assessed with open field) does not necessarily imply a deficit in swimming ability and so the MWM test was deemed a suitable test for assessing cognition in experimental PD (Vorhees and Williams, 2006) (Ma et al., 2014).

The lack of experience in using the 5-CSRTT rendered difficulty in obtaining valid data points for executive function impairment upon unilateral 6-OHDA injection into the MFB. However, other research groups have also studied the role of 6-OHDA in executive function (Marshall et al., 2019). Although Marshall and colleagues did not use the 5-CSRTT task, they instead used a series of attentional set shifting tasks. They documented that while rodents exhibited deficits in simple discrimination, no deficits were noted in reversal or extradimensional shifts. They also reported no notable differences in novel object recognition tasks. Thus, they concluded that injection of 6-OHDA into the MFB may not lead to executive impairment.

Mammals tend to freeze when exposed to both strange or noxious stimuli. The stimuli will also trigger autonomic nervous system activity, typically defecation. Therefore, to construct such stimuli for the rat, a simple method is to place the rat into a novel environment, such as an open field arena and monitor their behaviour (Denenberg, 1969). Anxiety-like behaviour induced by 6-OHDA was observed and attributable to dysregulation of neurotransmitter systems in such brain regions such as the prefrontal cortex, amygdala and striatum all being involved with anxiety (Vieira et al., 2019). Although some studies reported anxiety-like behaviour as early as one-week post lesion (Su et al., 2018), some studies reported contradictory findings. For example (Carvalho et al., 2013) did not detect any deficit in anxiety-like behaviour after unilateral MFB lesion in rats. The discrepancies are likely due to differences in the site of lesion, dosage and time post-injection, and also variation in the protocols used (Kim et al., 2019) (Su et al., 2018) (He et al., 2018). Here, 6-OHDA injection into rat MFB was found not to induce any anxiety-like behaviour.

LBs and aberrantly phosphorylated α–synuclein are characteristic hallmarks of PD (Spillantini et al., 1997; Spillantini et al., 1998b). One of the major drawbacks of experimental models that use 6-OHDA is that they do not develop LB inclusions (Tieu, 2011) (Meredith et al., 2008). A possible rationale for the lack of α–synuclein pathology being detected within the 6-OHDA model could be due to the lack of attempt from research groups to validate the presence of α–synuclein pathology given that 6-OHDA was primarily utilised for assessing drug induced dyskinesia and also for investigating behavioural deficits due to impairment of the nigrostriatal pathway. As alternative animal models of PD exist for examining neuropathology (α–synuclein PFFs, MPTP, paraquat and rotenone) less effort was focussed on 6-OHDA and α–synuclein pathology. Additionally, given that 6-OHDA mechanistically also impairs

mitochondrial function, similarly to other neurotoxin models (MPTP, paraquat and rotenone), it is not impossible that 6-OHDA may also induce and increase the aggregation of α–synuclein. Lastly, evidence from cell culture studies suggested that oxidative stress disrupts α–synuclein equilibrium, initiating the phosphorylation of α–synuclein (Musgrove et al., 2019; Scudamore and Ciossek, 2018) and 6-OHDA is known to trigger oxidative stress. The results shown within this thesis reflects this rationale, given that oxidative stress levels were elevated bilaterally concomitant with phosphorylated α–synuclein which was present bilaterally. Although TH cell loss was only apparent unilaterally, a number reasons could explain the presence of oxidative stress and phosphorylated α–synuclein but without cell death. Firstly, it was previously reported by Paumier et al. (2015) that cell loss within the nigra can be unilateral despite bilateral α-synuclein pathology therefore suggestive that an alternative mechanism may be responsible for mediating cell loss, other than α-synuclein. Secondly, in a more recent paper where α-synuclein was administered chronically into mice hippocampus, despite the presence of α-synuclein pathology, cell loss was absent (Legname et al., 2020).

Modified tau is also known to contribute to synapse loss in dementia. In a study comparing the contributions of total tau, phosphorylated tau and amyloid-beta (Aβ) to cognitive decline in the 3xTg-AD mouse model, it was noted that the most significant correlate of cognitive decline was increased phosphorylated tau levels (Huber et al., 2018). When phosphorylated tau levels were reduced in the Tg2576 mouse through passive immunotherapy using tau oligomer-specific monoclonal antibody treatment, cognitive impairments were reversed (Castillo-Carranza et al., 2014). A similar mechanism may contribute to cognitive deficits in PD, as accumulations of modified tau were reported in PD and PDD brain (Irwin and Hurtig, 2018; Irwin et al., 2013).

Although increases in tau phosphorylation in 6-OHDA-injected hippocampus were detected using immunohistochemical staining, this was not apparent by western blotting. The reasons for this discrepancy are not clear, although the presence of multiple tau fragments is indicative that the samples may have been degraded and this reason could also explain the high variation in total tau expression in Figure 4.16 E and Figure 4.16 G. The other possibility could also be due to natural variances in animals, but it is likely that as these samples and blot were repeated several times, some samples have undergone degradation more so than other samples in the same group contributing to the variability in total tau expression. Nevertheless, the results from immunohistochemical analysis demonstrate elevated levels of phosphorylated tau within the 6-OHDA injected rats. The findings are highly suggestive that oxidative stress induces tau changes that may contribute to cognitive deficits. The increase in levels of phosphorylated tau noted in hippocampal subfields indicates that unilateral lesions in the MFB, and or loss of SN neurons, can lead to further damage in connected regions. The hippocampus CA1 region is thought to be associated with spatial learning and impairment. Therefore, statistically increased levels of tau in CA1 in 6-OHDA rats, are in line with previous findings (Fu et al., 2017; Hatch et al., 2017; Ciupek et al., 2015).

A large number of kinases were shown to phosphorylate tau at various sites (Hanger et al., 2009). Glycogen synthase kinase 3-beta (GSK-3β) plays a critical role in many cellular functions including regulating microtubule affinity of tau, modulating microtubule dynamics and cell survival (Hanger et al., 2009). In SH-SY5Y cells, a cell line that shows similarity to SN neurons, (Chen et al., 2004) showed that 6-OHDA can regulate GSK-3β activity and significantly inhibited phosphorylation of GSK-3β at Ser9, therefore it was of interest to

understand from a exploratory aspect whether 6-OHDA would show findings similar to previously reported. However, here no changes in total or phosphorylated (inactive) GSK3β amounts were detected. 6-OHDA did induce the hyperphosphorylation of Tyr216, but Chen et al. (2004) showed that despite this little effect was shown on GSK-3β activity. There given the time restraint Tyr216 was not investigated within this thesis, but it should also be noted that the data here is preliminary and further experiments are required to explore potential roles for GSK-3β in this model.

Synaptic dysfunction is considered as one of the earliest events in the pathogenesis of neurodegenerative disorders, that underlies clinical features of the disease (Guo et al., 2017; Hanger et al., 2019; Rodriguez-Martin et al., 2013). Therefore, proteins present in synapses were examined by immunoblotting, as previously described.

No alterations in the pre-synaptic proteins examined in the cortex or hippocampus of 6-OHDA-injected rats relative to controls were noted. The post-synaptic protein, NR2B was also found unaltered in response to 6-OHDA. Interestingly, PSD-95 was reduced in the frontal cortex, but not the hippocampus following 6-OHDA injection, this could be associated with the changes found in tau phosphorylation, since tau is not only necessary for post-synaptic density maintenance (Guo et al., 2017) but small amounts of tau within dendrites are known to regulate PSD-95 levels (Guo et al., 2017). However, as it was only the hippocampus where phosphorylated tau was elevated but not in the frontal cortex, while in contrast PSD-95 was only elevated in the frontal cortex, additional experiments will need to performed to elucidate this.

4.10 Summary

To summarise the main results of this chapter, 6-OHDA led to depletion of dopaminergic cells within the nigrostriatal pathway. General gait imbalance and asymmetric fine motor impairment were also apparent, accompanied by deficits in cognition. Neuropathological examination revealed mild phosphorylation of α–synuclein in various brain regions, robust increase in oxidative stress levels, and increased tau phosphorylation in the hippocampus region. Lastly, minor reduction was noted in the post-synaptic marker PSD-95 within the frontal cortex, suggestive that 6-OHDA could play a role in influencing synaptic health in regions distinct from the site of injection. A reduction in interaction has previously been reported between NMDARs and Membrane-associated guanylate kinase (MAGUKs) in the striatum of the 6-OHDA lesion model (Gardoni et al., 2006). The normal role of MAGUKs are the major scaffolding proteins at the post synaptic density and they correlate with synaptic maturation strength, and are essential for the anchoring of AMPA and NMDA receptor complexes (Chen et al., 2015) while NMDARs have an integral role in controlling synaptic plasticity and memory function. In human PD cases analysis of Synapse-associated protein 97 (SAP97), GluA2 and GluN1 within the post-synaptic density compartment revealed a decrease in GluA2 within the ST, but an increase in SAP97 was observed in the hippocampus (Fourie et al., 2014). The normal role of SAP97 is regulation of interaction between receptors and downstream signalling molecules (Nash et al., 2005), while GluA2 and GluN1 are part of AMPA and NMDA receptors respectively, they are involved in maintenance of synaptic plasticity, memory function and transmission, therefore despite the degree of variability in overall synaptic protein expression levels, the proteins within the post synaptic compartment are associated in function and interlinked. Subsequently, it will be of interest to investigate firstly, if such changes noted by previous groups were firstly region specific and secondly,

influenced by changes in PSD-95 levels. Overall, further investigations are required to determine the mechanisms underlying this synaptic protein loss.

Taken together, these data suggest that 6-OHDA induces a robust increase in oxidative stress, and the elevated oxidative stress levels in turn contribute to the loss of SN neurons. The increase in oxidative stress and neuron loss within the SN is likely to release additional toxic factors to distal regions from the initial injection site to other regions in the brain and in turn, contribute to trigger cognitive abnormalities associated with mild increases in tau and α-synuclein phosphorylation in brain religions such as the frontal cortex and hippocampus. These data further elucidate the contributions of oxidative stress to disease progression and dementia in PDD.

Chapter 5-Discussion

5.1 Hypothesis of thesis

My hypothesis for the thesis work is that despite α–synuclein being a critical factor in Parkinson's disease (PD) pathogenesis, α–synuclein alone may not be sufficient to trigger neurodegeneration at early stages of the disease. Rather, it may be that additional factors such as oxidative stress are required to promote synapse and neuronal degeneration and in turn, α–synuclein spread from damaged synaptic terminals.

To test the hypothesis, two experimental PD models were established in parallel. Either α synuclein preformed fibrils (PFFs) or the classic neurotoxin 6-hydroxydopamine (6-OHDA) were stereotaxically injected into the medial forebrain bundle (MFB) region of Sprague Dawley rats. Rats were assessed in a series of behavioural tests, and brain tissues were collected and used for immunohistochemical and biochemical experiments.

In summary, the main findings deduced from the work of this thesis firstly demonstrated that α-synuclein PFFs can induce the phosphorylation of endogenous α-synuclein in locations which are distal to the MFB. These findings suggested that α-synuclein seeds spread from the MFB, mimicking the conventional spreading of pathological protein phenomenon as previously reported in the literature (Peng et al., 2018). However, despite α-synuclein spread, there were minimal changes in oxidative stress, tau phosphorylation or synaptic protein levels within the frontal cortex and hippocampal areas, and these were insufficient to cause robust behavioural phenotypes. A reduction in dopaminergic neurons within the substantia nigra (SN) was noted at 120 days post injection (d.p.i.). This was in line with previous findings where

progressive dopaminergic neuron loss occurs due to α–synuclein PFF (Paumier et al., 2015; Duffy et al., 2018; Abdelmotilib et al., 2017).

In contrast, 6-OHDA caused rapid neuronal death in the SN within a short time frame of 3 weeks post injection (w.p.i.). 6-OHDA also triggered the phosphorylation of tau in the hippocampus, and α–synuclein in regions distal from the injection site such as the frontal cortex and hippocampus. The induction of oxidative stress in conjunction with neuronal death, may be key in facilitating the spread of modified tau and α-synuclein, leading to neurodegenerative changes in regions related to cognition. These alterations likely underlie the deterioration of cognitive functions observed in 6-OHDA injected rats. Thus, data from this thesis supports the main hypothesis.

The three time points used here were established using previous literature as guidance (Luk et al., 2012a; Duffy et al., 2018c; Abdelmotilib et al., 2017). The conversion of endogenous α–synuclein to a phosphorylated pathological counterpart after α-synuclein PFF injection was noted from as early as 60 d.p.i. and was maintained until the last time point examined (120 d.p.i.). The phosphorylated α–synuclein was present in regions that were both in close proximity and distal to the MFB pathway. Structures such as the frontal cortex, striatum, hippocampus and SN region showed positive immunoreactivity for phosphorylated α–synuclein. For the first time, work from this thesis demonstrated that introducing α-synuclein PFFs into a bundle structure consisting of both axons and fibres, allows spread of abnormal α-synuclein.

Results from this thesis demonstrated that when injected stereotaxically into the MFB fibre system α-synuclein PFFs allowed the appearance of phosphorylated α-synuclein in neuroanatomically connected regions from 60 d.p.i. However, the phosphorylated α-synuclein noted across the 3 time points was less prominent compared to findings reported by others (Duffy et al., 2018a; Luk et al., 2012a). This is likely due to the injection site as the MFB consists predominantly of white matter tracts and is a complex fibre system thus uptake of PFFs may not be as efficient. Secondly, compared to other studies the rat brain is substantially bigger in size therefore it may require an extended time frame in order for more intense phosphorylated a-synuclein pathology to develop.

Despite the observation of phosphorylated α-synuclein pathology in various brain regions this was insufficient to trigger a motor or cognitive phenotype. The weak α-synuclein pathology also did not lead to changes in tau phosphorylation. This was anticipated as past literatures have rarely reported α-synuclein PFFs inducing tau phosphorylation in animal studies, unless with specific species of α-synuclein (Guo et al., 2013) or within a cell culture system (Waxman and Giasson, 2011). However, we were interested to investigate if there were any changes locally and thus we performed IHC, which confirmed few tau changes. However, due to the limited sample size additional experiments will be necessary to confirm these data. Based on the minimal IHC changes observed in phosphorylated tau, it was not unexpected that no tau changes were observed by western blot. In this model, injection of α-synuclein PFFs also did not lead to changes in synaptic protein levels. Past studies that have shown differences in synaptic protein amounts in response to PFFs have directly introduced PFFs to cultured neurons (Volpicelli-Daley et al., 2107) or via direct diffusion through patch clamp to single neurons (Wu et al.,2018). Overall, findings from this thesis add to a growing body of

knowledge that neuropathology requires an extended period of time to induce neurodegeneration. Furthermore, neuropathology may also not be sufficient to result in neuron loss. Although there was a trend in TH cell loss across the time points, there were brain regions with phosphorylated a-synuclein but absent of cell loss therefore suggesting that neuron loss is not solely dependent on the presence of phosphorylated α-synuclein.

6-OHDA is a neurotoxin commonly used as a mimetic for experiment model of PD. The TH cell loss along with motor impairments observed at 3 w.p.i. are consistent with findings from our lab and others (Shah et al., 2019; Ma et al., 2014). The visuospatial impairment is also consistent with findings reported by Ma et al. (2014). The observation of phosphorylated α-synuclein was unusual but not unexpected on the basis that other agents such as rotenone and MPTP also impair mitochondrial dysfunction leading to elevated oxidative stress and subsequently phosphorylation of α-synuclein (Scudamore et al., 2018). Therefore, as 6-OHDA is a free radical and is known to induce oxidative stress and impair mitochondria, it is likely for 6-OHDA to induce phosphorylation of α-synuclein. Additionally, since it has been long known that 6-OHDA does not induce LB pathology, it is possible that researchers have not further investigated this aspect. Secondly, 6-OHDA neurotoxin has not been used for the purpose of studying neuropathology, but rather for drug-induced dyskinesia and motor impairment therefore the possibility of 6-OHDA inducing phosphorylated α-synuclein may have been neglected. Tau phosphorylation within a 6-OHDA may not have been investigated too extensively previously, further previous studies have not clearly shown the correlation between elevation of tau and 6-OHDA. The precise mechanism underlying the increase in tau phosphorylation is possibly due to the elevated levels of oxidative stress induced by 6-OHDA. However, further studies will need to be conducted to better understand the mechanisms

involved. Although, increased levels of phosphorylated tau are shown to be associated with brain injury (Edwards et al., 2020) it is likely not to be the cause of elevated phosphorylated tau levels observed in Figure 4.17-4.19 as the contralateral hemisphere of control animals also show increased levels of tau phosphorylation. Injections were only performed on ipsilateral hemisphere.

Taken together, findings from the 6-OHDA model have shed insight into the role and importance of oxidative stress in PD-related neurodegeneration. In the context of this study, while neuropathology may not be sufficient to cause overt neurodegeneration, substantial increases in oxidative stress levels due to neuron loss and ROS (induced by 6-OHDA) can further trigger and promote disruptive changes throughout connected regions and contribute to neurodegeneration that may be mediated by changes in phosphorylated tau and reflected in reduced synaptic protein levels.

5.2 Limitations of this study

Uptake of a-synuclein PFFs within the MFB

A caveat to injecting α-synuclein PFFs into the MFB, is the inability to monitor whether uptake of α-synuclein PFFs is solely due to neuronal cells. Evidence has demonstrated that α-synuclein PFFs can also be transferred via astrocytes (Filippini et al., 2019), therefore nearby non-neuronal cells within the vicinity of the MFB site could potentially be involved in uptake and spread of α-synuclein. Further studies will need to investigate the transmission process.

Testing executive function in rats

The 5-choice serial reaction time test (5-CSRTT) was used here to examine executive function in rats, since this is the cognitive domain most affected in PDD. Due to technical difficulties and inexperience with the 5-CSRTT equipment, the data gathered from this test were considered inconclusive. Executive function tests for rats are currently limited. Therefore, it is desirable to repeat the 5-CSRTT with expert guidance, for example from Professor Tim Bussey at the University of Cambridge. It may also be of interest to extend this work to include labelling of parvalbumin expressing interneurons as demonstrated by (White et al., 2018a) which was found to be linked to changes in attention, at least in a mouse model of frontotemporal dementia/amyotrophic lateral sclerosis.

Neuron loss

There was a trend of neuron loss by 120 d.p.i. in the SN line with previous studies (Duffy et al., 2018; Luk et al., 2012) and it is likely a result of this structure being in close proximity to the MFB injection site. However, due to insufficient *n* numbers it is not possible to perform statistical analysis. Neuron loss was not investigated in the frontal and hippocampal regions this time but neurodegenerative changes in structures that are more distal from the MFB, may require an extended period of time to show degenerative changes, therefore it will be interesting to do so in future studies and at extended time points post injection.

Examination of phosphorylation at different tau sites and other tau modifications

Increases in tau phosphorylation were found here by immunohistochemistry but not Western blot. The immunohistochemistry data suggested that there were clusters of neurons

containing phosphorylated tau in the frontal cortex and hippocampus, as might be expected if there was a seeding event. These localised changes may therefore not be detectable when whole brain regions were homogenised for immunoblotting. Furthermore as only some modified species of α-synuclein can induce the accumulation of abnormal tau (Guo et al., 2013; Lim et al., 2019). The data obtained here suggest that the low abundance of phosphorylated tau observed in frontal cortex and hippocampus was not sufficient to induce tau phosphorylation. Alternatively, it may be that other neurodegeneration-associated cellular changes were not induced sufficiently by α-synuclein PFFs.

Nevertheless, it will be of interest to examine phosphorylation of tau at additional epitopes such as Tyr18 and Thr231 since phosphorylation at these two sites is suggested to occur at earlier disease stages than the epitopes examined in this thesis (Neddens et al., 2018). Moreover, phosphorylation at Tyr18 and Thr231 is suggested to promote disease progression (Neddens et al., 2018). Alternatively, additional tau modifications could be studied, for example using antibodies that detect conformational changes in tau such as MC1 (Jicha et al., 1997). Alterations in tau conformation represent the transition of tau from soluble to aggregated forms and is one of the earliest pathological alterations of tau in AD (Jeganathan et al., 2008; Haggerty et al., 2011).

Tau cleavage is also suggested to play a role in changes in tau phosphorylation and aggregation (Noble et al., 2013; Rissman et al., 2004; Cho and Johnson, 2004). Tau cleavage is typically assessed using immunoblots with antibodies directed against different parts of the tau molecules. This work may be hindered by the apparent degradation of the samples used for western blotting here. However, such studies elucidate changes in tau in response to the

treatment with α–synuclein or 6-OHDA that are associated with synaptic alterations and dementia in these rat models.

Tau mislocalisation from cytoplasm to synaptic compartments is associated with synaptic degeneration and dementia (Ittner et al., 2010; Hoover et al., 2010; Perez-Nievas et al., 2013). No alterations in synaptic tau amount was detected even at the latest time examined (120 d.p.i.) in rats injected with α-synuclein PFFs. Similarly, there were minimal changes if any, in synaptic proteins in these animals; and they exhibited no cognitive disruptions. In contrast, loss of the post-synaptic marker PSD-95 and deficits in spatial and reference memory were apparent in rats injected with 6-OHDA. Had time allowed, it would have been interesting to explore whether tau mislocalisation occurred within the 6-OHDA group.

Investigate glial involvement in detail

Due to time restraint, it was not possible within this thesis to further investigate in detail the involvement of glia within the two models. Although preliminary findings from this thesis did not show astrocytic activation, several studies have shown that glia is actively involved in α–synuclein PFF models. Reactive microgliosis precedes nigral degeneration after PFF administration (Duffy et al., 2018) and an increase in pro-inflammatory response in microglia, with elevated cytokine production was been shown (Su et al., 2008; Klegeris et al., 2008). Both microglia and astrocytes are thought to participate in clearing and degradation of extracellular α–synuclein (Ferreira and Romero Ramos, 2018; Fillipini et al., 2019), therefore it would be of interest to pursue the involvement of glia in the context of this PFF model. Given that the load of phosphorylated α–synuclein appeared to have declined from 90 d.p.i. to 120 d.p.i. it is plausible that glia was involved in clearing the phosphorylated α–synuclein.

Secondly, despite profound evidence demonstrating that 6-OHDA triggers activation of both astrocytes and microglia (Kuter et al., 2018), it is still necessary to examine the presence of astrocytes in addition to the frontal cortex region, such as the hippocampus. Furthermore, the use of GFAP as an astrocytic marker is ideal for detecting the cytoskeleton, though revealing little information about the morphology. Analysis of astrocytic morphology will provide a better indication of activation. An increase in the number of primary processes from the soma and the thickness of the processes from the soma is indicative of reactive astrocytic activity (Wilhelmsson et al., 2006). It is crucial to first detect changes in microglia as well given that both astrocytes and microglia are thought to act in combination in response to the insult (Guzman-Martinez et al., 2019; Vainchtein and Molofsky, 2020).

Examination of synaptic changes

Alterations at synapses underlie the clinical features of neurodegenerative diseases (Bereczki et al., 2016; (Bereczki et al., 2018; Aarsland et al., 2017). Synaptic changes are commonly assessed in tissues by measuring changes in the abundance of specific synaptic proteins. Here, two pre-synaptic (synaptophysin and synaptotagmin), and two post-synaptic proteins (NR2B and PSD-95) were assessed. Synaptic changes are highly variable amongst DLB and PD patients (Bridi and Hirth, 2018), therefore it may be necessary to assess additional synaptic proteins to gain a more comprehensive understanding of potential changes to synapses in the two models. Additional markers could include Synapsin 2, SNAP25, or Synphilin 1 which were found downregulated in PD postmortem studies (Dijkstra et al., 2015; Bereczki et al., 2016). Most animal model studies that have demonstrated synaptic changes are based on overexpression of α–synuclein (Lim et al., 2011; Masliah et al., 2011), or application of synuclein PFFs to cultured rodent neurons in culture (Wu et al., 2019; Volpicelli-Daley et al.,

2017). Thus, it is still unknown whether synaptic changes occur due to α-synuclein PFFs in a WT model system.

Lastly, the immunoblotting method used here may have resulted in some loss of synaptic protein content. Therefore, additional approaches, such as using super-resolution structured illumination microscopy (SIM) to quantify the synapse density (Hong et al., 2016) should be considered in conjunction with the immunoblotting technique to detect for synaptic protein changes.

The importance of specific regional effects

This thesis primarily focused on changes in the frontal cortex and hippocampus that are associated with alterations in motor function and cognition. However, due to the dopaminergic loss observed within the SN at 120 d.p.i., it would be beneficial to also examine this region for changes in tau phosphorylation and localisation, and synaptic protein disruptions. This will further clarify the mode of degeneration induced by α–synuclein PFFs in terms of selective vulnerability, location to lesion site and time required. In the 6-OHDA model, it is important to test the assertion that the rapid and extensive loss of neurons in this area is sufficient to drive α-synuclein spread and/or degeneration in the frontal cortex and hippocampus. This could be performed by selectively knocking down *SNCA* gene expression in the SN, or by administering a neuroprotective agent alongside 6-OHDA.

5.3 Future perspectives and remaining questions

Remaining questions and future studies which would complement the findings described in this thesis include the following suggestions.

It will be important to demonstrate that α-synuclein PFFs spread via the MFB pathway. Sagittal sections of the MFB at each of the three time points could be co-immunolabelled with MAP2, a marker for axons, and phosphorylated α-synuclein to detect the spread of α-synuclein PFFs along the MFB pathway. The extent of damage of neurons along the MFB was also not examined here, although it is plausible that damage to interneurons along the MFB may facilitate the spreading of pathological proteins to connecting regions. To investigate this, tissue could be cleared (Lai et al., 2018; Liu et al., 2016), and α-synuclein aggregates, phosphorylated tau and neurons can be co-labelled and visualised as a 3D reconstruction to enable better understanding of the relationship between these features, not just along the MFB pathway, but throughout the brain. Similarly, to find further if neuronal death in the SN contributes significantly to the spreading of pathological seeds and/or leads to a cascade of neurodegeneration events, structural magnetic resonance imaging (MRI) could be conducted to detect atrophy.

5.4 Overview of thesis

PD was discovered approximately 200 years ago by the British neurosurgeon James Parkinson. Since the initial discovery, great advances have been made in understanding the disease from all dimensions, from familial form to sporadic form with countless animal models being developed to mimic the disease. Despite this, there is still no cure for this debilitating disease. The aim of this thesis was not to provide a cure or drastic discovery that will immediately change the lives of those suffering from PD. However, this thesis did investigate a small yet critical aspect of the disease, namely to assess under which conditions dementia arises in PD. By understanding the importance of α-synuclein PFFs and oxidative stress in initiating neurodegenerative changes and cognitive abnormalities, it is hoped that a clear therapeutic

approach can be used to impede the onset of PD-related neurodegeneration. The data presented in this thesis indicate that α-synuclein alone is not sufficient to cause dementia in PD, and that accompanying marked oxidative stress and/or neuronal loss are required to induce cognitive decline.

α-Synuclein has been the centre piece of PD research since its initial discovery by Spillantini in 1997 (Spillantini et al., 1997). Lewy bodies (LBs) are a cardinal hallmark of postmortem PD brain. However, as it is not possible to detect end-stage α-synuclein pathology until postmortem examination, many of the earlier events leading to the final stages of disease remain unclear. Animal models created for studying PD have the tendency to exhibit end stage disease with full blown pathology and behavioural phenotypes. With this in mind, this thesis investigated the importance of α-synuclein PFFs independently. It is known that α-synuclein plays a key role in neurodegeneration and can influence the fibrillisation of tau (Giasson et al., 2003), as well as facilitating the spread of Aβ (Clinton et al., 2010; Bassil et al., 2020). As α-synuclein is the central component of LBs and also the main pathological hallmark of the disease, it is not surprising that α-synuclein is considered as the main villain that underlies neurodegeneration in PD.

However, results from this thesis suggest that α–synuclein PFFs require a prolonged period of time to exert neurodegenerative changes. Findings from a cellular seeding based model suggest that LB formation is the critical driving force for neurodegeneration, through the disruption of cellular functions including mitochondrial damage and synaptic deficits (Mahul-Mellier et al., 2020). Therefore, despite the abundance of phosphorylated α-synuclein induced by α-synuclein PFFs, due to the scarce LB inclusions in this model and the time frame

investigated, changes in tau phosphorylation and synaptic markers remained minimal and there was little impact on behavioural phenotypes. In contrast, concomitant with past literature, the role of oxidative stress seems integral for the neurodegeneration process. Oxidative stress leads to exacerbated disease progression in AD (Zhao and Zhao, 2013; Blesa et al., 2015) and findings from this thesis also suggest that a similar mechanism underlies the pathogenesis of PD. In the presence of elevated oxidative stress, acute changes associated with neurodegeneration occur, even in regions distal to the MFB (frontal and hippocampal regions).

PD is a multifaceted disease and the complex impairment of multiple cellular systems and neurotransmitters contribute to disease progression. The initiation site of PD remains unclear, while mechanisms such as impairment in ubiquitin proteasome system (UPS) system, mitochondria and environmental factors are triggers for sporadic PD (Aarsland et al., 2017). Spreading of pathological α-synuclein seeds to differential anatomical regions, reflect the fluidity of the disease (Braak et al., 2003). Selective vulnerability has led to some sub-neuronal populations being affected more than others (Luna et al., 2018).

Yet, findings from this thesis suggest that prior to the multifaceted impairment of cellular mechanisms, oxidative stress induced by 6-OHDA causes rapid and extensive neuron loss, and may also provide a primed environment where upon encounter with an external trigger, the neurodegeneration cascade proceeds. This results in impairment of multiple systems and development of modified proteins, spreading of pathology, and synaptic disruptions that ultimately cause both motor and cognitive impairment.

5.5 Conclusions

Oxidative stress is a key factor in initiating neurodegenerative changes that may contribute to the cognitive decline underlying dementia in PD. α-Synuclein alone does not appear sufficient to cause neurodegenerative changes leading to cognitive decline, at least not within a relatively short time span. Findings from this thesis provide key insights into the mechanisms of PD pathogenesis and suggest that attenuation of oxidative stress and/or neuroprotective strategies may confer therapeutic benefit for impeding the progression of PD-related dementia.

References

AARSLAND, D., ANDERSEN, K., LARSEN, J. P., LOLK, A. & KRAGH-SORENSEN, P. 2003. Prevalence and characteristics of dementia in Parkinson disease: an 8-year prospective study. *Arch Neurol,* 60**,** 387-92. (doi: 10.1001/archneur.60.3.387).

AARSLAND, D., CREESE, B., POLITIS, M., CHAUDHURI, K. R., FFYTCHE, D. H., WEINTRAUB, D. & BALLARD, C. 2017. Cognitive decline in Parkinson disease. *Nat Rev Neurol,* 13**,** 217-231. (doi: 10.1038/nrneurol.2017.27).

ABDELMOTILIB, H., MALTBIE, T., DELIC, V., LIU, Z., HU, X., FRASER, K. B., MOEHLE, M. S., STOYKA, L., ANABTAWI, N., KRENDELCHTCHIKOVA, V., VOLPICELLI-DALEY, L. A. & WEST, A. 2017. alpha-Synuclein fibril-induced inclusion spread in rats and mice correlates with dopaminergic Neurodegeneration. *Neurobiol Dis,* 105**,** 84-98. (doi: 10.1016/j.nbd.2017.05.014).

ABELIOVICH, A., SCHMITZ, Y., FARINAS, I., CHOI-LUNDBERG, D., HO, W. H., CASTILLO, P. E., SHINSKY, N., VERDUGO, J. M., ARMANINI, M., RYAN, A., HYNES, M., PHILLIPS, H., SULZER, D. & ROSENTHAL, A. 2000. Mice lacking alpha-synuclein display functional deficits in the nigrostriatal dopamine system. *Neuron,* 25**,** 239-52. (doi: 10.1016/s0896-6273(00)80886-7).

ABOUNIT, S., BOUSSET, L., LORIA, F., ZHU, S., DE CHAUMONT, F., PIERI, L., OLIVO-MARIN, J. C., MELKI, R. & ZURZOLO, C. 2016. Tunneling nanotubes spread fibrillar alpha-synuclein by intercellular trafficking of lysosomes. *EMBO J,* 35**,** 2120-2138. (doi: 10.15252/embj.201593411).

AGID, Y., JAVOY-AGID, F. & RUBERG, M. 1987. Biochemistry of neurotransmitters in Parkinson's disease. *In:* FAHN, S. (ed.) *Movement disorders.* Butterworth, London: Marsden.

AHARON-PERETZ, J., ROSENBAUM, H. & GERSHONI-BARUCH, R. 2004. Mutations in the glucocerebrosidase gene and Parkinson's disease in Ashkenazi Jews. *N Engl J Med,* 351**,** 1972-7. (doi: 10.1056/NEJMoa033277).

AHMARI, S. E. 2016. Using mice to model Obsessive Compulsive Disorder: From genes to circuits. *Neuroscience,* 321**,** 121-137. (doi: 10.1016/j.neuroscience.2015.11.009).

ALAFUZOFF, I., ARZBERGER, T., AL-SARRAJ, S., BODI, I., BOGDANOVIC, N., BRAAK, H., BUGIANI, O., DEL-TREDICI, K., FERRER, I., GELPI, E., GIACCONE, G., GRAEBER, M. B., INCE, P., KAMPHORST, W., KING, A., KORKOLOPOULOU, P., KOVACS, G. G., LARIONOV, S., MEYRONET, D., MONORANU, C., PARCHI, P., PATSOURIS, E., ROGGENDORF, W., SEILHEAN, D., TAGLIAVINI, F., STADELMANN, C., STREICHENBERGER, N., THAL, D. R., WHARTON, S. B. & KRETZSCHMAR, H. 2008. Staging of neurofibrillary pathology in Alzheimer's disease: a study of the BrainNet Europe Consortium. *Brain Pathol,* 18**,** 484-96. (doi: 10.1111/j.1750-3639.2008.00147.x).

ALAFUZOFF, I., INCE, P. G., ARZBERGER, T., AL-SARRAJ, S., BELL, J., BODI, I., BOGDANOVIC, N., BUGIANI, O., FERRER, I., GELPI, E., GENTLEMAN, S., GIACCONE, G., IRONSIDE, J. W., KAVANTZAS, N., KING, A., KORKOLOPOULOU, P., KOVACS, G. G., MEYRONET, D., MONORANU, C., PARCHI, P., PARKKINEN, L., PATSOURIS, E., ROGGENDORF, W., ROZEMULLER, A., STADELMANN-NESSLER, C., STREICHENBERGER, N., THAL, D. R. & KRETZSCHMAR, H. 2009. Staging/typing of Lewy body related alpha-synuclein pathology: a study of the BrainNet Europe Consortium. *Acta Neuropathol,* 117**,** 635-52. (doi: 10.1007/s00401-009-0523-2).

ALEXANDER, G. E. 2004. Biology of Parkinson's disease: pathogenesis and pathophysiology of a multisystem neurodegenerative disorder. *Dialogues Clin Neurosci,* 6**,** 259-80. (doi).

ANDERSEN, J. K. 2004. Oxidative stress in neurodegeneration: cause or consequence? *Nat Med,* 10 Suppl**,** S18-25. (doi: 10.1038/nrn1434).

ANDORFER, C., KRESS, Y., ESPINOZA, M., DE SILVA, R., TUCKER, K. L., BARDE, Y. A., DUFF, K. & DAVIES, P. 2003. Hyperphosphorylation and aggregation of tau in mice expressing normal human tau isoforms. *J Neurochem,* 86**,** 582-90. (doi: 10.1046/j.1471-4159.2003.01879.x).

AUGUSTINACK, J. C., SCHNEIDER, A., MANDELKOW, E. M. & HYMAN, B. T. 2002. Specific tau phosphorylation sites correlate with severity of neuronal cytopathology in Alzheimer's disease. *Acta Neuropathol,* 103**,** 26-35. (doi: 10.1007/s004010100423).

BABA, M., NAKAJO, S., TU, P. H., TOMITA, T., NAKAYA, K., LEE, V. M., TROJANOWSKI, J. Q. & IWATSUBO, T. 1998. Aggregation of alpha-synuclein in Lewy bodies of sporadic Parkinson's disease and dementia with Lewy bodies. *Am J Pathol,* 152**,** 879-84. (doi).

BANDOPADHYAY, R. 2016. Sequential Extraction of Soluble and Insoluble Alpha-Synuclein from Parkinsonian Brains. *J Vis Exp*. (107), 53415 (doi: 10.3791/53415).

BASSIL, F., BROWN, H. J., PATTABHIRAMAN, S., IWASYK, J. E., MAGHAMES, C. M., MEYMAND, E. S., COX, T. O., RIDDLE, D. M., ZHANG, B., TROJANOWSKI, J. Q. & LEE, V. M. 2020. Amyloid-Beta (Abeta) Plaques Promote Seeding and Spreading of Alpha-Synuclein and Tau in a Mouse Model of Lewy Body Disorders with Abeta Pathology. *Neuron,* 105**,** 260-275 e6. (doi: 10.1016/j.neuron.2019.10.010).

BEN ABDALLAH, N. M., FUSS, J., TRUSEL, M., GALSWORTHY, M. J., BOBSIN, K., COLACICCO, G., DEACON, R. M., RIVA, M. A., KELLENDONK, C., SPRENGEL, R., LIPP, H. P. & GASS, P. 2011. The puzzle box as a simple and efficient behavioral test for exploring impairments of general cognition and executive functions in mouse models of schizophrenia. *Exp Neurol,* 227**,** 42-52. (doi: 10.1016/j.expneurol.2010.09.008).

BERECZKI, D. 2010. The description of all four cardinal signs of Parkinson's disease in a Hungarian medical text published in 1690. *Parkinsonism Relat Disord,* 16**,** 290-3. (doi: 10.1016/j.parkreldis.2009.11.006).

BERECZKI, E., BRANCA, R. M., FRANCIS, P. T., PEREIRA, J. B., BAEK, J. H., HORTOBAGYI, T., WINBLAD, B., BALLARD, C., LEHTIO, J. & AARSLAND, D. 2018. Synaptic markers of cognitive decline in neurodegenerative diseases: a proteomic approach. *Brain,* 141**,** 582-595. (doi: 10.1093/brain/awx352).

BERECZKI, E., FRANCIS, P. T., HOWLETT, D., PEREIRA, J. B., HOGLUND, K., BOGSTEDT, A., CEDAZO-MINGUEZ, A., BAEK, J. H., HORTOBAGYI, T., ATTEMS, J., BALLARD, C. & AARSLAND, D. 2016. Synaptic proteins predict cognitive decline in Alzheimer's disease and Lewy body dementia. *Alzheimers Dement,* 12**,** 1149-1158. (doi: 10.1016/j.jalz.2016.04.005).

BEUREL, E., GRIECO, S. F. & JOPE, R. S. 2015. Glycogen synthase kinase-3 (GSK3): regulation, actions, and diseases. *Pharmacol Ther,* 148**,** 114-31. (doi: 10.1016/j.pharmthera.2014.11.016).

BEZARD, E. & PRZEDBORSKI, S. 2011. A tale on animal models of Parkinson's disease. *Mov Disord,* 26**,** 993-1002. (doi: 10.1002/mds.23696).

BJORKLUND, A. & DUNNETT, S. B. 2019. The Amphetamine Induced Rotation Test: A Re-Assessment of Its Use as a Tool to Monitor Motor Impairment and Functional Recovery in Rodent Models of Parkinson's Disease. *J Parkinsons Dis,* 9**,** 17-29. (doi: 10.3233/JPD-181525).

BJORKLUND, L. M., SANCHEZ-PERNAUTE, R., CHUNG, S., ANDERSSON, T., CHEN, I. Y., MCNAUGHT, K. S., BROWNELL, A. L., JENKINS, B. G., WAHLESTEDT, C., KIM, K. S. & ISACSON, O. 2002. Embryonic stem cells develop into functional dopaminergic neurons after transplantation in a Parkinson rat model. *Proc Natl Acad Sci U S A,* 99**,** 2344-9. (doi: 10.1073/pnas.022438099).

BLANDINI, F., ARMENTERO, M. T. & MARTIGNONI, E. 2008. The 6-hydroxydopamine model: news from the past. *Parkinsonism Relat Disord,* 14 Suppl 2**,** S124-9. (doi: 10.1016/j.parkreldis.2008.04.015).

BLAUWENDRAAT, C., NALLS, M. A. & SINGLETON, A. B. 2020. The genetic architecture of Parkinson's disease. *Lancet Neurol,* 19**,** 170-178. (doi: 10.1016/S1474-4422(19)30287-X).

BLESA, J., TRIGO-DAMAS, I., QUIROGA-VARELA, A. & JACKSON-LEWIS, V. R. 2015. Oxidative stress and Parkinson's disease. *Front Neuroanat,* 9**,** 91. (doi: 10.3389/fnana.2015.00091).

BOEVE, B. F., DICKSON, D. W., OLSON, E. J., SHEPARD, J. W., SILBER, M. H., FERMAN, T. J., AHLSKOG, J. E. & BENARROCH, E. E. 2007. Insights into REM sleep behavior disorder pathophysiology in brainstem-predominant Lewy body disease. *Sleep Med,* 8**,** 60-4. (doi: 10.1016/j.sleep.2006.08.017).

BOLISETTY, S. & JAIMES, E. A. 2013. Mitochondria and reactive oxygen species: physiology and pathophysiology. *Int J Mol Sci,* 14**,** 6306-44. (doi: 10.3390/ijms14036306).
BONIFATI, V., RIZZU, P., VAN BAREN, M. J., SCHAAP, O., BREEDVELD, G. J., KRIEGER, E., DEKKER, M. C., SQUITIERI, F., IBANEZ, P., JOOSSE, M., VAN DONGEN, J. W., VANACORE, N., VAN SWIETEN, J. C., BRICE, A., MECO, G., VAN DUIJN, C. M., OOSTRA, B. A. & HEUTINK, P. 2003. Mutations in the DJ-1 gene associated with autosomal recessive early-onset parkinsonism. *Science,* 299**,** 256-9. (doi: 10.1126/science.1077209).
BOVE, J. & PERIER, C. 2012. Neurotoxin-based models of Parkinson's disease. *Neuroscience,* 211**,** 51-76. (doi: 10.1016/j.neuroscience.2011.10.057).
BOVE, J., PROU, D., PERIER, C. & PRZEDBORSKI, S. 2005. Toxin-induced models of Parkinson's disease. *NeuroRx,* 2**,** 484-94. (doi: 10.1602/neurorx.2.3.484).
BRAAK, H. & BRAAK, E. 1991. Neuropathological stageing of Alzheimer-related changes. *Acta Neuropathol,* 82**,** 239-59. (doi: 10.1007/BF00308809).
BRAAK, H., DEL TREDICI, K., RUB, U., DE VOS, R. A., JANSEN STEUR, E. N. & BRAAK, E. 2003. Staging of brain pathology related to sporadic Parkinson's disease. *Neurobiol Aging,* 24**,** 197-211. (doi: 10.1016/s0197-4580(02)00065-9).
BRAAK, H., GHEBREMEDHIN, E., RUB, U., BRATZKE, H. & DEL TREDICI, K. 2004. Stages in the development of Parkinson's disease-related pathology. *Cell Tissue Res,* 318**,** 121-34. (doi: 10.1007/s00441-004-0956-9).
BRIDI, J. C. & HIRTH, F. 2018. Mechanisms of alpha-Synuclein Induced Synaptopathy in Parkinson's Disease. *Front Neurosci,* 12**,** 80. (doi: 10.3389/fnins.2018.00080).
BURKE, N. N., FAN, C. Y. & TRANG, T. 2016. Microglia in health and pain: impact of noxious early life events. *Exp Physiol,* 101**,** 1003-21. (doi: 10.1113/EP085714).
BURRE, J., SHARMA, M. & SUDHOF, T. C. 2018. Cell Biology and Pathophysiology of alpha-Synuclein. *Cold Spring Harb Perspect Med,* 8. (doi: 10.1101/cshperspect.a024091).
BURRE, J., SHARMA, M., TSETSENIS, T., BUCHMAN, V., ETHERTON, M. R. & SUDHOF, T. C. 2010. Alpha-synuclein promotes SNARE-complex assembly in vivo and in vitro. *Science,* 329**,** 1663-7. (doi: 10.1126/science.1195227).
CABREIRA, V. & MASSANO, J. 2019. [Parkinson's Disease: Clinical Review and Update]. *Acta Med Port,* 32**,** 661-670. (doi: 10.20344/amp.11978).
CARLSSON, A. 1959. The occurrence, distribution and physiological role of catecholamines in the nervous system. *Pharmacol Rev,* 11**,** 490-3. (doi).
CARLSSON, A., LINDQVIST, M., MAGNUSSON, T. & WALDECK, B. 1958. On the presence of 3-hydroxytyramine in brain. *Science,* 127**,** 471. (doi: 10.1126/science.127.3296.471).
CARVALHO, M. M., CAMPOS, F. L., COIMBRA, B., PEGO, J. M., RODRIGUES, C., LIMA, R., RODRIGUES, A. J., SOUSA, N. & SALGADO, A. J. 2013. Behavioral characterization of the 6-hydroxidopamine model of Parkinson's disease and pharmacological rescuing of non-motor deficits. *Mol Neurodegener,* 8**,** 14. (doi: 10.1186/1750-1326-8-14).
CASH, R., DENNIS, T., L'HEUREUX, R., RAISMAN, R., JAVOY-AGID, F. & SCATTON, B. 1987. Parkinson's disease and dementia: norepinephrine and dopamine in locus ceruleus. *Neurology,* 37**,** 42-6. (doi: 10.1212/wnl.37.1.42).
CASTILLO-CARRANZA, D. L., GUERRERO-MUNOZ, M. J., SENGUPTA, U., GERSON, J. E. & KAYED, R. 2018. alpha-Synuclein Oligomers Induce a Unique Toxic Tau Strain. *Biol Psychiatry,* 84**,** 499-508. (doi: 10.1016/j.biopsych.2017.12.018).
CASTILLO-CARRANZA, D. L., SENGUPTA, U., GUERRERO-MUNOZ, M. J., LASAGNA-REEVES, C. A., GERSON, J. E., SINGH, G., ESTES, D. M., BARRETT, A. D., DINELEY, K. T., JACKSON, G. R. & KAYED, R. 2014. Passive immunization with Tau oligomer monoclonal antibody reverses tauopathy phenotypes without affecting hyperphosphorylated neurofibrillary tangles. *J Neurosci,* 34**,** 4260-72. (doi: 10.1523/JNEUROSCI.3192-13.2014).
CENCI, M. A., WHISHAW, I. Q. & SCHALLERT, T. 2002. Animal models of neurological deficits: how relevant is the rat? *Nat Rev Neurosci,* 3**,** 574-9. (doi: 10.1038/nrn877).

CHANDRA, S., GALLARDO, G., FERNANDEZ-CHACON, R., SCHLUTER, O. M. & SUDHOF, T. C. 2005. Alpha-synuclein cooperates with CSPalpha in preventing neurodegeneration. *Cell,* 123**,** 383-96. (doi: 10.1016/j.cell.2005.09.028).

CHAUDHURI, K. R., HEALY, D. G., SCHAPIRA, A. H. & NATIONAL INSTITUTE FOR CLINICAL, E. 2006. Non-motor symptoms of Parkinson's disease: diagnosis and management. *Lancet Neurol,* 5**,** 235-45. (doi: 10.1016/S1474-4422(06)70373-8).

CHEN, G., BOWER, K. A., MA, C., FANG, S., THIELE, C. J. & LUO, J. 2004. Glycogen synthase kinase 3beta (GSK3beta) mediates 6-hydroxydopamine-induced neuronal death. *FASEB J,* 18**,** 1162-4. (doi: 10.1096/fj.04-1551fje).

CHEN, P. E., SPECHT, C. G., MORRIS, R. G. & SCHOEPFER, R. 2002. Spatial learning is unimpaired in mice containing a deletion of the alpha-synuclein locus. *Eur J Neurosci,* 16**,** 154-8. (doi: 10.1046/j.1460-9568.2002.02062.x).

CHEN, X., GUO, C. & KONG, J. 2012. Oxidative stress in neurodegenerative diseases. *Neural Regen Res,* 7**,** 376-85. (doi: 10.3969/j.issn.1673-5374.2012.05.009).

CHEN, X., LEVY, J. M., HOU, A., WINTERS, C., AZZAM, R., SOUSA, A. A., LEAPMAN, R. D., NICOLL, R. A. & REESE, T. S. 2015. PSD-95 family MAGUKs are essential for anchoring AMPA and NMDA receptor complexes at the postsynaptic density. *Proc Natl Acad Sci U S A,* 112**,** E6983-92. (doi: 10.1073/pnas.1517045112).

CHEN, Z. & ZHONG, C. 2014. Oxidative stress in Alzheimer's disease. *Neurosci Bull,* 30**,** 271-81. (doi: 10.1007/s12264-013-1423-y).

CHO, J. H. & JOHNSON, G. V. 2004. Glycogen synthase kinase 3 beta induces caspase-cleaved tau aggregation in situ. *J Biol Chem,* 279**,** 54716-23. (doi: 10.1074/jbc.M403364200).

CIUPEK, S. M., CHENG, J., ALI, Y. O., LU, H. C. & JI, D. 2015. Progressive functional impairments of hippocampal neurons in a tauopathy mouse model. *J Neurosci,* 35**,** 8118-31. (doi: 10.1523/JNEUROSCI.3130-14.2015).

CLINTON, L. K., BLURTON-JONES, M., MYCZEK, K., TROJANOWSKI, J. Q. & LAFERLA, F. M. 2010. Synergistic Interactions between Abeta, tau, and alpha-synuclein: acceleration of neuropathology and cognitive decline. *J Neurosci,* 30**,** 7281-9. (doi: 10.1523/JNEUROSCI.0490-10.2010).

COLOSIMO, C., HUGHES, A. J., KILFORD, L. & LEES, A. J. 2003. Lewy body cortical involvement may not always predict dementia in Parkinson's disease. *J Neurol Neurosurg Psychiatry,* 74**,** 852-6. (doi: 10.1136/jnnp.74.7.852).

COMPTA, Y., PARKKINEN, L., O'SULLIVAN, S. S., VANDROVCOVA, J., HOLTON, J. L., COLLINS, C., LASHLEY, T., KALLIS, C., WILLIAMS, D. R., DE SILVA, R., LEES, A. J. & REVESZ, T. 2011. Lewy- and Alzheimer-type pathologies in Parkinson's disease dementia: which is more important? *Brain,* 134**,** 1493-1505. (doi: 10.1093/brain/awr031).

COSTANZO, M., ABOUNIT, S., MARZO, L., DANCKAERT, A., CHAMOUN, Z., ROUX, P. & ZURZOLO, C. 2013. Transfer of polyglutamine aggregates in neuronal cells occurs in tunneling nanotubes. *J Cell Sci,* 126**,** 3678-85. (doi: 10.1242/jcs.126086).

CRIMINS, J. L., POOLER, A., POLYDORO, M., LUEBKE, J. I. & SPIRES-JONES, T. L. 2013. The intersection of amyloid beta and tau in glutamatergic synaptic dysfunction and collapse in Alzheimer's disease. *Ageing Res Rev,* 12**,** 757-63. (doi: 10.1016/j.arr.2013.03.002).

CROISIER, E., MORAN, L. B., DEXTER, D. T., PEARCE, R. K. & GRAEBER, M. B. 2005. Microglial inflammation in the parkinsonian substantia nigra: relationship to alpha-synuclein deposition. *J Neuroinflammation,* 2**,** 14. (doi: 10.1186/1742-2094-2-14).

DANZER, K. M., KRANICH, L. R., RUF, W. P., CAGSAL-GETKIN, O., WINSLOW, A. R., ZHU, L., VANDERBURG, C. R. & MCLEAN, P. J. 2012. Exosomal cell-to-cell transmission of alpha synuclein oligomers. *Mol Neurodegener,* 7**,** 42. (doi: 10.1186/1750-1326-7-42).

DAVIE, C. A. 2008. A review of Parkinson's disease. *Br Med Bull,* 86**,** 109-27. (doi: 10.1093/bmb/ldn013).

DAWSON, T. M. & DAWSON, V. L. 2010. The role of parkin in familial and sporadic Parkinson's disease. *Mov Disord,* 25 Suppl 1**,** S32-9. (doi: 10.1002/mds.22798).

DEL TREDICI, K., RUB, U., DE VOS, R. A., BOHL, J. R. & BRAAK, H. 2002. Where does parkinson disease pathology begin in the brain? *J Neuropathol Exp Neurol,* 61**,** 413-26. (doi: 10.1093/jnen/61.5.413).

DELONG, M. R. 1990. Primate models of movement disorders of basal ganglia origin. *Trends Neurosci,* 13**,** 281-5. (doi: 10.1016/0166-2236(90)90110-v).

DENENBERG, V. H. 1969. Open-field bheavior in the rat: what does it mean? *Ann N Y Acad Sci,* 159**,** 852-9. (doi: 10.1111/j.1749-6632.1969.tb12983.x).

DEUMENS, R., BLOKLAND, A. & PRICKAERTS, J. 2002. Modeling Parkinson's disease in rats: an evaluation of 6-OHDA lesions of the nigrostriatal pathway. *Exp Neurol,* 175**,** 303-17. (doi: 10.1006/exnr.2002.7891).

DI DOMENICO, A., CAROLA, G., CALATAYUD, C., PONS-ESPINAL, M., MUNOZ, J. P., RICHAUD-PATIN, Y., FERNANDEZ-CARASA, I., GUT, M., FAELLA, A., PARAMESWARAN, J., SORIANO, J., FERRER, I., TOLOSA, E., ZORZANO, A., CUERVO, A. M., RAYA, A. & CONSIGLIO, A. 2019. Patient-Specific iPSC-Derived Astrocytes Contribute to Non-Cell-Autonomous Neurodegeneration in Parkinson's Disease. *Stem Cell Reports,* 12**,** 213-229. (doi: 10.1016/j.stemcr.2018.12.011).

DIAS, V., JUNN, E. & MOURADIAN, M. M. 2013. The role of oxidative stress in Parkinson's disease. *J Parkinsons Dis,* 3**,** 461-91. (doi: 10.3233/JPD-130230).

DIJKSTRA, A. A., INGRASSIA, A., DE MENEZES, R. X., VAN KESTEREN, R. E., ROZEMULLER, A. J., HEUTINK, P. & VAN DE BERG, W. D. 2015. Evidence for Immune Response, Axonal Dysfunction and Reduced Endocytosis in the Substantia Nigra in Early Stage Parkinson's Disease. *PLoS One,* 10**,** e0128651. (doi: 10.1371/journal.pone.0128651).

DINER, I., NGUYEN, T. & SEYFRIED, N. T. 2017. Enrichment of Detergent-insoluble Protein Aggregates from Human Postmortem Brain. *J Vis Exp*. (128) 55835 (doi: 10.3791/55835).

DOBSON, C. M. 1999. Protein misfolding, evolution and disease. *Trends Biochem Sci,* 24**,** 329-32. (doi: 10.1016/s0968-0004(99)01445-0).

DOCHERTY, M. J. & BURN, D. J. 2010. Parkinson's disease dementia. *Curr Neurol Neurosci Rep,* 10**,** 292-8. (doi: 10.1007/s11910-010-0113-7).

DUDA, J. E., GIASSON, B. I., CHEN, Q., GUR, T. L., HURTIG, H. I., STERN, M. B., GOLLOMP, S. M., ISCHIROPOULOS, H., LEE, V. M. & TROJANOWSKI, J. Q. 2000. Widespread nitration of pathological inclusions in neurodegenerative synucleinopathies. *Am J Pathol,* 157**,** 1439-45. (doi: 10.1016/S0002-9440(10)64781-5).

DUFFY, M. F., COLLIER, T. J., PATTERSON, J. R., KEMP, C. J., FISCHER, D. L., STOLL, A. C. & SORTWELL, C. E. 2018a. Quality Over Quantity: Advantages of Using Alpha-Synuclein Preformed Fibril Triggered Synucleinopathy to Model Idiopathic Parkinson's Disease. *Front Neurosci,* 12**,** 621. (doi: 10.3389/fnins.2018.00621).

DUFFY, M. F., COLLIER, T. J., PATTERSON, J. R., KEMP, C. J., LUK, K. C., TANSEY, M. G., PAUMIER, K. L., KANAAN, N. M., FISCHER, D. L., POLINSKI, N. K., BARTH, O. L., HOWE, J. W., VAIKATH, N. N., MAJBOUR, N. K., EL-AGNAF, O. M. A. & SORTWELL, C. E. 2018b. Correction to: Lewy body-like alpha-synuclein inclusions trigger reactive microgliosis prior to nigral degeneration. *J Neuroinflammation,* 15**,** 169. (doi: 10.1186/s12974-018-1202-9).

DUFFY, M. F., COLLIER, T. J., PATTERSON, J. R., KEMP, C. J., LUK, K. C., TANSEY, M. G., PAUMIER, K. L., KANAAN, N. M., FISCHER, D. L., POLINSKI, N. K., BARTH, O. L., HOWE, J. W., VAIKATH, N. N., MAJBOUR, N. K., EL-AGNAF, O. M. A. & SORTWELL, C. E. 2018c. Lewy body-like alpha-synuclein inclusions trigger reactive microgliosis prior to nigral degeneration. *J Neuroinflammation,* 15**,** 129. (doi: 10.1186/s12974-018-1171-z).

DUKA, T., DUKA, V., JOYCE, J. N. & SIDHU, A. 2009. Alpha-Synuclein contributes to GSK-3beta-catalyzed Tau phosphorylation in Parkinson's disease models. *FASEB J,* 23**,** 2820-30. (doi: 10.1096/fj.08-120410).

DUKA, T., RUSNAK, M., DROLET, R. E., DUKA, V., WERSINGER, C., GOUDREAU, J. L. & SIDHU, A. 2006. Alpha-synuclein induces hyperphosphorylation of Tau in the MPTP model of parkinsonism. *FASEB J,* 20**,** 2302-12. (doi: 10.1096/fj.06-6092com).

DUTY, S. & JENNER, P. 2011. Animal models of Parkinson's disease: a source of novel treatments and clues to the cause of the disease. *Br J Pharmacol,* 164**,** 1357-91. (doi: 10.1111/j.1476-5381.2011.01426.x).

EDWARDS, G., 3RD, ZHAO, J., DASH, P. K., SOTO, C. & MORENO-GONZALEZ, I. 2020. Traumatic Brain Injury Induces Tau Aggregation and Spreading. *J Neurotrauma,* 37**,** 80-92. (doi: 10.1089/neu.2018.6348).

EMMANOUILIDOU, E., MELACHROINOU, K., ROUMELIOTIS, T., GARBIS, S. D., NTZOUNI, M., MARGARITIS, L. H., STEFANIS, L. & VEKRELLIS, K. 2010. Cell-produced alpha-synuclein is secreted in a calcium-dependent manner by exosomes and impacts neuronal survival. *J Neurosci,* 30**,** 6838-51. (doi: 10.1523/JNEUROSCI.5699-09.2010).

EMRE, M. 2003. What causes mental dysfunction in Parkinson's disease? *Mov Disord,* 18 Suppl 6**,** S63-71. (doi: 10.1002/mds.10565).

ENGELENDER, S. & ISACSON, O. 2017. The Threshold Theory for Parkinson's Disease. *Trends Neurosci,* 40**,** 4-14. (doi: 10.1016/j.tins.2016.10.008).

ESPINOZA, M., DE SILVA, R., DICKSON, D. W. & DAVIES, P. 2008. Differential incorporation of tau isoforms in Alzheimer's disease. *J Alzheimers Dis,* 14**,** 1-16. (doi: 10.3233/jad-2008-14101).

FALCON, B., NOAD, J., MCMAHON, H., RANDOW, F. & GOEDERT, M. 2018. Galectin-8-mediated selective autophagy protects against seeded tau aggregation. *J Biol Chem,* 293**,** 2438-2451. (doi: 10.1074/jbc.M117.809293).

FARRER, M., KACHERGUS, J., FORNO, L., LINCOLN, S., WANG, D. S., HULIHAN, M., MARAGANORE, D., GWINN-HARDY, K., WSZOLEK, Z., DICKSON, D. & LANGSTON, J. W. 2004. Comparison of kindreds with parkinsonism and alpha-synuclein genomic multiplications. *Ann Neurol,* 55**,** 174-9. (doi: 10.1002/ana.10846).

FEIGIN, V. L., VOS, T., NICHOLS, E., OWOLABI, M. O., CARROLL, W. M., DICHGANS, M., DEUSCHL, G., PARMAR, P., BRAININ, M. & MURRAY, C. 2020. The global burden of neurological disorders: translating evidence into policy. *Lancet Neurol,* 19**,** 255-265. (doi: 10.1016/S1474-4422(19)30411-9).

FILIPPINI, A., GENNARELLI, M. & RUSSO, I. 2019. alpha-Synuclein and Glia in Parkinson's Disease: A Beneficial or a Detrimental Duet for the Endo-Lysosomal System? *Cell Mol Neurobiol,* 39**,** 161-168. (doi: 10.1007/s10571-019-00649-9).

FITZGERALD, L. W. & DOKLA, C. P. 1989. Morris water task impairment and hypoactivity following cysteamine-induced reductions of somatostatin-like immunoreactivity. *Brain Res,* 505**,** 246-50. (doi: 10.1016/0006-8993(89)91450-9).

FLAVIN, W. P., BOUSSET, L., GREEN, Z. C., CHU, Y., SKARPATHIOTIS, S., CHANEY, M. J., KORDOWER, J. H., MELKI, R. & CAMPBELL, E. M. 2017. Endocytic vesicle rupture is a conserved mechanism of cellular invasion by amyloid proteins. *Acta Neuropathol,* 134**,** 629-653. (doi: 10.1007/s00401-017-1722-x).

FLEMING, S. M., ZHU, C., FERNAGUT, P. O., MEHTA, A., DICARLO, C. D., SEAMAN, R. L. & CHESSELET, M. F. 2004. Behavioral and immunohistochemical effects of chronic intravenous and subcutaneous infusions of varying doses of rotenone. *Exp Neurol,* 187**,** 418-29. (doi: 10.1016/j.expneurol.2004.01.023).

FORNAI, F., SCHLUTER, O. M., LENZI, P., GESI, M., RUFFOLI, R., FERRUCCI, M., LAZZERI, G., BUSCETI, C. L., PONTARELLI, F., BATTAGLIA, G., PELLEGRINI, A., NICOLETTI, F., RUGGIERI, S., PAPARELLI, A. & SUDHOF, T. C. 2005. Parkinson-like syndrome induced by continuous MPTP infusion: convergent roles of the ubiquitin-proteasome system and alpha-synuclein. *Proc Natl Acad Sci U S A,* 102**,** 3413-8. (doi: 10.1073/pnas.0409713102).

FOURIE, C., LI, D. & MONTGOMERY, J. M. 2014. The anchoring protein SAP97 influences the trafficking and localisation of multiple membrane channels. *Biochim Biophys Acta,* 1838**,** 589-94. (doi: 10.1016/j.bbamem.2013.03.015).

FRASIER, M., WALZER, M., MCCARTHY, L., MAGNUSON, D., LEE, J. M., HAAS, C., KAHLE, P. & WOLOZIN, B. 2005. Tau phosphorylation increases in symptomatic mice overexpressing A30P alpha-synuclein. *Exp Neurol,* 192**,** 274-87. (doi: 10.1016/j.expneurol.2004.07.016).

FREICHEL, C., NEUMANN, M., BALLARD, T., MULLER, V., WOOLLEY, M., OZMEN, L., BORRONI, E., KRETZSCHMAR, H. A., HAASS, C., SPOOREN, W. & KAHLE, P. J. 2007. Age-dependent cognitive decline and amygdala pathology in alpha-synuclein transgenic mice. *Neurobiol Aging,* 28**,** 1421-35. (doi: 10.1016/j.neurobiolaging.2006.06.013).

FU, H., RODRIGUEZ, G. A., HERMAN, M., EMRANI, S., NAHMANI, E., BARRETT, G., FIGUEROA, H. Y., GOLDBERG, E., HUSSAINI, S. A. & DUFF, K. E. 2017. Tau Pathology Induces Excitatory Neuron Loss, Grid Cell Dysfunction, and Spatial Memory Deficits Reminiscent of Early Alzheimer's Disease. *Neuron,* 93**,** 533-541 e5. (doi: 10.1016/j.neuron.2016.12.023).

FUJINO, G., NOGUCHI, T., MATSUZAWA, A., YAMAUCHI, S., SAITOH, M., TAKEDA, K. & ICHIJO, H. 2007. Thioredoxin and TRAF family proteins regulate reactive oxygen species-dependent activation of ASK1 through reciprocal modulation of the N-terminal homophilic interaction of ASK1. *Mol Cell Biol,* 27**,** 8152-63. (doi: 10.1128/MCB.00227-07).

GAGNE, J. J. & POWER, M. C. 2010. Anti-inflammatory drugs and risk of Parkinson disease: a meta-analysis. *Neurology,* 74**,** 995-1002. (doi: 10.1212/WNL.0b013e3181d5a4a3).

GALVIN, J. E., POLLACK, J. & MORRIS, J. C. 2006. Clinical phenotype of Parkinson disease dementia. *Neurology,* 67**,** 1605-11. (doi: 10.1212/01.wnl.0000242630.52203.8f).

GANGULY, G., CHAKRABARTI, S., CHATTERJEE, U. & SASO, L. 2017. Proteinopathy, oxidative stress and mitochondrial dysfunction: cross talk in Alzheimer's disease and Parkinson's disease. *Drug Des Devel Ther,* 11**,** 797-810. (doi: 10.2147/DDDT.S130514).

GARCIA-RUIZ, P. J., CHAUDHURI, K. R. & MARTINEZ-MARTIN, P. 2014. Non-motor symptoms of Parkinson's disease A review...from the past. *J Neurol Sci,* 338**,** 30-3. (doi: 10.1016/j.jns.2014.01.002).

GARDONI, F., PICCONI, B., GHIGLIERI, V., POLLI, F., BAGETTA, V., BERNARDI, G., CATTABENI, F., DI LUCA, M. & CALABRESI, P. 2006. A critical interaction between NR2B and MAGUK in L-DOPA induced dyskinesia. *J Neurosci,* 26**,** 2914-22. (doi: 10.1523/JNEUROSCI.5326-05.2006).

GASSOWSKA, M., CZAPSKI, G. A., PAJAK, B., CIESLIK, M., LENKIEWICZ, A. M. & ADAMCZYK, A. 2014. Extracellular alpha-synuclein leads to microtubule destabilization via GSK-3beta-dependent Tau phosphorylation in PC12 cells. *PLoS One,* 9**,** e94259. (doi: 10.1371/journal.pone.0094259).

GELDERS, G., BAEKELANDT, V. & VAN DER PERREN, A. 2018. Linking Neuroinflammation and Neurodegeneration in Parkinson's Disease. *J Immunol Res,* 2018**,** 4784268. (doi: 10.1155/2018/4784268).

GERFEN, C. R., ENGBER, T. M., MAHAN, L. C., SUSEL, Z., CHASE, T. N., MONSMA, F. J., JR. & SIBLEY, D. R. 1990. D1 and D2 dopamine receptor-regulated gene expression of striatonigral and striatopallidal neurons. *Science,* 250**,** 1429-32. (doi: 10.1126/science.2147780).

GERHARD, A., PAVESE, N., HOTTON, G., TURKHEIMER, F., ES, M., HAMMERS, A., EGGERT, K., OERTEL, W., BANATI, R. B. & BROOKS, D. J. 2006. In vivo imaging of microglial activation with [11C](R)-PK11195 PET in idiopathic Parkinson's disease. *Neurobiol Dis,* 21**,** 404-12. (doi: 10.1016/j.nbd.2005.08.002).

GIASSON, B. I., FORMAN, M. S., HIGUCHI, M., GOLBE, L. I., GRAVES, C. L., KOTZBAUER, P. T., TROJANOWSKI, J. Q. & LEE, V. M. 2003. Initiation and synergistic fibrillization of tau and alpha-synuclein. *Science,* 300**,** 636-40. (doi: 10.1126/science.1082324).

GIASSON, B. I., JAKES, R., GOEDERT, M., DUDA, J. E., LEIGHT, S., TROJANOWSKI, J. Q. & LEE, V. M. 2000. A panel of epitope-specific antibodies detects protein domains distributed throughout

human alpha-synuclein in Lewy bodies of Parkinson's disease. *J Neurosci Res,* 59**,** 528-33. (doi: 10.1002/(SICI)1097-4547(20000215)59:4<528::AID-JNR8>3.0.CO;2-0).
GIBB, W. R. & LEES, A. J. 1988a. A comparison of clinical and pathological features of young- and old-onset Parkinson's disease. *Neurology,* 38**,** 1402-6. (doi: 10.1212/wnl.38.9.1402).
GIBB, W. R. & LEES, A. J. 1988b. The relevance of the Lewy body to the pathogenesis of idiopathic Parkinson's disease. *J Neurol Neurosurg Psychiatry,* 51**,** 745-52. (doi: 10.1136/jnnp.51.6.745).
GLENNON, E. B., LAU, D. H., GABRIELE, R. M. C., TAYLOR, M. F., TROAKES, C., OPIE-MARTIN, S., ELLIOTT, C., KILLICK, R., HANGER, D. P., PEREZ-NIEVAS, B. G. & NOBLE, W. 2020. Bridging Integrator-1 protein loss in Alzheimer's disease promotes synaptic tau accumulation and disrupts tau release. *Brain Commun,* 2. (doi: 10.1093/braincomms/fcaa011).
GLINKA, Y., TIPTON, K. F. & YOUDIM, M. B. 1996. Nature of inhibition of mitochondrial respiratory complex I by 6-Hydroxydopamine. *J Neurochem,* 66**,** 2004-10. (doi: 10.1046/j.1471-4159.1996.66052004.x).
GOEDERT, M., SPILLANTINI, M. G. & DAVIES, S. W. 1998. Filamentous nerve cell inclusions in neurodegenerative diseases. *Curr Opin Neurobiol,* 8**,** 619-32. (doi: 10.1016/s0959-4388(98)80090-1).
GOETZ, C. G. 2011. The history of Parkinson's disease: early clinical descriptions and neurological therapies. *Cold Spring Harb Perspect Med,* 1**,** a008862. (doi: 10.1101/cshperspect.a008862).
GOMEZ-TORTOSA, E., NEWELL, K., IRIZARRY, M. C., SANDERS, J. L. & HYMAN, B. T. 2000. alpha-Synuclein immunoreactivity in dementia with Lewy bodies: morphological staging and comparison with ubiquitin immunostaining. *Acta Neuropathol,* 99**,** 352-7. (doi: 10.1007/s004010051135).
GOREN, B., MIMBAY, Z., BILICI, N., ZARIFOGLU, M., OGUL, E. & KORFALI, E. 2009. Investigation of neuroprotective effects of cyclooxygenase inhibitors in the 6-hydroxydopamine induced rat Parkinson model. *Turk Neurosurg,* 19**,** 230-6. (doi).
GRATWICKE, J., JAHANSHAHI, M. & FOLTYNIE, T. 2015. Parkinson's disease dementia: a neural networks perspective. *Brain,* 138**,** 1454-76. (doi: 10.1093/brain/awv104).
GRAY, M. T. & WOULFE, J. M. 2015. Striatal blood-brain barrier permeability in Parkinson's disease. *J Cereb Blood Flow Metab,* 35**,** 747-50. (doi: 10.1038/jcbfm.2015.32).
GREALISH, S., MATTSSON, B., DRAXLER, P. & BJORKLUND, A. 2010. Characterisation of behavioural and neurodegenerative changes induced by intranigral 6-hydroxydopamine lesions in a mouse model of Parkinson's disease. *Eur J Neurosci,* 31**,** 2266-78. (doi: 10.1111/j.1460-9568.2010.07265.x).
GRETEN-HARRISON, B., POLYDORO, M., MORIMOTO-TOMITA, M., DIAO, L., WILLIAMS, A. M., NIE, E. H., MAKANI, S., TIAN, N., CASTILLO, P. E., BUCHMAN, V. L. & CHANDRA, S. S. 2010. alphabetagamma-Synuclein triple knockout mice reveal age-dependent neuronal dysfunction. *Proc Natl Acad Sci U S A,* 107**,** 19573-8. (doi: 10.1073/pnas.1005005107).
GUO, J. L., COVELL, D. J., DANIELS, J. P., IBA, M., STIEBER, A., ZHANG, B., RIDDLE, D. M., KWONG, L. K., XU, Y., TROJANOWSKI, J. Q. & LEE, V. M. 2013. Distinct alpha-synuclein strains differentially promote tau inclusions in neurons. *Cell,* 154**,** 103-17. (doi: 10.1016/j.cell.2013.05.057).
GUO, J. L. & LEE, V. M. 2011. Seeding of normal Tau by pathological Tau conformers drives pathogenesis of Alzheimer-like tangles. *J Biol Chem,* 286**,** 15317-31. (doi: 10.1074/jbc.M110.209296).
GUO, T., NOBLE, W. & HANGER, D. P. 2017. Roles of tau protein in health and disease. *Acta Neuropathol,* 133**,** 665-704. (doi: 10.1007/s00401-017-1707-9).
GUZMAN-MARTINEZ, L., MACCIONI, R. B., ANDRADE, V., NAVARRETE, L. P., PASTOR, M. G. & RAMOS-ESCOBAR, N. 2019. Neuroinflammation as a Common Feature of Neurodegenerative Disorders. *Front Pharmacol,* 10**,** 1008. (doi: 10.3389/fphar.2019.01008).
HAASS, C. & SELKOE, D. J. 2007. Soluble protein oligomers in neurodegeneration: lessons from the Alzheimer's amyloid beta-peptide. *Nat Rev Mol Cell Biol,* 8**,** 101-12. (doi: 10.1038/nrm2101).

HAGGERTY, T., CREDLE, J., RODRIGUEZ, O., WILLS, J., OAKS, A. W., MASLIAH, E. & SIDHU, A. 2011. Hyperphosphorylated Tau in an alpha-synuclein-overexpressing transgenic model of Parkinson's disease. *Eur J Neurosci,* 33**,** 1598-610. (doi: 10.1111/j.1460-9568.2011.07660.x).

HALLIDAY, G., LEES, A. & STERN, M. 2011. Milestones in Parkinson's disease--clinical and pathologic features. *Mov Disord,* 26**,** 1015-21. (doi: 10.1002/mds.23669).

HALLIDAY, G. M., LEVERENZ, J. B., SCHNEIDER, J. S. & ADLER, C. H. 2014. The neurobiological basis of cognitive impairment in Parkinson's disease. *Mov Disord,* 29**,** 634-50. (doi: 10.1002/mds.25857).

HANGER, D. P., ANDERTON, B. H. & NOBLE, W. 2009. Tau phosphorylation: the therapeutic challenge for neurodegenerative disease. *Trends Mol Med,* 15**,** 112-9. (doi: 10.1016/j.molmed.2009.01.003).

HANGER, D. P., BYERS, H. L., WRAY, S., LEUNG, K. Y., SAXTON, M. J., SEEREERAM, A., REYNOLDS, C. H., WARD, M. A. & ANDERTON, B. H. 2007. Novel phosphorylation sites in tau from Alzheimer brain support a role for casein kinase 1 in disease pathogenesis. *J Biol Chem,* 282**,** 23645-54. (doi: 10.1074/jbc.M703269200).

HANGER, D. P., GONIOTAKI, D. & NOBLE, W. 2019. Synaptic Localisation of Tau. *Adv Exp Med Biol,* 1184**,** 105-112. (doi: 10.1007/978-981-32-9358-8_9).

HATCH, R. J., WEI, Y., XIA, D. & GOTZ, J. 2017. Hyperphosphorylated tau causes reduced hippocampal CA1 excitability by relocating the axon initial segment. *Acta Neuropathol,* 133**,** 717-730. (doi: 10.1007/s00401-017-1674-1).

HE, Z., GUO, J. L., MCBRIDE, J. D., NARASIMHAN, S., KIM, H., CHANGOLKAR, L., ZHANG, B., GATHAGAN, R. J., YUE, C., DENGLER, C., STIEBER, A., NITLA, M., COULTER, D. A., ABEL, T., BRUNDEN, K. R., TROJANOWSKI, J. Q. & LEE, V. M. 2018. Amyloid-beta plaques enhance Alzheimer's brain tau-seeded pathologies by facilitating neuritic plaque tau aggregation. *Nat Med,* 24**,** 29-38. (doi: 10.1038/nm.4443).

HELY, M. A., REID, W. G., ADENA, M. A., HALLIDAY, G. M. & MORRIS, J. G. 2008. The Sydney multicenter study of Parkinson's disease: the inevitability of dementia at 20 years. *Mov Disord,* 23**,** 837-44. (doi: 10.1002/mds.21956).

HENDERSON, M. X., CORNBLATH, E. J., DARWICH, A., ZHANG, B., BROWN, H., GATHAGAN, R. J., SANDLER, R. M., BASSETT, D. S., TROJANOWSKI, J. Q. & LEE, V. M. Y. 2019a. Spread of alpha-synuclein pathology through the brain connectome is modulated by selective vulnerability and predicted by network analysis. *Nat Neurosci,* 22**,** 1248-1257. (doi: 10.1038/s41593-019-0457-5).

HENDERSON, M. X., SENGUPTA, M., TROJANOWSKI, J. Q. & LEE, V. M. Y. 2019b. Alzheimer's disease tau is a prominent pathology in LRRK2 Parkinson's disease. *Acta Neuropathol Commun,* 7**,** 183. (doi: 10.1186/s40478-019-0836-x).

HERNANDEZ-BALTAZAR, D., ZAVALA-FLORES, L. M. & VILLANUEVA-OLIVO, A. 2017. The 6-hydroxydopamine model and parkinsonian pathophysiology: Novel findings in an older model. *Neurologia,* 32**,** 533-539. (doi: 10.1016/j.nrl.2015.06.011).

HEUER, A. & DUNNETT, S. B. 2013. Characterisation of spatial neglect induced by unilateral 6-OHDA lesions on a choice reaction time task in rats. *Behav Brain Res,* 237**,** 215-22. (doi: 10.1016/j.bbr.2012.09.038).

HEUER, A., SMITH, G. A. & DUNNETT, S. B. 2013. Comparison of 6-hydroxydopamine lesions of the substantia nigra and the medial forebrain bundle on a lateralised choice reaction time task in mice. *Eur J Neurosci,* 37**,** 294-302. (doi: 10.1111/ejn.12036).

HEUER, A., SMITH, G. A., LELOS, M. J., LANE, E. L. & DUNNETT, S. B. 2012. Unilateral nigrostriatal 6-hydroxydopamine lesions in mice I: motor impairments identify extent of dopamine depletion at three different lesion sites. *Behav Brain Res,* 228**,** 30-43. (doi: 10.1016/j.bbr.2011.11.027).

HICKEY, M. A. & CHESSELET, M. F. 2012. Behavioural Assessment of Genetic Mouse Models of Huntington's Disease. *In:* LANE, E. L. & DUNNETT, S. B. (eds.) *Animal Models of Movement Disorders.* Humana.

HIJAZ, B. A. & VOLPICELLI-DALEY, L. A. 2020. Initiation and propagation of alpha-synuclein aggregation in the nervous system. *Mol Neurodegener,* 15**,** 19. (doi: 10.1186/s13024-020-00368-6).

HOLDORFF, B. 2002. Friedrich Heinrich Lewy (1885-1950) and his work. *J Hist Neurosci,* 11**,** 19-28. (doi: 10.1076/jhin.11.1.19.9106).

HOLMES, B. B., DEVOS, S. L., KFOURY, N., LI, M., JACKS, R., YANAMANDRA, K., OUIDJA, M. O., BRODSKY, F. M., MARASA, J., BAGCHI, D. P., KOTZBAUER, P. T., MILLER, T. M., PAPY-GARCIA, D. & DIAMOND, M. I. 2013. Heparan sulfate proteoglycans mediate internalization and propagation of specific proteopathic seeds. *Proc Natl Acad Sci U S A,* 110**,** E3138-47. (doi: 10.1073/pnas.1301440110).

HOLMQVIST, S., CHUTNA, O., BOUSSET, L., ALDRIN-KIRK, P., LI, W., BJORKLUND, T., WANG, Z. Y., ROYBON, L., MELKI, R. & LI, J. Y. 2014. Direct evidence of Parkinson pathology spread from the gastrointestinal tract to the brain in rats. *Acta Neuropathol,* 128**,** 805-20. (doi: 10.1007/s00401-014-1343-6).

HONG, S., BEJA-GLASSER, V. F., NFONOYIM, B. M., FROUIN, A., LI, S., RAMAKRISHNAN, S., MERRY, K. M., SHI, Q., ROSENTHAL, A., BARRES, B. A., LEMERE, C. A., SELKOE, D. J. & STEVENS, B. 2016. Complement and microglia mediate early synapse loss in Alzheimer mouse models. *Science,* 352**,** 712-716. (doi: 10.1126/science.aad8373).

HOOVER, B. R., REED, M. N., SU, J., PENROD, R. D., KOTILINEK, L. A., GRANT, M. K., PITSTICK, R., CARLSON, G. A., LANIER, L. M., YUAN, L. L., ASHE, K. H. & LIAO, D. 2010. Tau mislocalization to dendritic spines mediates synaptic dysfunction independently of neurodegeneration. *Neuron,* 68**,** 1067-81. (doi: 10.1016/j.neuron.2010.11.030).

HORNER, A. E., HEATH, C. J., HVOSLEF-EIDE, M., KENT, B. A., KIM, C. H., NILSSON, S. R., ALSIO, J., OOMEN, C. A., HOLMES, A., SAKSIDA, L. M. & BUSSEY, T. J. 2013. The touchscreen operant platform for testing learning and memory in rats and mice. *Nat Protoc,* 8**,** 1961-84. (doi: 10.1038/nprot.2013.122).

HU, S., HU, M., LIU, J., ZHANG, B., ZHANG, Z., ZHOU, F. H., WANG, L. & DONG, J. 2020. Phosphorylation of Tau and alpha-Synuclein Induced Neurodegeneration in MPTP Mouse Model of Parkinson's Disease. *Neuropsychiatr Dis Treat,* 16**,** 651-663. (doi: 10.2147/NDT.S235562).

HUBER, C. M., YEE, C., MAY, T., DHANALA, A. & MITCHELL, C. S. 2018. Cognitive Decline in Preclinical Alzheimer's Disease: Amyloid-Beta versus Tauopathy. *J Alzheimers Dis,* 61**,** 265-281. (doi: 10.3233/JAD-170490).

HWANG, O. 2013. Role of oxidative stress in Parkinson's disease. *Exp Neurobiol,* 22**,** 11-7. (doi: 10.5607/en.2013.22.1.11).

IANCU, R., MOHAPEL, P., BRUNDIN, P. & PAUL, G. 2005. Behavioral characterization of a unilateral 6-OHDA-lesion model of Parkinson's disease in mice. *Behav Brain Res,* 162**,** 1-10. (doi: 10.1016/j.bbr.2005.02.023).

IRIZARRY, M. C., GROWDON, W., GOMEZ-ISLA, T., NEWELL, K., GEORGE, J. M., CLAYTON, D. F. & HYMAN, B. T. 1998. Nigral and cortical Lewy bodies and dystrophic nigral neurites in Parkinson's disease and cortical Lewy body disease contain alpha-synuclein immunoreactivity. *J Neuropathol Exp Neurol,* 57**,** 334-7. (doi: 10.1097/00005072-199804000-00005).

IRWIN, D. J. & HURTIG, H. I. 2018. The Contribution of Tau, Amyloid-Beta and Alpha-Synuclein Pathology to Dementia in Lewy Body Disorders. *J Alzheimers Dis Parkinsonism,* 8. (doi: 10.4172/2161-0460.1000444).

IRWIN, D. J., LEE, V. M. & TROJANOWSKI, J. Q. 2013. Parkinson's disease dementia: convergence of alpha-synuclein, tau and amyloid-beta pathologies. *Nat Rev Neurosci,* 14**,** 626-36. (doi: 10.1038/nrn3549).

IRWIN, D. J., WHITE, M. T., TOLEDO, J. B., XIE, S. X., ROBINSON, J. L., VAN DEERLIN, V., LEE, V. M., LEVERENZ, J. B., MONTINE, T. J., DUDA, J. E., HURTIG, H. I. & TROJANOWSKI, J. Q. 2012. Neuropathologic substrates of Parkinson disease dementia. *Ann Neurol,* 72**,** 587-98. (doi: 10.1002/ana.23659).

ISEKI, E., TOGO, T., SUZUKI, K., KATSUSE, O., MARUI, W., DE SILVA, R., LEES, A., YAMAMOTO, T. & KOSAKA, K. 2003. Dementia with Lewy bodies from the perspective of tauopathy. *Acta Neuropathol,* 105**,** 265-70. (doi: 10.1007/s00401-002-0644-3).

ITTNER, L. M., KE, Y. D., DELERUE, F., BI, M., GLADBACH, A., VAN EERSEL, J., WOLFING, H., CHIENG, B. C., CHRISTIE, M. J., NAPIER, I. A., ECKERT, A., STAUFENBIEL, M., HARDEMAN, E. & GOTZ, J. 2010. Dendritic function of tau mediates amyloid-beta toxicity in Alzheimer's disease mouse models. *Cell,* 142**,** 387-97. (doi: 10.1016/j.cell.2010.06.036).

JEGANATHAN, S., HASCHER, A., CHINNATHAMBI, S., BIERNAT, J., MANDELKOW, E. M. & MANDELKOW, E. 2008. Proline-directed pseudo-phosphorylation at AT8 and PHF1 epitopes induces a compaction of the paperclip folding of Tau and generates a pathological (MC-1) conformation. *J Biol Chem,* 283**,** 32066-76. (doi: 10.1074/jbc.M805300200).

JENNER, P. & LANGSTON, J. W. 2011. Explaining ADAGIO: a critical review of the biological basis for the clinical effects of rasagiline. *Mov Disord,* 26**,** 2316-23. (doi: 10.1002/mds.23926).

JENSEN, P. H., HAGER, H., NIELSEN, M. S., HOJRUP, P., GLIEMANN, J. & JAKES, R. 1999. alpha-synuclein binds to Tau and stimulates the protein kinase A-catalyzed tau phosphorylation of serine residues 262 and 356. *J Biol Chem,* 274**,** 25481-9. (doi: 10.1074/jbc.274.36.25481).

JHA, M. K. & MORRISON, B. M. 2018. Glia-neuron energy metabolism in health and diseases: New insights into the role of nervous system metabolic transporters. *Exp Neurol,* 309**,** 23-31. (doi: 10.1016/j.expneurol.2018.07.009).

JOE, E. H., CHOI, D. J., AN, J., EUN, J. H., JOU, I. & PARK, S. 2018. Astrocytes, Microglia, and Parkinson's Disease. *Exp Neurobiol,* 27**,** 77-87. (doi: 10.5607/en.2018.27.2.77).

JONSSON, G. 1983. Monoamine neurotoxins. In Handbook of chemical neuroanatomy. *In:* BJORKLUND, A. & HOKFELT, T. (eds.) *Methods in chemical neuroanatomy.* Amersterdam: Elsevier.

JUCKER, M. & WALKER, L. C. 2013. Self-propagation of pathogenic protein aggregates in neurodegenerative diseases. *Nature,* 501**,** 45-51. (doi: 10.1038/nature12481).

KALAITZAKIS, M. E., GRAEBER, M. B., GENTLEMAN, S. M. & PEARCE, R. K. 2008. The dorsal motor nucleus of the vagus is not an obligatory trigger site of Parkinson's disease: a critical analysis of alpha-synuclein staging. *Neuropathol Appl Neurobiol,* 34**,** 284-95. (doi: 10.1111/j.1365-2990.2007.00923.x).

KANNARKAT, G. T., BOSS, J. M. & TANSEY, M. G. 2013. The role of innate and adaptive immunity in Parkinson's disease. *J Parkinsons Dis,* 3**,** 493-514. (doi: 10.3233/JPD-130250).

KASONGO, D. W., DE LEO, G., VICARIO, N., LEANZA, G. & LEGNAME, G. 2020. Chronic alpha-Synuclein Accumulation in Rat Hippocampus Induces Lewy Bodies Formation and Specific Cognitive Impairments. *eNeuro,* 7. (doi: 10.1523/ENEURO.0009-20.2020).

KIM, G. H., KIM, J. E., RHIE, S. J. & YOON, S. 2015. The Role of Oxidative Stress in Neurodegenerative Diseases. *Exp Neurobiol,* 24**,** 325-40. (doi: 10.5607/en.2015.24.4.325).

KIM, H., AHRLUND-RICHTER, S., WANG, X., DEISSEROTH, K. & CARLEN, M. 2016. Prefrontal Parvalbumin Neurons in Control of Attention. *Cell,* 164**,** 208-218. (doi: 10.1016/j.cell.2015.11.038).

KIM, S., KWON, S. H., KAM, T. I., PANICKER, N., KARUPPAGOUNDER, S. S., LEE, S., LEE, J. H., KIM, W. R., KOOK, M., FOSS, C. A., SHEN, C., LEE, H., KULKARNI, S., PASRICHA, P. J., LEE, G., POMPER, M. G., DAWSON, V. L., DAWSON, T. M. & KO, H. S. 2019. Transneuronal Propagation of

Pathologic alpha-Synuclein from the Gut to the Brain Models Parkinson's Disease. *Neuron,* 103**,** 627-641 e7. (doi: 10.1016/j.neuron.2019.05.035).
KIN, K., YASUHARA, T., KAMEDA, M. & DATE, I. 2019. Animal Models for Parkinson's Disease Research: Trends in the 2000s. *Int J Mol Sci,* 20. (doi: 10.3390/ijms20215402).
KIRIK, D., ANNETT, L. E., BURGER, C., MUZYCZKA, N., MANDEL, R. J. & BJORKLUND, A. 2003. Nigrostriatal alpha-synucleinopathy induced by viral vector-mediated overexpression of human alpha-synuclein: a new primate model of Parkinson's disease. *Proc Natl Acad Sci U S A,* 100**,** 2884-9. (doi: 10.1073/pnas.0536383100).
KIRIK, D., ROSENBLAD, C. & BJORKLUND, A. 1998. Characterization of behavioral and neurodegenerative changes following partial lesions of the nigrostriatal dopamine system induced by intrastriatal 6-hydroxydopamine in the rat. *Exp Neurol,* 152**,** 259-77. (doi: 10.1006/exnr.1998.6848).
KLEGERIS, A., PELECH, S., GIASSON, B. I., MAGUIRE, J., ZHANG, H., MCGEER, E. G. & MCGEER, P. L. 2008. Alpha-synuclein activates stress signaling protein kinases in THP-1 cells and microglia. *Neurobiol Aging,* 29**,** 739-52. (doi: 10.1016/j.neurobiolaging.2006.11.013).
KRUGER, R., KUHN, W., MULLER, T., WOITALLA, D., GRAEBER, M., KOSEL, S., PRZUNTEK, H., EPPLEN, J. T., SCHOLS, L. & RIESS, O. 1998. Ala30Pro mutation in the gene encoding alpha-synuclein in Parkinson's disease. *Nat Genet,* 18**,** 106-8. (doi: 10.1038/ng0298-106).
KUTER, K., OLECH, L. & GLOWACKA, U. 2018. Prolonged Dysfunction of Astrocytes and Activation of Microglia Accelerate Degeneration of Dopaminergic Neurons in the Rat Substantia Nigra and Block Compensation of Early Motor Dysfunction Induced by 6-OHDA. *Mol Neurobiol,* 55**,** 3049-3066. (doi: 10.1007/s12035-017-0529-z).
LAI, H. M., LIU, A. K. L., NG, H. H. M., GOLDFINGER, M. H., CHAU, T. W., DEFELICE, J., TILLEY, B. S., WONG, W. M., WU, W. & GENTLEMAN, S. M. 2018. Next generation histology methods for three-dimensional imaging of fresh and archival human brain tissues. *Nat Commun,* 9**,** 1066. (doi: 10.1038/s41467-018-03359-w).
LEE, V. M., BRUNDEN, K. R., HUTTON, M. & TROJANOWSKI, J. Q. 2011. Developing therapeutic approaches to tau, selected kinases, and related neuronal protein targets. *Cold Spring Harb Perspect Med,* 1**,** a006437. (doi: 10.1101/cshperspect.a006437).
LEE, Y., DAWSON, V. L. & DAWSON, T. M. 2012. Animal models of Parkinson's disease: vertebrate genetics. *Cold Spring Harb Perspect Med,* 2. (doi: 10.1101/cshperspect.a009324).
LEES, A. J., HARDY, J. & REVESZ, T. 2009. Parkinson's disease. *Lancet,* 373**,** 2055-66. (doi: 10.1016/S0140-6736(09)60492-X).
LEES, A. J., TOLOSA, E. & OLANOW, C. W. 2015. Four pioneers of L-dopa treatment: Arvid Carlsson, Oleh Hornykiewicz, George Cotzias, and Melvin Yahr. *Mov Disord,* 30**,** 19-36. (doi: 10.1002/mds.26120).
LEHMKUHLE, M. J., BHANGOO, S. S. & KIPKE, D. R. 2009. The electrocorticogram signal can be modulated with deep brain stimulation of the subthalamic nucleus in the hemiparkinsonian rat. *J Neurophysiol,* 102**,** 1811-20. (doi: 10.1152/jn.90844.2008).
LESAGE, S., ANHEIM, M., LETOURNEL, F., BOUSSET, L., HONORE, A., ROZAS, N., PIERI, L., MADIONA, K., DURR, A., MELKI, R., VERNY, C., BRICE, A. & FRENCH PARKINSON'S DISEASE GENETICS STUDY, G. 2013. G51D alpha-synuclein mutation causes a novel parkinsonian-pyramidal syndrome. *Ann Neurol,* 73**,** 459-71. (doi: 10.1002/ana.23894).
LEVIN, B. E., LLABRE, M. M., REISMAN, S., WEINER, W. J., SANCHEZ-RAMOS, J., SINGER, C. & BROWN, M. C. 1991. Visuospatial impairment in Parkinson's disease. *Neurology,* 41**,** 365-9. (doi: 10.1212/wnl.41.3.365).
LEWIS, S. J., DOVE, A., ROBBINS, T. W., BARKER, R. A. & OWEN, A. M. 2003. Cognitive impairments in early Parkinson's disease are accompanied by reductions in activity in frontostriatal neural circuitry. *J Neurosci,* 23**,** 6351-6. (doi).
LIDDELOW, S. A. & BARRES, B. A. 2017. Reactive Astrocytes: Production, Function, and Therapeutic Potential. *Immunity,* 46**,** 957-967. (doi: 10.1016/j.immuni.2017.06.006).

LIDDELOW, S. A., GUTTENPLAN, K. A., CLARKE, L. E., BENNETT, F. C., BOHLEN, C. J., SCHIRMER, L., BENNETT, M. L., MUNCH, A. E., CHUNG, W. S., PETERSON, T. C., WILTON, D. K., FROUIN, A., NAPIER, B. A., PANICKER, N., KUMAR, M., BUCKWALTER, M. S., ROWITCH, D. H., DAWSON, V. L., DAWSON, T. M., STEVENS, B. & BARRES, B. A. 2017. Neurotoxic reactive astrocytes are induced by activated microglia. *Nature,* 541**,** 481-487. (doi: 10.1038/nature21029).

LIGUORI, I., RUSSO, G., CURCIO, F., BULLI, G., ARAN, L., DELLA-MORTE, D., GARGIULO, G., TESTA, G., CACCIATORE, F., BONADUCE, D. & ABETE, P. 2018. Oxidative stress, aging, and diseases. *Clin Interv Aging,* 13**,** 757-772. (doi: 10.2147/CIA.S158513).

LIM, Y., KEHM, V. M., LEE, E. B., SOPER, J. H., LI, C., TROJANOWSKI, J. Q. & LEE, V. M. 2011. alpha-Syn suppression reverses synaptic and memory defects in a mouse model of dementia with Lewy bodies. *J Neurosci,* 31**,** 10076-87. (doi: 10.1523/JNEUROSCI.0618-11.2011).

LIN, M. T. & BEAL, M. F. 2006. Mitochondrial dysfunction and oxidative stress in neurodegenerative diseases. *Nature,* 443**,** 787-95. (doi: 10.1038/nature05292).

LINDSTROM, V., GUSTAFSSON, G., SANDERS, L. H., HOWLETT, E. H., SIGVARDSON, J., KASRAYAN, A., INGELSSON, M., BERGSTROM, J. & ERLANDSSON, A. 2017. Extensive uptake of alpha-synuclein oligomers in astrocytes results in sustained intracellular deposits and mitochondrial damage. *Mol Cell Neurosci,* 82**,** 143-156. (doi: 10.1016/j.mcn.2017.04.009).

LIPTON, D. M., GONZALES, B. J. & CITRI, A. 2019. Dorsal Striatal Circuits for Habits, Compulsions and Addictions. *Front Syst Neurosci,* 13**,** 28. (doi: 10.3389/fnsys.2019.00028).

LIU, A. K., HURRY, M. E., NG, O. T., DEFELICE, J., LAI, H. M., PEARCE, R. K., WONG, G. T., CHANG, R. C. & GENTLEMAN, S. M. 2016. Bringing CLARITY to the human brain: visualization of Lewy pathology in three dimensions. *Neuropathol Appl Neurobiol,* 42**,** 573-87. (doi: 10.1111/nan.12293).

LIU, Z., GALEMMO, R. A., JR., FRASER, K. B., MOEHLE, M. S., SEN, S., VOLPICELLI-DALEY, L. A., DELUCAS, L. J., ROSS, L. J., VALIYAVEETTIL, J., MOUKHA-CHAFIQ, O., PATHAK, A. K., ANANTHAN, S., KEZAR, H., WHITE, E. L., GUPTA, V., MADDRY, J. A., SUTO, M. J. & WEST, A. B. 2014. Unique functional and structural properties of the LRRK2 protein ATP-binding pocket. *J Biol Chem,* 289**,** 32937-51. (doi: 10.1074/jbc.M114.602318).

LORIA, F., VARGAS, J. Y., BOUSSET, L., SYAN, S., SALLES, A., MELKI, R. & ZURZOLO, C. 2017. alpha-Synuclein transfer between neurons and astrocytes indicates that astrocytes play a role in degradation rather than in spreading. *Acta Neuropathol,* 134**,** 789-808. (doi: 10.1007/s00401-017-1746-2).

LUK, K. C., COVELL, D. J., KEHM, V. M., ZHANG, B., SONG, I. Y., BYRNE, M. D., PITKIN, R. M., DECKER, S. C., TROJANOWSKI, J. Q. & LEE, V. M. 2016. Molecular and Biological Compatibility with Host Alpha-Synuclein Influences Fibril Pathogenicity. *Cell Rep,* 16**,** 3373-3387. (doi: 10.1016/j.celrep.2016.08.053).

LUK, K. C., KEHM, V., CARROLL, J., ZHANG, B., O'BRIEN, P., TROJANOWSKI, J. Q. & LEE, V. M. 2012a. Pathological alpha-synuclein transmission initiates Parkinson-like neurodegeneration in nontransgenic mice. *Science,* 338**,** 949-53. (doi: 10.1126/science.1227157).

LUK, K. C., KEHM, V. M., ZHANG, B., O'BRIEN, P., TROJANOWSKI, J. Q. & LEE, V. M. 2012b. Intracerebral inoculation of pathological alpha-synuclein initiates a rapidly progressive neurodegenerative alpha-synucleinopathy in mice. *J Exp Med,* 209**,** 975-86. (doi: 10.1084/jem.20112457).

LUK, K. C., SONG, C., O'BRIEN, P., STIEBER, A., BRANCH, J. R., BRUNDEN, K. R., TROJANOWSKI, J. Q. & LEE, V. M. 2009. Exogenous alpha-synuclein fibrils seed the formation of Lewy body-like intracellular inclusions in cultured cells. *Proc Natl Acad Sci U S A,* 106**,** 20051-6. (doi: 10.1073/pnas.0908005106).

LUNA, E., DECKER, S. C., RIDDLE, D. M., CAPUTO, A., ZHANG, B., COLE, T., CASWELL, C., XIE, S. X., LEE, V. M. Y. & LUK, K. C. 2018. Differential alpha-synuclein expression contributes to selective vulnerability of hippocampal neuron subpopulations to fibril-induced toxicity. *Acta Neuropathol,* 135**,** 855-875. (doi: 10.1007/s00401-018-1829-8).

LUSCHER, C. 2016. The Emergence of a Circuit Model for Addiction. *Annu Rev Neurosci,* 39**,** 257-76. (doi: 10.1146/annurev-neuro-070815-013920).

LUTHMAN, J., FREDRIKSSON, A., SUNDSTROM, E., JONSSON, G. & ARCHER, T. 1989. Selective lesion of central dopamine or noradrenaline neuron systems in the neonatal rat: motor behavior and monoamine alterations at adult stage. *Behav Brain Res,* 33**,** 267-77. (doi: 10.1016/s0166-4328(89)80121-4).

MA, Y., ZHAN, M., OUYANG, L., LI, Y., CHEN, S., WU, J., CHEN, J., LUO, C. & LEI, W. 2014. The effects of unilateral 6-OHDA lesion in medial forebrain bundle on the motor, cognitive dysfunctions and vulnerability of different striatal interneuron types in rats. *Behav Brain Res,* 266**,** 37-45. (doi: 10.1016/j.bbr.2014.02.039).

MAHUL-MELLIER, A. L., BURTSCHER, J., MAHARJAN, N., WEERENS, L., CROISIER, M., KUTTLER, F., LELEU, M., KNOTT, G. W. & LASHUEL, H. A. 2020. The process of Lewy body formation, rather than simply alpha-synuclein fibrillization, is one of the major drivers of neurodegeneration. *Proc Natl Acad Sci U S A,* 117**,** 4971-4982. (doi: 10.1073/pnas.1913904117).

MAINGAY, M., ROMERO-RAMOS, M., CARTA, M. & KIRIK, D. 2006. Ventral tegmental area dopamine neurons are resistant to human mutant alpha-synuclein overexpression. *Neurobiol Dis,* 23**,** 522-32. (doi: 10.1016/j.nbd.2006.04.007).

MANFREDSSON, F. P., LUK, K. C., BENSKEY, M. J., GEZER, A., GARCIA, J., KUHN, N. C., SANDOVAL, I. M., PATTERSON, J. R., O'MARA, A., YONKERS, R. & KORDOWER, J. H. 2018. Induction of alpha-synuclein pathology in the enteric nervous system of the rat and non-human primate results in gastrointestinal dysmotility and transient CNS pathology. *Neurobiol Dis,* 112**,** 106-118. (doi: 10.1016/j.nbd.2018.01.008).

MAR, A. C., HORNER, A. E., NILSSON, S. R., ALSIO, J., KENT, B. A., KIM, C. H., HOLMES, A., SAKSIDA, L. M. & BUSSEY, T. J. 2013. The touchscreen operant platform for assessing executive function in rats and mice. *Nat Protoc,* 8**,** 1985-2005. (doi: 10.1038/nprot.2013.123).

MARRAS, C. & CHAUDHURI, K. R. 2016. Nonmotor features of Parkinson's disease subtypes. *Mov Disord,* 31**,** 1095-102. (doi: 10.1002/mds.26510).

MARSDEN, C. D. 1983. Neuromelanin and Parkinson's disease. *J Neural Transm Suppl,* 19**,** 121-41. (doi).

MARSHALL, C. A., KING, K. M. & KORTAGERE, S. 2019. Limitations of the rat medial forebrain lesion model to study prefrontal cortex mediated cognitive tasks in Parkinson's disease. *Brain Res,* 1702**,** 105-113. (doi: 10.1016/j.brainres.2018.03.035).

MASLIAH, E., ROCKENSTEIN, E., MANTE, M., CREWS, L., SPENCER, B., ADAME, A., PATRICK, C., TREJO, M., UBHI, K., ROHN, T. T., MUELLER-STEINER, S., SEUBERT, P., BARBOUR, R., MCCONLOGUE, L., BUTTINI, M., GAMES, D. & SCHENK, D. 2011. Passive immunization reduces behavioral and neuropathological deficits in an alpha-synuclein transgenic model of Lewy body disease. *PLoS One,* 6**,** e19338. (doi: 10.1371/journal.pone.0019338).

MASUDA-SUZUKAKE, M., NONAKA, T., HOSOKAWA, M., OIKAWA, T., ARAI, T., AKIYAMA, H., MANN, D. M. & HASEGAWA, M. 2013. Prion-like spreading of pathological alpha-synuclein in brain. *Brain,* 136**,** 1128-38. (doi: 10.1093/brain/awt037).

MAZZONI, P., SHABBOTT, B. & CORTES, J. C. 2012. Motor control abnormalities in Parkinson's disease. *Cold Spring Harb Perspect Med,* 2**,** a009282. (doi: 10.1101/cshperspect.a009282).

MCCANN, H., STEVENS, C. H., CARTWRIGHT, H. & HALLIDAY, G. M. 2014. alpha-Synucleinopathy phenotypes. *Parkinsonism Relat Disord,* 20 Suppl 1**,** S62-7. (doi: 10.1016/S1353-8020(13)70017-8).

MCGREGOR, M. M. & NELSON, A. B. 2019. Circuit Mechanisms of Parkinson's Disease. *Neuron,* 101**,** 1042-1056. (doi: 10.1016/j.neuron.2019.03.004).

MCMULLEN, N. T. & ALMLI, C. R. 1981. Cell types within the medial forebrain bundle: a Golgi study of preoptic and hypothalamic neurons in the rat. *Am J Anat,* 161**,** 323-40. (doi: 10.1002/aja.1001610306).

MEADE, R. M., FAIRLIE, D. P. & MASON, J. M. 2019. Alpha-synuclein structure and Parkinson's disease - lessons and emerging principles. *Mol Neurodegener,* 14**,** 29. (doi: 10.1186/s13024-019-0329-1).

MEREDITH, G. E. & KANG, U. J. 2006. Behavioral models of Parkinson's disease in rodents: a new look at an old problem. *Mov Disord,* 21**,** 1595-606. (doi: 10.1002/mds.21010).

MEREDITH, G. E., SONSALLA, P. K. & CHESSELET, M. F. 2008. Animal models of Parkinson's disease progression. *Acta Neuropathol,* 115**,** 385-98. (doi: 10.1007/s00401-008-0350-x).

MERTENS, B., MASSIE, A., MICHOTTE, Y. & SARRE, S. 2009. Effect of nigrostriatal damage induced by 6-hydroxydopamine on the expression of glial cell line-derived neurotrophic factor in the striatum of the rat. *Neuroscience,* 162**,** 148-54. (doi: 10.1016/j.neuroscience.2009.04.036).

MILBER, J. M., NOORIGIAN, J. V., MORLEY, J. F., PETROVITCH, H., WHITE, L., ROSS, G. W. & DUDA, J. E. 2012. Lewy pathology is not the first sign of degeneration in vulnerable neurons in Parkinson disease. *Neurology,* 79**,** 2307-14. (doi: 10.1212/WNL.0b013e318278fe32).

MILLHOUSE, O. E. 1969. A Golgi study of the desending medial forebrain bundle. *Brain Res,* 15**,** 341-63. (doi: 10.1016/0006-8993(69)90161-9).

MIRZA, B., HADBERG, H., THOMSEN, P. & MOOS, T. 2000. The absence of reactive astrocytosis is indicative of a unique inflammatory process in Parkinson's disease. *Neuroscience,* 95**,** 425-32. (doi: 10.1016/s0306-4522(99)00455-8).

MONTSE, A., PERE, V., CARME, J., FRANCESC, V. & EDUARDO, T. 2001. Visuospatial deficits in Parkinson's disease assessed by judgment of line orientation test: error analyses and practice effects. *J Clin Exp Neuropsychol,* 23**,** 592-8. (doi: 10.1076/jcen.23.5.592.1248).

MORALES, I., SANCHEZ, A., RODRIGUEZ-SABATE, C. & RODRIGUEZ, M. 2015. The degeneration of dopaminergic synapses in Parkinson's disease: A selective animal model. *Behav Brain Res,* 289**,** 19-28. (doi: 10.1016/j.bbr.2015.04.019).

MORALES, R., MORENO-GONZALEZ, I. & SOTO, C. 2013. Cross-seeding of misfolded proteins: implications for etiology and pathogenesis of protein misfolding diseases. *PLoS Pathog,* 9**,** e1003537. (doi: 10.1371/journal.ppat.1003537).

MOUSSAUD, S., JONES, D. R., MOUSSAUD-LAMODIERE, E. L., DELENCLOS, M., ROSS, O. A. & MCLEAN, P. J. 2014. Alpha-synuclein and tau: teammates in neurodegeneration? *Mol Neurodegener,* 9**,** 43. (doi: 10.1186/1750-1326-9-43).

MUNOZ, P., HUENCHUGUALA, S., PARIS, I. & SEGURA-AGUILAR, J. 2012. Dopamine oxidation and autophagy. *Parkinsons Dis,* 2012**,** 920953. (doi: 10.1155/2012/920953).

MUNTANE, G., DALFO, E., MARTINEZ, A. & FERRER, I. 2008. Phosphorylation of tau and alpha-synuclein in synaptic-enriched fractions of the frontal cortex in Alzheimer's disease, and in Parkinson's disease and related alpha-synucleinopathies. *Neuroscience,* 152**,** 913-23. (doi: 10.1016/j.neuroscience.2008.01.030).

MURPHY, K. E. & HALLIDAY, G. M. 2014. Glucocerebrosidase deficits in sporadic Parkinson disease. *Autophagy,* 10**,** 1350-1. (doi: 10.4161/auto.29074).

MUSGROVE, R. E., HELWIG, M., BAE, E. J., ABOUTALEBI, H., LEE, S. J., ULUSOY, A. & DI MONTE, D. A. 2019. Oxidative stress in vagal neurons promotes parkinsonian pathology and intercellular alpha-synuclein transfer. *J Clin Invest,* 130**,** 3738-3753. (doi: 10.1172/JCI127330).

NARASIMHAN, S., GUO, J. L., CHANGOLKAR, L., STIEBER, A., MCBRIDE, J. D., SILVA, L. V., HE, Z., ZHANG, B., GATHAGAN, R. J., TROJANOWSKI, J. Q. & LEE, V. M. Y. 2017. Pathological Tau Strains from Human Brains Recapitulate the Diversity of Tauopathies in Nontransgenic Mouse Brain. *J Neurosci,* 37**,** 11406-11423. (doi: 10.1523/JNEUROSCI.1230-17.2017).

NASH, J. E., JOHNSTON, T. H., COLLINGRIDGE, G. L., GARNER, C. C. & BROTCHIE, J. M. 2005. Subcellular redistribution of the synapse-associated proteins PSD-95 and SAP97 in animal models of Parkinson's disease and L-DOPA-induced dyskinesia. *FASEB J,* 19**,** 583-5. (doi: 10.1096/fj.04-1854fje).

NEDDENS, J., TEMMEL, M., FLUNKERT, S., KERSCHBAUMER, B., HOELLER, C., LOEFFLER, T., NIEDERKOFLER, V., DAUM, G., ATTEMS, J. & HUTTER-PAIER, B. 2018. Phosphorylation of

different tau sites during progression of Alzheimer's disease. *Acta Neuropathol Commun,* 6**,** 52. (doi: 10.1186/s40478-018-0557-6).

NEUMANN, M., KAHLE, P. J., GIASSON, B. I., OZMEN, L., BORRONI, E., SPOOREN, W., MULLER, V., ODOY, S., FUJIWARA, H., HASEGAWA, M., IWATSUBO, T., TROJANOWSKI, J. Q., KRETZSCHMAR, H. A. & HAASS, C. 2002. Misfolded proteinase K-resistant hyperphosphorylated alpha-synuclein in aged transgenic mice with locomotor deterioration and in human alpha-synucleinopathies. *J Clin Invest,* 110**,** 1429-39. (doi: 10.1172/JCI15777).

NIEUWENHUYS, R., GEERAEDTS, L. M. & VEENING, J. G. 1982. The medial forebrain bundle of the rat. I. General introduction. *J Comp Neurol,* 206**,** 49-81. (doi: 10.1002/cne.902060106).

NISHIOKA, K., HASHIZUME, Y., TAKANASHI, M., DAIDA, K., LI, Y., YOSHINO, H., TAMBASCO, N., PRONTERA, P., HATTORI, Y., UEDA, A., WATANABE, H. & HATTORI, N. 2020. Pathological findings in a patient with alpha-synuclein p.A53T and familial Parkinson's disease. *Parkinsonism Relat Disord,* 81**,** 183-187. (doi: 10.1016/j.parkreldis.2020.11.001).

NOBILI, A., LATAGLIATA, E. C., VISCOMI, M. T., CAVALLUCCI, V., CUTULI, D., GIACOVAZZO, G., KRASHIA, P., RIZZO, F. R., MARINO, R., FEDERICI, M., DE BARTOLO, P., AVERSA, D., DELL'ACQUA, M. C., CORDELLA, A., SANCANDI, M., KELLER, F., PETROSINI, L., PUGLISI-ALLEGRA, S., MERCURI, N. B., COCCURELLO, R., BERRETTA, N. & D'AMELIO, M. 2017. Dopamine neuronal loss contributes to memory and reward dysfunction in a model of Alzheimer's disease. *Nat Commun,* 8**,** 14727. (doi: 10.1038/ncomms14727).

NOBLE, W., HANGER, D. P., MILLER, C. C. & LOVESTONE, S. 2013. The importance of tau phosphorylation for neurodegenerative diseases. *Front Neurol,* 4**,** 83. (doi: 10.3389/fneur.2013.00083).

NOBLE, W. & SPIRES-JONES, T. L. 2019. Sleep well to slow Alzheimer's progression? *Science,* 363**,** 813-814. (doi: 10.1126/science.aaw5583).

NORMAN, A. B., LU, S. Y., KLUG, J. M. & NORGREN, R. B. 1993. Sensitization of c-fos expression in rat striatum following multiple challenges with D-amphetamine. *Brain Res,* 603**,** 125-8. (doi: 10.1016/0006-8993(93)91308-f).

NORRIS, E. H. & GIASSON, B. I. 2005. Role of oxidative damage in protein aggregation associated with Parkinson's disease and related disorders. *Antioxid Redox Signal,* 7**,** 672-84. (doi: 10.1089/ars.2005.7.672).

OBESO, J. A., RODRIGUEZ-OROZ, M. C., GOETZ, C. G., MARIN, C., KORDOWER, J. H., RODRIGUEZ, M., HIRSCH, E. C., FARRER, M., SCHAPIRA, A. H. & HALLIDAY, G. 2010. Missing pieces in the Parkinson's disease puzzle. *Nat Med,* 16**,** 653-61. (doi: 10.1038/nm.2165).

OCZKOWSKA, A., KOZUBSKI, W., LIANERI, M. & DORSZEWSKA, J. 2013. Mutations in PRKN and SNCA Genes Important for the Progress of Parkinson's Disease. *Curr Genomics,* 14**,** 502-17. (doi: 10.2174/1389202914666131210205839).

OKUN, M. S. & KOEHLER, P. J. 2007. Paul Blocq and (psychogenic) astasia abasia. *Mov Disord,* 22**,** 1373-8. (doi: 10.1002/mds.21474).

OKUZUMI, A., KUROSAWA, M., HATANO, T., TAKANASHI, M., NOJIRI, S., FUKUHARA, T., YAMANAKA, T., MIYAZAKI, H., YOSHINAGA, S., FURUKAWA, Y., SHIMOGORI, T., HATTORI, N. & NUKINA, N. 2018. Rapid dissemination of alpha-synuclein seeds through neural circuits in an in-vivo prion-like seeding experiment. *Acta Neuropathol Commun,* 6**,** 96. (doi: 10.1186/s40478-018-0587-0).

OLGIATI, S., THOMAS, A., QUADRI, M., BREEDVELD, G. J., GRAAFLAND, J., EUSSEN, H., DOUBEN, H., DE KLEIN, A., ONOFRJ, M. & BONIFATI, V. 2015. Early-onset parkinsonism caused by alpha-synuclein gene triplication: Clinical and genetic findings in a novel family. *Parkinsonism Relat Disord,* 21**,** 981-6. (doi: 10.1016/j.parkreldis.2015.06.005).

OSTERBERG, V. R., SPINELLI, K. J., WESTON, L. J., LUK, K. C., WOLTJER, R. L. & UNNI, V. K. 2015. Progressive aggregation of alpha-synuclein and selective degeneration of lewy inclusion-bearing neurons in a mouse model of parkinsonism. *Cell Rep,* 10**,** 1252-60. (doi: 10.1016/j.celrep.2015.01.060).

PARK, S. E., SONG, K. I., KIM, H., CHUNG, S. & YOUN, I. 2018. Graded 6-OHDA-induced dopamine depletion in the nigrostriatal pathway evokes progressive pathological neuronal activities in the subthalamic nucleus of a hemi-parkinsonian mouse. *Behav Brain Res,* 344**,** 42-47. (doi: 10.1016/j.bbr.2018.02.014).

PARKKINEN, L., PIRTTILA, T. & ALAFUZOFF, I. 2008. Applicability of current staging/categorization of alpha-synuclein pathology and their clinical relevance. *Acta Neuropathol,* 115**,** 399-407. (doi: 10.1007/s00401-008-0346-6).

PATTERSON, J. R., DUFFY, M. F., KEMP, C. J., HOWE, J. W., COLLIER, T. J., STOLL, A. C., MILLER, K. M., PATEL, P., LEVINE, N., MOORE, D. J., LUK, K. C., FLEMING, S. M., KANAAN, N. M., PAUMIER, K. L., EL-AGNAF, O. M. A. & SORTWELL, C. E. 2019. Time course and magnitude of alpha-synuclein inclusion formation and nigrostriatal degeneration in the rat model of synucleinopathy triggered by intrastriatal alpha-synuclein preformed fibrils. *Neurobiol Dis,* 130**,** 104525. (doi: 10.1016/j.nbd.2019.104525).

PAUMIER, K. L., LUK, K. C., MANFREDSSON, F. P., KANAAN, N. M., LIPTON, J. W., COLLIER, T. J., STEECE-COLLIER, K., KEMP, C. J., CELANO, S., SCHULZ, E., SANDOVAL, I. M., FLEMING, S., DIRR, E., POLINSKI, N. K., TROJANOWSKI, J. Q., LEE, V. M. & SORTWELL, C. E. 2015. Intrastriatal injection of pre-formed mouse alpha-synuclein fibrils into rats triggers alpha-synuclein pathology and bilateral nigrostriatal degeneration. *Neurobiol Dis,* 82**,** 185-199. (doi: 10.1016/j.nbd.2015.06.003).

PAXINOU, E., CHEN, Q., WEISSE, M., GIASSON, B. I., NORRIS, E. H., RUETER, S. M., TROJANOWSKI, J. Q., LEE, V. M. & ISCHIROPOULOS, H. 2001. Induction of alpha-synuclein aggregation by intracellular nitrative insult. *J Neurosci,* 21**,** 8053-61. (doi).

PENG, C., GATHAGAN, R. J., COVELL, D. J., MEDELLIN, C., STIEBER, A., ROBINSON, J. L., ZHANG, B., PITKIN, R. M., OLUFEMI, M. F., LUK, K. C., TROJANOWSKI, J. Q. & LEE, V. M. 2018. Cellular milieu imparts distinct pathological alpha-synuclein strains in alpha-synucleinopathies. *Nature,* 557**,** 558-563. (doi: 10.1038/s41586-018-0104-4).

PENG, C., TROJANOWSKI, J. Q. & LEE, V. M. 2020. Protein transmission in neurodegenerative disease. *Nat Rev Neurol,* 16**,** 199-212. (doi: 10.1038/s41582-020-0333-7).

PEREIRA, J. B., IBARRETXE-BILBAO, N., MARTI, M. J., COMPTA, Y., JUNQUE, C., BARGALLO, N. & TOLOSA, E. 2012. Assessment of cortical degeneration in patients with Parkinson's disease by voxel-based morphometry, cortical folding, and cortical thickness. *Hum Brain Mapp,* 33**,** 2521-34. (doi: 10.1002/hbm.21378).

PERESE, D. A., ULMAN, J., VIOLA, J., EWING, S. E. & BANKIEWICZ, K. S. 1989. A 6-hydroxydopamine-induced selective parkinsonian rat model. *Brain Res,* 494**,** 285-93. (doi: 10.1016/0006-8993(89)90597-0).

PEREZ-NIEVAS, B. G., STEIN, T. D., TAI, H. C., DOLS-ICARDO, O., SCOTTON, T. C., BARROETA-ESPAR, I., FERNANDEZ-CARBALLO, L., DE MUNAIN, E. L., PEREZ, J., MARQUIE, M., SERRANO-POZO, A., FROSCH, M. P., LOWE, V., PARISI, J. E., PETERSEN, R. C., IKONOMOVIC, M. D., LOPEZ, O. L., KLUNK, W., HYMAN, B. T. & GOMEZ-ISLA, T. 2013. Dissecting phenotypic traits linked to human resilience to Alzheimer's pathology. *Brain,* 136**,** 2510-26. (doi: 10.1093/brain/awt171).

PETERSEN, S. E. & POSNER, M. I. 2012. The attention system of the human brain: 20 years after. *Annu Rev Neurosci,* 35**,** 73-89. (doi: 10.1146/annurev-neuro-062111-150525).

PICCONI, B., PICCOLI, G. & CALABRESI, P. 2012. Synaptic dysfunction in Parkinson's disease. *Adv Exp Med Biol,* 970**,** 553-72. (doi: 10.1007/978-3-7091-0932-8_24).

POEHLER, A. M., XIANG, W., SPITZER, P., MAY, V. E., MEIXNER, H., ROCKENSTEIN, E., CHUTNA, O., OUTEIRO, T. F., WINKLER, J., MASLIAH, E. & KLUCKEN, J. 2014. Autophagy modulates SNCA/alpha-synuclein release, thereby generating a hostile microenvironment. *Autophagy,* 10**,** 2171-92. (doi: 10.4161/auto.36436).

POEWE, W., SEPPI, K., TANNER, C. M., HALLIDAY, G. M., BRUNDIN, P., VOLKMANN, J., SCHRAG, A. E. & LANG, A. E. 2017. Parkinson disease. *Nat Rev Dis Primers,* 3**,** 17013. (doi: 10.1038/nrdp.2017.13).

POLINSKI, N. K., VOLPICELLI-DALEY, L. A., SORTWELL, C. E., LUK, K. C., CREMADES, N., GOTTLER, L. M., FROULA, J., DUFFY, M. F., LEE, V. M. Y., MARTINEZ, T. N. & DAVE, K. D. 2018. Best Practices for Generating and Using Alpha-Synuclein Pre-Formed Fibrils to Model Parkinson's Disease in Rodents. *J Parkinsons Dis,* 8**,** 303-322. (doi: 10.3233/JPD-171248).

POLYMEROPOULOS, M. H., LAVEDAN, C., LEROY, E., IDE, S. E., DEHEJIA, A., DUTRA, A., PIKE, B., ROOT, H., RUBENSTEIN, J., BOYER, R., STENROOS, E. S., CHANDRASEKHARAPPA, S., ATHANASSIADOU, A., PAPAPETROPOULOS, T., JOHNSON, W. G., LAZZARINI, A. M., DUVOISIN, R. C., DI IORIO, G., GOLBE, L. I. & NUSSBAUM, R. L. 1997. Mutation in the alpha-synuclein gene identified in families with Parkinson's disease. *Science,* 276**,** 2045-7. (doi: 10.1126/science.276.5321.2045).

POOLER, A. M., NOBLE, W. & HANGER, D. P. 2014. A role for tau at the synapse in Alzheimer's disease pathogenesis. *Neuropharmacology,* 76 Pt A**,** 1-8. (doi: 10.1016/j.neuropharm.2013.09.018).

PRAJAPATI, S. K., GARABADU, D. & KRISHNAMURTHY, S. 2017. Coenzyme Q10 Prevents Mitochondrial Dysfunction and Facilitates Pharmacological Activity of Atorvastatin in 6-OHDA Induced Dopaminergic Toxicity in Rats. *Neurotox Res,* 31**,** 478-492. (doi: 10.1007/s12640-016-9693-6).

RABILLOUD, T. 2009. Detergents and chaotropes for protein solubilization before two-dimensional electrophoresis. *Methods Mol Biol,* 528**,** 259-67. (doi: 10.1007/978-1-60327-310-7_18).

RAUDINO, F. 2001. Non motor off in Parkinson's disease. *Acta Neurol Scand,* 104**,** 312-5. (doi: 10.1034/j.1600-0404.2001.00357.x).

REY, N. L., GEORGE, S., STEINER, J. A., MADAJ, Z., LUK, K. C., TROJANOWSKI, J. Q., LEE, V. M. & BRUNDIN, P. 2018. Spread of aggregates after olfactory bulb injection of alpha-synuclein fibrils is associated with early neuronal loss and is reduced long term. *Acta Neuropathol,* 135**,** 65-83. (doi: 10.1007/s00401-017-1792-9).

REY, N. L., PETIT, G. H., BOUSSET, L., MELKI, R. & BRUNDIN, P. 2013. Transfer of human alpha-synuclein from the olfactory bulb to interconnected brain regions in mice. *Acta Neuropathol,* 126**,** 555-73. (doi: 10.1007/s00401-013-1160-3).

RIETDIJK, C. D., PEREZ-PARDO, P., GARSSEN, J., VAN WEZEL, R. J. & KRANEVELD, A. D. 2017. Exploring Braak's Hypothesis of Parkinson's Disease. *Front Neurol,* 8**,** 37. (doi: 10.3389/fneur.2017.00037).

RISSMAN, R. A., POON, W. W., BLURTON-JONES, M., ODDO, S., TORP, R., VITEK, M. P., LAFERLA, F. M., ROHN, T. T. & COTMAN, C. W. 2004. Caspase-cleavage of tau is an early event in Alzheimer disease tangle pathology. *J Clin Invest,* 114**,** 121-30. (doi: 10.1172/JCI20640).

RODRIGUEZ-MARTIN, T., CUCHILLO-IBANEZ, I., NOBLE, W., NYENYA, F., ANDERTON, B. H. & HANGER, D. P. 2013. Tau phosphorylation affects its axonal transport and degradation. *Neurobiol Aging,* 34**,** 2146-57. (doi: 10.1016/j.neurobiolaging.2013.03.015).

ROZAS, G., GUERRA, M. J. & LABANDEIRA-GARCIA, J. L. 1997. An automated rotarod method for quantitative drug-free evaluation of overall motor deficits in rat models of parkinsonism. *Brain Res Brain Res Protoc,* 2**,** 75-84. (doi: 10.1016/s1385-299x(97)00034-2).

SACINO, A. N., BROOKS, M. M., CHAKRABARTY, P., SAHA, K., KHOSHBOUEI, H., GOLDE, T. E. & GIASSON, B. I. 2017. Proteolysis of alpha-synuclein fibrils in the lysosomal pathway limits induction of inclusion pathology. *J Neurochem,* 140**,** 662-678. (doi: 10.1111/jnc.13743).

SANO, I., GAMO, T., KAKIMOTO, Y., TANIGUCHI, K., TAKESADA, M. & NISHINUMA, K. 1959. Distribution of catechol compounds in human brain. *Biochim Biophys Acta,* 32**,** 586-7. (doi: 10.1016/0006-3002(59)90652-3).

SARRE, S., YUAN, H., JONKERS, N., VAN HEMELRIJCK, A., EBINGER, G. & MICHOTTE, Y. 2004. In vivo characterization of somatodendritic dopamine release in the substantia nigra of 6-

hydroxydopamine-lesioned rats. *J Neurochem,* 90**,** 29-39. (doi: 10.1111/j.1471-4159.2004.02471.x).
SAUER, H. & OERTEL, W. H. 1994. Progressive degeneration of nigrostriatal dopamine neurons following intrastriatal terminal lesions with 6-hydroxydopamine: a combined retrograde tracing and immunocytochemical study in the rat. *Neuroscience,* 59**,** 401-15. (doi: 10.1016/0306-4522(94)90605-x).
SCHMIDT, N. & FERGER, B. 2001. Neuroprotective effects of (+/-)-kavain in the MPTP mouse model of Parkinson's disease. *Synapse,* 40**,** 47-54. (doi: 10.1002/1098-2396(200104)40:1<47::AID-SYN1025>3.0.CO;2-S).
SCHNEIDER, J. A., LI, J. L., LI, Y., WILSON, R. S., KORDOWER, J. H. & BENNETT, D. A. 2006. Substantia nigra tangles are related to gait impairment in older persons. *Ann Neurol,* 59**,** 166-73. (doi: 10.1002/ana.20723).
SCUDAMORE, O. & CIOSSEK, T. 2018. Increased Oxidative Stress Exacerbates alpha-Synuclein Aggregation In Vivo. *J Neuropathol Exp Neurol,* 77**,** 443-453. (doi: 10.1093/jnen/nly024).
SENIOR, S. L., NINKINA, N., DEACON, R., BANNERMAN, D., BUCHMAN, V. L., CRAGG, S. J. & WADE-MARTINS, R. 2008. Increased striatal dopamine release and hyperdopaminergic-like behaviour in mice lacking both alpha-synuclein and gamma-synuclein. *Eur J Neurosci,* 27**,** 947-57. (doi: 10.1111/j.1460-9568.2008.06055.x).
SHAH, A., HAN, P., WONG, M. Y., CHANG, R. C. & LEGIDO-QUIGLEY, C. 2019. Palmitate and Stearate are Increased in the Plasma in a 6-OHDA Model of Parkinson's Disease. *Metabolites,* 9. (doi: 10.3390/metabo9020031).
SHIOSAKA, S., TOHYAMA, M., TAKAGI, H., TAKAHASHI, Y., SAITOH, Y., SAKUMOTO, T., NAKAGAWA, H. & SHIMIZU, N. 1980. Ascending and descending components of the medial forebrain bundle in the rat as demonstrated by the horseradish peroxidase-blue reaction. I. Forebrain and upper brain stem. *Exp Brain Res,* 39**,** 377-88. (doi: 10.1007/BF00239302).
SIMIC, G., BABIC LEKO, M., WRAY, S., HARRINGTON, C., DELALLE, I., JOVANOV-MILOSEVIC, N., BAZADONA, D., BUEE, L., DE SILVA, R., DI GIOVANNI, G., WISCHIK, C. & HOF, P. R. 2016. Tau Protein Hyperphosphorylation and Aggregation in Alzheimer's Disease and Other Tauopathies, and Possible Neuroprotective Strategies. *Biomolecules,* 6**,** 6. (doi: 10.3390/biom6010006).
SINGH, B., COVELO, A., MARTELL-MARTINEZ, H., NANCLARES, C., SHERMAN, M. A., OKEMATTI, E., MEINTS, J., TERAVSKIS, P. J., GALLARDO, C., SAVONENKO, A. V., BENNEYWORTH, M. A., LESNE, S. E., LIAO, D., ARAQUE, A. & LEE, M. K. 2019. Tau is required for progressive synaptic and memory deficits in a transgenic mouse model of alpha-synucleinopathy. *Acta Neuropathol,* 138**,** 551-574. (doi: 10.1007/s00401-019-02032-w).
SINGLETON, A. B., FARRER, M., JOHNSON, J., SINGLETON, A., HAGUE, S., KACHERGUS, J., HULIHAN, M., PEURALINNA, T., DUTRA, A., NUSSBAUM, R., LINCOLN, S., CRAWLEY, A., HANSON, M., MARAGANORE, D., ADLER, C., COOKSON, M. R., MUENTER, M., BAPTISTA, M., MILLER, D., BLANCATO, J., HARDY, J. & GWINN-HARDY, K. 2003. alpha-Synuclein locus triplication causes Parkinson's disease. *Science,* 302**,** 841. (doi: 10.1126/science.1090278).
SMITH, G. P. & YOUNG, R. C. 1974. A new experimental model of hypokinesia. *Adv Neurol,* 5**,** 427-32. (doi).
SOFRONIEW, M. V. & VINTERS, H. V. 2010. Astrocytes: biology and pathology. *Acta Neuropathol,* 119**,** 7-35. (doi: 10.1007/s00401-009-0619-8).
SPENCER, B., DESPLATS, P. A., OVERK, C. R., VALERA-MARTIN, E., RISSMAN, R. A., WU, C., MANTE, M., ADAME, A., FLORIO, J., ROCKENSTEIN, E. & MASLIAH, E. 2016. Reducing Endogenous alpha-Synuclein Mitigates the Degeneration of Selective Neuronal Populations in an Alzheimer's Disease Transgenic Mouse Model. *J Neurosci,* 36**,** 7971-84. (doi: 10.1523/JNEUROSCI.0775-16.2016).
SPILLANTINI, M. G., CROWTHER, R. A., JAKES, R., CAIRNS, N. J., LANTOS, P. L. & GOEDERT, M. 1998a. Filamentous alpha-synuclein inclusions link multiple system atrophy with Parkinson's disease

and dementia with Lewy bodies. *Neurosci Lett,* 251**,** 205-8. (doi: 10.1016/s0304-3940(98)00504-7).
SPILLANTINI, M. G., CROWTHER, R. A., JAKES, R., HASEGAWA, M. & GOEDERT, M. 1998b. alpha-Synuclein in filamentous inclusions of Lewy bodies from Parkinson's disease and dementia with lewy bodies. *Proc Natl Acad Sci U S A,* 95**,** 6469-73. (doi: 10.1073/pnas.95.11.6469).
SPILLANTINI, M. G., SCHMIDT, M. L., LEE, V. M., TROJANOWSKI, J. Q., JAKES, R. & GOEDERT, M. 1997. Alpha-synuclein in Lewy bodies. *Nature,* 388**,** 839-40. (doi: 10.1038/42166).
SPIRES-JONES, T. L., ATTEMS, J. & THAL, D. R. 2017. Interactions of pathological proteins in neurodegenerative diseases. *Acta Neuropathol,* 134**,** 187-205. (doi: 10.1007/s00401-017-1709-7).
STANIC, D., FINKELSTEIN, D. I., BOURKE, D. W., DRAGO, J. & HORNE, M. K. 2003. Timecourse of striatal re-innervation following lesions of dopaminergic SNpc neurons of the rat. *Eur J Neurosci,* 18**,** 1175-88. (doi: 10.1046/j.1460-9568.2003.02800.x).
STEFANIS, L. 2012. alpha-Synuclein in Parkinson's disease. *Cold Spring Harb Perspect Med,* 2**,** a009399. (doi: 10.1101/cshperspect.a009399).
STROHAKER, T., JUNG, B. C., LIOU, S. H., FERNANDEZ, C. O., RIEDEL, D., BECKER, S., HALLIDAY, G. M., BENNATI, M., KIM, W. S., LEE, S. J. & ZWECKSTETTER, M. 2019. Structural heterogeneity of alpha-synuclein fibrils amplified from patient brain extracts. *Nat Commun,* 10**,** 5535. (doi: 10.1038/s41467-019-13564-w).
SU, R. J., ZHEN, J. L., WANG, W., ZHANG, J. L., ZHENG, Y. & WANG, X. M. 2018. Time-course behavioral features are correlated with Parkinson's diseaseassociated pathology in a 6-hydroxydopamine hemiparkinsonian rat model. *Mol Med Rep,* 17**,** 3356-3363. (doi: 10.3892/mmr.2017.8277).
SU, X., FISCHER, D. L., LI, X., BANKIEWICZ, K., SORTWELL, C. E. & FEDEROFF, H. J. 2017. Alpha-Synuclein mRNA Is Not Increased in Sporadic PD and Alpha-Synuclein Accumulation Does Not Block GDNF Signaling in Parkinson's Disease and Disease Models. *Mol Ther,* 25**,** 2231-2235. (doi: 10.1016/j.ymthe.2017.04.018).
SU, X., MAGUIRE-ZEISS, K. A., GIULIANO, R., PRIFTI, L., VENKATESH, K. & FEDEROFF, H. J. 2008. Synuclein activates microglia in a model of Parkinson's disease. *Neurobiol Aging,* 29**,** 1690-701. (doi: 10.1016/j.neurobiolaging.2007.04.006).
TAI, H. C., SERRANO-POZO, A., HASHIMOTO, T., FROSCH, M. P., SPIRES-JONES, T. L. & HYMAN, B. T. 2012. The synaptic accumulation of hyperphosphorylated tau oligomers in Alzheimer disease is associated with dysfunction of the ubiquitin-proteasome system. *Am J Pathol,* 181**,** 1426-35. (doi: 10.1016/j.ajpath.2012.06.033).
TAN, E. K., CHANDRAN, V. R., FOOK-CHONG, S., SHEN, H., YEW, K., TEOH, M. L., YUEN, Y. & ZHAO, Y. 2005. Alpha-synuclein mRNA expression in sporadic Parkinson's disease. *Mov Disord,* 20**,** 620-3. (doi: 10.1002/mds.20391).
TAO, H., LIU, W., SIMMONS, B. N., HARRIS, H. K., COX, T. C. & MASSIAH, M. A. 2010. Purifying natively folded proteins from inclusion bodies using sarkosyl, Triton X-100, and CHAPS. *Biotechniques,* 48**,** 61-4. (doi: 10.2144/000113304).
TAYEBI, N., CALLAHAN, M., MADIKE, V., STUBBLEFIELD, B. K., ORVISKY, E., KRASNEWICH, D., FILLANO, J. J. & SIDRANSKY, E. 2001. Gaucher disease and parkinsonism: a phenotypic and genotypic characterization. *Mol Genet Metab,* 73**,** 313-21. (doi: 10.1006/mgme.2001.3201).
TAYLOR, J. P., HARDY, J. & FISCHBECK, K. H. 2002. Toxic proteins in neurodegenerative disease. *Science,* 296**,** 1991-5. (doi: 10.1126/science.1067122).
TERAVSKIS, P. J., COVELO, A., MILLER, E. C., SINGH, B., MARTELL-MARTINEZ, H. A., BENNEYWORTH, M. A., GALLARDO, C., OXNARD, B. R., ARAQUE, A., LEE, M. K. & LIAO, D. 2018. A53T Mutant Alpha-Synuclein Induces Tau-Dependent Postsynaptic Impairment Independently of Neurodegenerative Changes. *J Neurosci,* 38**,** 9754-9767. (doi: 10.1523/JNEUROSCI.0344-18.2018).

TIEU, K. 2011. A guide to neurotoxic animal models of Parkinson's disease. *Cold Spring Harb Perspect Med,* 1**,** a009316. (doi: 10.1101/cshperspect.a009316).
TONG, J., WONG, H., GUTTMAN, M., ANG, L. C., FORNO, L. S., SHIMADZU, M., RAJPUT, A. H., MUENTER, M. D., KISH, S. J., HORNYKIEWICZ, O. & FURUKAWA, Y. 2010. Brain alpha-synuclein accumulation in multiple system atrophy, Parkinson's disease and progressive supranuclear palsy: a comparative investigation. *Brain,* 133**,** 172-88. (doi: 10.1093/brain/awp282).
TROIANO, R. & SIEGEL, A. 1978a. Efferent connections of the basal forebrain in the cat: the nucleus accumbens. *Exp Neurol,* 61**,** 185-97. (doi: 10.1016/0014-4886(78)90190-5).
TROIANO, R. & SIEGEL, A. 1978b. Efferent connections of the basal forebrain in the cat: the substantia innominata. *Exp Neurol,* 61**,** 198-213. (doi: 10.1016/0014-4886(78)90191-7).
TROJANOWSKI, J. Q. & LEE, V. M. 1998. Aggregation of neurofilament and alpha-synuclein proteins in Lewy bodies: implications for the pathogenesis of Parkinson disease and Lewy body dementia. *Arch Neurol,* 55**,** 151-2. (doi: 10.1001/archneur.55.2.151).
TURTURICI, G., TINNIRELLO, R., SCONZO, G. & GERACI, F. 2014. Extracellular membrane vesicles as a mechanism of cell-to-cell communication: advantages and disadvantages. *Am J Physiol Cell Physiol,* 306**,** C621-33. (doi: 10.1152/ajpcell.00228.2013).
UHL, G. R., HEDREEN, J. C. & PRICE, D. L. 1985. Parkinson's disease: loss of neurons from the ventral tegmental area contralateral to therapeutic surgical lesions. *Neurology,* 35**,** 1215-8. (doi: 10.1212/wnl.35.8.1215).
UHL, G. R., WALTHER, D., MASH, D., FAUCHEUX, B. & JAVOY-AGID, F. 1994. Dopamine transporter messenger RNA in Parkinson's disease and control substantia nigra neurons. *Ann Neurol,* 35**,** 494-8. (doi: 10.1002/ana.410350421).
UNGERSTEDT, U. 1968. 6-Hydroxy-dopamine induced degeneration of central monoamine neurons. *Eur J Pharmacol,* 5**,** 107-10. (doi: 10.1016/0014-2999(68)90164-7).
UNGERSTEDT, U. & ARBUTHNOTT, G. W. 1970. Quantitative recording of rotational behavior in rats after 6-hydroxy-dopamine lesions of the nigrostriatal dopamine system. *Brain Res,* 24**,** 485-93. (doi: 10.1016/0006-8993(70)90187-3).
UVERSKY, V. N. 2007. Neuropathology, biochemistry, and biophysics of alpha-synuclein aggregation. *J Neurochem,* 103**,** 17-37. (doi: 10.1111/j.1471-4159.2007.04764.x).
VAINCHTEIN, I. D. & MOLOFSKY, A. V. 2020. Astrocytes and Microglia: In Sickness and in Health. *Trends Neurosci,* 43**,** 144-154. (doi: 10.1016/j.tins.2020.01.003).
VALENTE, E. M., ABOU-SLEIMAN, P. M., CAPUTO, V., MUQIT, M. M., HARVEY, K., GISPERT, S., ALI, Z., DEL TURCO, D., BENTIVOGLIO, A. R., HEALY, D. G., ALBANESE, A., NUSSBAUM, R., GONZALEZ-MALDONADO, R., DELLER, T., SALVI, S., CORTELLI, P., GILKS, W. P., LATCHMAN, D. S., HARVEY, R. J., DALLAPICCOLA, B., AUBURGER, G. & WOOD, N. W. 2004. Hereditary early-onset Parkinson's disease caused by mutations in PINK1. *Science,* 304**,** 1158-60. (doi: 10.1126/science.1096284).
VASILI, E., DOMINGUEZ-MEIJIDE, A. & OUTEIRO, T. F. 2019. Spreading of alpha-Synuclein and Tau: A Systematic Comparison of the Mechanisms Involved. *Front Mol Neurosci,* 12**,** 107. (doi: 10.3389/fnmol.2019.00107).
VEENING, J. G., SWANSON, L. W., COWAN, W. M., NIEUWENHUYS, R. & GEERAEDTS, L. M. 1982. The medial forebrain bundle of the rat. II. An autoradiographic study of the topography of the major descending and ascending components. *J Comp Neurol,* 206**,** 82-108. (doi: 10.1002/cne.902060107).
VIEIRA, J. C. F., BASSANI, T. B., SANTIAGO, R. M., DE, O. G. G., ZANOVELI, J. M., DA CUNHA, C. & VITAL, M. 2019. Anxiety-like behavior induced by 6-OHDA animal model of Parkinson's disease may be related to a dysregulation of neurotransmitter systems in brain areas related to anxiety. *Behav Brain Res,* 371**,** 111981. (doi: 10.1016/j.bbr.2019.111981).
VILARINO-GUELL, C., WIDER, C., ROSS, O. A., DACHSEL, J. C., KACHERGUS, J. M., LINCOLN, S. J., SOTO-ORTOLAZA, A. I., COBB, S. A., WILHOITE, G. J., BACON, J. A., BEHROUZ, B., MELROSE, H. L.,

HENTATI, E., PUSCHMANN, A., EVANS, D. M., CONIBEAR, E., WASSERMAN, W. W., AASLY, J. O., BURKHARD, P. R., DJALDETTI, R., GHIKA, J., HENTATI, F., KRYGOWSKA-WAJS, A., LYNCH, T., MELAMED, E., RAJPUT, A., RAJPUT, A. H., SOLIDA, A., WU, R. M., UITTI, R. J., WSZOLEK, Z. K., VINGERHOETS, F. & FARRER, M. J. 2011. VPS35 mutations in Parkinson disease. *Am J Hum Genet,* 89**,** 162-7. (doi: 10.1016/j.ajhg.2011.06.001).

VOLPICELLI-DALEY, L. A. 2017. Effects of alpha-synuclein on axonal transport. *Neurobiol Dis,* 105**,** 321-327. (doi: 10.1016/j.nbd.2016.12.008).

VOLPICELLI-DALEY, L. A., GAMBLE, K. L., SCHULTHEISS, C. E., RIDDLE, D. M., WEST, A. B. & LEE, V. M. 2014a. Formation of alpha-synuclein Lewy neurite-like aggregates in axons impedes the transport of distinct endosomes. *Mol Biol Cell,* 25**,** 4010-23. (doi: 10.1091/mbc.E14-02-0741).

VOLPICELLI-DALEY, L. A., KIRIK, D., STOYKA, L. E., STANDAERT, D. G. & HARMS, A. S. 2016. How can rAAV-alpha-synuclein and the fibril alpha-synuclein models advance our understanding of Parkinson's disease? *J Neurochem,* 139 Suppl 1**,** 131-155. (doi: 10.1111/jnc.13627).

VOLPICELLI-DALEY, L. A., LUK, K. C. & LEE, V. M. 2014b. Addition of exogenous alpha-synuclein preformed fibrils to primary neuronal cultures to seed recruitment of endogenous alpha-synuclein to Lewy body and Lewy neurite-like aggregates. *Nat Protoc,* 9**,** 2135-46. (doi: 10.1038/nprot.2014.143).

VOLPICELLI-DALEY, L. A., LUK, K. C., PATEL, T. P., TANIK, S. A., RIDDLE, D. M., STIEBER, A., MEANEY, D. F., TROJANOWSKI, J. Q. & LEE, V. M. 2011. Exogenous alpha-synuclein fibrils induce Lewy body pathology leading to synaptic dysfunction and neuron death. *Neuron,* 72**,** 57-71. (doi: 10.1016/j.neuron.2011.08.033).

VORHEES, C. V. & WILLIAMS, M. T. 2006. Morris water maze: procedures for assessing spatial and related forms of learning and memory. *Nat Protoc,* 1**,** 848-58. (doi: 10.1038/nprot.2006.116).

WAXMAN, E. A. & GIASSON, B. I. 2011. Induction of intracellular tau aggregation is promoted by alpha-synuclein seeds and provides novel insights into the hyperphosphorylation of tau. *J Neurosci,* 31**,** 7604-18. (doi: 10.1523/JNEUROSCI.0297-11.2011).

WHITE, M. A., KIM, E., DUFFY, A., ADALBERT, R., PHILLIPS, B. U., PETERS, O. M., STEPHENSON, J., YANG, S., MASSENZIO, F., LIN, Z., ANDREWS, S., SEGONDS-PICHON, A., METTERVILLE, J., SAKSIDA, L. M., MEAD, R., RIBCHESTER, R. R., BARHOMI, Y., SERRE, T., COLEMAN, M. P., FALLON, J. R., BUSSEY, T. J., BROWN, R. H., JR. & SREEDHARAN, J. 2018a. Publisher Correction: TDP-43 gains function due to perturbed autoregulation in a Tardbp knock-in mouse model of ALS-FTD. *Nat Neurosci,* 21**,** 1138. (doi: 10.1038/s41593-018-0160-y).

WHITE, M. A., KIM, E., DUFFY, A., ADALBERT, R., PHILLIPS, B. U., PETERS, O. M., STEPHENSON, J., YANG, S., MASSENZIO, F., LIN, Z., ANDREWS, S., SEGONDS-PICHON, A., METTERVILLE, J., SAKSIDA, L. M., MEAD, R., RIBCHESTER, R. R., BARHOMI, Y., SERRE, T., COLEMAN, M. P., FALLON, J. R., BUSSEY, T. J., BROWN, R. H., JR. & SREEDHARAN, J. 2018b. TDP-43 gains function due to perturbed autoregulation in a Tardbp knock-in mouse model of ALS-FTD. *Nat Neurosci,* 21**,** 552-563. (doi: 10.1038/s41593-018-0113-5).

WICHMANN, T. & DELONG, M. R. 2003. Pathophysiology of Parkinson's disease: the MPTP primate model of the human disorder. *Ann N Y Acad Sci,* 991**,** 199-213. (doi: 10.1111/j.1749-6632.2003.tb07477.x).

WILHELMSSON, U., BUSHONG, E. A., PRICE, D. L., SMARR, B. L., PHUNG, V., TERADA, M., ELLISMAN, M. H. & PEKNY, M. 2006. Redefining the concept of reactive astrocytes as cells that remain within their unique domains upon reaction to injury. *Proc Natl Acad Sci U S A,* 103**,** 17513-8. (doi: 10.1073/pnas.0602841103).

WILLS, J., JONES, J., HAGGERTY, T., DUKA, V., JOYCE, J. N. & SIDHU, A. 2010. Elevated tauopathy and alpha-synuclein pathology in postmortem Parkinson's disease brains with and without dementia. *Exp Neurol,* 225**,** 210-8. (doi: 10.1016/j.expneurol.2010.06.017).

WINKLER, C., KIRIK, D., BJORKLUND, A. & CENCI, M. A. 2002. L-DOPA-induced dyskinesia in the intrastriatal 6-hydroxydopamine model of parkinson's disease: relation to motor and cellular parameters of nigrostriatal function. *Neurobiol Dis,* 10**,** 165-86. (doi: 10.1006/nbdi.2002.0499).

WRIGHT WILLIS, A., EVANOFF, B. A., LIAN, M., CRISWELL, S. R. & RACETTE, B. A. 2010. Geographic and ethnic variation in Parkinson disease: a population-based study of US Medicare beneficiaries. *Neuroepidemiology,* 34**,** 143-51. (doi: 10.1159/000275491).

WU, Q., TAKANO, H., RIDDLE, D. M., TROJANOWSKI, J. Q., COULTER, D. A. & LEE, V. M. 2019. alpha-Synuclein (alphaSyn) Preformed Fibrils Induce Endogenous alphaSyn Aggregation, Compromise Synaptic Activity and Enhance Synapse Loss in Cultured Excitatory Hippocampal Neurons. *J Neurosci,* 39**,** 5080-5094. (doi: 10.1523/JNEUROSCI.0060-19.2019).

XILOURI, M., BREKK, O. R. & STEFANIS, L. 2013. alpha-Synuclein and protein degradation systems: a reciprocal relationship. *Mol Neurobiol,* 47**,** 537-51. (doi: 10.1007/s12035-012-8341-2).

XILOURI, M., VOGIATZI, T., VEKRELLIS, K., PARK, D. & STEFANIS, L. 2009. Abberant alpha-synuclein confers toxicity to neurons in part through inhibition of chaperone-mediated autophagy. *PLoS One,* 4**,** e5515. (doi: 10.1371/journal.pone.0005515).

YANG, Z. & WANG, K. K. 2015. Glial fibrillary acidic protein: from intermediate filament assembly and gliosis to neurobiomarker. *Trends Neurosci,* 38**,** 364-74. (doi: 10.1016/j.tins.2015.04.003).

YORITAKA, A., HATTORI, N., UCHIDA, K., TANAKA, M., STADTMAN, E. R. & MIZUNO, Y. 1996. Immunohistochemical detection of 4-hydroxynonenal protein adducts in Parkinson disease. *Proc Natl Acad Sci U S A,* 93**,** 2696-701. (doi: 10.1073/pnas.93.7.2696).

YOU, R., LIU, Y. & CHANG, R. C. 2019. A Behavioral Test Battery for the Repeated Assessment of Motor Skills, Mood, and Cognition in Mice. *J Vis Exp*. (145) (doi: 10.3791/58973).

ZAMANIAN, J. L., XU, L., FOO, L. C., NOURI, N., ZHOU, L., GIFFARD, R. G. & BARRES, B. A. 2012. Genomic analysis of reactive astrogliosis. *J Neurosci,* 32**,** 6391-410. (doi: 10.1523/JNEUROSCI.6221-11.2012).

ZEMPEL, H. & MANDELKOW, E. 2014. Lost after translation: missorting of Tau protein and consequences for Alzheimer disease. *Trends Neurosci,* 37**,** 721-32. (doi: 10.1016/j.tins.2014.08.004).

ZHAI, S., TANIMURA, A., GRAVES, S. M., SHEN, W. & SURMEIER, D. J. 2018. Striatal synapses, circuits, and Parkinson's disease. *Curr Opin Neurobiol,* 48**,** 9-16. (doi: 10.1016/j.conb.2017.08.004).

ZHANG, B., KEHM, V., GATHAGAN, R., LEIGHT, S. N., TROJANOWSKI, J. Q., LEE, V. M. & LUK, K. C. 2019. Stereotaxic Targeting of Alpha-Synuclein Pathology in Mouse Brain Using Preformed Fibrils. *Methods Mol Biol,* 1948**,** 45-57. (doi: 10.1007/978-1-4939-9124-2_5).

ZHANG, J., PERRY, G., SMITH, M. A., ROBERTSON, D., OLSON, S. J., GRAHAM, D. G. & MONTINE, T. J. 1999. Parkinson's disease is associated with oxidative damage to cytoplasmic DNA and RNA in substantia nigra neurons. *Am J Pathol,* 154**,** 1423-9. (doi: 10.1016/S0002-9440(10)65396-5).

ZHAO, Y. & ZHAO, B. 2013. Oxidative stress and the pathogenesis of Alzheimer's disease. *Oxid Med Cell Longev,* 2013**,** 316523. (doi: 10.1155/2013/316523).

ZHOU, J., BROE, M., HUANG, Y., ANDERSON, J. P., GAI, W. P., MILWARD, E. A., PORRITT, M., HOWELLS, D., HUGHES, A. J., WANG, X. & HALLIDAY, G. M. 2011. Changes in the solubility and phosphorylation of alpha-synuclein over the course of Parkinson's disease. *Acta Neuropathol,* 121**,** 695-704. (doi: 10.1007/s00401-011-0815-1).

ZHOU, L., MCINNES, J., WIERDA, K., HOLT, M., HERRMANN, A. G., JACKSON, R. J., WANG, Y. C., SWERTS, J., BEYENS, J., MISKIEWICZ, K., VILAIN, S., DEWACHTER, I., MOECHARS, D., DE STROOPER, B., SPIRES-JONES, T. L., DE WIT, J. & VERSTREKEN, P. 2017. Tau association with synaptic vesicles causes presynaptic dysfunction. *Nat Commun,* 8**,** 15295. (doi: 10.1038/ncomms15295).

ZIMPRICH, A., BENET-PAGES, A., STRUHAL, W., GRAF, E., ECK, S. H., OFFMAN, M. N., HAUBENBERGER, D., SPIELBERGER, S., SCHULTE, E. C., LICHTNER, P., ROSSLE, S. C., KLOPP, N.,

WOLF, E., SEPPI, K., PIRKER, W., PRESSLAUER, S., MOLLENHAUER, B., KATZENSCHLAGER, R., FOKI, T., HOTZY, C., REINTHALER, E., HARUTYUNYAN, A., KRALOVICS, R., PETERS, A., ZIMPRICH, F., BRUCKE, T., POEWE, W., AUFF, E., TRENKWALDER, C., ROST, B., RANSMAYR, G., WINKELMANN, J., MEITINGER, T. & STROM, T. M. 2011. A mutation in VPS35, encoding a subunit of the retromer complex, causes late-onset Parkinson disease. *Am J Hum Genet,* 89**,** 168-75. (doi: 10.1016/j.ajhg.2011.06.008).

ZHAO, Y. & ZHAO, B. 2013. Oxidative stress and the pathogenesis of Alzheimer's disease. Oxid Med Cell Longev, 2013, 316523.

ZHOU, J., BROE, M., HUANG, Y., ANDERSON, J. P., GAI, W. P., MILWARD, E. A., PORRITT, M., HOWELLS, D., HUGHES, A. J., WANG, X. & HALLIDAY, G. M. 2011. Changes in the solubility and phosphorylation of alpha-synuclein over the course of Parkinson's disease. Acta Neuropathol, 121, 695-704.

ZHOU, L., MCINNES, J., WIERDA, K., HOLT, M., HERRMANN, A. G., JACKSON, R. J., WANG, Y. C., SWERTS, J., BEYENS, J., MISKIEWICZ, K., VILAIN, S., DEWACHTER, I., MOECHARS, D., DE STROOPER, B., SPIRES-JONES, T. L., DE WIT, J. & VERSTREKEN, P. 2017. Tau association with synaptic vesicles causes presynaptic dysfunction. *Nat Commun,* 8**,** 15295.

Appendix 1- Statstistics table for all data within thesis

Figure	Groups	F Value	Significance
A) 60 d.p.i. latency	Treatment (Veh vs PFFs) Timepoint (training day) Interaction (treatment x timepoint)	F (4, 24) = 25.49 F (1, 6) = 1.819 F (4, 24) = 0.1110	P=02261 P<0.0001 P=0.9775
B) 90 d.p.i. latency	Treatment (Veh vs PFFs) Timepoint (training day) Interaction (treatment x timepoint)	F (4, 24) =1.827 F (1, 6) = 32.07 F (4, 24) = 1.170	P=0.2252 P<0.0001 P=0.3489
120 d.p.i. latency	Treatment (Veh vs PFFs) Timepoint (training day) Interaction (treatment x timepoint)	F (4, 20) = 0.06062 F (1, 5) = 36.34 F (4, 20) = 0.5010	P=0.8153 P<0.0001 P=0.7353
60 d.p.i. quadrant preferences	Treatment (Veh vs PFFs) Performance (target quadrant crossings) Interaction (treatment vs performance)	F (3, 48) = 0.9696 F (3, 48) = 0.06062 F (1, 48) = 1.186	P=0.4149 P=0.8153 P=0.2816
90 d.p.i quadrant preferences	Treatment (Veh vs PFFs) Performance (target quadrant crossings) Interaction (treatment vs performance)	F (3, 36) = 0.9628 F (1.977, 23.73) = 8.531 F (1, 12) = 0.07314	P=0.4208 P=0.0017 P=0.7914
120 d.p.i quadrant preferences	Treatment (Veh vs PFFs) Performance (target quadrant crossings) Interaction (treatment vs performance)	F (3, 24) = 10.63 F (1, 20) = 10.09 F (3, 20) = 3.106	P=0.8091 P=0.0047 P=0.0496

Figure 4.8 MWM			
A)Training curve	Treatment (Veh vs 6-OHDA) Timepoint (training day) Interaction (treatment x timepoint)	F (4, 36) = 11.68 F (1, 9) = 17.75 F (4, 36) = 1.888	P P<0.0001 P=0.0023 P=0.1338
B) Quadrant preference	Treatment (Veh vs PFFs) Performance (target quadrant crossings) Interaction (treatment vs performance)	F (3, 27) = 11.19 F (1, 9) = 1.326 F (3, 27) = 6.070	P<0.0001 P=0.2791 P=0.0027